Activities of the

Oil Implementation Task Force

Reporting Period September–November 1990

62

Contracts for field projects
and supporting research on . . .

Enhanced Oil Recovery

Reporting Period January–March 1990

DOE/BC-90/2
(DE90000262)
PROGRESS REVIEW

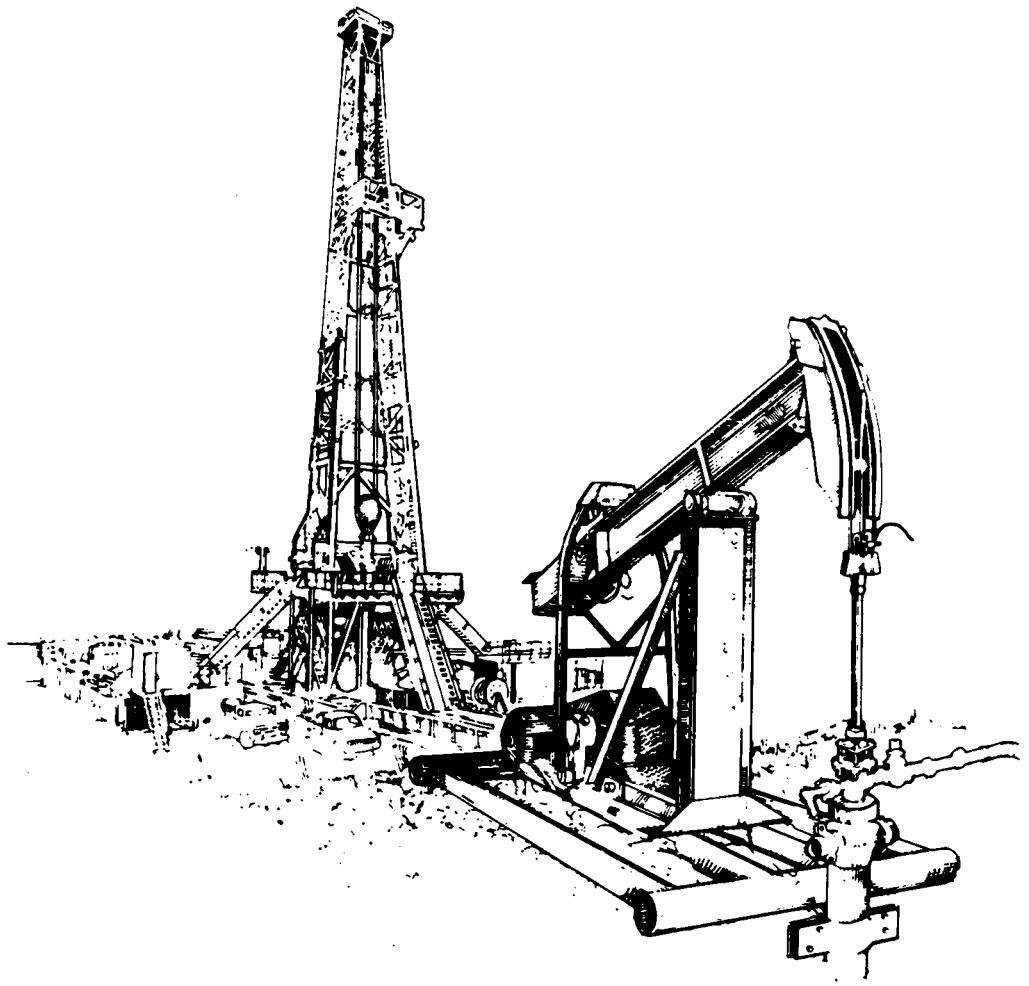

United States Department of Energy
Office of Oil, Gas, and Shale Technology
and Bartlesville Project Office

DISCLAIMER

Available to DOE and DOE contractors from the Office of Scientific and Technical Information, P.O. Box 62, Oak Ridge, Tennessee 37831; prices available from (615)576-8401, FTS 626-8401.

Available to the public from the National Technical Information Service, U.S. Department of Commerce, 5285 Port Royal Rd., Springfield, Virginia 22161.

Printed in the United States of America

NOTE: Beginning with this volume, the Quarterly Progress Review will include a separate section reporting activities of the Oil Implementation Task Force (OITF), as well as the standard reports on Enhanced Oil Recovery projects. Each section will have its own separate indexing and pagination.

SECTION INDEX **Pages**

SECTION I

Activities of the Oil Implementation Task Force

U.S. Department of Energy
Washington, D.C. 20545

ROBERT H. GENTILE
Assistant Secretary
for Fossil Energy
Room 4G-084 Forrestal Building
Telephone Number (202) 586-4695

MARVIN SINGER
Deputy Assistant Secretary for Oil,
Gas, Shale, and Special
Technologies

ROBERT L. FOLSTEIN
Director, Oil Implementation
Task Force

DOE/BC-90/2
(DE90000262)
Distribution Category UC-122

PROGRESS REVIEW NO. 62

ACTIVITIES OF THE OIL IMPLEMENTATION TASK FORCE

September-November, 1990

Date Published - December 1990

UNITED STATES DEPARTMENT OF ENERGY

INDEX

DOE Members of the
Oil Implementation Task Force

DIRECTORY

Name	Phone number	Task Force function
	U.S. Department of Energy **Oil, Gas, Shale and Special Technologies** **Mail Stop D-123, Washington, D.C. 20545**	
Ralph Avellanet	301-353-2737 – FTS 745-2737	Heavy Oil
Marvin Brooks	301-353-4462 – FTS 233-4462	AEPT
Edward Ferrero	301-353-2790 – FTS 233-2790	AEPT Alternate
Robert Folstein	301-353-2709 – FTS 233-2709	Chairman
Arthur Hartstein	301-353-2760 – FTS 233-2760	Environment
Carolyn Klym	301-353-2430 – FTS 233-2430	Administrative
Ronald Parent	301-353-3484 – FTS 233-3484	Planning & Schedule
Linda Simons	301-353-2703 – FTS 233-2703	Secretary
	U.S. Department of Energy **Headquarters, Forrestal Building** **Washington, D.C. 20585**	
William Hochheiser	202-586-5614 – FTS 896-5614	Geoscience
Nancy Johnson	202-586-6458 – FTS 896-6458	Environmental Policy
Elena S. Melchert	202-586-5095 – FTS 896-5095	Naval Petrol. Reserve
	Bartlesville Project Office **P.O. Box 1398** **Bartlesville, Oklahoma 74005**	
Edith Allison	918-337-4390 – FTS 745-4390	Manager, Reservoir Class I
Jerry Casteel	918-337-4412 – FTS 745-4412	Supporting Research
R. Michael Ray	918-337-4403 – FTS 745-4403	Data & Analysis
Thomas Reid	918-337-4233 – FTS 745-4233	Heavy Oil
H. A. Tiedemann	918-337-4293 – FTS 745-4293	Technology Transfer
	Morgantown Energy Technology Center **P.O. Box 880** **Morgantown, West Virginia 26505**	
James Ammer	304-291-4383 – FTS 923-4383	Tar Sands
John Guide	304-291-4930 – FTS 923-4930	Assistant Chairman
	Pittsburgh Energy Technology Center **P.O. Box 10940** **Pittsburgh, Pennsylvania 15326-0940**	
James J. Lacey	412-892-6144 – FTS 723-6144	Reservoir Field Tests
Dale Siciliano	412-892-6208 – FTS 723-6208	Procurement
	Metairie Site Office **900 Commerce East** **New Orleans, Louisiana 70123**	
E. B. Nuckols	504-734-4806 – FTS 686-4806	Manager, Reservoir Class II

INTRODUCTION TO THE OIL IMPLEMENTATION TASK FORCE

In August, 1990, Robert H. Gentile, The Department of Energy's Assistant Secretary for Fossil Energy, appointed a Task Force, comprising technical and management expertise, to put into place the Department's new Oil Research Program Implementation Plan. This new plan grew out of DOE's continuing effort to formulate a National Energy Strategy.

The previous program emphasis on long-term, high-risk research has been redirected to address the needs of current conditions in the petroleum industry. The 1986 price collapse, falling domestic production, and increased well abandonments that threaten future access to reservoirs containing a vast potential of recoverable oil were the major factors that led to this new direction.

In 1987 the Department initiated a study that highlighted the risk to national energy security posed by rising imports and pointed to the need for greater efforts in research. This recommendation was reinforced in an independent study by the Energy Research Advisory Board, which emphasized greater integration and coordination of geoscience and extraction research.

DOE sent a team of technical and management experts across the country to canvass the entire petroleum industry — majors, independents, consultants, service companies, universities — to obtain input on what they thought was needed to increase domestic production. Information gained from this effort led to a DOE Enhanced Oil Recovery (EOR) Initiative that recommended expansion of the research program to include near- and mid-term measures to improve domestic production, inclusion of mobile as well as immobile oil, and emphasis on technology transfer, particularly in relation to the independent producer.

In 1988, Congress directed DOE's Office of Fossil Energy to create, as part of a Hydrocarbon Geoscience Research Strategy, a plan to refocus oil research programs with a specific goal of increasing domestic oil production. In late 1989 and early 1990 the Department held a series of public hearings throughout the U.S., heard hundreds of witnesses and gathered thousands of pages of testimony from a cross-section of the nation. These meetings provided the background material for the formulation of a National Energy Strategy that seeks to strike a balance between competing resources and national priorities in arriving at a sensible, cohesive approach to a national energy policy.

Other concurrent studies emphasized additional facets of the energy security situation. Analysis by DOE's Tertiary Oil Recovery Information System (TORIS), an extensive compilation of petroleum-related information, disclosed the urgency posed by the increasing rate of well abandonment. The Hydrocarbon Geoscience Research Coordinating Committee, in cooperation with the Geoscience Institute for Oil and Gas Recovery Research, published a strategy document that urged a balance of near-, mid- and long-term research, and stressed the need to increase our understanding of reservoir complexities.

In response to these studies, on January 31, 1990, DOE announced its new Oil Research Program Implementation Plan. It recommended a program of field-based research on prioritized classes of reservoirs to rapidly demonstrate cost-effective advances in recovery technology. Under this new plan a balance of near-, mid- and long-term research will pursue the goals of better reservoir knowledge and improved recovery technologies. Research results will need to be evaluated at reservoir scale to be of value.

Building upon its predecessor, the plan establishes a program of highly targeted research, development and demonstration in collaboration with the states, industry and the academic community. It focuses on the reduction of technical and economic constraints on producibility to realize the enormous potential of the resource remaining in known domestic reservoirs. The program sets three time-specific goals:

- In the near term (within five years), preserve access to reservoirs with high recovery potential that are rapidly approaching their economic limits and are in danger of being abandoned.
- In the mid term (within ten years), develop, test and transfer the best, currently defined, advanced technologies to operators of the reservoirs with the greatest potential for incremental recovery.
- In the long term, develop sufficient fundamental understanding to define new recovery techniques for the oil left after application of the most advanced, currently defined mid-term processes, and for major classes of reservoirs for which no advanced technologies are anticipated to be available.

The primary goal of the new Oil Research Program is to increase domestic producibility and preserve access to those reservoirs containing the largest volumes of oil that are at the greatest risk of being abandoned.

A vast resource remains in existing reservoirs after conventional recovery. Of the more than 500 billion barrels of original oil in place in the U.S., less than ⅓ has been produced, and a mere 5% — less than 30 billion barrels — remains as proven reserves. With well-designed research and effective technology transfer, reserve additions of 76 billion barrels are possible within the next ten years — 15 billion barrels in the near-term (within five years), at present economic conditions with currently available and proven technologies. For the mid-term research component (five to ten years) reserve additions of 61 billion barrels are possible with the application of currently identified, yet-to-be-proven technologies.

The top priority for the Task Force is to preserve access to those reservoirs that have the largest potential for oil recovery. TORIS analysis shows that the present abandonment rate of 17-18,000 wells a year threatens future access to a significant portion of our oil resource. Calculations based on the principal reservoirs in nine states, representing over 75% of the remaining resource in the Lower-48, indicate that by 1987 access to 40% of the remaining oil in place had been abandoned. Even at $34 per barrel nearly 60% of the resource could be abandoned by the year 2000, and more than three quarters would be lost by the early 21st century if lower prices persist and technology advances are delayed (see References).

The first step in preserving reservoir access is identifying those reservoirs with significant remaining oil in place that are at the greatest risk of being abandoned. Information relating to the 3700 reservoirs contained in TORIS's reservoir database is being expanded and refined. Using TORIS in an ongoing Multi-State Study, BPO and the Interstate Oil Compact Commission have classified nearly 2000 of the nation's 2500 largest reservoirs, covering 25 of the 29 oil-producing states and 65% of the original oil in place. The reservoirs have been tentatively grouped into 25 classes, 16 sandstone and 9 carbonate, based on common geologic characteristics, and their associated production potential is being estimated.

The Task Force will prioritize the reservoir classes, based on volume of remaining oil in place, risk of abandonment, and the expectation that DOE-sponsored research can contribute to improved recovery. A preliminary selection for the first reservoir class has been made from the clastic reservoirs. Other selections will be made in the succeeding months.

Industry and other public comment on the reservoir selection process and the research needs of each class will be used along with other data to make the final selections and to design research keyed to the needs of the particular reservoir class. Field demonstrations of both currently existing and promising new recovery techniques will be implemented in reservoirs where they are deemed applicable. Successful results will be made available through DOE's Technology Transfer Program, and will be directed particularly to operators in the reservoirs where the results are applicable.

The Task Force is proceeding with these multiple approaches. Data is being collected, refined and analyzed to provide criteria for ranking and selection of reservoir classes, and plans are being made for the first of a series of meetings on the selection process. Reports on the activities of the various Task Force Teams are contained in this volume, and will continue in subsequent volumes.

References

1. U.S. Department of Energy, Bartlesville Project Office, "Abandonment Rates of the Known Domestic Oil Resource," DOE/BC-89/6/SP, November 1989.
2. U.S. Department of Energy, "Oil Research Program Implementation Plan," DOE/FE-0188P, April 1990.

TORIS DATA AND ANALYSIS

Data and Analysis Manager:
R. Michael Ray
Bartlesville Project Office

Report Period: September-November 1990

Objectives

The role of TORIS data and analysis in the work of the Task Force is to:

- Provide baseline data for the classification of reservoirs, the determination of urgency relative to abandonment, the geographic distribution of reservoirs, and the identification of applicable recovery processes.
- Provide baseline data to prioritize reservoir classes.
- Estimate the impact of research and development successes and failures on increasing the economic producibility of the known remaining oil resources in each reservoir class.

Summary of Progress

Supporting Data for Class and Reservoir Selection Criteria

Data Collection and Updating – The criteria for the selection of reservoir classes and individual reservoirs to be considered for research projects are derived from data contained in TORIS. Through the Multi-State Study, being conducted by Interstate Oil Compact Commission (IOCC) and the Geoscience Institute for Oil and Gas Recovery Research, funded by a grant from DOE, the existing TORIS data is being updated on a state-by-state basis. Data has been collected from 1979 reservoirs in 23 states, representing an original-oil-in-place total of 319.9 billion barrels. The collection effort is complete except for the southeast Gulf region (see Figures 1-3).

EOR Process and Operator Profile Data Collection – A substantial amount of information on enhanced oil recovery (EOR) processes and operator profiles was collected for use in the EOR and advanced secondary recovery (ASR) recovery potential analyses. EOR process data was obtained from the EOR project databases maintained by both DOE and by the Oil & Gas Journal. The data was reported on a field-by-field basis in each of the top 5 reservoir classes, and included the process, operator, start year, project status, and other information.

Petroleum Information Services provided detailed field-by-field information on operator profiles, including operator name, percentage of field production for each operator (for 1989 and from 1985 to 1989), number of producing wells for each operator, and field/reservoir annual production and well counts for the 1985-1989 period.

Technical Analysis

Multi-State Classification System – The TORIS data was analyzed to determine a new base-case, Lower-48, light oil recovery potential, and to assess the impacts of research and development, technology advances, oil prices, and the timing of abandonment on incremental recovery and economics. These results were reported by reservoir class.

The Original reservoir classification system was modified to one in which all TORIS reservoirs are classified by geologic characteristics. The classification was revised initially by the Geoscience Institute, and that version reviewed by an IOCC committee. The resulting system was then regrouped to reduce the number of geological classes in order to further focus the research and development programs. The reduction was accomplished by developing an indicator of reservoir heterogeneity derived from reservoir performance. Geologically similar reservoirs were given trial groupings, and statistical tests were applied to the heterogeneity indicators to evaluate the final 25 groupings, which are shown in Figure 4. The original and remaining oil in place and the number of reservoirs in each class are shown in Figure 5.

Oil Recovery Target Analysis – The 25 reservoir classes were analyzed for oil recovery potential using enhanced oil recovery (EOR) methods. Three levels of assessment were run: 1) near-term (1-5 years), oil at $20/bbl, with the existing level of technology; 2) mid-term (5-10 years), oil at $32/bbl, with advanced technology; and 3) long-term (beyond 10 years), the oil still remaining after mid-term recovery.

The completed EOR portion of the analysis indicates a total of 164 billion barrels of oil remaining in place in the analyzed TORIS reservoirs (Figure 6). In the near-term at $20/bbl, two-thirds of that total (over 100 billion barrels) is contained in the delta, dolomitized shelf and structured slope-basin reservoir classes, but well over half of those potential reserves are at risk of abandonment by 1995 (Figure 7). Nearly all of the near-term EOR recovery potential resides in the dolomitized shelf and unstructured delta classes; most of the delta potential is at risk of abandonment by 1995, but very little of the shelf total was projected to be at risk (Figures 8 and 9). For the mid-term, at $32/bbl, the bulk of the EOR recovery potential is contained in the delta, dolomitized shelf, structured slope-basin, and unstructured strandplain classes; significantly greater proportions of these potential reserves are projected to remain by 1995 (Figure 10 and 11).

A similar analysis for recovery potential using ASR and combined EOR and ASR methods is still in progress.

Reservoir Class Ranking And Selection Process

Using the data and analyses cited above, the Task Force is formulating criteria by which the various reservoir classes can be ranked and prioritized for implementation of recovery research projects. A considerable complex of interrelated data is being considered: remaining-oil-in-place, operator profile, recovery potential at various oil prices, risk of abandonment, the changing status of reservoirs from near-term to mid-term operation, and many other parameters.

Various members of the Task Force have suggested ranking schemes based on combinations of some or all of the above data. These suggestions are currently being evaluated and the actual ranking criteria will be developed by the end of 1990.

*Status of Supporting Data for Selection Criteria***

Criteria	% Complete
• Resource target	100
• Near- term recovery potential	50*
• Mid- term recovery potential	50*
• Urgency of R&D due to resource abandonment	50*
• Technology constraints	-
• Operator profile	100
• Geographic distribution	100
• Environmental consequences	-

* Pending completion of Advanced Secondary Recovery results
** Subject to quality control review

06M0670

Figure 1

Preliminary data subject to change.

Geographic Distribution of Reservoirs in the Multi-State Analysis

Region	States	Target Reservoirs
Southeastern Gulf	Alabama	1
	Arkansas	41
	Florida	4
	Louisiana	440
	Mississippi	76
Central	Kansas	78
	Montana[1]	78
	Nebraska	38
	North Dakota	49
	South Dakota	1
Eastern	Illinois	55
	Indiana	3
	Michigan	5
	Kentucky*	25
	Ohio*	8
	Pennsylvania*	6
	West Virginia*	27
Rocky Mountain	Colorado	63
	Montana[2]	20
	Utah	22
	Wyoming	161
Pacific	Alaska	8
	California	232
3-State Region	New Mexico	94
	Oklahoma	120
	Texas	869
	Total	2,528

[1] Williston Basin; [2] Exclusive of Williston Basin;
* Appalachian data coverage insufficient; study will determine feasibility of expanded data collection

06M0670

Figure 2

Preliminary data subject to change.

Status of Data Collection Effort

(Completed to Date)

Regions	# of States	# of Reservoirs	Total OOIP (Bil. Bbl)
IOCC Multi-State			
• S.E. Gulf Region	2*	125	6.5
• Other Regions	18	791	147.4
TORIS Three-State (Texas, Oklahoma, New Mexico)	3	1,063	166.0
Total All Regions	23	1,979	319.9

* Partially completed (22%)

Figure 3

Preliminary data subject to change.

Regrouped Geological Reservoir Classification System

Clastic Reservoirs

Depositional System	Structure
• Eolian	Structured Unstructured
• Alluvial Fan	All
• Fluvial	Structured Unstructured
• Delta	Structured Unstructured
• Strandplain • Strandplain - Other • Barrier Cores & Shorefaces	Structured Unstructured Unstructured
• Shelf • Shelf - Other • Sand Ridges	Structured Unstructured Unstructured
• Slope-Basin • Slope-Basin - Other • Turbidite Fans	Structured Unstructured Unstructured

Carbonate Reservoirs

Depositional System	Diagenesis
• Peritidal	Dolomitized Non-Dolomitized
• Shelf	Dolomitized (Evaporites) Dolomitized Non-Dolomitized
• Reefs • Reefs - Other • Atolls	Dolomitized Non-Dolomitized Non-Dolomitized
• Slope-Basin	All

Figure 4

Preliminary data subject to change.

Geologic Classification System for TORIS Light Oil Reservoirs

Oil Quantities by Geologic Class (MMBbl) Based on 1,824 Reservoirs

Class Title	OOIP	ROIP	Number of Reservoirs
Clastics:			
Delta Unstructured	44,270.8	28,383.5	369
Delta Structured	20,549.5	10,790.0	189
Slope-Basin Turbidite Fans - Unstructured	15,928.6	10,760.7	65
Slope-Basin Structured	12,437.2	8,607.2	20
Strandplain Barr. Cores-Shrface Unstruct.	11,183.5	6,672.8	135
Strandplain Structured	10,841.4	6,491.3	66
Slope-Basin Other Unstructured	7,467.0	6,257.2	49
Shelf Sand Ridges Unstructured	6,434.8	4,341.3	25
Shelf Other Unstructured	5,936.5	4,257.9	67
Strandplain Other Unstructured	4,446.1	2,981.0	74
Fluvial Unstructured	3,100.7	2,040.8	38
Shelf Structured	3,781.3	1,939.9	25
Eolian Structured	3,508.7	1,537.4	18
Eolian Unstructured	2,508.1	1,437.5	38
Alluvial Fan	1,202.4	880.5	18
Fluvial Structured	1,169.1	867.0	13
Clastic Totals	154,765.7	98,246.0	1,209
Carbonates:			
Shelf Dolomitized (Evaporites)	40,485.6	25,303.8	134
Shelf Dolomitized	23,676.8	15,158.8	110
Shelf Non-Dolomitized	8,351.0	6,286.2	69
Peritidal Dolomitized	8,360.4	5,887.8	98
Reefs Other Non-Dolomitized	5,950.4	4,360.0	34
Peritidal Non-Dolomitized	5,888.4	3,752.0	73
Reefs Atolls Non-Dolomitized	5,695.1	2,765.5	45
Reefs Dolomitized	2,412.7	1,449.6	30
Slope-Basin	1,825.0	971.3	22
Carbonate Totals	102,645.2	65,935.1	615
Light Oil Totals	257,411.0	164,181.1	1,824
Heavy Oil Totals	37,830.9	26,329.3	122
Unclassified Reservoirs	2,699.1	1,709.5	32
Prudhoe Bay	22,000.0	12,320.0	1
Grand Totals	319,941.0	204,539.9	1,979

Figure 5

Preliminary data subject to change.

Geological Classes Ranked by Remaining Oil in Place
Light Oil Reservoirs in TORIS

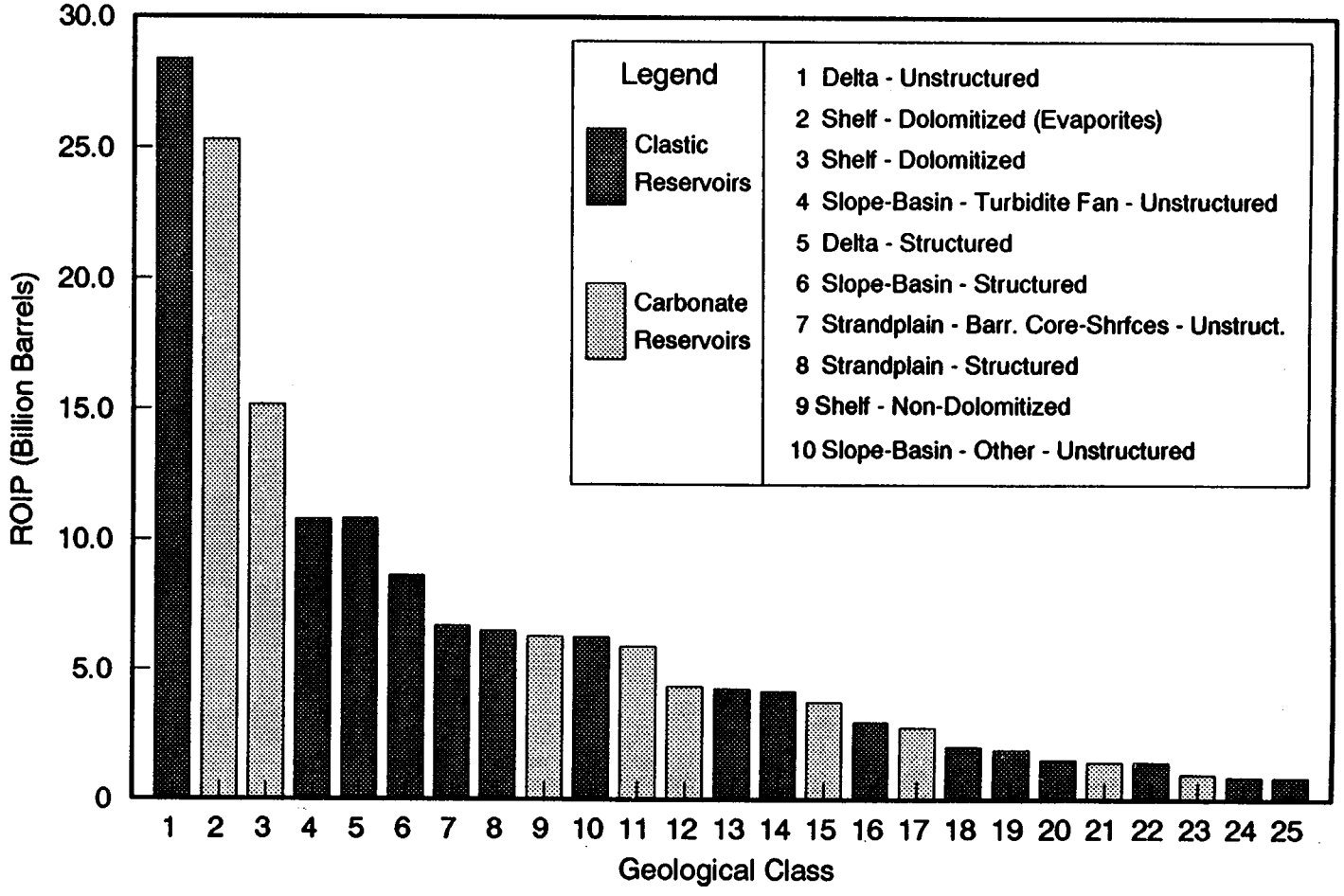

Figure 6

Preliminary data subject to change.

Projected Status of Remaining Oil in Place

Light Oil Reservoirs in TORIS

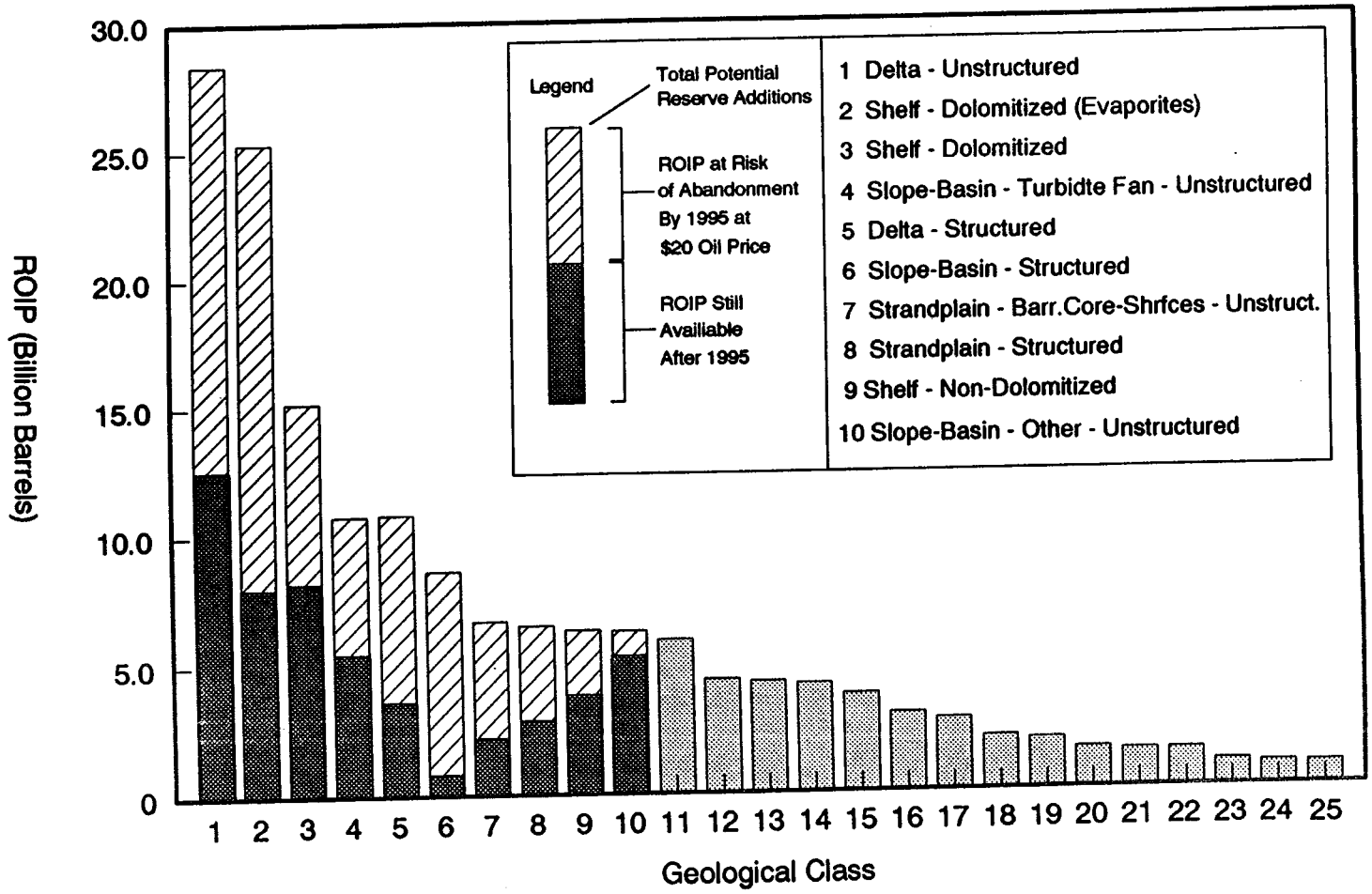

Figure 7

Preliminary data subject to change.

Near-Term EOR Potential By Geological Class for Light Oil Reservoirs in TORIS

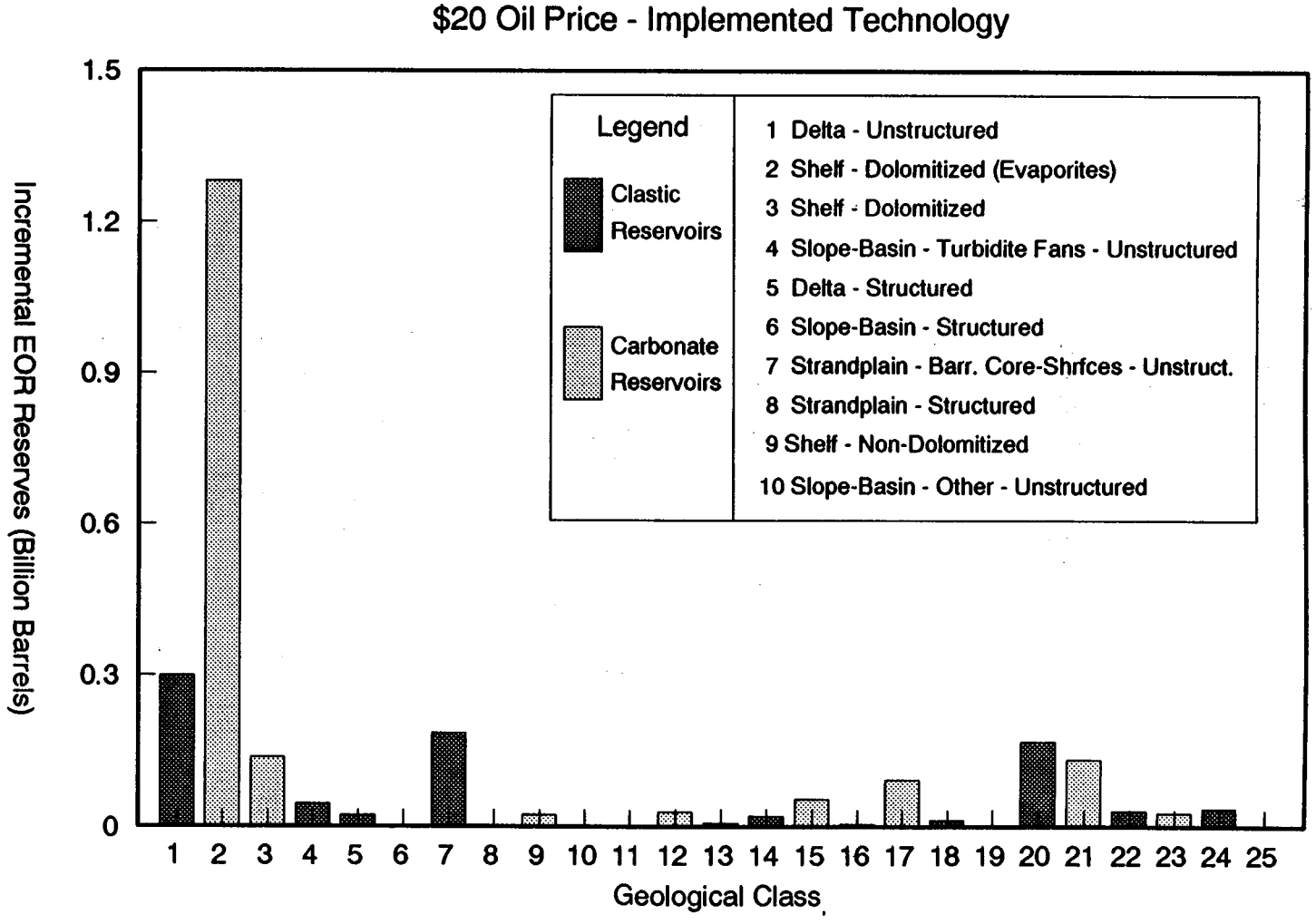

Figure 8

Preliminary data subject to change.

Near-Term Projected Status of EOR Reserves
Light Oil Reservoirs in TORIS

$20 Oil Price - Implemented Technology

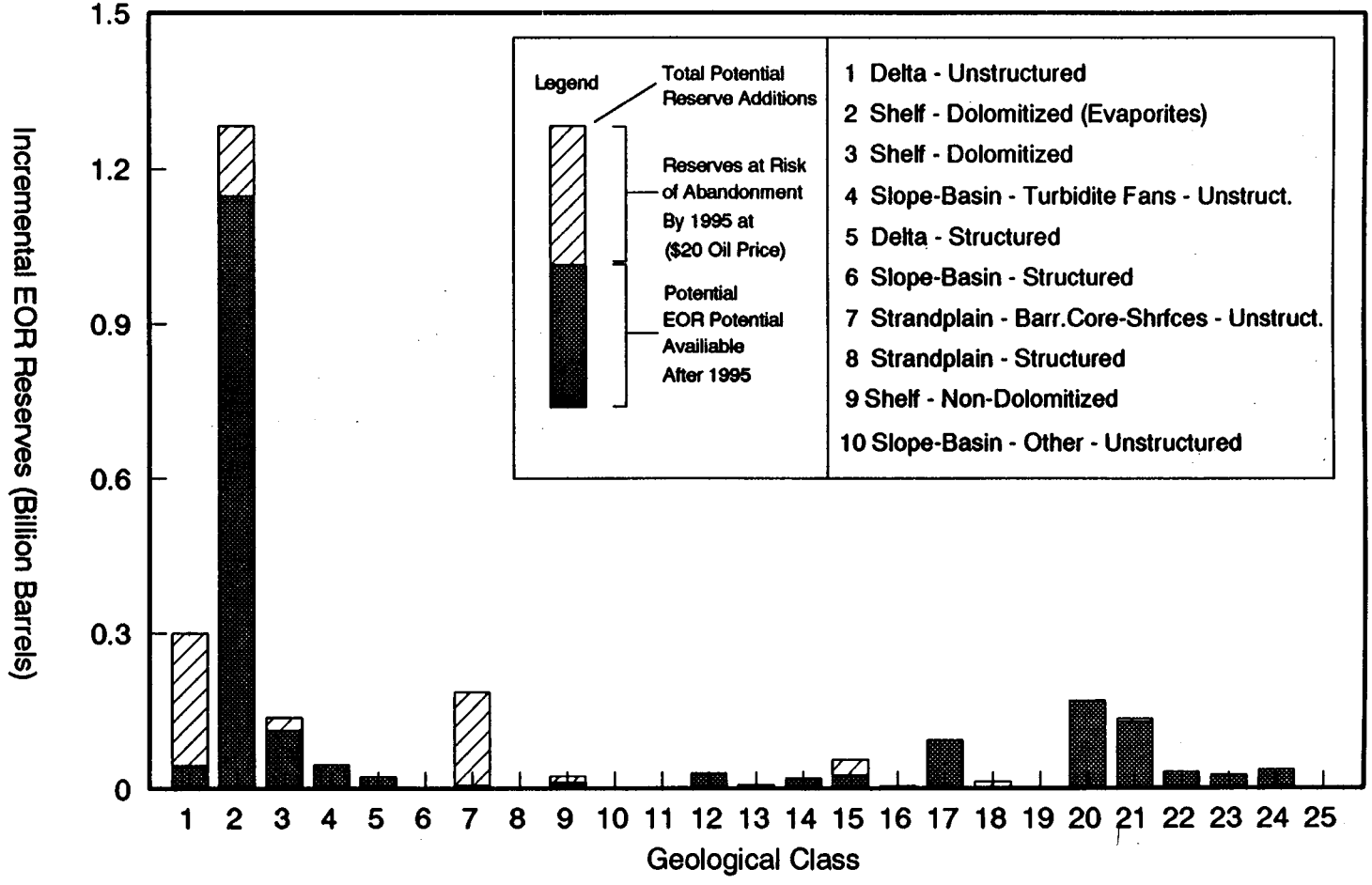

Figure 9

Preliminary data subject to change.

Mid-Term EOR Potential By Geological Class for Light Oil Reservoirs in TORIS

$32 Oil Price - Advanced Technology

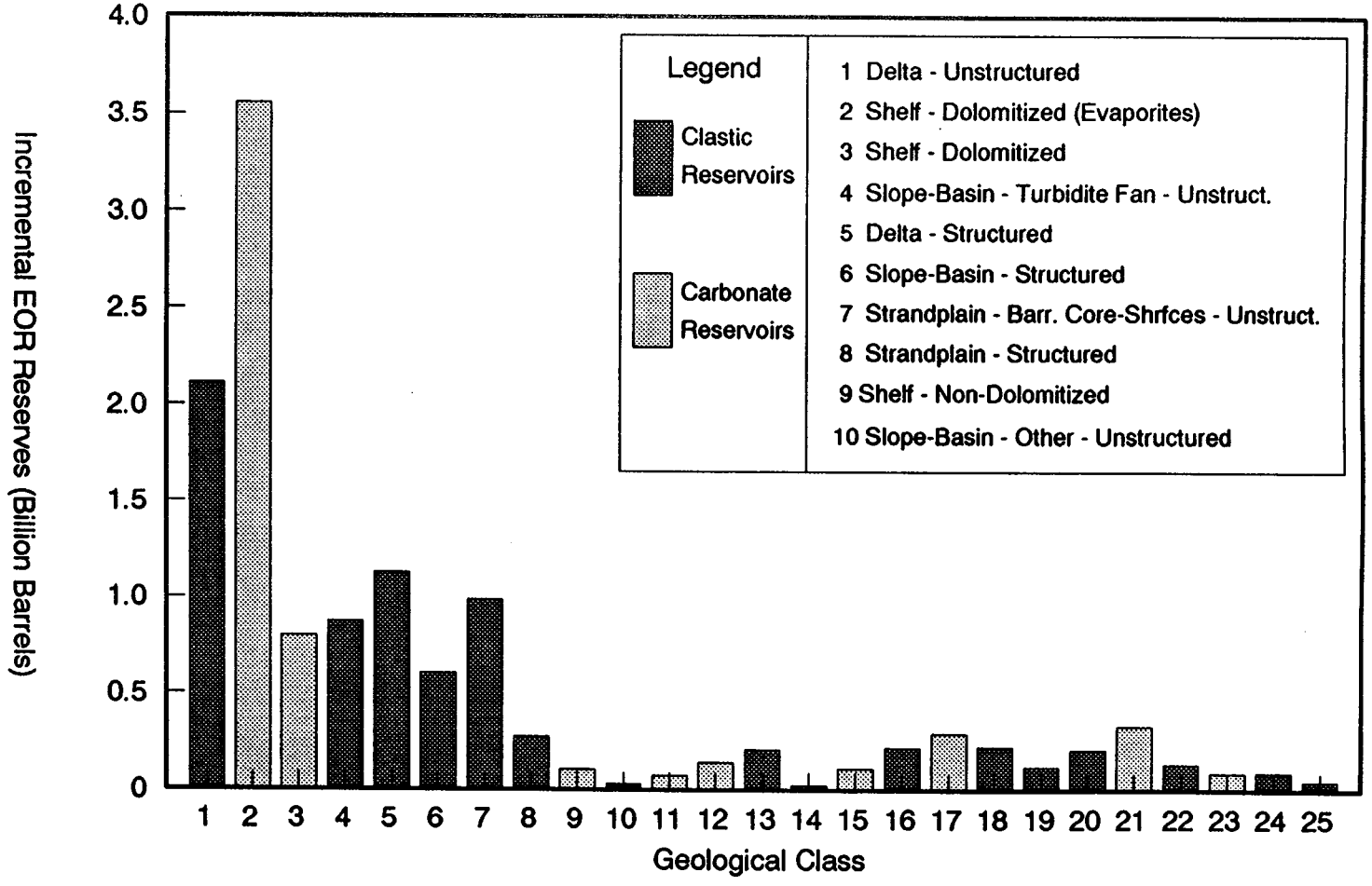

Figure 10

Preliminary data subject to change.

Mid-Term Projected Status of EOR Reserves
Light Oil Reservoirs in TORIS

$32 Oil Price - Advanced Technology

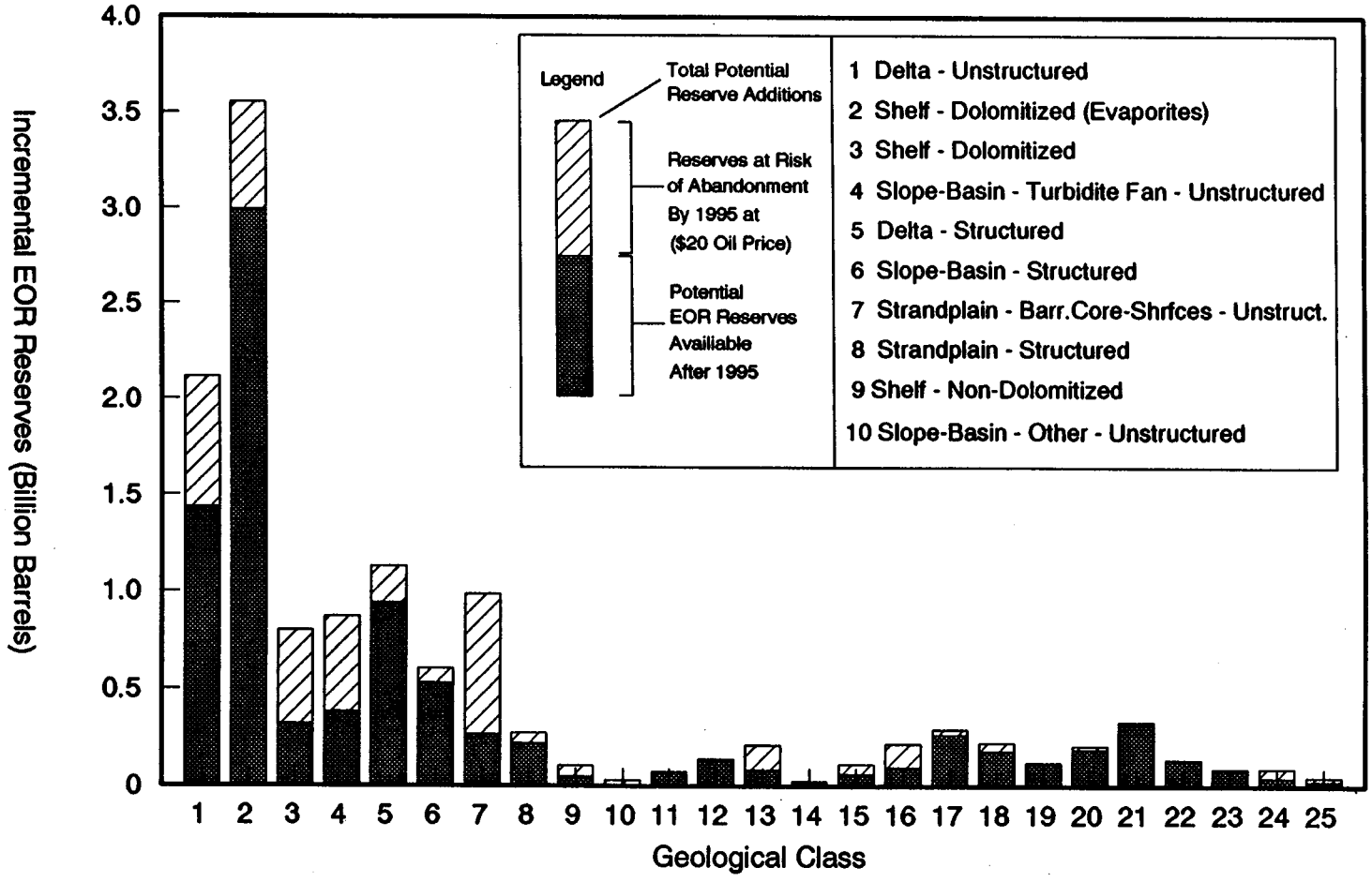

Figure 11

Preliminary data subject to change.

FIELD RESEARCH, DEVELOPMENT AND DEMONSTRATION

Reservoir Class I Manager:
Edith Allison
Bartlesville Project Office

Reservoir Class II Manager:
E. B. Nuckols
Metairie Site Office

Reporting Period: September-November 1990

Objectives

The Field Research, Development and Demonstration (RD&D) effort will contribute to the Oil Implementation Plan objectives by: 1) selecting for study several classes of reservoirs, each of which has a common geologic history; 2) soliciting industry and other public input regarding technical constraints to improved production and mechanisms for overcoming those constraints for each class of reservoirs; 3) implementing near-term demonstrations of conventional technology that will assist operators in maintaining production and preventing abandonment of oil resources; 4) conducting research to better characterize the reservoirs in the class, and 5) implementing field demonstrations of advanced technology to overcome the reservoir constraints identified in the characterization research.

Summary of Progress

Selection of Reservoir Classes

The formal selection process for the first two reservoir classes is under way. Final selections will be made after the Task Force completes evaluation of available Tertiary Oil Recovery Information System (TORIS) data on the volume of the resource and the risk of abandonment for the reservoir classes, as well as information on geographic distribution of the reservoirs and technological uncertainty of potential recovery techniques.

The Class Managers, assisted by George Stosur, Enhanced Oil Recovery Program Manager, contacted industry, university, service company and National Laboratory scientists to obtain comment and opinion on the potential of high-priority reservoir types for improved production, the expected obstacles to achieving improved production, and the technologies most appropriate to understanding the reservoirs. The Class Managers also evaluated the interest of various industry, service and research segments in working cooperatively with DOE on field studies.

Reservoir Selection, Research and Public Meeting Activities

A management plan and schedule have been developed for activities leading to: 1) technical symposia and public meetings for discussion of the first two reservoir classes, 2) publication of a reference text on engineering and geologic characteristics of the reservoirs and potentials for improved recovery, and 3) preparation and release of competitive solicitations for research keyed to specific reservoir classes.

A preliminary selection for Class 1 has been made. Unstructured deltaic reservoirs were chosen on the basis of having a large potential for recoverable oil and high risk of abandonment. Reservoirs of this class are widespread in the U.S., occurring predominantly in the Appalachian basin (W. Virginia, Ohio, Kentucky and Pennsylvania), Illinois basin (Illinois and Indiana), Denver-Julesburg basin (Colorado and Nebraska), Green River basin (Wyoming), Anadarko basin (Oklahoma, Kansas, Texas Panhandle, and Colorado), Mississippi salt basin (Mississippi), and North Central Texas Strawn sands.

These reservoirs are characterized by lack of continuity of productive flow units, which results in low recovery efficiency, leaving a large volume of mobile oil (the target for geologically targeted infill drilling and waterflooding) as well as immobile oil (a chemical flooding target).

A Technical Symposium, to be held in Dallas on January 29 and 30, 1991, will provide an overview of constraints and near-term and mid-term technological advances affecting the producibility of oil resources in the unstructured deltaic formations. The symposium will provide an opportunity for operators and other technical personnel to share information about their problems and technical experiences working in deltaic reservoirs. (Information regarding details of this symposium is included at the end of this report.)

December 14, 1990

Dear Colleague:

On behalf of the Department of Energy, I would like to extend an invitation to attend and participate in a Symposium on "Opportunities to Improve Oil Productivity in Unstructured Deltaic Reservoirs." The symposium, to be hosted by Assistant Secretary of Energy for Fossil Energy Robert H. Gentile, will be held on January 29 - 30, 1991 at the Hyatt Regency DFW (East Tower) in Dallas, Texas.

This invitation is being extended to technical personnel and managers in companies operating in U.S. fields with unstructured deltaic formations. ("Unstructured deltas" can be defined as deltaic reservoirs in which production is not severely constrained by structural compartmentalization.) Unstructured deltaic formations have been identified by DOE as the reservoir class with the largest known remaining oil resource in the Lower-48 states and with the greatest urgency relative to abandonment. We encourage the attendance and participation of appropriate geological and engineering E&P personnel.

The purpose of the symposium is to provide an opportunity for oil producers, service companies, reservoir characterization experts, and other technical managers to share information regarding problems encountered in deltaic reservoirs, approaches to resolving them, and the potential of current or future technologies to address them. As shown in the attached preliminary symposium program, we have already identified a number of problems and related technologies and invited a variety of technical experts to discuss them. The symposium has been designed to allow for interactive exchange of problems and solutions. Operators will benefit from the sharing of concerns, problems, and ideas. The Department of Energy will also benefit from the symposium by gaining insight to operators' perspectives on problems and solutions in unstructured deltaic reservoirs.

If you wish to attend, please complete and return the registration card enclosed in the preliminary program by January 14, 1990. Advance registration is strongly recommended. We will send you additional information after receipt of your registration. Also, if there are others in your firm who you think should attend, please feel free to copy and distribute this invitation to them.

We appreciate your interest in this symposium and look forward to seeing you in Dallas. Please feel free to call us at the numbers in the program if you need additional information.

Sincerely,

Edith C. Allison
Reservoir Class 1 Manager

Enclosures

A Symposium On

Opportunities to Improve Oil Productivity in Unstructured Deltaic Reservoirs

January 29-30, 1991

Hyatt Regency DFW
East Tower
Dallas-Fort Worth International Airport
Dallas, Texas

Sponsored By
U.S. Department of Energy
Office of Fossil Energy

The purpose of this symposium is to provide an overview of technical constraints and advances affecting the producibility of oil resources from unstructured deltaic formations in U.S. reservoirs. The symposium should be attended by key reservoir engineers and geological staff of firms operating in reservoirs with unstructured deltaic formations. The symposium offers an opportunity for operators and technical personnel to share their experiences and constraints in deltaic reservoirs. The symposium is offered free of charge to participants.

Symposium Information

Who Should Attend

The symposium is intended for senior reservoir engineers and geologists, technical managers, independent operators, and other appropriate personnel working in deltaic reservoirs. Attendance of multiple personnel from companies who may have differing experience in different field and reservoir settings is encouraged. Please feel free to distribute copies of this notice to other appropriate personnel.

Symposium Registration

Please complete the attached registration card and return it to Ms. Carolyn Klym, U.S. Department of Energy, Office of Fossil Energy, FE-30, Room D-109, Germantown, Maryland 20585. Registrations should be received **no later than January 14, 1991.** On-site registration will be available beginning at 9:00 AM on Tuesday, January 29. About ten days before the meeting, advance registrants will receive a packet of additional information discussing general characteristics of deltaic reservoirs and other important information. (If you are unable to attend, but wish to receive the technical packet, please check the appropriate box on the reply card.)

Location

The meeting will be held in the Hyatt Regency-DFW Hotel, East Tower, a full service hotel located at the Dallas/Fort Worth International Airport.

Accommodations

A block of rooms has been reserved until January 14, 1991. **Please call the hotel directly at 1-800-233-1234 for reservations** and mention the "DOE Unstructured Deltaic Reservoirs Symposium."

Proceedings

A complete set of symposium proceedings will be published after the meeting and distributed to all meeting participants. Persons not attending may request proceedings by returning the enclosed card.

Additional Information

Questions regarding registration may be addressed to Ms. Carolyn Klym or Ms. Linda Simons at (301) 353-2430. Other questions related to the program or other technical aspects of the symposium should be addressed to Ms. Edith Allison at (918) 337-4390 or Mr. E.B. Nuckols at (504) 734-4806.

About the DOE Oil Research Program

In 1988, Congress directed DOE's Office of Fossil Energy to create, as part of a Hydrocarbon Geoscience Research Strategy, a plan to refocus oil research programs with a specific goal of increasing domestic oil production.

The *Oil Research Program Implementation Plan* lays out a clear path for structuring research programs to focus on critical problems limiting the producibility of known remaining oil resources in specific classes of reservoirs. The plan calls for addressing identified research needs on a prioritized basis, determined by the resource potential and timing of abandonment of reservoirs in each class.

Through focused near-term, mid-term, and long-term research, development, and demonstration (RD&D) efforts, the program seeks to stimulate application of existing technologies to retain access to reservoirs, complete development and promote application of technologies currently in the R&D phase, and, through improved understanding of the problems of the nation's priority reservoir classes, to design new R&D efforts that will result in technologies, processes, and products to resolve them.

To begin implementation of the new plan, the Department has appointed a task force that marshals the technical resources of the Enhanced Oil Recovery program, the Office of Geoscience Research, and complementary Fossil Energy R&D programs. The task force is also drawing on expertise from the university research community, the producing and service industries, and other experts to accomplish the plan's goals of technology development, improved economics, environmental protection, and technology transfer and application.

Throughout the process, the task force will strive to enhance technology transfer efforts, encourage demonstrations, and solicit external industry, academic, state, and private sector participation.

This symposium will offer the opportunity for an exchange of ideas about problems and potential solutions in unstructured deltas. Unstructured deltaic reservoirs have been selected as the first area of focus on the basis of the known remaining oil in place and the timing of resource abandonment. The Department of Energy appreciates your interest and participation in this important work.

Symposium Program -- Tuesday, January 29, 1991

9:00 On-Site Registration

Introductory Session

This session will briefly explain the Department of Energy's refocused light oil RD&D plan and describe the characteristics of unstructured deltaic reservoirs (reservoirs in which production is not severely constrained by structural compartmentalization). This will provide the context for the technical sessions.

10:00 **Introductions**
Edith C. Allison, Reservoir Class 1 Manager, DOE Bartlesville Project Office

DOE's R&D Approach: Focusing on Problems Encountered in Specific Reservoir Classes
Robert H. Gentile, Assistant Secretary for Fossil Energy, U.S. Department of Energy

DOE's Oil R&D Plan and Objectives of the Symposium
Edith C. Allison, Reservoir Class 1 Manager, DOE Bartlesville Project Office

Reservoir Classification System and Selection Methodology
R. Michael Ray, Deputy Director, DOE Bartlesville Project Office

Geologic and Engineering Characteristics of Deltaic Reservoirs
E.B. Nuckols, Reservoir Class 2 Manager, DOE Metairie (La.) Site Office

10:45 **Discussion Period**

11:30 **Lunch** (A no-host, a la carte buffet will be available to attendees in the Hyatt Regency DFW)

Technical Session 1: Reservoir Characterization in Deltaic Reservoirs

The session will address critical technologies necessary to improve the description, analysis, and prediction of reservoir properties affecting oil productivity in deltaic reservoirs. Participants will explore the potential for these technologies to enhance productivity in the near-term and mid-term. The session will highlight potential constraints to implementing these technologies. Five experts will briefly discuss relevant aspects. Each presentation will be followed by a 10-15 minute question period. A discussion period will conclude the session.

1:00 **Reservoir Characterization of the Illinois Basin Including Deltaic Sands**
Donald F. Oltz, Oil and Gas Section Head, Illinois State Geological Survey

Seismic Applications to Reservoir Characterization
James H. Justice, Research Scientist, Mobil Oil Corporation

Petrophysical Evaluation of Deltaic Reservoirs
Steve Crary, Interpretive Development Staff Engineer, Schlumberger Well Services

COFFEE BREAK (15 minutes)

Reservoir Modeling: Advanced Reservoir Simulation -- Experience in the Big Muddy Field, Wyoming
Gary Pope, Director, Center for Petroleum and Geosystems Engineering, University of Texas

Variability in Deltaic Reservoir Heterogeneity: Implications for Mobile and Residual Oil Recovery
Robert J. Finley, Associate Director and Noel Tyler, Program Director, Texas Bureau of Economic Geology

4:00 **Discussion Period** -- Problems and experience with characterization of unstructured deltaic reservoirs

5:00 **Adjournment**

Symposium Program -- Wednesday, January 30, 1991

Technical Session 2 -- Extraction Technologies

This session will address the application of advanced extraction technologies to improve oil productivity, including broader application of conventional technologies in the near term and demonstration of advanced technologies that have been tested and could be effective in the mid-term. The session will also consider constraints to implementing these technologies. The session will follow the same format as Technical Session 1.

8:00 **Drilling Technology: Advances in Directional Drilling**
William Maurer, President, Maurer Engineering

An Analysis of Infill Drilling in the Hugoton Gas Field
Riley Needham, Manager of Production Technology, Phillips Petroleum Company

Review of Surfactant Flooding in the Illinois Basin -- Robinson Sand
Ron Smith, Manager, Petroleum Recovery Technology, Marathon Oil Company

Completion Engineering -- Where We Are Today/Needs for the Future
Gerald Coulter, Division Completion Engineer, Oryx Energy Company

COFFEE BREAK (15 minutes)

Completion/Maintenance Technologies: Organic Formation Damage
Kenneth M. Barker, Research Fellow, Petrolite Inc.

11:00 **Discussion Period** -- Extraction Technologies

NOON **Lunch** (A no-host, a la carte buffet will be available to attendees in the Hyatt Regency DFW)

Technical Session 3 -- Operational Constraints

This session will focus on the environmental and regulatory constraints to increased production in deltaic reservoirs and R&D requirements to address them. The session will consist of speaker presentations and questions and answers for speakers and moderators.

1:00 **Lessons Learned at Loudon Surfactant Pilots**
Edward D. Holstein, Reservoir Engineering Coordinator, Exxon Company, U.S.A.

Economic and Regulatory Constraints
James Russell, President, Russell Petroleum

Environmental Constraints
Cheryl Stark, Manager, Environmental Affairs, Milpark Drilling Fluids Company

Data Availability
Philip Stark, Vice President of Technical Marketing, Petroleum Information Corporation

2:30 **Discussion Period** -- Environmental and Economic Constraints

3:45 **Wrap-Up Comments and Questions**

4:00 **Symposium Adjourned**

RESEARCH SUPPORT – CHARACTERIZATION OF CLASS 1 RESERVOIRS

Project Leader:
Susan Jackson
National Institute for Petroleum and Energy Research (NIPER)

Reporting Period: September-November 1990

Objectives

The objective of this project is to summarize the generally available knowledge about the geological and production characteristics of Class 1, clastic deltaic system reservoirs, and to determine in what areas further investigation would have the greatest potential for preserving economic access to the oil resource.

Summary of Progress

Histograms and cross-plots of parameters contained in TORIS are being used to determine the degree of variability of petrophysical and production characteristics with the Class 1 reservoirs and the similarities and differences among the plays selected for study. A "first look" at the reservoir characteristics indicates a wide range of values for many of the parameters; however, correlation of primary recovery to well spacing, permeability, Dykstra-Parsons coefficient, and oil gravity are evident.

Five plays were selected as a sample to determine characteristics of deltaic reservoirs. Selection was based on geographic distribution, delta type, and availability of data:

- Cherokee sands – primarily fluvial-dominated deltaic deposits in Oklahoma and Kansas.
- Dakota Formation, including the D sand and J sand – mixed wave- and fluvial-dominated deltaic deposits in Colorado and Nebraska.
- Frontier Formation – undifferentiated deltaic deposits in Wyoming.
- Strawn Formation – primarily fluvial-dominated deltaic deposits in Texas.
- Wilcox Formation – mixed but predominantly fluvial-dominated deltaic deposits in Texas, Louisiana and Mississippi.

DOE cost-shared EOR projects provide abundant data and are being used insofar as possible in the study. Collation of information on three of these projects (Burbank Field, producing from the Cherokee sand; Big Muddy Field, producing from the Frontier Formation; and Main Consolidated Field, producing from the Robinson sand) is nearly complete. Data collection from other reservoirs is currently under way.

SECTION II

Enhanced Oil Recovery Progress Reviews

U.S. Department of Energy
Washington, D.C. 20545

ROBERT H. GENTILE
Assistant Secretary
for Fossil Energy
Room 4G-084 Forrestal Building
Telephone Number (202) 586-4695

MARVIN SINGER
Deputy Assistant Secretary for Oil,
Gas, Shale, and Special
Technologies

JAMES D. BATCHELOR
Director for Oil, Gas,
and Shale Technology

ARTHUR HARTSTEIN
Deputy Director of Oil, Gas,
and Shale Technology

J. J. STOSUR
Enhanced Oil Recovery Program Manager
Mail Stop D-116, Germantown
Telephone Number (301) 353-2749

Bartlesville Project Office
P.O. Box 1398
Bartlesville, Oklahoma 74005
Telephone No. 918/337-4401

THOMAS C. WESSON
Director

R. M. RAY
Deputy Director

FRED W. BURTCH
Program Coordinator,
Enhanced Oil Recovery

HERBERT A. TIEDEMANN
Project Manager for
Technology Transfer

DOE/BC-90/2
(DE90000262)
Distribution Category UC-122

PROGRESS REVIEW NO. 62

CONTRACTS FOR FIELD PROJECTS AND SUPPORTING RESEARCH ON ENHANCED OIL RECOVERY

Date Published - December 1990

UNITED STATES DEPARTMENT OF ENERGY

PUBLICATIONS LIST

Bartlesville Project Office

Thomas C. Wesson, *Director*

AVAILABILITY OF PUBLICATIONS

The Department of Energy makes the results of all DOE-funded research and development efforts available to DOE and DOE contractors from the **Office of Scientific and Technical Information, P.O. Box 62, Oak Ridge, TN 37831; prices available from (615) 576-8401, FTS 626-8401.**

Available to the public from the **National Technical Information Service, U.S. Department of Commerce, 5285 Port Royal Road, Springfield, VA 22161; prices available from (703) 487-4650.**

Give the full title of the report and the report number.

Sometimes there are slight delays between the time reports are shipped to NTIS and the time it takes for NTIS to process the reports and make them available. Accordingly, if NTIS advises you that a specific report is not yet available, we will provide one copy of any individual report as long as our limited supply lasts. Please help us in our effort to eliminate wasteful spending on government publications by requesting only those publications needed. Order by the report number listed at the beginning of each citation and enclose a self-addressed mailing label. Available from **DOE Bartlesville Project Office, ATTN: Herbert A. Tiedemann, P.O. Box 1398, Bartlesville, OK 74005; (918) 337-4293.**

Quarterly Reports

DOE/BC–89/3 **Contracts for Field Projects and Supporting Research on Enhanced Oil Recovery. Progress Review No. 59. Quarter ending June 30, 1989. May 1990. Order No. DE90000206.** Status reports are given for various enhanced oil recovery and gas recovery projects sponsored by the Department of Energy. The field tests and supporting research on enhanced oil recovery include chemical flooding, gas displacement, thermal/heavy oil, resource assessment, geoscience technology, microbial technology, novel technology, and environmental technology.

Chemical Flooding

DOE/BC/10841–15 **Modeling and Optimizing Surfactant Structure to Improve Oil Recovery by Chemical Flooding at the University of Texas – Final Report. The University of Texas. April 1990. 120 pp. DE90000230.** Adsorption of surfactant from aqueous solutions is a complex function of a relatively large set of variables including the solution pH, electrolyte composition, temperature, and surfactant concentration as well as the surface characteristics of the mineral and surfactant molecular structure. Because of this complexity, an accurate model to tie the variables together is essential. This made the development of an adsorption theory foremost to this project. A model surface, titanium dioxide, was selected for the initial studies. A particular sample of TiO_2 was studied extensively (surface titration, ESCA, electrophoretic mobility, and electronmicroscopy) and was used as a model system for comparison with predictions. The parameters describing naturally occurring minerals (clays, silica, etc..) were incorporated into the theory once the titanium dioxide system was adequately modeled.

DOE/BC/10842–10 **Flow in Porous Media, Phase Behavior and Ultralow Interfacial Tensions: Mechanisms of Enhanced Petroleum Recovery. Second Annual Report for the Period October 1, 1986 to September 30, 1987. University of Minnesota. May 1990. 232 pp. Order No. DE90000238.** This report summarizes the results of research performed during the fiscal year. The goals of this program are to develop ideas, instruments, techniques, data, and skills needed to elucidate the basic mechanisms of phase behavior and ultralow interfacial tensions. The emphasis of the research program is on understanding basic physical and chemical mechanisms with the goal of transforming this knowledge into the concepts and mathematical formulations needed for engineering process design and analysis. The research progress is described in detail in subsequent sections of the report.

DOE/BC/10842–15 **Flow in Porous Media, Phase Behavior and Ultralow Interfacial Tensions: Mechanisms of Enhanced Petroleum Recovery. Third Annual Report for the Period October 1, 1987 to September 30, 1988. University of Minnesota. May 1990. Order No. DE90000239.** This report summarizes the results of research performed during the fiscal year. The goals of this program are to develop ideas, instruments, techniques, data, and skills needed to elucidate the basic mechanisms of phase behavior and ultralow interfacial tensions. The emphasis of the research program is on understanding basic physical and chemical mechanisms with the goal of transforming this knowledge into the concepts and mathematical formulations needed for engineering process design and analysis. The research progress is reported in detail.

DOE/BC/10844–20 **Polymers for Mobility Control in Enhanced Oil Recovery. Final Report. University of Southern Mississippi. June 1990. 124 pp. Order No. DE90000243.** This report summarizes the work performed during FY 1989 which focused on the preparation, characterization and rheological study of copolymers possessing intra- or intermolecular associations. Associative copolymers of acrylamide with N-alkylacrylamides; terpolymers of acrylamide, N-decylacrylamide, and NaAMPS, NaA, or NaAMB; and copolymers of acrylamide with the zwitterionic AMPDAPS monomer have been shown to possess rheological behavior of potential in EOR processes. The salt-induced conformational responses and resulting association mechanisms are being studied by a number of techniques including rheometry, gel permeation chromatography, quasielastic light scattering, and fluorescence spectroscopy.

Carbon Dioxide Flooding

DOE/FE/61114–2 **Development of Effective Gas Solvents Including Carbon Dioxide for the Improved Recovery of West Sak Oil. Final Report. University of Alaska Fairbanks. June 1990. 324 pp. Order No. DE90000241.** The West Sak reservoir located on the North Slope of Alaska is estimated to contain up to 25 billion barrels of heavy oil in place and represents the largest known heavy oil accumulation in the United States. The absence of natural drive mechanism in this reservoir makes it a target for enhanced oil recovery processes. The research undertaken in this project pertains to study of thermal and miscible processes for the recovery of West Sak crude. This report provides a description of the West Sak reservoir along with the petrophysical properties of various sand members based on the analysis of well log data; experimentally measured fluid properties (PVT) of West Sak crude and phase behavior of CO_2-West Sak crude mixtures; slim tube experiments, asphaltene precipitation tests and equation of state predictions (in presence and absence of aqueous phase) conducted to study applicability of miscible flooding with enriched hydrocarbon gas solvents and carbon dioxide.

Thermal Recovery

DOE/BC/14126–18 **A Comparison of Relative Permeability from Centrifuging Versus Coreflooding. SUPRI TR 72. Stanford University. May 1990. 184 pp. Order No. DE90000234.** Relative permeability and capillary pressure data from both

centrifuge and coreflooding experiments on the same Berea sandstone will be analyzed using both analytical and simulation techniques. A linear two phase simulation model of fluid displacement from a core will be built. Capillary, gravity, and viscous effects will be included.

DOE/BC/14126–19 **Characterization of Steam Foam Surfactants Through One-Dimensional Sandpack Experiments. SUPRI TR 73. Stanford University. May 1990. 176 pp. Order No. DE90000235.** The efficiency of a steamflood may be increased by the use of surfactants that spontaneously generate steam foam when injected into an oil reservoir. Ideally, the foam preferentially forms in high permeability streaks and oil depleted regions of the reservoir through which the steam would otherwise channel. The foam diverts the steam through regions previously uncontacted by the injected steam. This report describes an experimental program conducted to study the foam-forming characteristics of a range of different surfactants. Both commerically available and experimental surfactants were tested in a one-dimensional sandpack under controlled conditions of pressures and temperatures similar to those encountered in California oil fields. Steam and nitrogen were continuously injected into the sandpack which contained neither clay nor oil. The surfactant solutions were injected in discrete slugs of finite duration allowing transient phenomena such as the persistence of the foam to be studied. Under the conditions of the experiment, long-chain alpha olefin sulphonate surfactants were found to generate the strongest foams. Internal olefin sulphonates, linear toluene sulphonates and linear xylene sulphonate surfactants generated just as strong foams but only at successively high concentrations. It was found that the strength of the foam produced by a surfactant of a particular chemical structure increased with increasing alkyl chain length. The novel use of heat flux sensors attached to the outside of the sandpack allowed a better understanding of the heat transfer mechanisms operating within the system. Such an understanding is necessary if the experimental observations are to be interpreted correctly.

DOE/BC/14126–21 **A Semianalytical Model for Linear Steam Drive. SUPRI TR 75. Stanford University. May 1990. 168 pp. Order No. DE90000237.** A semianalytical model (SAM) has been developed for one-dimensional linear systems and two-dimensional linear cross-sectional systems. Wells are located at both systems and two-dimensional linear cross-sectional systems. Wells are located at both ends of the reservoir. At the injection well, wet steam is injected at a constant rate and enthalpy. The production well produces at a constant flowing bottomhole pressure. The SAM includes formation dip, compressible formation, water, and oil, and thermal expansion of the formation, water, and oil. The model automatically calculates the steam zone steam saturation and includes the water front and overburden heat losses. The two-dimensional model also includes gravity override of steam.

DOE/BC/14126–23 **Modification of Buckley-Leverett and JBN Methods for Power-Law Fluids. Topical Report. University of Southern California. May 1990. 26 pp. Order No. DE90000240.** Injection of non-Newtonian fluids for mobility control is a standard operation in oil recovery. While the description of the fluid rheology during the simultaneous flow of two immiscible phases is in general complicated, significant progress is possible when one of the fluids is of the power-law type. In the latter case the standard methods for flow description and analysis of experimental data must be modified. This paper presents such an approach for one-dimensional immiscible displacement. Considered in this report are the application of the Buckley-Leverett method and the modification of the JBN technique for measurement of relative permeabilities. The effects of rate and fluid rheology on the displacement features are investigated. It is shown that substantial errors may arise by the direct use of the original JBN method in interpreting unsteady-state experiments. A general modification of the technique is also proposed.

DOE/BC/14126–24 **Steady-State, Vapor-Liquid Concurrent Flow: Relative Permeabilities and End Effects. Topical Report. University of Southern California. June 1990. 48 pp. Order No. DE90000242.** This paper presents a systematic study of the saturation and temperature distributions in steady-state, vapor-liquid flows and examines the sensitivity to parameters such as injection rate, permeability and core length. Two sets are analyzed, one pertaining to the simultaneous injection of a two-phase mixture and another involving phase change (liquid to vapor) within the core. End effects and, in general, effects associated with capillary heterogeneity are analyzed in detail.

Microbial Enhanced Oil Recovery

BNL 43788 **Effects of Selected Thermophilic Microorganisms on Crude Oils at Elevated Temperatures and Pressures. 1989 Annual Report. Brookhaven National Laboratory. May 1990. 44 pp. Order No. DE90000233.** Work performed on this project shows that microbial enhanced oil recovery (MEOR) is promising and the biotechnology resulting from this work may be transferable. Systematic studies are being done that deal with the effects of thermophilic bacteria on the chemical and physical properties of selected types of crude oils at elevated temperatures and pressures comparable to those of reservoir conditions. Current studies indicate that during the biotreatment several properties of crude oils are affected. The oils are (1) emulsified, (2) acidified, (3) there is a qualitative and quantitative change in light and heavy fractions of the crudes, (4) there are chemical changes in fractions containing sulfur compounds, and (5) the qualitative and quantitative chemical and physical changes appear to be microbial species dependent. In order to analyze for these changes in the crudes, several instruments have been purchased and dedicated to this program. The results generated in the past fiscal year describing (1) through (5) are discussed in this report.

Geoscience Technology

NIPER–448 **Fluid Flow Behavior Through Rock-Slab Micromodels in Relation to Other Micromodels. Topical Report. National Institute for Petroleum and Energy Research. June 1990. 32 pp. Order No. DE90000244.** A new technique was developed to visualize fluid movement and rock-fluid interaction in the pores of reservoir rocks. It consists of fabricating micromodels containing rock slabs of 3 millimeter thickness and using sensitive image acquisition, recording, and enhancement systems to perform time-and-motion analyses of high-speed events. Displacement experiments were performed using these rock-slab micromodels and two other types of micromodels: an etched-glass network model (HEG) and a chemically consolidated grain-packed (cryolite) model. The tests included several cycles of imbibition and drainage. Comprehensive steady-state tests were also performed in the two simplified (HEG and cryolite) models, which included two-phase and three-phase flows with gas/water, oil/water, and gas/oil/water systems. The results were compared to understand the scope and limitations of these micromodel techniques. The observations are summarized as: (1) behaviors in the simplified models were very sensitive to operating conditions; (2) end effects and fluid redistributions were not evident; and (3) many observations differed from those with the rock-slab micromodel. Another important feature of the rock-slab micromodel was the absence of fluid by-passing at confining surfaces (boundary effects), which usually distorts the true mechanisms.

Resource Assessment

DOE/BC/14000–2 **Producing Unrecovered Mobile Oil: Evaluation of Potential Economically Recoverable Reserves in Texas, Oklahoma, and New Mexico. ICF Resources Incorporated and the Bureau of Economic Geology, The University of Texas. May 1990. 168 pp. Order No. DE90000232.** This report is part of a coordinated series of research efforts designed to prepare preliminary evaluations of important components of the domestic unrecovered oil resource. The specific resource of interest is the oil that is displaceable by water and remains in the Nation's reservoirs after conventional production. Integrated geologic, engineering, and economic evaluations in this series estimate future reserve additions from this unrecovered mobile oil (UMO) resource under various circumstances. The individual studies consider the effects of changes in oil prices and advances in production technology on the economic recovery potential of the UMO resource. Several recovery technologies are evaluated, including the use of waterflooding in conjunction with infill drilling to displace and produce UMO at decreased well spacings.

Fundamental Petroleum Chemistry

NIPER–468 **Thermodynamics of the Hydrodenitrogenation of Quinoline. Topical Report. National Institute for Petroleum and Energy Research. June 1990.**

48 pp. DE90000245. A thermodynamic analysis, based on accurate experimental Gibbs energies of formation was completed for the key hydrogen-consuming steps in the HDN reaction network for quinoline. The results were compared with literature reaction studies in all cases. The concept of "crossover temperature" is discussed, and is shown to be a valuable tool in the interpretation of literature reaction-study results. The report begins in the form of a "primer," in which the problem of aromatics content in diesel fuel is used as a "simple" example of thermodynamics at work in the "real world" of the process engineer. This problem has been the topic of several regulatory efforts in California and by the federal government. There exists some question of whether the proposed maximum aromatics content can be achieved and whether the aromatics content decreases concomitantly with decreases in sulfur content due to processing conditions. Through the "crossover-temperature" concept, the report outlines how the conditions necessary for efficient attainment of low-aromatics levels can be attained. The results are compared with an exhaustive reaction study reported in the literature. Methods of nitrogen removal from aromatic materials are discussed in light of the finds of the thermodynamic analyses. It is concluded that the removal of nitrogen from heterocyclic aromatic nitrogen-containing compounds with conventional hydrodesulfurization catalysts, temperatures, and hydrogen pressures occurs under "thermodynamic control" with unavoidably high hydrogen consumption. The report also concludes that to reduce hydrogen consumption in the HDN of quinoline, two criteria must be met; (1) the catalyst must hydrogenate the nitrogen-containing ring while leaving the aromatic ring untouched (i.e., form only 1,2,3,4-tetrahydroquinoline), and (2) the catalyst must remove the nitrogen from the product of the first step (2-propylaniline) without hydrogenation of the aromatic ring. Conditions under which these conditions are possible are discussed.

NIPER–469 **Critical Property and High-Temperature Heat-Capacity Measurements on Quinoline and 5,6,7,8-Tetrahydroquinoline. Topical Report. National Institute for Petroleum and Energy Research. June 1990. 36 pp. Order No. DE90000246.** Critical property and high-temperature heat capacity measurements on quinoline and 5,6,7,8-tetrahydroquinoline are reported. From the measurements, critical temperatures of (787 ± 2)K and (746 ± 2)K, and critical densities of (336 ± 3) kg mol^{-1} (304 ± 3) kg mol^{-1} were obtained for quinoline and 5,6,7,8-tetrahydroquinoline, respectively. Critical pressures of (4820 ± 50) kPa and (3975 ± 40) kPa, respectively, were derived from the fitting procedures used. The results from the high-temperature heat capacity measurements were combined with earlier reported measurements at lower temperatures to obtain ideal-gas thermodynamic functions for both quinoline and 5,6,7,8-tetrahydroquinoline in the temperature range 298.15 K to 700 K. The derived values are compared with literature values. Densities for quinoline, estimated using the experimental critical properties determined in this research and extended corresponding states, are compared with literature measurements. Agreement is excellent with a maximum difference of 0.14 percent at 298 K. Using critical properties estimated via group-contribution methods the agreement is not so good. The difference between experimental and calculated values averages 4.5 percent.

INDEX

COMPANIES AND INSTITUTIONS

CONTENTS BY EOR PROCESS

DOE Technical Project Officers for Enhanced Oil Recovery

DIRECTORY

Name	Phone number	Name of contractor
U. S. Department of Energy Oil, Gas, and Shale Technology Mail Stop, D-116 GTN, Washington, D.C. 20545		
J. J. Stosur	301/353-2749	
Bartlesville Project Office P. O. Box 1398 Bartlesville, Oklahoma 74005		
Edith C. Allison	918/337-4390 - FTS 745-4390	Brookhaven National Laboratory Idaho National Engineering Laboratory National Institute for Petroleum and Energy Research Sandia National Laboratories Texas A&M University University of Oklahoma University of Texas at Austin
Jerry F. Casteel	918/337-4412 - FTS 745-4412	Columbia University Johns Hopkins University National Institute for Petroleum and Energy Research New Mexico Institute of Mining and Technology Texas A&M University University of Texas at Austin
Alex B. Crawley	918/337-4406 - FTS 745-4406	National Institute for Petroleum and Energy Research
Robert E. Lemmon	918/337-4405 - FTS 745-4405	Blackhawk Geosciences Inc. Colorado School of Mines Lawrence Livermore National Laboratory Los Alamos National Laboratory National Institute for Petroleum and Energy Research Pennsylvania State University Sandia National Laboratories University of Alaska University of California, Berkeley University of Michigan University of Texas at Austin Western Research Institute
Chandra Nautiyal	918/337-4409 - FTS 745-4409	Geological Survey of Alabama Kansas Geological Survey National Institute for Petroleum and Energy Research University of Texas at Austin
R. Michael Ray	918/337-4403 - FTS 745-4403	Illinois Department of Energy and Natural Resources Oklahoma Geological Survey
Thomas B. Reid	918/337-4233 - FTS 745-4233	Lawrence Berkeley Laboratory Lawrence Livermore National Laboratory National Institute for Petroleum and Energy Research Petrolphysics, Inc. Union Carbide Corporation University of Southern California
Morgantown Energy Technology Center P. O. Box 880 Morgantown, W. Va. 26505		
Royal J. Watts	304/291-4218 - FTS 923-4218	Morgantown Energy Technology Center New Mexico Institute of Mining and Technology Stanford University

CHEMICAL FLOODING—SUPPORTING RESEARCH

INTERACTIONS OF STRUCTURALLY MODIFIED SURFACTANTS WITH RESERVOIR MINERALS: CALORIMETRIC, SPECTROSCOPIC, AND ELECTROKINETIC STUDY

Contract No. DE-FG22-89BC14432

Columbia University
New York, N.Y.

Contract Date: July 1, 1989
Anticipated Completion: June 30, 1990
Government Award: $99,935

Principal Investigator:
P. Somasundaran

Project Manager:
Jerry F. Casteel
Bartlesville Project Office

Reporting Period: Jan. 1–Mar. 31, 1990

Objective

The objective of this project is to elucidate mechanisms of adsorption of structurally modified surfactants on reservoir minerals and to develop a full understanding of the effect of the surfactant structure on the nature of the adsorbed layers at the molecular level. An additional aim is to study the adsorption of surfactant mixtures on simple well-characterized minerals and on complex minerals representing real conditions. The practical goal of these studies is the identification of the optimum surfactant structures and their combinations for micellar flooding.

Summary of Technical Progress

In enhanced oil recovery by micellar flooding, adsorption of surfactants on reservoir minerals represents a major problem. An understanding of the mechanisms of adsorption and the effect of different parameters on adsorption is important in this regard. Among the different parameters, surfactant structure plays a crucial role in determining the adsorption characteristics.[1-4] In addition, surfactants used in chemical flooding processes are invariably mixtures of surfactants of different structures. Since mixtures do not generally behave like single surfactants, studies with well-defined surfactant mixtures of pure surfactants are needed to reliably model the behavior in actual systems.[5-10] The adsorption behavior of each component from mixtures (especially in anionic–nonionic systems) need to be explored because chromatographical adsorption of the components will not only cause loss of surfactants but will also change the compositional balance for maximum oil recovery.

Last quarter, the enthalpies of micellization of the alkyl xylene sulfonates as measured by microcalorimetry were reported. The studies indicated that entropy was the main driving force for micellization and that the enthalpy and entropy of micellization changed as a function of the position of sulfonate and methyl groups on the benzene ring of alkyl xylene sulfonates.

During this quarter, the enthalpy of adsorption of alkyl xylene sulfonates on alumina was measured and the results are reported. The change in the electrokinetic potential of alumina after the adsorption of the alkyl xylene sulfonates was also examined in order to understand the charge characteristics of the surfactants. Also, the adsorption of different mixtures of sodium dodecyl sulfate and ethoxylated alcohol on kaolinite is reported.

Experimental Procedures

Materials

The surfactants used, 4C11 124 *m*-xylene sulfonate (124MXS) and 4C11 135 *m*-xylene sulfonate (135MXS), were obtained from ARCO Exploration and Technology Company. The surfactants were specified to be at least 97% isomerically pure. Their structures are given below:

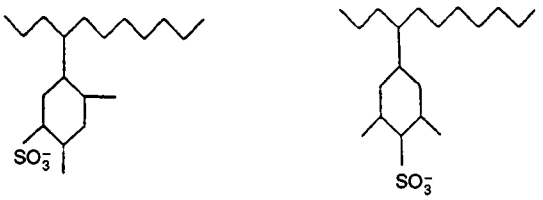

124MXS 135MXS

Sodium dodecyl sulfate purchased from Fluka Chemicals was specified to be 99% pure and was used as received. Octa ethylene glycol *n*-dodecyl ether ($C_{12}EO_8OH$) purchased from Nikko Chemicals was specified to be 98% pure and was used as received.

A high-purity Linde A alumina purchased from Union Carbide was used. The specific surface area was determined by nitrogen adsorption to be 15 m^2/g.

A well-crystallized sample of Georgia Kaolinite purchased from the clay repository at the University of Missouri was subjected to an ion-exchange treatment[11] to yield homoionic kaolinite. The surface area determined by nitrogen adsorption was 8.2 m^2/g.

Experimental Conditions

All the experiments with *m*-xylene sulfonates were carried out at 43.3°C and at a constant ionic strength of 3×10^{-2} kmol/m^3 NaCl. The adsorption of anionic–nonionic surfactant mixtures was carried out at 25°C and at an ionic strength of 3×10^{-2} kmol/m^3 NaCl.

Methods

Surfactant analysis. The anionic surfactants were analyzed by a two-phase titration technique.[12] The nonionic surfactant was analyzed with high-performance liquid chromatography (HPLC) with refractive index detection. The stationary phase was a C_{18} bonded silica column, and the mobile phase was a 90:10 mixture of acetonitrile and water.

Microcalorimetry. Calorimetric experiments were performed using an LKB 2107 differential microcalorimetry system. The description of the instrument and its working principles were given in the last quarterly report.[13] For measuring the enthalpy of adsorption, the sample cell was filled with alumina slurry and the surfactant solution of desired concentration. The reference cell was loaded with supernatant of alumina slurry and the surfactant solution of the same concentration in the sample cell. In this manner, the heat of dilution of the surfactant and its interaction with the dissolved species was automatically subtracted from the heat of reaction in the sample cell. The heat of dilution of the slurry was measured separately and subtracted from the reaction heat. Also, through mass balance calculations, the amount of demicellization was calculated. Then with the heat of micellization known, the heat of demicellization of the surfactant was calculated and subtracted from the reaction heat.

Electrokinetics. The electrokinetic potential of the mineral was measured using a Zeta Meter Model D system.

Results

Enthalpy of Adsorption of *m*-Xylene Sulfonates

The adsorption isotherms of the 124MXS and 135MXS, which were reported earlier, are given for reference in Fig. 1. The 135MXS adsorbs more than the 124MXS under premicellar conditions, but both have the same plateau value above the critical micelle concentration

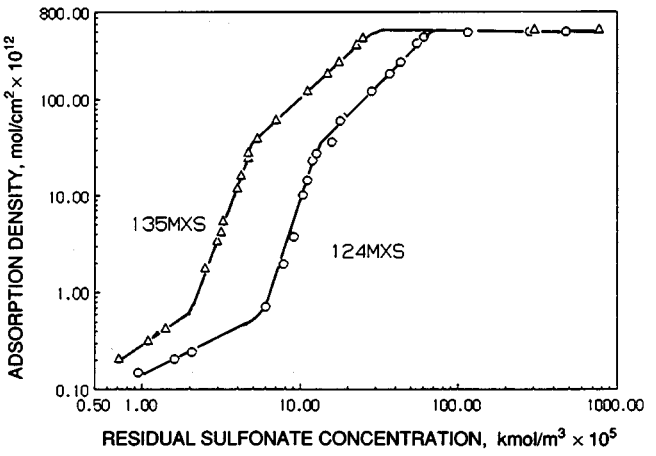

Fig. 1 Adsorption of 124MXS and 135 MXS on alumina.

(CMC). The lower adsorption of 124MXS was considered to be the result of the increased steric hindrance to the packing of the molecules in the hemimicelles arising from the position of the methyl groups on the aromatic ring. However, the reason for the lower adsorption of 124MXS at low concentrations, where the adsorption is the result of electrostatic attraction to the positively charged mineral, is not clear. To elucidate the mechanisms of the adsorption of the two surfactants, the adsorption enthalpies were measured. The differential adsorption enthalpy of the two surfactants as a function of the adsorption density is shown in Fig. 2. The enthalpy of adsorption of the two surfactants

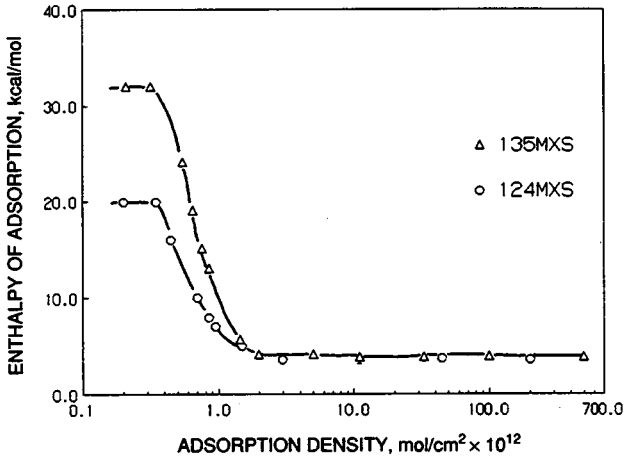

Fig. 2 Differential adsorption enthalpy of 124MXS and 135MXS on alumina.

is exothermic at all adsorption densities and decreases rapidly with the formation of surfactant aggregates through hemimicellization. This indicates that like the formation of micelles, the formation of hemimicelles is also entropy driven. The enthalpy of adsorption of the 135MXS is higher than that of the 124MXS at low adsorption densities indicating greater attraction to the mineral which results in its higher adsorption in region I as seen from Fig. 1. This greater attraction to the mineral could be the result of 135MXS being more negatively charged than 124MXS. This was tested by measuring the electrokinetic potential after adsorption of the two surfactants, and this will be discussed later. Once hemimicelles form, the enthalpy of adsorption of the two surfactants is the same. The free energy of hemimicellization of 135MXS is higher than that of 124MXS as evidenced by its greater adsorption. Since the enthalpy of hemimicellization is the same, the entropy of hemimicellization is higher for the 135MXS than for 124MXS. The entropy results from two contributions: a negative contribution caused by the ordering of the surfactant in the aggregate and a positive and major contribution from the release of the water molecules structured around the hydrocarbon tail upon its association. The tighter the packing of the molecules in the aggregates, the more water molecules will be released and the higher the entropy. Thus, the higher entropy of hemimicellization of 135MXS could indicate a tighter packing of the molecules, which was what was initially speculated as the reason for its higher adsorption. The actual calculations of the free energy and entropy are in progress and shall be reported subsequently.

Electrokinetic Potential of Alumina

The zeta potential of alumina after the adsorption of the two surfactants as a function of the adsorption density is shown in Fig. 3. The zeta potential is the same for the two

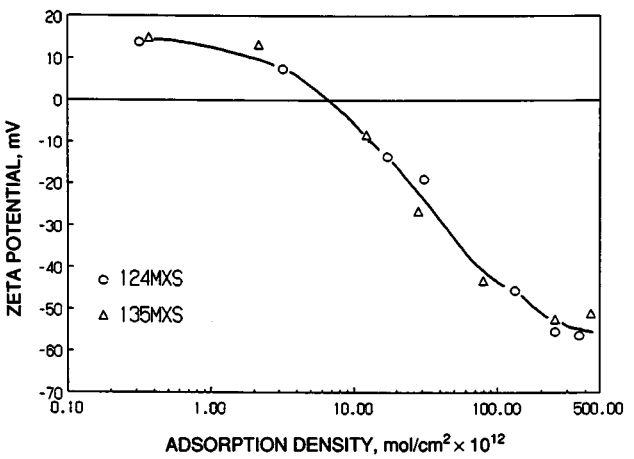

Fig. 3 Zeta potential of alumina after adsorption of 124MXS and 135MXS.

surfactants at all the adsorption densities studied. This indicates that the charge characteristics of the two surfactants are the same or that the technique is not sensitive to such small changes in the charge of the surfactant; this does not explain the greater attraction of 135MXS to the mineral at low concentrations. One possible reason could be that the water molecules near the alumina surface being structured are relatively less hydrophilic[14] and 135MXS as a result of its greater hydrophobicity (as measured by HPLC) is drawn more to the interface than 124MXS.

Adsorption of Sodium Dodecyl Sulfate–Ethoxylated Alcohol Mixtures on Kaolinite

The adsorption of different mixtures of dodecyl sulfate and ethoxylated alcohol on kaolinite was investigated and the results are shown in Figs. 4, 5, and 6. In Fig. 4, the adsorption isotherm for dodecyl sulfate from the mixtures is shown along with the isotherm for pure dodecyl sulfate. Under premicellar conditions, the adsorption of dodecyl sulfate is increased by the presence of the nonionic surfactant. However, above the CMC, the plateau adsorption decreases with increase in the amount of the nonionic

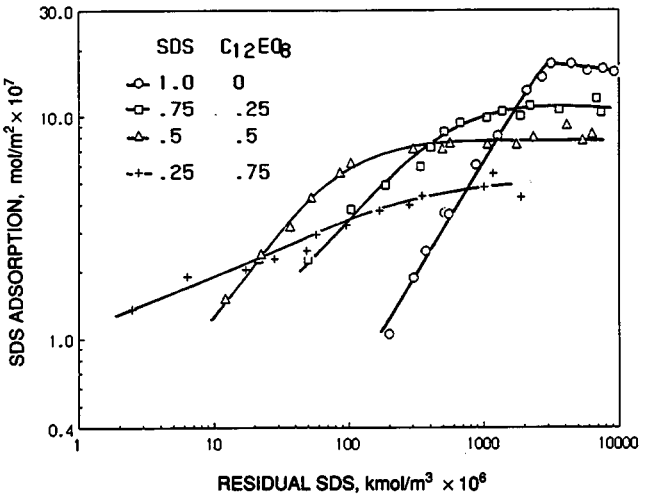

Fig. 4 Adsorption of sodium dodecyl sulfate on (SDS) kaolinite from sodium dodecyl sulfate–ethoxylated alcohol mixtures.

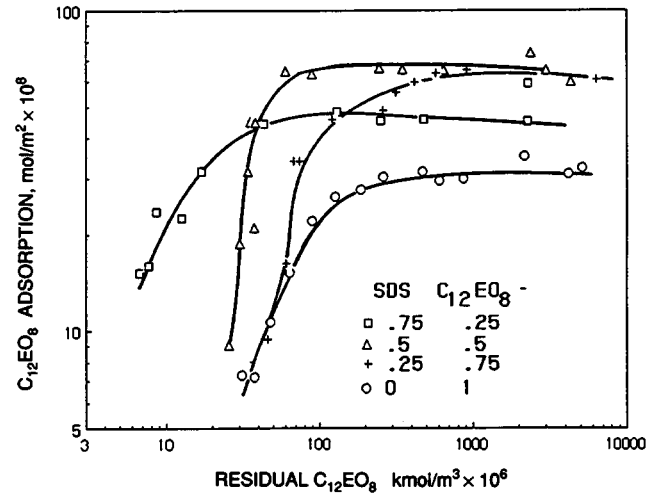

Fig. 5 Adsorption of ethoxylated alcohol (EO_8) on kaolinate from sodium dodecyl sulfate–ethoxylated alcohol mixtures.

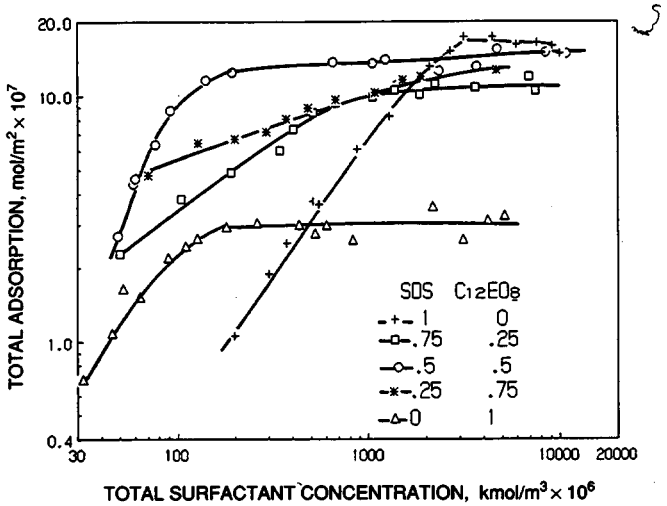

Fig. 6 Total adsorption of sodium dodecyl sulfate–ethoxylated alcohol mixtures on kaolinite.

surfactant in the mixture. The initial enhancement in the adsorption of the anionic surfactant is the result of its cooperative interactions with the nonionic surfactant. The nonionic surfactant interacts with the anionic one through hydrophobic attraction between the hydrocarbon tails and being more surface active induces greater adsorption of the anionic. Also, the nonionic reduces the electrostatic repulsion between the anionic molecules, resulting in greater adsorption of the anionic. However, once the nonionic begins to coadsorb with sodium dodecyl sulfate, the bulky ethoxyl groups create steric hindrance to the packing of the molecules, and this can result in decreased adsorption above the CMC. The component adsorption of the nonionic surfactant from the mixtures is plotted in Fig. 5. As in the case of the anionic surfactant, the adsorption of the nonionic surfactant increases with an increase in the amount of the anionic surfactant. The adsorption of the nonionic alone on kaolinite is low, and with an increase in the adsorption of the sodium dodecyl sulfate, more nonionic adsorbs through chain–chain interaction. Unlike in the case of sodium dodecyl sulfate, the plateau adsorption from the mixtures is higher than that of the pure nonionic surfactant. Most interestingly, there is no correlation of the plateau adsorption with the amount of sodium dodecyl sulfate in the mixture. The highest adsorption is obtained for a 50:50 anionic–nonionic surfactant mixture. The plateau adsorption proceeds through the formation of bilayers. Such an adsorption by bilayer formation is dependent on the packing of the molecules on the surface, which in turn seems to be related to the molar ratio of the two surfactants in the mixture. Further experiments to test this hypothesis are under way and shall be reported subsequently. The total adsorption of the mixtures is shown in Fig. 6. Again there is no correlation of the adsorption with the molar ratios of the two surfactants. The maximum adsorption is obtained for a 50:50 mixture which seems to indicate that the adsorption of the mixture is dominated by the nonionic surfactant.

References

1. P. Somasundaran, R. Middleton, and K. V. Viswanathan, in Structure/Performance Relationship in Surfactants, M. J. Rosen (Ed.), *ACS Symp. Ser.*, 253: 270-290 (1984).
2. N. M. van Os, G. J. Danne, and T. A. B. M. Bolsman, *J. Colloid Interface Sci.*, 115: 402 (1987).
3. N. M. van Os, G. J. Danne, and T. A. B. M. Bolsman, *J. Colloid Interface Sci.*, 123: 267 (1988).
4. M. J. Rosen, Z. H. Zhu, B. Gu, and D. S. Murphy, *Langmuir*, 4: 1273 (1988).
5. P. Somasundaran, *Adsorption from Flooding Solutions in Porous Media*, Annual Report submitted to DOE, NSF, and a Consortium of Supporting Industrial Organizations, Columbia University, New York, 1987.
6. P. M. Holland, in Phenomena in Mixed Surfactant Systems, J. F. Scamehorn (Ed.), *ACS Symp. Ser.*, 311: 102 (1986).
7. J. F. Scamehorn, R. S. Schechter, and W. H. Wade, *J. Disp. Sci. Tech.*, 3: 261 (1982).
8. D. G. Hall and R. W. Huddleston, *Colloids Surf.*, 13: 209 (1985).

9. E. Fu, *DES Thesis*, Columbia University, New York (1988).
10. J. H. Harwell, B. L. Roberts, and J. F. Scamehorn, *Colloids Surf.*, 32: 1 (1988).
11. P. A. Siracusa and P. Somasundaran, *J. Colloid Interface Sci.*, 114: 184 (1986).
12. Z. Li and M. J. Rosen, *Anal. Chem.*, 53: 516 (1981).
13. P. Somasundaran, *Interactions of Structurally Modified Surfactants with Reservoir Minerals: Calorimetric, Spectroscopic and Electrokinetic Study*, October 15, 1989–January 15, 1990, Quarterly Report submitted to Department of Energy.
14. W. Drost-Hansen, Structure of Water Near Solid Interfaces, in *Chemistry and Physics of Interfaces-2*, Sydney Ross (Ed.), American Chemical Society Publications, Washington, D.C. (1971).

FLUID DIVERSION AND SWEEP IMPROVEMENT WITH CHEMICAL GELS IN OIL RECOVERY PROCESSES

Contract No. FG07-89BC14447

New Mexico Institute of Mining and Technology
Soccoro, N. Mex.

Contract Date: May 1, 1989
Anticipated Completion: Aug. 1, 1992
Government Award: $272,674

Principal Investigators:
Randall S. Seright
Frank S. Kovarik
F. David Martin

Project Manager:
Jerry F. Casteel
Bartlesville Project Office

Reporting Period: Jan. 1–Mar. 31, 1990

Objectives

The objectives of this project are to examine the mechanisms by which gel treatments divert fluids in reservoirs and to establish where and how gel treatments are best applied. Several different types of gelants are being examined, including polymer-based gelants, a monomer-based gelant, and a colloidal silica gelant. This research is directed at gel applications in water injection wells, in production wells, and in high-pressure gas floods. The work will establish how the flow properties of gels and gelling agents are influenced by permeability, lithology, and wettability. Other goals include determining the proper placement of gelants, the stability of in-place gels, and the types of gels required for the various oil recovery processes and for different scales of reservoir heterogeneity.

Summary of Technical Progress

Fabrication of Two-Dimensional Glass Micromodels

A previous report details techniques for preparing the two-dimensional glass micromodels that are being used in this project. The techniques described represent improvements on methods that were developed earlier at the New Mexico Petroleum Recovery Research Center.

Impact of Gelation pH, Rock Permeability, and Lithology on the Performance of a Monomer-Based Gel

For many of the gels that are currently used in enhanced oil recovery, the gelation reaction is very sensitive to pH. Often, an optimum pH exists at which the strongest gels form. At other pH values, weak gels may form, or gelation may not occur at all. Commonly, the optimum pH for gelation is not near neutral pH. Also, most gel formulations have very little buffering capacity (i.e., their pH may be changed very easily). On the other hand, clay and carbonate minerals in reservoir rocks usually have a tremendous capacity to buffer aqueous solutions near neutral pH. Thus, even though a gelant is injected at the optimum pH for gelation, the rock may quickly change the pH to a less optimum value.

A previous report describes an experimental investigation of the effects of gelation pH on the performance of a resorcinol–formaldehyde gel. This gel has been used in field applications and was chosen for study because its placement in porous media is not complicated by some of the factors that influence placement of polymeric gelling agents (i.e., permeability- and lithology-dependent retention of polymers and metallic cross-linkers).

Beaker studies and core experiments were performed with both unbuffered gelants and gelants that were buffered at a variety of pH values. The product formed by the reaction of resorcinol with formaldehyde depends on pH. During studies of gelation in beakers, the strongest resorcinol–formaldehyde gels are formed at pH=9. At pH=9, a strong gel that is clear and red is formed. The inherent permeability to water for this gel (no rock) is 6 μD. As the initial pH is decreased, gel formation becomes less perfect. With an initial pH of 7, an opaque orange–white gel is formed during beaker tests, and some free water remains after the reaction. As initial pH value is decreased below 7, the final ratio of free water to gel increases.

During core experiments, residual resistance factors are very high (10^3 to 10^4) for gelants buffered and formed at pH=9. Tracer studies reveal that this gel occupies 87 to 99% of the available pore volume. As pH is decreased dur-

ing core experiments, the gelation reaction is inhibited. In particular, as gelation pH decreases from 7 to 6, residual resistance factors decrease sharply from high to low values (e.g., from ≈1000 to 1). Tracer studies show that the fraction of the pore volume occupied by the gel generally decreases over this pH range. In many core experiments, the results suggest that, upon first exposure to a given fluid velocity, a certain amount of gel breaks down to allow a flow path through the porous medium. Flow of brine through this porous medium then appears more or less Newtonian until the previous maximum in fluid velocity is exceeded.

In general, residual resistance factors (F_{rr}) increased with decreased permeability. For a given permeability, however, F_{rr} values can be significantly higher in sandstones than in carbonate cores. A simple mathematical model was used to assess whether pH effects can be exploited to optimize gel placement in injection wells. The results suggest that pH effects usually will not eliminate the need for zone isolation during gel placement in radial flow (unfractured injection wells). Insights obtained by studying this relatively simple gel system may be valuable when assessing the performance of more complicated gels in fluid diversion.

Rheology of Chromium(III)–Xanthan Gels and Gelants in Porous Media

Experiments were performed to probe the rheology of chromium(III)–xanthan gels and gelants in porous media. Details are given in another report. For a large fraction of the time prior to gelation, 90-ppm Cr^{3+} did not significantly affect the rheology in porous media of a 3000-ppm xanthan solution.

For gel formulations containing 3000-ppm xanthan and 90-ppm Cr^{3+}, residual resistance factors in Berea sandstone were not much greater than those for xanthan solutions without Cr^{3+}. Clay and carbonate minerals in Berea probably forced the gelation reaction to occur near neutral pH rather than at the injection pH (3.8). In beaker tests, rigid gels are formed from Cr^{3+}–xanthan gelants at pH≈4, but gelation is not apparent for the same formulation at pH=7. Previous researchers reported large residual resistance factors for more dilute Cr^{3+}–xanthan gels in clean sandpacks. The discrepancy between these results and those of previous researchers may be explained in that the lack of clay and carbonate minerals in sandpacks may have allowed gelation to occur at low pH values rather than at neutral pH. Thus the buffering action of reservoir rocks should be considered when evaluating gel performance in the laboratory.

Additional studies were performed with a gelant that contained 4000-ppm xanthan and 154-ppm Cr^{3+}. With this composition, a rigid gel was formed in a beaker at pH=4, but gelation was not evident at pH=7. Even so, the composition injected at pH=7 provided substantial residual resistance factors (30-714) in Berea sandstone. Tracer studies indicated that the gel occupied between 0 and 45% of the original pore volume, depending on the initial pH of the gelant and the core permeability. Tracer studies also revealed that the gel increased dispersivity values in Berea by factors ranging from 5.5 to 17.8. For this gel in 483-mD Berea, residual resistance factors were quite high (50-714), even though tracer studies indicated that the pore volume occupied by the gel was near zero. Perhaps small gel particles lodge in pore throats and thereby dramatically reduce brine permeability without occupying much volume. Residual resistance factors provided by these gels decreased significantly with increased fluid flux and could be described by a power-law relation over the flux range from 0.025 to 16 ft/d.

Laboratory measurements of gel properties in 66-mD Berea and in 483-mD Berea were used during example calculations to show that the apparent "shear-thinning" nature of residual resistance factors will not eliminate the need for zone isolation during gel placement in unfractured injection wells.

A Preliminary Study of Permeability Reduction for CO_2 and Water Using a Resorcinol–Formaldehyde Gel

Another report describes a preliminary study of the effects of a resorcinol–formaldehyde gel on the flow of CO_2 and brine in Berea sandstone. The gelant was buffered at pH=6.5. During the first injection of brine after gelation, the F_{rr} for brine averaged 192. This value was insensitive to fluid injection rate for flux values between 0.2 and 15.7 ft/d. During subsequent CO_2 injection, the F_{rr} value for CO_2 averaged 23.7. Returning to brine injection yielded an average F_{rr} value of 27.1. These observations were briefly compared with results from a previous study. In this work, tracer studies were performed to determine the fraction of the pore volume that was occupied by CO_2 and/or gel during each of the various stages of the experiments. The procedures examined during this study will provide a basis for future experiments.

OIL RECOVERY ENHANCEMENT FROM FRACTURED, LOW-PERMEABILITY RESERVOIRS

Contract No. DE-FG07-89BC14444

Texas A&M University
College Station, Tex.

Contract Date: June 13, 1989
Anticipated Completion: Sept. 1, 1992
Government Award: $256,000
(Current Year)

Principal Investigator:
S. Poston

Project Manager:
Jerry F. Casteel
Bartlesville Project Office

Reporting Period: Jan. 1–Mar. 31, 1990

Objective

The objective of this project is to develop and advance new concepts and technology to increase oil and possibly gas recovery from fractured, low-matrix permeability reservoirs. The overall study is to encompass geological, geophysical, laboratory, and imaging flow studies and analytical and computer modeling as well as field trials.

Summary of Technical Progress

Interpreting and Predicting Natural Fractures

Geological Studies

During this reporting period the earlier work of Corbett et al. was extended. The distortional strain area for specimens that had previously been deformed at a confining pressure of 10 MPa, 24°C and at a strain rate of 10^{-4} s^{-1} was determined. The distortional strain energy is the area measured under the stress–strain curve up to an arbitrary 3% strain. The total trace length of fractures observed at the surface of each of the cylindrical specimens (10 cm long and 5 cm in diameter) was determined as a measure of the fracture development (abundance) in each of the specimens.

The results of these studies indicate that fracture abundance (greater fracture trace length) increases with increasing distortional strain energy (specimen strength in the brittle regime), although the relationship does not seem to be linear.

Plans and commitments for field work to be conducted by Dr. Kevin Corbett during the summer have been formulated. The assignment is to (1) collect blocks of the Austin Chalk for further laboratory experimental deformation tests, X-ray analyses, and microscopic examination; (2) determine from measurements made in the field if the intact block size of naturally fractured Austin Chalk or the fracture surface area per unit volume can be characterized by fractal geometry; (3) obtain more data on fracture abundance vs. bedding thickness per several lithologies; and (4) map fracture vein arrays in several localities where different lithologies exist with a view toward getting data on fracture lengths, types, and densities of intersections and fracture throat sizes.

Geophysical Studies

Two sets of Austin Chalk data have been obtained and transferred to storage for analysis. Frequency spectra have been generated on selected raw traces. The studies show that the frequency content of the seismic signals lies between 8 and 25 Hz. The form of the seismic wavelet has been extracted from the data, and a deconvolution operator has been generated to extend the wavelet frequencies to over 60 Hz. The results of the deconvolution process are shown in Fig. 1. Part (a) of Fig. 1 is a segment of a trace before the deconvolution operator was applied, whereas part (b) of Fig. 1 shows the same trace segment after deconvolution. The increase in the high-frequency content is clearly evident in part (b), where the events at about 90, 140, 180, 220, and 360 ms are more readily resolvable compared to the same events in part (a).

The process of stacking the seismic data to look for the seismic effects of the fractures is in progress. Preliminary study of the deconvolved seismic traces shows high-frequency signals that may be associated with the fractures. There will be a more definitive picture of the seismic effects once the stacked seismic data are generated.

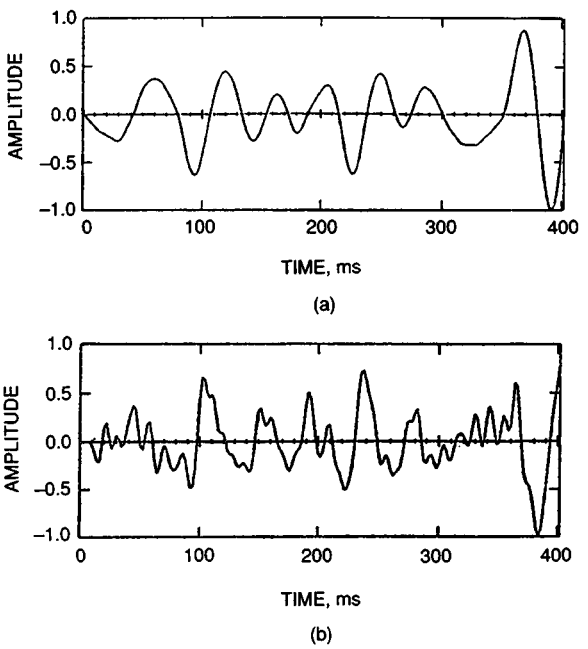

Fig. 1 Segment of T 15 from Shot 21 before (a) and after (b) deconvolution was applied.

Relating Recovery to Log Signatures

Geological Studies

The response of common well logs has been correlated with the stages of maturity in the source rock. The resistivity, density–porosity, and neutron porosity logs indicate three zones: the immature zone, the accumulation zone, and the migration zone. Furthermore, the true resistivity of the mature source can be correlated with water saturation in cores (Fig. 2). The potential reservoir zone has resistivities between 9 and 40 Ω-m, which indicates water saturation in the range of 45 to 75%. These values also suggest a moveable oil saturation of 10 to 20%. The oil saturation values represent the oil still in the source rock available for migration to support sustained oil production after the fractures have been drained.

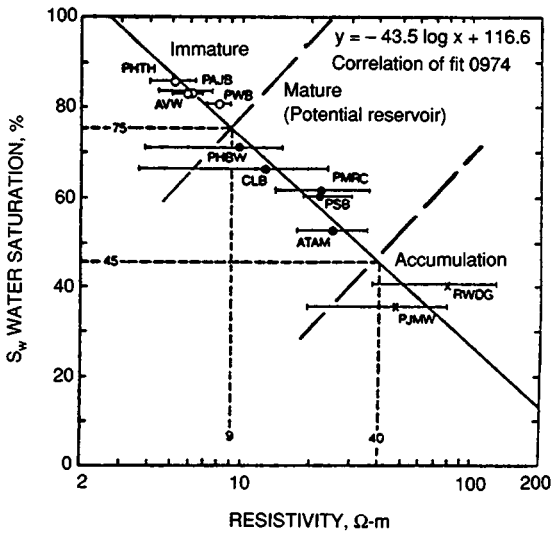

Fig. 2 Illustration showing relation of core resistivity to water saturation.

The next phase of the project will attempt to correlate oil production from the Austin Chalk to the volume of moveable oil determined from the resistivity logs. An area in the Big Wells field, Dimmit County, Tex., has been selected for the initial production study.

Petroleum Engineering

The type curves generated specifically for the fractured reservoir situation were used to analyze several Austin Chalk wells. However, the fracture half-length and storage-compressibility values must be known with some certainty for the analysis to be used quantitatively. The area of study for the preliminary analysis was too large to permit the reservoir characteristics or permeability to be determined quantitatively.

The next step is to apply the analysis technique to a smaller area with more geological and reservoir control. A six-well section in Dimmit County, Tex., has been selected. Well logs, core analysis, and completion and production data have been obtained.

Laboratory Studies of the Imbibition Process

Laboratory Displacement Studies

The student conducting these experiments has completed all degree requirements. A new graduate student has been selected and is presently constructing glass imbibition cells to add to the data assembled during the initial efforts.

Magnetic Resonance Imaging Studies

The magnetic resonance imaging (MRI) and computerized tomography (CT) imaging equipment has not been operational because of the move to the new building and various malfunctions. However, during this time interval a new core holder has been designed. The core holder will be able to accept 1-in.-OD core and is rated at 2000 psig and 250°F. The holder has been fabricated, and pressure and image testing is to be initiated this week.

Computerized Tomography Studies

A new graduate student will conduct imbibition studies on the CT scanner. These studies are to be dovetailed with the MRI work. An extensive literature review is being conducted to acquaint the student with CT work. The CT equipment should become operational within 2 weeks.

Mathematical Modeling

Efforts were concentrated in two separate but similar studies:

1. Work was conducted to develop a simplified fractured reservoir model to be used in the analysis of a CO_2-enriched waterflood and to model the corresponding recovery improvement. A set of equations was formulated describing the saturation distribution as well as production performance within the fracture for a simple water–oil system. The following equations should adequately describe the waterflood process.

The continuity equation for linear reservoirs:

$$-\frac{\partial q_w}{\partial x} - W'_{Iu} = W_r L\, \phi_{fe} \frac{\partial S_w}{\partial t}$$

where $\partial q_w/\partial x$ is the flow term in the x direction (L^4/t) and W'_{Iu} is the rate of water imbibition/unit fracture length (L^4/t).

Rate of water imbibition–unitary fracture length

$$W'_{Iu} = \frac{N_{maRu}}{\tau_I} \int_0^t e^{-(t-\theta)/\tau_I} \frac{\partial S_w}{\partial \theta}\, d\theta$$

where N_{maRu} = total oil recovery from the matrix unit fracture length; $f(C_{CO_2})$ (L^3/L)
τ_I = matrix block imbibition time; $f(C_{CO_2})$, (t)
t = time, t
S_w = mobile water saturation (fraction)
θ = integration parameter

2. A three-dimensional, compositional simulator is being modified for dual-porosity, dual-permeability systems. The input and output data sections were modified to expedite the simulation data file. The input data section was divided into: (a) reservoir geometry, (b) rock properties, (c) fluid properties, (d) rock and fluid properties, (e) operational parameters, and (f) simulation parameters.

Reference

1. D. Corbett, M. Friedman, and J. Spang, Fracture Development and Mechanical Stratigraphy of Austin Chalk, Texas, *Am. Assoc. Pet. Geol.*, 71(1) (1987).

DEVELOPMENT OF IMPROVED SURFACTANT FLOODING METHODS

Cooperative Agreement DE-FC22-83FE60149, Project BE4A

National Institute for Petroleum and Energy Research
Bartlesville, Okla.

Contract Date: Oct. 1, 1983
Anticipated Completion: Sept. 30, 1990
Funding for FY 1990: $605,000

Principal Investigator:
Leo A. Noll

Project Manager:
Jerry F. Casteel
Bartlesville Project Office

Reporting Period: Jan. 1–Mar. 31, 1990

Objectives

The objective of this work is to develop more effective surfactant flooding systems that have broader tolerance to variations in salinity. Specific objectives are: (1) to determine if surfactant systems of similar hydrophilic–lipophilic balance (HLB) and solubility parameter values can be combined so that salinity tolerance and resistance to chromatographic separation are improved and to study the solution properties of such mixtures; (2) to study the use of alkaline additives to surfactant systems for light oils; and (3) to use this information to develop improved surfactant-property relationships.

Summary of Technical Progress

Mixed Surfactant Systems

Screening interfacial tension (IFT) measurements were conducted for a binary mixture of an alpha-olefin sulfonate (AOS), Shell's AOS 1416, and a carboxymethylated ethoxylated (CME) surfactant, Sandoz Chemicals' RS-16, with *n*-decane as the hydrocarbon component. *N*-pentanol was added to the mixtures as a cosurfactant. Severe gel formation was observed in most of the different salinity mixtures tested. The addition of the CME surfactant did not alleviate the formation of gels in the test mixtures. Reliable IFT measurements were not possible under these conditions. All the IFT measurements were conducted at a low fixed total surfactant concentration of 2 wt %.

The IFT measurements were also conducted for the binary mixture of an alkyl-aryl sulfonate (AAS), Shell's Enordet LXS-1314, and a CME surfactant, Sandoz Chemicals' JA-6, with *n*-decane. The relatively low-phase separation temperature of JA-6 (<24°C at 0.5 wt % NaCl salinity) became a hindrance in the desired experimental measurements, even at the low concentration of 0.1 wt % JA-6. These results were compared with the IFT values measured from the previous binary system containing LXS-1314 and RS-16 surfactants.[1] The main difference between the two CME surfactants is in the primary (R_1) hydrocarbon chain length and the degree of ethoxylation. For the RS-16 surfactant, the R_1 structure is a C_{16} to C_{18} group and the degree of ethoxylation is 8, whereas the JA-6 surfactant has a structure of C_{13} and a degree of ethoxylation of 3. Previous results have shown that the JA-6 alone can exhibit relatively low IFT values with *n*-dodecane and *n*-decane at salinity ranges greater than 15 wt %.[2]

Interfacial tension measurements were conducted for Sandoz Chemicals' RS-16 alone over a wide range of salinity from 5 to 20 wt % NaCl with *n*-decane. Intermediate IFT values of about 10^{-1} mN/m have been measured. These IFT values are lower than those previously observed for this surfactant with *n*-dodecane at a salinity from 10 to 20 wt % NaCl. The IFT measurements using this surfactant alone were conducted to provide the base-case values when the total surfactant concentration in the formulation was replaced primarily by the CME surfactant. The results of these measurements are presented in Fig. 1.

Two other CME surfactants are currently being tested as secondary surfactants: Sandoz Chemicals' MA-18 and Hüls' CES 6.5. MA-18 is an *n*-nonylphenol-based CME with an average of 9 ethylene oxide (EO) groups, and CES 6.5 is an i-nonylphenol-based CME with an average of 6.5 EO groups. These CME surfactants yielded relatively higher phase separation temperatures in previous studies. For the IFT measurements, an equal ratio of the two surfactants

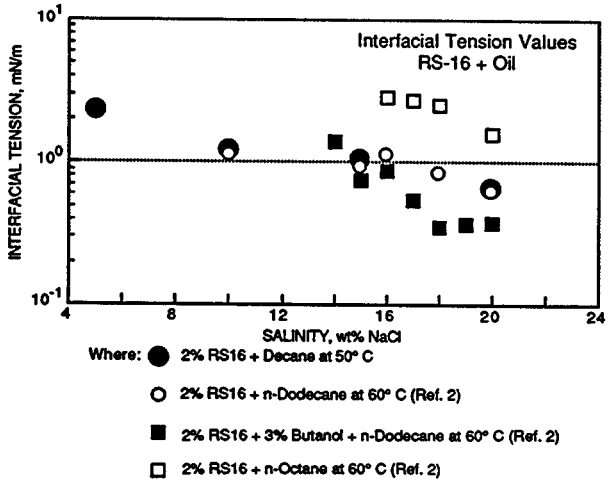

Fig. 1 Interfacial tension measurements for a carboxymethylated ethoxylated surfactant, Sandoz Chemicals' RS-16 + *n*-decane at 50°C.

(1:1) was added to the primary surfactant LXS-1314. Relatively low IFT values have been measured, less than 10^{-2} mN/m at a salinity of about 3 wt % NaCl. These measurements were conducted using surfactant formulations containing only 10% CME surfactants of the total surfactant concentration. No unfavorable phase behavior has been observed under these conditions. Additional IFT measurements were conducted for this surfactant system with *n*-decane at different salinities. The proportion of AAS to CME surfactants was varied to investigate the extent of the improvement in salinity tolerance of the overall system. The IFT measurements yielded fairly uniform values of IFT (about 10^{-2} mN/m) over a broad range of salinities (0.5 to 9 wt % NaCl) as a function of the different surfactant proportions tested. Similar IFT measurements were conducted using North Burbank Unit (NBU) oil and the surfactant systems tested. Reasonable values of IFT were obtained for this system when using NBU oil. The results of the study are presented in Fig. 2. Additional work is

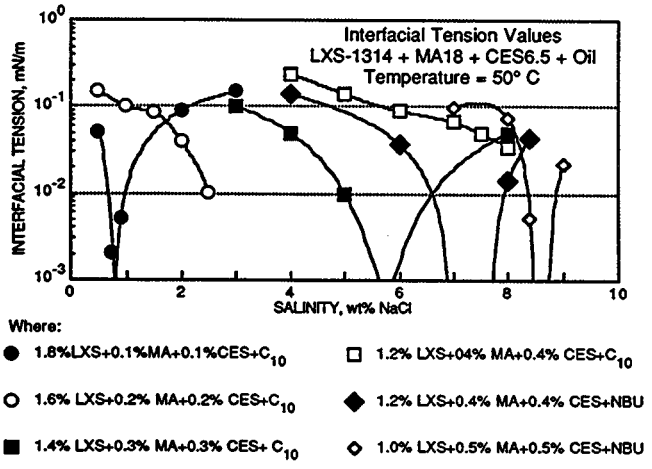

Fig. 2 Interfacial tension measurements using LXS-1314 with MA-18 and CES 6.5 at 50°C.

under way to investigate further extending the salinity coverage of this system to higher levels (above 9 wt % NaCl) while maintaining fairly uniform, relatively low IFT values. Phase behavior studies using this surfactant system will also be initiated.

Adsorption of Mixed Surfactant Systems

Static adsorption tests were conducted using a binary mixture of an AAS, Enordet LXS-1314, and an ethoxylated sulfate, GAF Alipal® CO-436, in 3% NaCl at ambient temperature. Solutions containing only LXS-1314 separated into two phases at this brine concentration. The ethoxylated sulfate was added to improve the solubility of the AAS. Solutions containing both surfactants in 3% brine were cloudy but did not phase separate. Significant reduction of surfactant loss was observed for the binary mixtures as compared with the solution containing only LXS-1314. Results are shown in Table 1.

TABLE 1

Surfactant Loss of a Mixed Surfactant System on Crushed Berea Sandstone at Ambient Temperature

LXS-1314 concentration, %	CO-436 concentration, %	Surfactant loss, mg/g
0.991	0	46.8 ± 1.4
0.891	0.113	1.59 ± 0.14
0.794	0.209	2.36 ± 0.37
0.708	0.336	1.03 ± 0.27
0	0.331	0.59 ± 0.02

Therefore, addition of an ethoxylated anionic surfactant was effective in extending the useful salinity range for an AAS. Surfactant loss may still be excessive for economical oil recovery, and additional methods to reduce surfactant loss, such as the use of sacrificial agents, may be desirable.

Surfactant concentrations for these measurements were determined using high-pressure liquid chromatography (HPLC) techniques. The surfactants were detected using an ultraviolet (UV) absorption at 272 nm after separation on a reverse-phase chromatographic column. Both these surfactants eluted from the column at about the same time using a mobile phase solvent of 33% H_2O, 22% MeOH, and 45% CH_3CN. The combined area of the overlapping peaks was proportional to both the LXS-1314 and the CO-436 surfactant concentrations. Figure 3 shows a three-dimensional graph of peak area as a function of the amount of each type of surfactant in the injected sample.

Studies are under way to determine the surfactant loss for a ternary surfactant mixture containing LXS-1314, and two CME surfactants, Sandoz M-18 and Hüls CES 6.5. The addition of the CME surfactants has extended the salinity tolerance of the LXS-1314 surfactant to 9 wt % NaCl, as

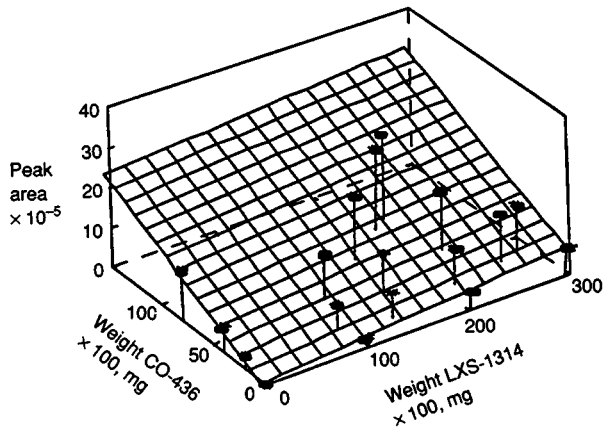

Fig. 3 Chromatographic peak area as a function of concentration in a binary surfactant system, LXS-1314 and CO-436.

described in the previous section. This surfactant system exhibits some useful analytical features. The HPLC elution peaks for the LXS and CME surfactants do not overlap. Therefore, separate evaluation of surfactant loss of each surfactant type can be determined in static tests.

In addition, analytical methods were investigated this quarter to prepare aqueous samples collected during coreflood experiments for surfactant concentration analysis using the HPLC. These collected fractions often contain polymers and emulsions that can cause problems during the surfactant analysis. Adsorption of the surfactant on a small reverse-phase filter, washing with water to remove water-soluble salts and polymer, and removal of the surfactant from the filter with acetonitrile was used to clean up small samples. The amount of surfactant in the sample was then measured with HPLC techniques. However, any presence of oil in the sample could cause severe interference in the UV detection of the surfactant. Acetonitrile could remove UV absorbing components from the oil, which would completely mask the signal produced by the surfactant. Therefore, the technique can only be used for surfactant in the brine eluting after a coreflood experiment.

Dilution Calorimetry of Mixed Surfactant Systems

Dilution calorimetric studies of an AAS, LXS-1314 in water and in 0.5% brine, as well as a mixture of Sandopan RS-16 with LXS at 25, 50, and 90°C are near completion. Since a sodium chloride brine at elevated temperatures can be quite corrosive to the calorimeter, the brine used in these experiments is 0.933% sodium sulfate. This concentration was chosen since it has the same osmosity as a 0.5% solution of sodium chloride.

The solution of LXS in brine is cloudy, perhaps from the presence of liquid crystals. These solutions were shaken well, and samples were taken and immediately put into the calorimeter. There is very little detectable heat of dilution of LXS in brine at any of the three temperatures. The runs at 90° are undergoing repetition. The reason for the small heat effect is probably because the solutions have phase separated, so the dilution calorimetry is dealing with solutions of constant, very low concentration.

The solutions of LXS in water and of the mixture are both clear. The heats of dilution of the LXS in water are the largest of the present series at all three temperatures. However, they are much lower than those observed for the pure surfactant decyltrimethylammonium bromide, or those observed with Chaser SD1000 or Sandopan MA-18. The heats of dilution of the mixture in brine are between those of the LXS in brine and LXS in water, but closer to the LXS–brine results.

The calculation of heats of dilution for all surfactants at all temperatures is near completion. However, to extract the solution properties, it is still necessary to fit the data to a relative apparent molar enthalpy curve. This fitting will be done early next quarter.

Additives for Surfactant Formulations

Two low acid number, light crude oils were screened with phase behavior tests to identify salinity ranges and pH ranges where alkaline agents will be useful as additive agents to low-concentration synthetic surfactant formulations. Light crude oils from Teapot Dome (Wyoming) oil field and Delaware–Childers (Oklahoma) oil field were used for the tests, which were conducted at the respective reservoir temperatures.

Teapot Dome oil was tested with 0.1% Petrostep B-100, a commercial anionic EOR surfactant, and with 0.1% Neodol 25-9, a commercial alcohol ethoxylate. It is essential that the pH be maintained at a low level to minimize deleterious mineral–alkali reactions because there is considerable kaolinite in the Upper and Lower Shannon sandstones. Salinity scans were conducted at pH 8.2 and pH 9.5. A pH effect was observed. At the higher pH, more of the phase behavior samples exhibited slow water-breakout rates, and the optimal salinity appeared to be higher at the higher pH. These results with the Teapot Dome oil are encouraging, and some samples were selected for further study via IFT measurements.

Delaware–Childers oil was tested at pH levels from 9.5 to 10.5 with the same surfactants. Many of the samples exhibited slow water-breakout rates, and certain samples were selected for further study via IFT measurements.

If the results of the IFT measurements with the two oils are encouraging, then coreflooding tests will be designed to test the oil recovery efficiency of surfactant formulations that contain alkaline additives. IFT experiments are currently being conducted at reservoir temperature and pH 9.5 with the Delaware–Childers (Oklahoma) oil. If the IFT results at reservoir temperature (30°C) are not favorable, then the corefloods will be conducted at 52°C, where favorable IFT values were previously obtained. These chemical formulations will be designed so that the cost of the com-

mercial EOR surfactant, on scale-up to a field situation, will be minimal.

References

1. National Institute for Petroleum and Energy Research, *Quarterly Technical Report for October 1–December 31, 1989,* DOE Report NIPER-463, Vol. II, pp. 28-33, February 1990.
2. A. Strycker, *Selection and Design of Ethoxylated Carboxylates for Chemical Flooding,* DOE Report NIPER-449, September 1989.

DEVELOPMENT OF IMPROVED ALKALINE FLOODING METHODS

Cooperative Agreement DE-FC22-83FE60149, Project BE4B

National Institute for Petroleum and Energy Research
Bartlesville, Okla.

Contract Date: Oct. 1, 1983
Anticipated Completion: Sept. 30, 1990
Funding for FY 1990: $140,000

Principal Investigator:
Troy R. French

Project Manager:
Thomas B. Reid
Bartlesville Project Office

Reporting Period: Jan. 1–Mar. 31, 1990

Objectives

The objective of this project is to develop cost-effective and efficient chemical flooding formulations with surfactant-enhanced, low-pH alkaline systems. Specific objectives for FY90 are to: (1) investigate the applicability of alkaline–surfactant flooding for use in reservoirs with crude oils having very low acid numbers, (2) test commercially available enhanced oil recovery (EOR) chemicals that could be used in a pilot alkaline flood, and (3) compare the effect of divalent ions on surfactant loss and the transient interfacial tension (IFT) behavior of carbonate–surfactant systems with the effects previously observed for carbonate–phosphate–surfactant mixtures.

Summary of Technical Progress

The results of phase behavior tests and IFT measurements with a heavy, low-acid crude oil provided further evidence that surfactant-enhanced alkaline flooding may be effective for recovery of oils that have low acid numbers. It was also shown that phase behavior tests may be of little value for the identification of optimal salinities for surfactant-enhanced alkaline systems when the crude oils have very low acid numbers.

Several very low-pH alkaline systems formulated with commercially available surfactants were tested for possible use in the Wilmington (California) field; however, the optimum salinities were found to be too high for use in that field.

Application to Enhanced Oil Recovery

Prior work has shown that the acidic content of a crude oil, which is usually expressed as acid number, is not necessarily a reliable indicator of how amenable an oil is to alkaline flooding.[1] If surfactant-enhanced alkaline flooding methods can be applied to recover crude oils with low acid content, then the target resource for this technology would be greater than was previously thought.

Low-Acid Crude

Phase behavior tests and IFT measurements were conducted with Densmore (Kansas) crude oil and two commercial surfactants at pH 9.3. The objectives of the experiments were to determine if this low-acid (total acid number, 0.27 mg of KOH/g of oil) heavy oil is a candidate for alkaline flooding and if phase behavior tests can be used to predict the IFT behavior of low-acid crude oils under alkaline conditions.

One series of experiments was conducted at pH 9.3 with 0.1% active anionic surfactant (Petrostep B-100). The IFT over a salinity range is shown in Fig. 1. Very low IFT values were obtained over the entire salinity range, and this provided evidence that even low-acid oils will respond favorably to surfactant-enhanced alkaline flooding. It was not possible to predict this IFT behavior from the results of either static or dynamic phase behavior tests.

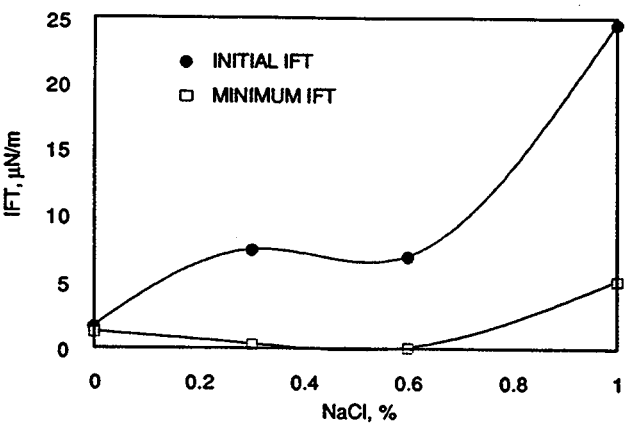

Fig. 1 Densmore (Kansas) crude oil salinity scan, 0.1% Petrostep B-100 surfactant, 52°C, pH 9.3.

Another pH 9.3 system was formulated with a nonionic surfactant (Neodol 25-9). The IFT over a salinity range is shown in Fig. 2. Very low IFT values were measured above 4% NaCl concentration. These results are encouraging because traditional high-pH systems produce very low IFT values only at very low salinities. It was not possible to predict this IFT behavior from either static or dynamic phase behavior tests.

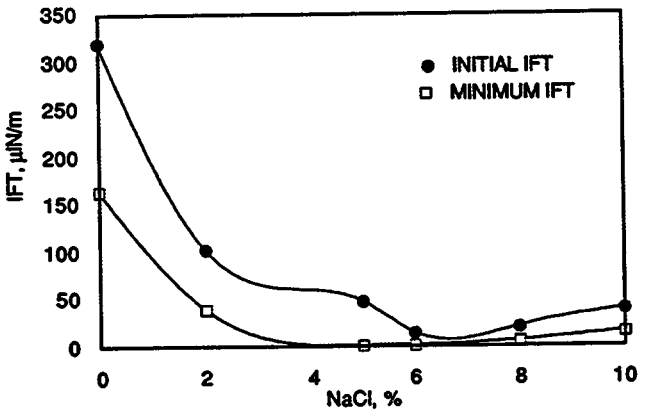

Fig. 2 Densmore (Kansas) crude oil salinity scan, 0.1% Neodol 25-9 surfactant, 52°C, pH 9.3.

The lack of correlation between the phase behavior tests and IFT measurements appears to hold true for medium-pH (9.3) alkaline systems when the oil is nonacidic or slightly acidic. The same behavior was also observed when very low-pH (8.2) surfactant–alkaline systems were tested with acidic oils. Under these conditions, phase behavior testing appears to have little value, and IFT measurements must be relied upon for evaluation.

It was previously believed that a high acid number was essential for alkaline flooding to be successful. These and other results[2] that were previously reported indicate that surfactant-enhanced alkaline flooding may also be an effective EOR method with low-acid crude oils.

Acidic Crude

Phase behavior tests were conducted with the Wilmington (California) crude oil and four commercial surfactants at pH 8.2. The surfactants tested were Igepon T-33 (sodium N-methyl-N-oleoyltaurate), Igepal CA-720 (an octylphenol ethoxylate), and Igepal CO-730 and CO-850 (both nonylphenol ethoxylates). The Wilmington oil has an acid number of 1.59 mg of KOH/g of oil, and this is believed to be the first time that Wilmington oil has been tested at pH 8.2 with these particular commercial surfactants.

Many of the samples showed slow water-breakout rates, which was encouraging, and the Igepon T-33 and Igepal CA-720 series were selected for IFT measurements. The IFT over a salinity range is shown for 0.1% active Igepon T-33 in Fig. 3. The Igepon T-33 system IFT decreased over the salinity range tested to a low of 17.1 μN/m at 9% NaCl concentration. Apparently the optimal salinity is above 9% NaCl concentration. The high optimum salinity is interesting but occurs at too high a salinity to be used in the Wilmington field.

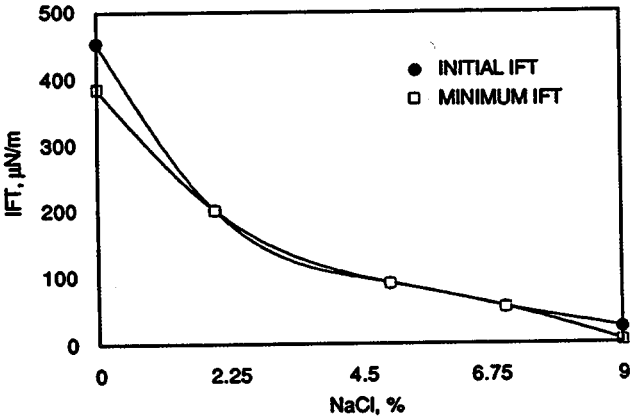

Fig. 3 Wilmington (California) crude oil salinity scan, 0.1% Igepon T-33 surfactant, 52°C, pH 8.2.

In the Igepon T-33 system, there was no correlation between measured IFT values and the results of dynamic phase behavior tests. There was, however, a correlation with the static phase behavior tests. At 7 and 9% NaCl concentrations, aqueous and oil phases showed considerable activity at the oil–water interface before the phases were dynamically shaken.

The IFT over a salinity range is shown in Fig. 4 for the system formulated at pH 8.2 with Igepal CA-720 surfactant. The IFT behavior of this system was similar to that of the Igepon T-33. The lowest IFT occurred at the highest salinity tested (7%), and the optimum salinity was

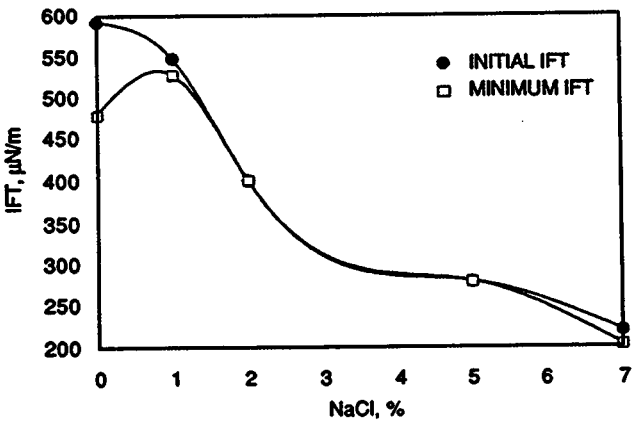

Fig. 4 Wilmington (California) crude oil salinity scan, 0.1% Igepon T-33 surfactant, 52°C, pH 8.2.

probably higher. There was no correlation between the measured IFT values and the results of either dynamic or static phase behavior tests, perhaps because no ultralow IFT values were obtained with this system.

Conclusions

Surfactant-enhanced alkaline flooding should be effective for the recovery of low-acid crude oils. Phase behavior tests are of limited value when designing a surfactant-enhanced alkaline flooding system for use with low-acid crude oils, and primary reliance should be placed on IFT measurements.

References

1. T. R. French, *Design and Optimization of Phosphate-Containing Alkaline Flooding Formulations,* DOE Report NIPER-446, September 1989.
2. T. R. French and T. E. Burchfield, *Design and Optimization of Alkaline Flooding Formulations,* paper SPE/DOE 20238, presented at the Seventh SPE/DOE Symposium on Enhanced Oil Recovery, Tulsa, Okla., April 22–25, 1990.

DEVELOPMENT OF IMPROVED MOBILITY CONTROL METHODS

Cooperative Agreement DE-FC22-83FE60149, Project BE4C

National Institute for Petroleum and Energy Research
Bartlesville, Okla.

Contract Date: Oct. 1, 1983
Anticipated Completion: Sept. 30, 1990
Funding for FY 1990: $200,000

Principal Investigators:
Troy R. French
Hong W. Gao

Project Manager:
Jerry F. Casteel
Bartlesville Project Office

Reporting Period: Jan. 1–Mar. 31, 1990

Objectives

The objectives of this project are to determine the applicability of low-molecular-weight polymer gels for mobility-control applications and the effects of permeability and depth of gel penetration on oil recovery efficiency.

Summary of Technical Progress

Screening tests showed that polymer gel systems prepared with a low-molecular-weight (400,000 daltons) polyacrylamide polymer that was 20% hydrolyzed gelled at a faster rate and retained higher gel strength than those prepared with a low-molecular-weight (400,000 daltons) polyacrylamide polymer that was 10% hydrolyzed. Under the screening conditions, no viscosity enhancement was observed in samples prepared with polymers having a degree of hydrolysis equal to or greater than 30%.

Simulation runs were performed with a quarter of a five-spot, two-layer reservoir model with $k_v k_h = 0.001$. Under the same simulated conditions, decreasing the ratio between the permeability in the top layer and that in the bottom layer decreased the fractional oil recovery. The simulation results showed that the fractional oil recovery is a function of the ratio of the permeability of the two layers but independent of the absolute values of each layer. This result holds true for both waterfloods and gel-treated waterfloods.

Application to EOR

Mechanical degradation of high-molecular-weight polyacrylamides is a problem in field applications. A mobility-control system based on cross-linking a low-molecular-weight polyacrylamide may be much less susceptible to mechanical degradation. A permeability modification simulator is very useful to facilitate the design of treatments and assess potential fields for permeability-modification treatments using gelled polymers.

Screening Tests

For the investigation of the effect of the degree of hydrolysis on gelation kinetics and gel strength, screening tests were conducted on samples prepared with four low-molecular-weight polyacrylamide polymers that were 10% (HPAM1), 20% (HPAM1-20), 30% (HPAM1-30), and 40% (HPAM1-40) hydrolyzed and a Cr(III) cross-linker in 53 meq/L NaCl (pH = 4.8) at room temperature, 22.4°C. The three polymers, HPAM1-20, HPAM1-30, and HPAM1-40, were prepared by hydrolyzing a low-molecular-weight polymer (HPAM1) in alkaline solutions[1] and purified by precipitation twice from aqueous solution. Polymer concentrations used in screening tests ranged from 13,000 to 17,000 ppm, and Cr(III) concentrations used ranged from 75 to 150 ppm. Before mixing, all stock solutions were adjusted to pH = 4.8. After mixing, samples were sealed under a nitrogen atmosphere and allowed to age with continuous agitation on a shaker. Viscosity measurements were used to monitor the process of gelation.

Results showed that with the concentrations of polymer and Cr(III) used, precipitate was formed in all samples prepared with HPAM1-40. Precipitate was also formed in samples prepared with HPAM1-30 at a polymer concentration of 13,000 ppm and Cr(III) concentrations greater than 100 ppm and at a polymer concentration of 15,000 ppm and Cr(III) concentrations greater than 150 ppm. For the samples prepared with HPAM1-20, precipitate formed only in two samples that contained 13,000 ppm of polymer and Cr(III) concentrations greater than 150 ppm. These results indicated that, at the same polymer concentration, the maximum concentration of Cr(III) that could be used to cross-link the polymers without forming precipitate in the solution decreased with the increase in the degree of hydrolysis.

Viscosity measurements on samples that did not form precipitate showed that no viscosity enhancement was observed in samples prepared with HPAM1-30. Viscosity enhancement was observed in samples prepared with HPAM1 and HPAM1-20, which were 10 and 20% hydrolyzed, respectively. Comparison of measured viscosities as a function of time showed that, at the same polymer and Cr(III) concentrations, the gel systems prepared with HPAM1-20 gave a faster rate of gelation reaction and stronger gel strength than those prepared with HPAM1. Typical results are shown in Figs. 1 and 2 for two gel systems (13,000-ppm polymer/100-ppm Cr(III) and 15,000-ppm polymer/100-ppm Cr(III). As shown in these two figures, gelation was complete within 3 d in samples prepared with HPAM1-20, which was 20% hydrolyzed, under continuous agitation. Gelation was also complete within 3 d in other samples prepared with HPAM1-20 under continuous agitation. Results also showed that gel strength increased with polymer concentration (Figs. 1 and 2) and Cr(III) concentration. Further gelation tests with a Brookfield viscometer will be conducted with samples prepared with HPAM1 and HPAM1-20 and compared with each other.

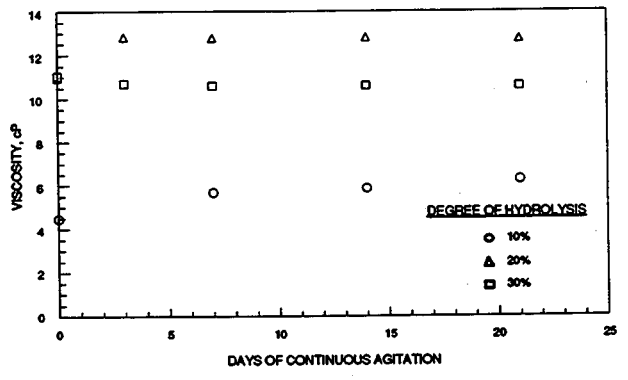

Fig. 1 Gelation as a function of time for gel systems prepared with polymers of different degrees of hydrolysis and aged with continuous agitation on a shaker at 22.4°C. Polymer concentration was 13,000 ppm, and Cr(III) concentration was 100 ppm in 53 meq/L NaCl, pH 4.8. Shear rate = 5.96 s^{-1}.

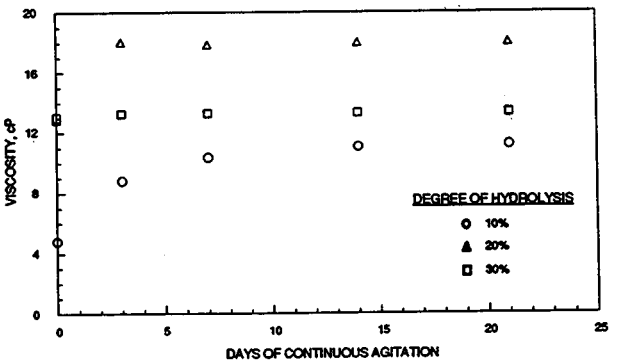

Fig. 2 Gelation as a function of time for gel systems prepared with polymers of different degrees of hydrolysis and aged with continuous agitation on a shaker at 22.4°C. Polymer concentration was 15,000 ppm, and Cr(III) concentration was 100 ppm in 53 meq/L NaCl, pH 4.8. Shear rate = 5.96 s^{-1}.

Permeability Modification

Three-dimensional simulation runs using a NIPER permeability-modification simulator were conducted on a quarter of a five-spot, two-layer reservoir model to investigate the effects of permeability and initiation time of a polymer gel treatment on oil recovery in a waterflood. The length and width of the reservoir model used was 1000 ft, and each layer was 15 ft thick. The oil viscosity was 3 cP, and water viscosity was 0.8 cP. The porosity was 20%. The slug size of the gel system injected was 0.0025 PV (1 yr = 0.1827 PV). Concentrations of the chemicals used were 3000 ppm for polymer, 1000 ppm for dichromate, and 1400 ppm for thiourea. Detailed fluid properties used in the simulation runs are listed elsewhere.[1]

In the simulation runs, the permeability in the top layer varied from 10 to 300 mD, and that in the bottom layer varied from 100 to 3000 mD. The ratio of the vertical permeability to the horizontal permeability was kept at a constant ($k_v/k_h = 0.001$). Results showed that at a constant ratio of k_1/k_2, where k_1 and k_2 are the horizontal permeabilities in the top and bottom layers, respectively, fractional oil recovery from a gel treatment in the injection well was not sensitive to the magnitudes of k_1 and k_2, as is shown in Fig. 3. This can be attributed to the very similar distributions of the residual resistance factor in all three reservoirs after the gel treatment. Similar distributions of residual resistance factor resulted in similar ratios of the horizontal permeabilities in two layers and similar water injection profiles in all three reservoirs (Table 1). Therefore oil recovery was about the same. Results also showed that fractional oil recovery from a waterflood at a constant ratio of k_1/k_2 was also insensitive to the magnitudes of the permeabilities in the two layers. Under all simulated conditions, an early start of the gel treatment resulted in an early increase in the incremental oil recovery. Typical results are shown in Fig. 4 for a reservoir having k_1 = 10 mD and k_2 = 100 mD.

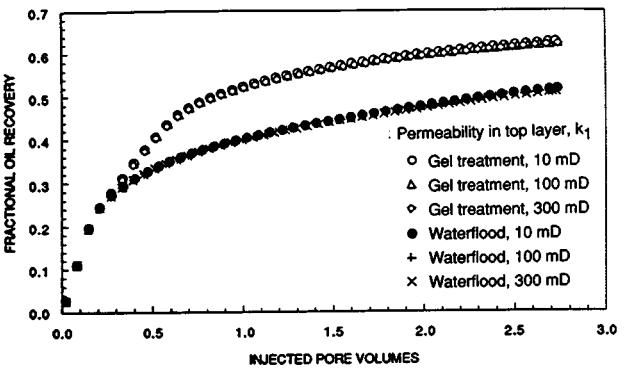

Fig. 3 Effect of permeability on oil recovery after a gel treatment in an injection well at k_1 (top layer)/k_2 (bottom layer) = 0.1; k_v/k_h = 0.001; 0.0025 PV of gel was initiated at 1 y; 1 y = 0.1825 PV.

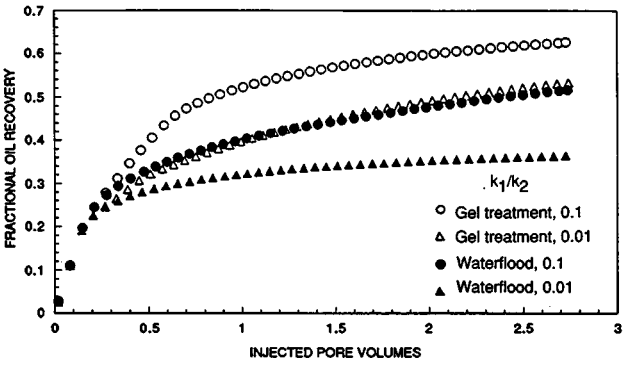

Fig. 5 Effect of k_1/k_2 on fractional oil recovery. k_1 (permeability in top layer) = 10 mD; k_v/k_h = 0.001; 0.0025 PV of gel was initiated at 1 y; 1 y = 0.1827 PV.

TABLE 1

Amount of Injected Water Flowing into the Top Layer in an Injection Well (STB/d)

Permeability of top layer–permeability of bottom layer, mD–mD	Days before gel treatment	Days after gel treatment								
		5	25	365	730	1461	2192	2923	4385	4785
300–3000	38	535	533	469	451	453	454	454	454	454
100–1000	31	535	533	470	451	453	454		454	454
10–100	25	535	533	453	450	452	453	453	454	454
10–1000	1	504	415	155	169	179	183	186	188	188

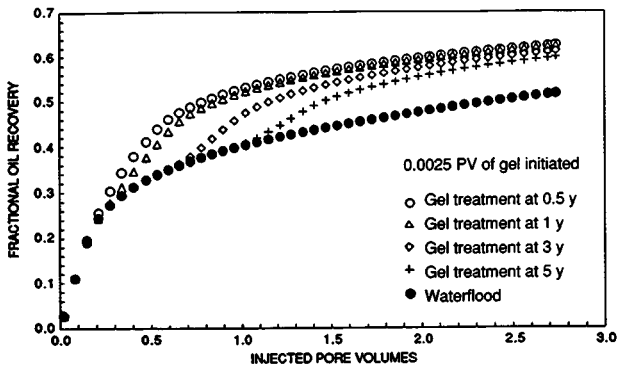

Fig. 4 Effect of initiation time of a polymer gel treatment in an injection well in a reservoir having horizontal permeabilities of 10 mD in the top layer and 100 mD in the bottom layer. k_v/k_h = 0.001; 1 y = 0.1825 PV.

Simulation runs were also conducted to investigate the effect of the ratio k_1/k_2 (0.1 and 0.01) on the fractional oil recovery. Results showed that fractional oil recovery from a gel treatment in the injection well increased with increasing k_1/k_2 (Fig. 5). This can be attributed to different water-injection profiles in these reservoirs. After the gel treatment, the amounts of the injected water that went to the top low-permeability layer decreased with decreasing k_1/k_2 (Table 1). Hence more oil in the top layer of the reservoir having a higher k_1/k_2 value was swept out than that in a reservoir having a smaller k_1/k_2 value. In all cases, gel treatments were effective in increasing incremental oil recovery over that of waterflood. Under simulated conditions, an early start of the gel treatment also resulted in an early increase in the incremental oil recovery regardless of the ratio of k_1/k_2, as shown in Fig. 6 for the reservoir having k_1 = 10 mD and k_2 = 1000 mD.

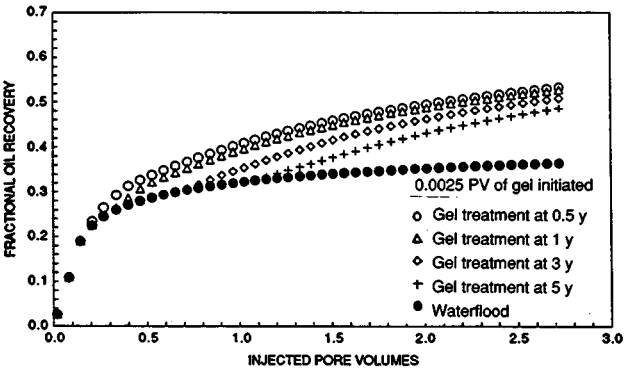

Fig. 6 Effect of initiation time of a polymer gel treatment in an injection well in a reservoir having horizontal permeabilities of 10 mD in the top layer and 1000 mD in the bottom layer. k_v/k_h = 0.001; 1 y = 0.1825 PV.

Reference

1. H. W. Gao and M. M. Chang, *A Three-Dimensional, Three-Phase Simulator for Permeability Modification Treatments Using Gelled Polymers*, DOE Report NIPER-388, March 1990.

GAS DISPLACEMENT— SUPPORTING RESEARCH

ENHANCED OIL RECOVERY MODEL DEVELOPMENT AND VALIDATION

Morgantown Energy Technology Center
Morgantown, W. Va.

FY90 Total Project Cost: $200,000

Principal Investigator:
Rodney A. Geisbrecht

Project Manager:
Royal J. Watts
Morgantown Energy Technology Center

Reporting Period: Jan. 1–Mar. 31, 1990

Objectives

Plans for FY 1990 are organized into corefloods, microvisual models, pore-level mechanistic modeling, and reservoir simulation techniques. Corefloods will primarily focus on the relative merits of ex situ and in situ foam generation with the possibility of measuring carbon dioxide (CO_2) flowing fraction under reservoir conditions. Pore-level network simulators will be used to explore basic mechanisms in foam flow, such as division, trapping, and mobilization. Microvisual models will be used in conjunction with network simulators and will also be used to screen surfactants on the basis of fluid–fluid interactions at reservoir conditions. Reservoir simulation techniques accounting for the fluid-flow instabilities associated with foaming flow (trapping) will be pursued.

Summary of Technical Progress

Background

Progress was made in two areas during the reporting period. First, a flow rule that describes formation of leave-behind lamellae in pore-scale network simulators was tested. In addition to accounting for experimentally observed mobility reductions, the simulations generated insights into the scaling laws that govern practical applications of the leave-behind mobility control technique. Second, a recent coreflood test of leave-behind mobility control in tertiary oil recovery was assessed. Oil recovery and relative permeability curves showed no interferences between mobility control and oil-recovery processes.

Mechanistic Models

In the limit of completely stable and immobile leave-behind lamellae, "foaming" surfactants have a predictable effect on the relative permeability of a nonwetting phase displacing a wetting phase. A leave-behind lamella forms in

the throat between two pores whenever nonwetting fluid invades a pore that is connected to another pore that is already filled by the nonwetting phase. The surfactant-stabilized leave-behind lamella block flow paths and thus create dendrites of trapped nonwetting phase which do not contribute to flow conductivity. These effects were replicated in two different stochastic, pore-scale network simulators (invasion percolation and diffusion-limited aggregation).

Relative permeability reduction factors were generated by normalizing the flow capacity with leave-behind lamellae to that without leave-behind lamellae. Predicted relative permeability reduction factors and corresponding leave-behind lamellae distributions are shown in Figs. 1 and 2. With bond mapping (mapping of pore throats through which flow occurs), as opposed to site mapping (mapping of pores filled with invading fluid), computer graphics were used to depict the patterns of leave-behind lamallae. Bond mapping is particularly effective with the complex leave-behind lamella distributions of large networks. For completely stable and immobile lamellae, bond maps correspond to modified Bethe trees—or mazes—whose singular paths could be traced either genealogically or through solution of the corresponding Laplace equation for flow through the nonuniform network of active and inactive bonds.

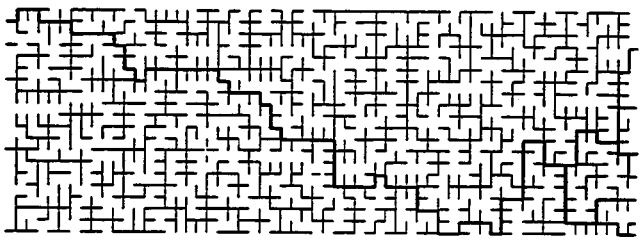

Fig. 1 Leave-behind according to invasion percolation model (Note: flow is from left to right, connected path is bold, and relative permeability reduction factor is 31.3).

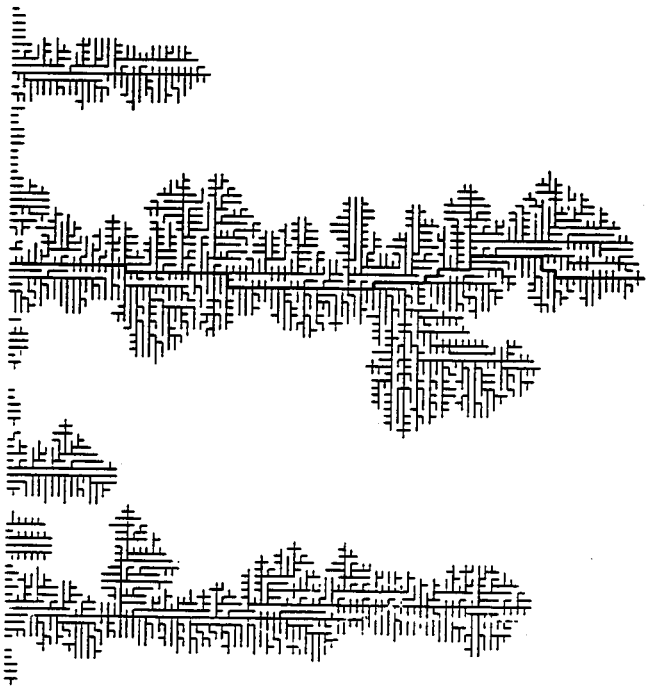

Fig. 2 Leave-behind according to diffusion limited aggregation model (Note: flow is from left to right, connected path is bold, and relative permeability reduction factor is 11.1).

Process Simulation

An assessment was made of a recently completed coreflood test of surfactant-based mobility control for dense CO_2 in a tertiary oil recovery mode (an oil-saturated porous medium was flooded in sequence by brine, surfactant solution, and CO_2). The test illustrates a base case in which no interferences between mobility control and oil recovery occurred.

Mobilized oil did not seriously destabilize leave-behind films vital to mobility control, as evidenced by a mobility reduction factor only partially less than that obtained in comparable experiments without oil. Leave-behind films did not significantly impede mass transfer vital to oil recovery, as evidenced by a recovery close to the theoretical maximum.

A 3.91- by 75-cm Berea core of 500-mD permeability was used for the test. Fluids included a 42.6 API mineral oil (Pennzoil's Penetech), a 2 wt % sodium chloride brine, and a 0.2 wt % solution in brine of an ethoxylated ammonium sulfate surfactant (GAF's Alipal CD-128). Recovery of waterflood residual oil was approximately 82.5% after 2.6 pore volumes (PV) of CO_2 were injected at 72°F and 1600 psi. The recovery curve indicated a two-component, immiscible extraction with a solvent-rich phase containing oil in the 2 mol % range. This is consistent with the expected phase behavior since the mineral oil used was a "white" paraffinic fraction in the C_{13} to C_{16} range. Confirming phase equilibrium calculations were made with a three-phase Peng–Robinson equation of state tuned to data[1] (interaction coefficient = 0.095) for the CO_2/n-$C_{16}H_{34}$ binary in the subcritical region as shown in Fig. 3 and Tables 1 and 2.

A subtle aspect of the recovery curve was its asymptotic behavior, leveling off at about 85% in this particular experiment. The asymptotic behavior may be the result of selective extraction of volatile oil components, incomplete sweep efficiency caused by gravity override or viscous fingering, or water shielding of isolated oil ganglia. Diffusion of oil species from dendrites of trapped nonwetting phase is an additional possibility when surfactants are used to control mobility. The mass transfer of trapped species out of a three-dimensional network of dendrites occupying a cylindrical region axisymmetric to a flowing channel conforms to the diffusivity equation in an annular region with closed outer boundary and constant potential on the inner boundary. The general solution was originally reported for the equivalent constant pressure well testing problem with a slightly compressible fluid.[2,3] The predicted

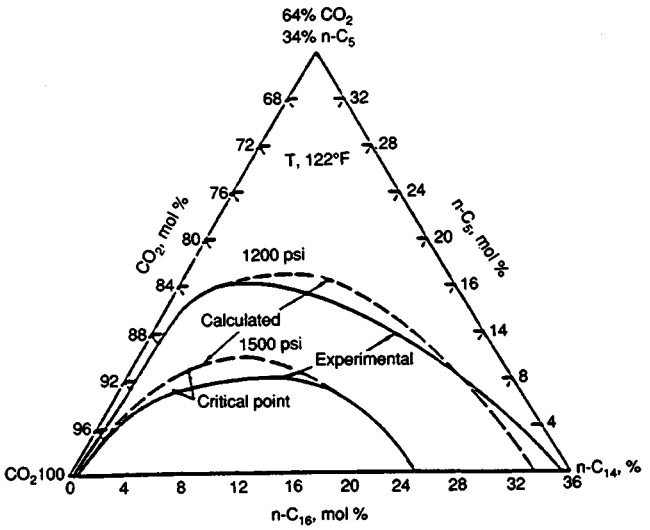

Fig. 3 CO_2/n-C_5/n-C_{16} ternary at 122°F.

TABLE 1

CO_2/n-C_{16} Binary at 122°F/1500 psi

```
SOLN METHOD (SSM=1, ASSM=2, NP=3): 1  ITMAX: 300
E/EV/ER/EL/EU:  0.10E-07  0.10E-01  0.60E+00  0.10E-04  0.10E-02
K-START (EXT=0, INT=1): 0
I-FAST (OFF=0, ON=1): 1
I-POWELL (OFF=0, ON=1): 0
 5
CO2          304.200    72.800     0.225    44.000
C13          675.800    17.000     0.623   184.000
C16          717.000    14.000     0.742   226.000
C15          707.000    15.000     0.706   212.000
C14          694.000    16.000     0.679   198.000
   0.00000   0.09500    0.09500    0.09500   0.09500
   0.09500   0.00000    0.00000    0.00000   0.00000
   0.09500   0.00000    0.00000    0.00000   0.00000
   0.09500   0.00000    0.00000    0.00000   0.00000
   0.09500   0.00000    0.00000    0.00000   0.00000
   323.000   102.000     0    0     0    0     0    0
   0.90000   0.00000    0.10000    0.00000   0.00000
CONVERGENCE AFTER 17 V-L ITERATIONS
INITIAL SSM ITS:  0  ASSM(NP) ITS:  0  SWITCHES:  0
VAP MOL FR:  0.608     VAP VOL FR:  0.543     VAP Z:  0.386
LIQ MOL FR:  0.392     LIQ VOL FR:  0.457     LIQ Z:  0.503
VAP MOL FRAC:
  0.9966  0.0000  0.0034  0.0000  0.0000
LIQ MOL FRAC:
  0.7500  0.0000  0.2500  0.0000  0.0000
```

TABLE 2

CO_2/n-C_{16} Binary at 72°F/1600 psi

```
SOLN METHOD (SSM=1, ASSM=2, NP=3): 1  ITMAX: 300
E/EV/ER/EL/EU:  0.10E-07  0.10E-01  0.60E+00  0.10E-04  0.10E-02
K-START (EXT=0, INT=1): 0
I-FAST (OFF=0, ON=1): 1
I-POWELL (OFF=0, ON=1): 0
 5
CO2          304.200    72.800     0.225    44.000
C13          675.800    17.000     0.623   184.000
C16          717.000    14.000     0.742   226.000
C15          707.000    15.000     0.706   212.000
C14          694.000    16.000     0.679   198.000
   0.00000   0.09500    0.09500    0.09500   0.09500
   0.09500   0.00000    0.00000    0.00000   0.00000
   0.09500   0.00000    0.00000    0.00000   0.00000
   0.09500   0.00000    0.00000    0.00000   0.00000
   0.09500   0.00000    0.00000    0.00000   0.00000
   295.000   110.000     0    0     0    0     0    0
   0.90000   0.00000    0.10000    0.00000   0.00000
CONVERGENCE AFTER 23 V-L ITERATIONS
INITIAL SSM ITS:  0  ASSM(NP) ITS:  0  SWITCHES:  0
VAP MOL FR:  0.599     VAP VOL FR:  0.415     VAP Z:  0.258
LIQ MOL FR:  0.401     LIQ VOL FR:  0.585     LIQ Z:  0.543
VAP MOL FRAC:
  0.9881  0.0000  0.0119  0.0000  0.0000
LIQ MOL FRAC:
  0.7682  0.0000  0.2318  0.0000  0.0000
```

time for recovery of 90% of trapped species is estimated to be at least on the order of 1 h without taking into account tortuosity. Although this time scale is short in field scale, a careful interpretation of laboratory-scale experiments in which dendritic trapping is an important aspect may be required.

References

1. R. K. Mehra, R. A. Heidemann, and K. Aziz, *Soc. Pet. Eng. J.*, 2: 66 (February 1982).
2. H. S. Carslaw and J. C. Jaeger, *Conduction of Heat in Solids*, Sec. 13.4, p. 332, *Oxford University Press*, New York, 1959.
3. A. T. Chatas, cited in Katz et al., *Handbook of Natural Gas Engineering*, p. 412, McGraw Hill Book Co., New York, 1953.

QUANTIFICATION OF MOBILITY CONTROL IN ENHANCED RECOVERY OF LIGHT OIL BY CARBON DIOXIDE

Morgantown Energy Technology Center
Morgantown, W. Va.

FY90 Total Project Cost: $550,000

Principal Investigator:
Duane H. Smith

Project Manager:
Royal J. Watts
Morgantown Energy Technology Center

Reporting Period: Jan. 1–Mar. 31, 1990

Objectives

The current objective of the Morgantown Energy Technology Center (METC) enhanced oil recovery (EOR) research is to conduct experimental and theoretical studies to improve the recovery efficiency of the carbon dioxide (CO_2) miscible flooding process. Since reducing the mobility ratio seems to provide efficient flood performance, the research is being directed to the study and use of viscous CO_2. The technique involves the use of surfactants to generate a CO_2 dispersion that would retard the growth of viscous fingers and also act as an in situ diverting agent. The merits of CO_2 dispersion will be determined by performing linear core-flow studies on large-scale systems. This effort will be supplemented by theoretical and experimental studies of CO_2 dispersions, studies of the effects of altered wettability of rock surfaces, and determination of in situ saturation profiles as probed by X-ray computerized tomography (CT) and nuclear magnetic resonance (NMR) imaging. The laboratory data will also be used to test the METC composition model, and the model will be used to plan critical experiments.

Summary of Technical Progress

The foams (or emulsions) created by capillary snap-off in CO_2 mobility control commonly produce pressure gradients in excess of 500 psi/ft in steady-state relative permeability measurements.[1] Pressure gradients of this magnitude are far too large for use in the field to modify CO_2 mobilities and could even hinder the use of CO_2 foams as blocking agents by making it difficult to inject the foaming agent.

Hence, as part of the search for ways to avoid excessive near-well pressure gradients from CO_2 dispersions, a systematic study of the relationships among phase behavior, fluid saturations, and dispersions (i.e., emulsion and foam) morphologies is being conducted.[2–7] Also, the flow properties of CO_2 foams (at typical miscible-flood pressures) are being studied to better characterize their utility for field processes.

Flow Rate–Pressure Drop Relationships for CO_2 Foam Flow at Reservoir Pressure

Pressure drops that result from foam flow at different frontal advance rates were measured in fired Berea core, at 72°F and a back pressure of 1540 psi. The test employed a 2.5-cm-diameter by 3.9-cm-long core with an absolute permeability for water of 60 mD. The foam was generated by simultaneous injection of CO_2 and surfactant solution (0.1 wt % Alipal CD-128 in 2 wt % NaCl brine) at a fractional flow of CO_2 of 0.88. Pressure drop readings were taken when steady-state was reached. The results are presented in Fig. 1 as a plot of logarithm of the pressure gradient vs. logarithm of the frontal advance velocity. The following power–law relationship was obtained from a fit to the data:

$$(dp / dl) = 2.45\ V^{0.73} \qquad (1)$$

where (dp / dl) is the pressure gradient across the core at steady-state flow (MPa/m) and V is the Darcy (superficial) velocity (m/d).

The value of the exponent in Eq. 1 is close to the theoretical value of 0.66 (Ref. 8) for bubble flow in smooth capillaries. Within the experimental uncertainties, it is identical to the value of 0.71 measured for the flow of N_2 foams in sandstone.[9]

The pressure drop vs. velocity can be converted to a shear stress vs. shear rate relationship; thus, the apparent viscosity, U, can be written as:

$$U_{app} = KV^{n-1} \qquad (2)$$

where n = 0.73 and K is a constant. When treated as a single phase, foam seems to behave as shear-thinning fluid (apparent viscosity decreases as the shear rate or flow velocity increases) when the fractional flow of CO_2 (inlet foam quality) is maintained constant. Although Eq. 2 can be useful, one should remember that the macroscopic pressure drop depends on microscopic, pore level events that are not yet completely elucidated.[10]

For easier comparison with field practice, Figs. 2 and 3 replot the data from Fig. 1 in terms of apparent viscosity vs. velocity, and mobility vs. velocity (in customary units). Figure 2 indicates that lower apparent viscosities are found at high superficial velocities. However, the decrease may be too small to significantly improve foam injectivity.

Mobility Control by Means of Low Molecular Weight Surfactants

The use of low molecular weight surfactants at concentrations below their critical micelle concentrations may prove to be the most effective way to improve CO_2 mobility control. These materials may make it possible to use foams and/or other types of true fluid dispersions without creation of excessive pressure gradients. Studies of low molecular weight anionic surfactants have been reported

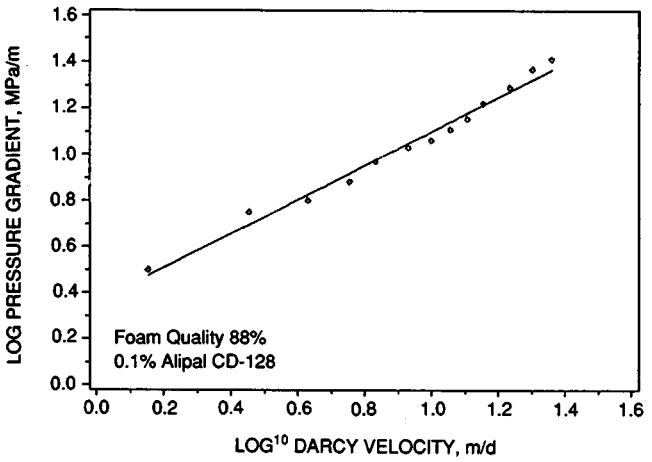

Fig. 1 Demonstration that the pressure gradient from a flow of a CO_2 foam depends exponentially on the flow rate and measurement of the exponent and preexponential factor.

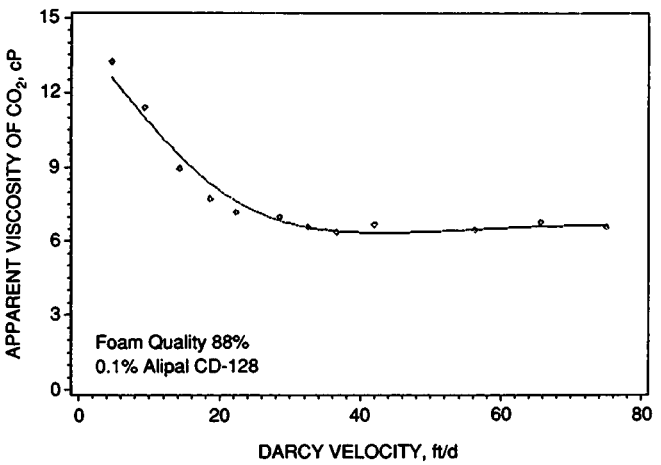

Fig. 2 Apparent viscosity when the foam of Fig. 1 is treated as a single fluid.

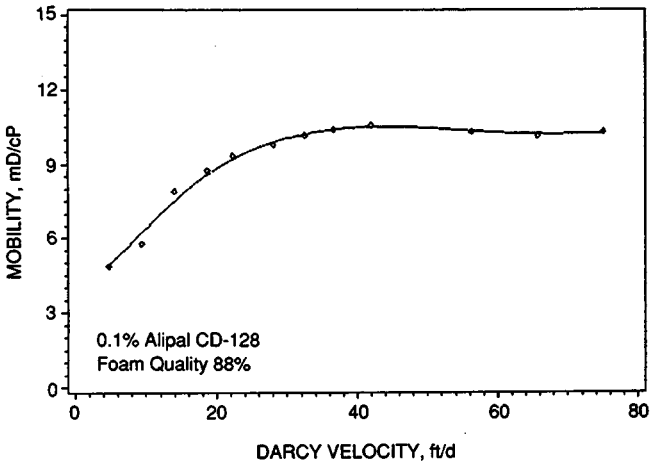

Fig. 3 Fluid mobility when the foam of Fig. 1 is treated as a single fluid.

in the literature;[11] this laboratory has been investigating low molecular weight nonionic surfactants.[2–7].

One of the concerns with any foaming agent is its formation of emulsions when the surfactant solution mixes with oil. An advantage of low molecular weight nonionic surfactants is that their emulsions are relatively unstable. Nevertheless, it is important to determine what emulsion morphologies (e.g., oil-in-water or water-in-oil) will form as a function of reservoir parameters such as temperature and oil saturation. This information is summarized by the dispersion morphology diagram, which is somewhat like a phase diagram, except that it gives not only the amounts and compositions of the phases, but also their state of physical dispersion.

It is widely claimed that below a certain temperature, called the phase inversion temperature (PIT), all emulsions are oil-in-water and that above this temperature all emulsions are water-in-oil. Previously this belief was shown to be incorrect for the compounds studied when the phase saturations change at constant temperature.[2–5].However, because the PIT is measured by changes of temperature at constant composition, previous studies left open the possibility that the emulsion behavior might be path dependent (i.e., for a given temperature and fluid saturation, the emulsion morphologies produced by changes of saturation at constant temperature might be different from those produced by change of temperature at constant system composition).

Phase inversion temperature (PIT)-type measurements have been made, with the temperature at constant system composition and with the use of only compositions for which the number of phases always remained two.[12](The concentration of surfactant in the 2-butoxyethanol/decane/10 mM NaCl brine mixtures was less than the minimum needed to form a middle phase.) Figure 4 shows the emulsion morphology as a function of temperature and saturation (i.e., volume fraction) of the

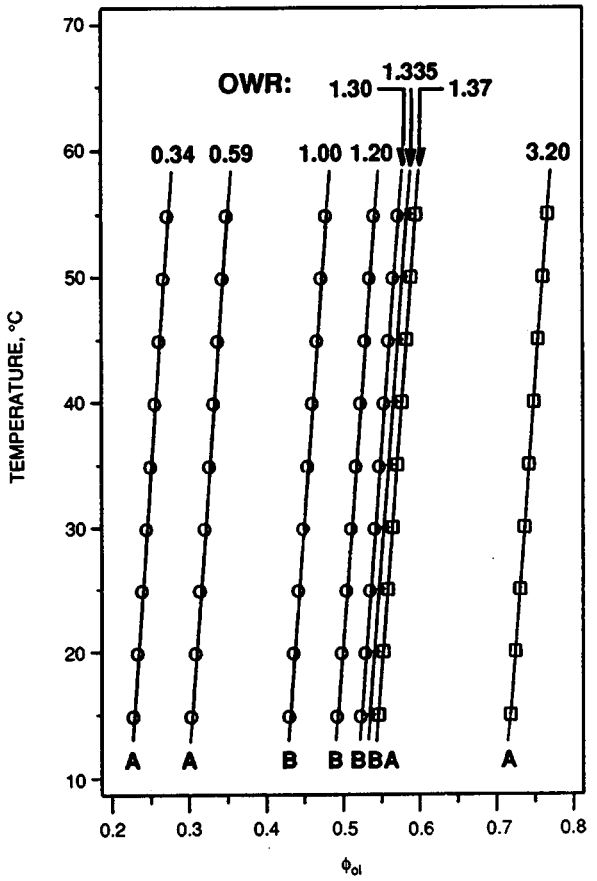

Fig. 4 Emulsion morphology as a function of temperature and saturation of the oleic phase for a series of 2-butoxyethanol/decane/water mixtures of constant compositions. Squares, water-in-oil emulsions; circles, oil-in-water emulsions.

oleic phase for a series of mixtures. (The lines showing the experimental paths are slightly tilted because the thermal expansivities of the conjugate phases are slightly different and the phase compositions also change slightly with temperature.) The squares indicate water-in-oil emulsions, whereas the circles denote oil-in-water emulsions. (The morphologies were determined from the electrical conductivities of the emulsions.)

As illustrated by Fig. 4 (Ref. 12), at relatively large ratios of aqueous phase to oleic phase, the morphology was oil-in-water at all temperatures. This was true regardless of whether the temperature was below, above, or within the temperature range at which three phases would have formed at larger surfactant concentrations. Similarly, at relatively large ratios of oleic phase to aqueous phase, all emulsions were water-in-oil, regardless of temperature. Hence, at least for this particular combination of low molecular weight nonionic mobility control agent and light oil, the PIT idea is incorrect. Regardless of whether the temperature is below or above the PIT, either oil-in-water or water-in-oil emulsions may form, and the choice depends on the oil and water saturations.

References

1. H. O. Lee and J. Heller, *Laboratory Measurements of CO_2-Foam Mobility*, SPE/DOE 17363, presented at the SPE/DOE Sixth Symposium on Enhanced Oil Recovery, Tulsa, Okla., April 17–20, 1988.
2. D. H. Smith and K.-H. Lim, A Phase and Electrical Conductivity Study of Model Oilfield Dispersions, SPE 18496, *Proceedings of the SPE International Symposium on Oilfield Chemistry, Houston, Tex., Feb. 8–10, 1989*, Society of Petroleum Engineers, Richardson, Tex., (August 1990) (in press).
3. U.S. Department of Energy, Enhanced Oil Recovery Group *Enhanced Oil Recovery, Progress Review No. 58*, Quarter Ending March 31, 1989, DOE/BC-89/2.
4. U.S. Department of Energy, Enhanced Oil Recovery Group *Enhanced Oil Recovery, Progress Review No. 60*, Quarter Ending September 30, 1989, DOE/BC-89/4.
5. D. H. Smith and K.-H. Lim, Morphology and Inversion of Dispersions of Two Fluids in Systems of Three and Four Thermodynamic Dimensions, *J. Phys. Chem.* 94: 3746 (1990).
6. D. H. Smith and K-H. Lim, An Experimental Test of Catastrophe and Critical-Scaling Theories of Emulsion Inversion, *Langmuir* (1990) (in press).
7. K.-H. Lim and D. H. Smith, Electrical Conductivities of Concentrated Emulsions and Their Fit by Conductivity Models, *J. Dispersion Sci. Technol.* (1990) (in press).
8. G. J. Hirasaki and J. B. Lawson, Mechanism of Foam Flow in Porous Media: Apparent Viscosity in Smooth Capillaries, *Soc. Pet. Eng. J.*, 176-190, (April 1985).
9. F. Friedman, W. H. Chen, and P. A. Gauglitz, *Experimental and Simulation Study of High-Temperature Foam Displacement in Porous Media*, SPE/DOE 17357, presented at the SPE/DOE 6th Symposium on Enhanced Oil Recovery, Tulsa, Okla., April 17–20, 1988.
10. D. H. Smith, (Ed.), *Surfactant-Based Mobility Control: Progress in Miscible Flood Enhanced Oil Recovery*, American Chemical Society, Washington, D.C., 1988.
11. M. I. Kuhlman et al., *Carbon Dioxide Foams with Surfactant Used Below Their Critical Micelle Concentrations*, SPE/DOE 20192, presented at the SPE/DOE Seventh Symposium on Enhanced Oil Recovery, Tulsa, Okla., April 22–25, 1990.
12. D. H. Smith and K.-H. Lim, Temperature Dependence of Emulsion Morphologies and the Dispersion Morphology Diagram, *J. Phys. Chem.* (submitted for publication).

ENHANCED OIL RECOVERY SYSTEMS ANALYSIS

Morgantown Energy Technology Center
Morgantown, W. Va.

FY90 Total Project Cost: $150,000

Principal Investigators:
James R. Ammer
Allen C. Brummert

Project Manager:
Royal J. Watts
Morgantown Energy Technology Center

Reporting Period: Jan. 1–Mar. 31, 1990

Objectives

The overall goal of the Systems Analysis Project is to incorporate results of laboratory investigations, model enhancements, and field experimental work into a systems approach to predict oil recovery and to estimate the increase in reserves for improved technology.

Specific objectives for FY90 include:

1. *Advanced Technology Assessment Study in the Delaware Basin*—Screening criteria will be used to select reservoirs amenable to carbon dioxide (CO_2) miscible enhanced oil recovery (EOR). These reservoirs will be categorized using the CO_2 predictive model (CO2PM) to identify the increase in reserves that results from applying advanced technologies.

- Screen reservoirs to determine the applicability of CO_2 miscible EOR.
- Collect and input reservoir data for use in CO2PM.
- Categorize reservoirs on the basis of physical and geological characteristics.
- Select a representative reservoir from each category for simulation studies.
- Review CO2PM and recommend changes for modeling advanced technologies. Specific technologies being investigated are horizontal wells and CO_2–foam.

2. *University of Wyoming Horizontal Well Study*—Validate laboratory results through history matching and conduct optimization studies for field-scale floods.

- Investigate if viscous fingering affected laboratory results.
- History match laboratory results.

3. *Simulation Studies*—Two field simulation studies are being conducted to obtain a better understanding of the CO_2 displacement process. Once a history match has been obtained on these fields, the application of advanced technologies can be investigated through simulation studies that benefit from having a more accurately defined reservoir.

- Industry Cooperative Simulation Study
  - — Match the primary production history.
  - — Match the waterflood history.
- Griffithsville Simulation Study
  - — Match the waterflood history.
  - — Match the CO_2 tertiary flood history.

Summary of Technical Progress

Advanced Technology Assessment Study in the Delaware Basin

A literature search and study of geologic maps was continued to determine what oil fields exist in the Delaware Basin and to gather physical and geologic data about each field. To date, 152 oil fields have been identified. The Petroleum Information (PI) Well History Control System Permian Basin data tapes are currently being reviewed to identify any additional fields and collect data. The PI Permian Basin data are stored on 15 tapes, of which 9 have been searched. The Texas Railroad Commission was contacted and will be sending a copy of their most recent annual report as well as their survey of enhanced recovery operations. The New Mexico Oil Conservation was contacted and indicated that all the New Mexico data are available from PI.

Model development work to incorporate mobility control with CO_2–foam into CO2PM was initiated. The model is being based on the fractional flow theory to be consistent with the existing CO2PM code. Literature is being reviewed for information on related processes (e.g., micellar–polymer flooding).

University of Wyoming Horizontal Well Study

Sensitivity runs were made with a test version of the Computer Modeling Group's (CMG's) compositional simulator (which has the capability to model viscous fingering) for values of the fingering parameter (beta) = 1000, 100, 10, and 1 for both the horizontal and vertical injection well scenarios. Predicted oil recovery for a horizontal well run having a beta = 10 fell within 5% of the experimental results. Predicted oil recovery for a vertical well run with beta = 1 fell within 10 to 15% of the experimental results. Simulations with beta values of 100 and 1000 produced results nearly identical to CMG's compositional model without fingering. Simulations are currently being made for the vertical scenario to investigate the grid orientation effect.

An abstract, titled *Modeling the Performance of Horizontal Injection Wells in Carbon Dioxide Miscible Displacement Processes,* was written and submitted to the Reservoir Simulation Symposium. The abstract discusses the modeling work of the University of Wyoming laboratory experiments.

Industry Cooperative Simulation Study

Additional grid blocks were added to the northwest corner of the field to provide pressure support to wells in the area. This helped to raise simulator-predicted pressure so that all wells in the field had a higher simulator-predicted pressure compared to field-measured pressure. Thus global changes can be made to the field without adversely affecting wells in the northwest corner.

A simulation run was then completed in which the absolute permeability was reduced field wide by 20%. This increased the accuracy of the pressure matches for several more wells. However, there are still several wells with poor pressure matches. Therefore it was decided to proceed to the saturation match, water/oil and gas/oil ratios, to determine if enough gas is being produced from the field since only liquid (oil and water) rates can be specified in CMG's black oil model.

Griffithsville Simulation Study

Work continued on preparing a technical note on the Griffithsville study.

IMPROVEMENT OF CO_2 FLOOD PERFORMANCE

Contract No. DE-FC21-84MC21136

New Mexico Institute of Mining and Technology
Petroleum Recovery Research Center
Socorro, N.Mex

Contract Date: April 1984
Anticipated Completion: September 1990

Total Project Cost:

DOE	$1,615,000
State of New Mexico	981,000
Industry	1,366,000
Total	$3,962,000

Principal Investigators:
John P. Heller
F. David Martin

Project Manager:
Royal J. Watts
Morgantown Energy Technology Center

Reporting Period: Jan. 1–Mar. 31, 1990

Objectives

The research to be performed in this project is intended to produce quantitative measurements of the influence of CO_2 flood performance of the following:

- Displacement with pure and impure CO_2.
- Evaluation and improvement of flow uniformity.

The experimental investigations and accompanying analysis and interpretation are designed to build understanding of fundamental physical mechanisms as a basis for improved performance prediction and for optimization of process performance.

Task 1: Displacement with Pure and Impure CO_2

The study of the effects of small amounts of impurities (N_2, C_1, C_2, and C_3) in the CO_2 stream on phase behavior and fluid properties of CO_2–crude oil systems has been initiated this quarter. Ten continuous phase equilibrium (CPE) runs are scheduled with a recombined Wasson San Andres crude oil sample from the Willard Unit Well No. 279 (ARCO). Run conditions range from 1500 to 2000 psia at 105°F with ~10 mol % contamination of the CO_2.

Previous research at the Petroleum Recovery Research Center (PRRC) involved static phase behavior measurements with a crude oil from the Wasson field in Gaines and Yoakum Counties, Tex. Experiments were performed with a stock tank oil and two recombined oil mixtures containing 312 and 602 scf/bbl of solution gas at varying temperatures. New experiments are being planned using the recombined Wasson oil with 312 scf/bbl of solution gas. Dynamic phase behavior measurements will be made, and slim-tube experiments are scheduled to determine the minimum miscibility pressure of the recombined oil with pure CO_2. Additionally, pressure–temperature scans will be performed with varying amounts of CO_2 to visually confirm the appropriate three-phase boundary.

In the area of micromodel studies, flow visualization experiments have been conducted in the high-pressure micromodel apparatus to study the effect of pregenerated foam injections (PRE) on oil recovery in the modified layered micromodel (MLAY). Initial saturation was Maljamar separator oil with connate water. Results from these displacements are compared to previous experiments involving simultaneous injection of CO_2 and surfactant solution (SAG) into the MLAY micromodel saturated with Maljamar separator oil with connate water. Operating conditions for the displacements were 1320 psig and 90 ± 0.1°F. Pregenerated foam was produced by simultaneous injection of CO_2 and surfactant solution into a Berea sandstone core; the resulting foam was then injected into the micromodel. Three gas/liquid ratios were used, and all exhibited similar results after 1.5 pore volumes injected (PVI) with over 95% recovery after 2.5 PVI. Comparing the PRE displacements with the SAG displacements shows that the PRE displacements had higher oil recoveries, caused by the high-density foam that consistently blocked pores and caused excellent fluid diversion.

In the previous corefloods using the CO_2 foam coreflood apparatus, the experiments were run in the absence of oil. This was intended to determine the maximum mobility reductions caused by foam without the deleterious effect of oil. During last quarter, the experiments were run for the purpose of displacing oil from the cores. Six experiments were run. In the first two experiments, brine was displaced from a homogeneous core with simultaneous injection of CO_2 and brine, and with CO_2 and surfactant solution. In two other experiments, oil was displaced from the same homogeneous core with simultaneous injection of CO_2 and brine, and with CO_2 and surfactant solution. In two more experiments, corefloods were performed with a heterogeneous core of Berea that had a concentric hole in the middle filled with sand.

In the investigation of the effect of free and solution gas on the development of miscibility, the Peng–Robinson Equation of State (PREOS) was used to model the fluid properties of Wasson crude oil. The approach in this work was to obtain an optimal match between the PREOS calculations and the available experimental data by adjusting the equation of state (EOS) parameters. The heptanes plus (C_{7+}) were grouped into five pseudocomponents. The critical properties, the acentric factors, and the binary interaction coefficients for each pseudocomponent group were obtained from the available correlations. The EOS parameters were systematically adjusted until a selected set of parameters was obtained to provide the best match with the experimental pressure–composition data.

During this quarter, the mechanistic foam flood simulator was used to perform a history match with one of the CO_2 coreflood experiments to determine the model parameters. This experiment was conducted at 100°F and 1000 psig with a flow rate of 75 cc/h. The CO_2 and surfactant solutions were simultaneously injected into a Berea core, initially saturated with 1% NaCl brine, with a volumetric ratio of 2:1. The simulation results matched well with the experimental results. Using the matched parameters, the simulator was then used to predict liquid production and pressure drop history for comparison with the results of a foam coreflood experiment. This experiment was performed at a flow rate of 62.5 cc/h with a gas/liquid volumetric ratio of 4:1. Simulation and experimental results were in good agreement for pressure drop and liquid production. To find the optimal values for the model parameters used in the simulator, sensitivity analyses will be continued. The model description and user's manual for the mechanistic foam simulator (MFS 2.1) have been completed as a separate report and have been distributed to supporters of this project.

Task 2: CO_2 Mobility Control and Flow Heterogeneities

Task 2 of this project consists of three interrelated topics with common relevance to the degree of uniformity in flow and displacement. Special emphasis is placed on the recovery efficiency of CO_2 floods. The first of the topics is directly concerned with various aspects of the heterogeneity of reservoir rock, while the second and third topics involve the development of methods of mobility control, especially

for CO_2 floods. Significant progress has been made in each area during this quarter. This work is briefly described.

Rock Heterogeneity

The research on rock heterogeneity includes investigation of the statistical properties of generated or synthetic fields and has produced results of interest in the wider domain that has come to be known as reservoir characterization. A paper, entitled *Generation and Testing of Random Fields and the Conditional Simulation of Reservoirs* has been prepared for presentation at the International Technical Meeting of the Petroleum Society of CIM/SPE in Calgary, Canada. This presentation will compare three current methods by which synthetic random fields are generated and will also demonstrate a mathematical procedure by which these fields can be "conditioned" to take into account (or "honor") known data. A two-dimensional (2-D) conditional simulation has been developed to investigate the effect of conditioning, using the fluid flow simulator developed at New Mexico Tech. During this quarter, some effort was also made to develop PC software by which to display quantitative color contour maps of the permeability or corresponding covariance fields. Examples of these images have been prepared for presentation at the Calgary meeting. This work also investigates the classical statistical properties of actual reservoir rocks and their mathematical representation. In particular, the form of permeability distribution that occurs in nature has been of continuing interest. Although some doubt exists about the general nature of the distribution, statistical tabulations have frequently found log-normal distributions of permeability within well-defined horizons or groups of similar sediments. In each of the three methods for generating synthetic fields [the Source Point Method, the Fast Fourier Transform Method, and the Turning Bands Method (TBM)], it is possible to specify in advance the form of the overall distribution desired. Research confirmed that the actually generated distribution matched the desired log-normal form in all of the cases. It has become apparent as a result of this work and previous research that statistical symmetry of the spatial correlation structure is also important to examine and, on this criterion, it seems that one of the methods for generating synthetic fields (the TBM) often introduces unwelcome artifacts.

Of interest to many is the work aimed at the production of a set of "type curves" by which a field operator could interpret the produced tracer concentration curves in terms of the geostatistical heterogeneity parameters. Some novel numerical simulation techniques are employed in the calculations. These procedures include the generation of synthetic, heterogeneous permeability fields, followed by deterministic solution of the pressure field by a finite-difference calculation. The flow of the fluid-carrying tracer is represented by the motion of isoconcentration lines. This work will also be presented in a national meeting, that of the American Geophysical Union in Baltimore, Md. The presentation is entitled "Quantifying Permeability Heterogeneity Using an Improved Numerical Simulation of a Field Tracer Test."

Laboratory-scale heterogeneities are also being studied, using a variety of techniques.

Mobility Control—Direct Thickeners

In this quarter, major emphasis has been placed on the synthesis of a special new class of the associative "Method II" polymers. These terminally functionalized polymers are called "telechelic ionomers." In them, functional groups are selectively placed at the ends of the polymer chains. Thus, when such ionomers associate in solution in a nonpolar fluidlike dense CO_2, they produce longer and more hydrodynamically active aggregates much more efficiently.

Because of the great sensitivity of polymer solubility in CO_2 to molecular weight, it is important to produce polymers of the greatest chain length consistent with solubility requirements, and thus to synthesize a distribution of molecular weights as narrow as possible.

Controlled synthesis of well-defined polymer structures is required to achieve these objectives. Precisely defined networks may be obtained by use of so-called inifer methods of end-linking the prepolymers, capped with a suitable functional group such as chlorine. The prepolymers are dehydrochlorinated to produce polymers with terminal double bonds that direct the attack of sulfonic acid groups. These sulfonated polymers are then neutralized with metal hydroxides or acetates to yield sulfonated telechelic polymers.

As examples of these, the solubility of a number of telechelic ionomers has been synthesized, characterized, and tested during this quarter. This required the preliminary synthesis of "initiators" such as 1,4-bis(1-hydroxyl-1-methylethyl) benzene (Binifer) and 1,3,5-tris(1-chloro-1-methylethyl) benzene (Trinifer). These polyfunctional initiators are called "inifers" (initiator-transfer agents). The polymerizations were carried out under an inert (nitrogen) atmosphere in dicloromethane at moderately low (–65 and –40°C, respectively) temperatures and stopped by the addition of methanol.

Polymers have been characterized by the use of Fourier Transform Infrared (FTIR) Spectrometry, Vapor Pressure Osmometry (VPO) Spectrometry, and Gel Permeation Chromatography (GPC). The infrared (IR) spectra show characteristic absorption bands corresponding to the chlorine, aromatic, and sulfonate groups that make it possible, by analyzing intermediate products, to follow the progress of the synthesis procedures. The GPC and VPO data enable the molecular weight distributions and the number average molecular weights of the products to be measured.

Mobility Control—CO_2–Foam

The second means of mobility control for CO_2 floods is the use of CO_2–foam. Research and development work on

the use of this additive has reached the stage of application. Current work is directed at the enlargement of the database through the testing of more diverse core material and surfactants.

One of the most economically important properties of the surfactants is the extent of their adsorption onto the pore walls of reservoir rock. To determine this, a dynamic adsorption experiment has been used. In this procedure, a small slug of surfactant solution is introduced into the input stream during flow of brine through a core. The measurement of surfactant concentration as a function of time then provides data by which both the chromatographic delay and the surfactant retention or irreversible adsorption can be calculated.

During the past quarter, experimental capabilities for the measurement of surfactant concentration in the effluent stream from the core have been redesigned. Experiments have been performed on two methods for conducting this analysis—by the measurement of ultraviolet (UV) absorption of characteristic chromophores or light-absorbing groups in the surfactant molecules, and by the direct measurement of the surface tension of the effluent by a modified drop-weight method (MDWM). Although the direct application of the first method is possible only for certain surfactants (such as those containing aromatic rings or unsaturated bonds), it seems possible to find chemicals that can combine chemically with other surfactants to form distinctive chromophores. Some candidate chemicals have been examined for this property but at this time none that could be used have been found.

On the other hand, the MDWM seems to be quite practical, at least for surfactant concentrations below the critical micelle concentration (CMC). It is necessary, in the use of this method, to maintain a constant flow rate (or at least a rate known with better-than-usual precision) through the core. This is because the MDWM involves only the measurement of time intervals between the emerging drops and does not distinguish between variations in the rate and the expected signal, the variations in surface tension of the liquid produced from the core. An apparatus has been constructed so considerable precision can be maintained, both in the measurement of interdrop intervals and in the elimination of rate fluctuations.

During this quarter, the foam durability apparatus has been used to test two new surfactants. This apparatus enables the production and observation of CO_2–foam at reservoir conditions of temperature and pressure. Both of the surfactants tested recently are manufactured by Chevron Chemical Company. The first of these, Chevron Chaser CD1040, is a brine-tolerant sulfonate surfactant designed for use in sandstone reservoirs at temperatures up to 93°C. The second surfactant, Chevron Chaser CD1050, is also specified as brine tolerant but has been designed specifically for carbonate reservoir CO_2 floods.

Measurements of the interfacial tension (IFT) between the dense CO_2 and several surfactant concentrations, prepared in a 1% brine solution, were conducted at 40°C and 2500 psi. Values for the CMC of the surfactants under these conditions were also obtained from these measurements. The CMC of Chevron Chaser CD1040 was determined to be about 0.15 wt % and that of CD1050 about 0.05 wt %.

The decay of foam as a function of time can also be measured in this apparatus. In contact with the mixed brine used in these experiments (0.5% NaCl and 0.5% $CaCl_2$), CO_2–foam produced by the CD1050 was much longer lasting at all surfactant concentrations than that produced by CD1040 solutions. Although the measurements are interesting, it is uncertain what standards should be applied in this area, other than a minimum requirement that the CO_2 bubbles should not coalesce immediately on contact with each other—that is, that the foam should persist for at least a few minutes.

FIELD VERIFICATION OF CO_2–FOAM

Contract No. DE-FG21-89MC26031

New Mexico Institute of Mining and Technology
Petroleum Recovery Research Center
Socorro, N. Mex.

Contract Date: September 1989
Anticipated Completion: September 1993

Total Project Cost:

DOE	**$2,000,000**
Contractor	**$2,000,000**
Total	**$4,000,000**

Principal Investigators:
F. David Martin
John P. Heller
William W. Weiss

Project Manager:
Royal J. Watts
Morgantown Energy Technology Center

Reporting Period: Jan. 1–Mar. 31, 1990

Objectives

The objectives of this project are to (1) evaluate the use of foaming agents to improve the efficiency of CO_2 flooding in a New Mexico reservoir, and (2) prove the

concept of CO_2–foam in the field by selecting a suitable reservoir where CO_2 flooding is ongoing, and characterizing the reservoir, modeling the process, and verifying the effectiveness and economics.

Reservoir studies, laboratory tests, simulation runs, and field tests will be conducted to evaluate the use of foam for mobility control or fluid diversion in a CO_2 flood. Seven tasks were identified for the successful completion of this 4-yr project: (1) site evaluation and selection; (2) initial site-specific plan; (3) CO_2–foam mobility tests; (4) reservoir simulation; (5) slug and injectant design; (6) implementation; and (7) evaluation.

Summary of Technical Progress

As discussed in the last quarterly report, a suitable site in New Mexico has been identified as appropriate for the proposed work. The initial site-specific plan is being developed.

SCALEUP OF MISCIBLE FLOOD PROCESSES

Contract No. DE-FG21-89MC26253

Stanford University
Stanford, Calif.

Contract Date: July 1989
Anticipated Completion: July 1992

Total Project Cost:

DOE	$736,000
Contractor	0
Total	$736,000

Principal Investigator:
F. M. Orr, Jr.

Project Manager:
Royal J. Watts
Morgantown Energy Technology Center

Reporting Period: Jan. 1–Mar. 31, 1990

Objectives

The research effort is to develop improved procedures for scaling predictions of miscible flood performance from laboratory scale, where the process is experimentally accessible to field scale and where more accurate performance predictions are needed.

Summary of Technical Progress

Phase Behavior, Fluid Properties, and Flow

Work continued on development of a technique in use of SFC to measure binary interaction parameters for CO_2–hydrocarbon pairs. Any equation of state (EOS) representation of the phase behavior of a CO_2–crude oil system requires that EOS parameters such as the critical pressure (P_c), critical temperature (T_c), and accentric factor (ω) be known or estimated. In addition, accurate portrayal of equilibrium phase behavior requires the use of a binary interaction parameter (K_{ij}) for each pair of components. Although values of T_c, P_c, ω, and K_{ij} are tabulated for *n*-alkanes up to about C_{20} and for a few other hydrocarbons, data for heavy hydrocarbons present in crude oils are generally not available. Estimates of T_c, P_c, and ω can be made from correlations, but values of K_{ij} are usually treated as adjustable parameters. The goal of this work is to develop a method for efficient determination of reasonable values of K_{ij} for hydrocarbons present in crude oils. To do this, retention time is calculated for a given hydrocarbon with the Peng–Robinson EOS and the value of K_{ij} required to give the observed value is determined.

An analysis has been performed by the method of the characteristics of effects of volume change on mixing in CO_2 and N_2 floods. The resulting calculations demonstrate quantitatively how local displacement velocity is reduced when low-density CO_2 dissolves in undisplaced oil, where it has a much higher apparent density. That change in volume as CO_2 changes phase can result in CO_2 breakthrough that occurs after more than one pore volume of CO_2 (at its injection density) has been injected. The calculations completed to date indicate that, although flow velocity changes, composition path behavior is affected much less. Thus the picture of composition path behavior that emerges from calculations performed on the assumption of no volume change on mixing is still reasonably accurate when volume change is present.

Progress has also been made using the method of characteristics. Solutions for linear one-dimensional (1-D) vaporizing gas drives can be transformed in a straightforward way to yield solutions for flow in radial systems. In addition, the problem of interfering shocks in binary displacements (CO_2–decane) has been solved. Such problems

arise in slug injection processes, for example. They are more difficult than continuous injection problems because the shock initiated at the trailing edge of the injected slug (of CO_2, for example) catches up and interacts with shocks initiated by the step change at the front of the injected slug. Extension of this work to three-component systems is now under way. The goal is to develop a detailed theory of the behavior of CO_2 slugs followed by a chase gas such as methane or nitrogen. Such a theory would allow rational design of slug sizes to eliminate adverse effects of chase gas phase behavior.

Patterns and Scales of Nonuniform Flow

A technique with which the permeability distribution in a two-dimensional (2-D) bead-pack model can be estimated from the positions of fronts of dyed fluid in unit mobility displacements has been developed. The resulting permeability field is then used as input to simulations of the growth of viscous fingers in adverse mobility displacements.

Interaction of Nonuniform Flow, Crossflow, and Phase Behavior in Large-Scale Flows

Experiments to investigate capillary crossflow have been performed. Although the eventual goal of those experiments is to investigate interactions of phase equilibrium and combined effects of gravity drainage and capillary crossflow, the first set of experiments was performed with equilibrated mixtures of isooctane, brine and isopropanol, a system for which phase composition, density, and interfacial tension data are available. Hence, phases did not change composition during the experiment. The results described below are surprising. Faster recovery of oil was observed when interfacial tension between the oil initially in place and the imbibing brine was lower, despite the fact that the density difference between phases was also lower. Because capillary forces are proportional to interfacial tension, slower capillary imbibition was expected. The reasons for the observed behavior are still under investigation.

STATISTICALLY DESIGNED STUDY OF PARAMETERS OF A CARBON DIOXIDE EQUATION OF STATE

Contract No. DE-AC22-89BC14200

Johns Hopkins University
Baltimore, Md.

Contract Date: Sept. 29, 1989
Anticipated Completion: Sept. 28, 1990
Government Award: $205,350

Principal Investigators:
Marc D. Donohue
Daniel Q. Naiman
Gang Jin
Joseph R. Loehe

Project Manager:
Jerry F. Casteel
Bartlesville Project Office

Reporting Period: Jan. 1–Mar. 31, 1990

Objective

The objective of this project is to select equations of state to calculate the thermodynamic properties of carbon dioxide (CO_2) and its mixtures relevant to enhanced oil recovery (EOR). A statistically designed factorial or fractional factorial computer analysis is used to study these equations of state. The purpose of this study is to determine the importance and sensitivity of thermodynamic variables and of the parameters in the equations. An important aspect of this is to determine how the accuracy and/or precision of these parameters affect the agreement with experimental data.

Summary of Technical Progress

During the last quarter, efforts were concentrated in two areas: (1) Testing the reliability of the equation by comparing calculated mixture critical points with experimental data, and (2) selecting equations of state for the statistical studies.

In the first area, several computer programs have been developed in which a generalized mathematical algorithm

was used for mixture critical point calculations. The calculated critical temperatures and critical pressures for ten binary mixtures and three multicomponent systems were compared with experimental values.

On the basis of the results of the reliability tests and the results of the accuracy tests carried out during the first quarter, accuracy rankings and overall rankings were given for the eleven equations of state. After analyzing the rankings and considering the simplicity of the equations and the availability of parameters in the equations, two equations of state, the Adachi–Lu–Sugie (ALS)[1] and the Suresh–Elliott–Donohue (SED)[2] equations, were chosen for future statistical studies.

Reliability Test (Critical Point Calculations)

Since the operating temperature and pressure in a petroleum reservoir are always near or above the critical temperature of the fluid mixture and since the phase behavior of fluid mixtures in a petroleum reservoir is complex at these operating conditions,[3,4] an equation of state (EOS) used in EOR design and simulation must be reliable in its description of phase behavior of CO_2 mixtures near the mixture critical points. Therefore mixture critical points were selected as one of the key thermodynamic variables to study to test the reliability of each equation.

After a review of the simplicity and results of the accuracy test, the ALS equation was tested for these critical point calculations. Since the SED equation is the cubic equation that is based on molecular theory, this equation was included in this test as well. Also, because of the wide industrial use of the Redlich–Kwong–Soave (RKS)[5] and the Peng–Robinson (PR)[6] equations, they were tested also. The four cubic equations of state (RKS, PR, ALS and SED equations) were used to calculate critical temperatures and critical pressures for a number of multiple-component mixtures at different compositions. These systems include five alkane–alkane binary mixtures, five CO_2–alkane binary mixtures, two ternary alkane mixtures, and one mixture containing six components of alkanes.

The rigorous thermodynamic definition of a mixture critical point was originally given by Gibbs.[7] The definition shows that a critical state must obey two restrictions: the second and third derivatives of Gibbs energy with respect to composition (mole number or mole fraction) must be zero. In the literature, these restrictions are presented in several different forms. Nevertheless, the independent variables most frequently used in these forms are pressure and temperature. However, since all equations of state are written in an explicit form for pressure and give several roots for volume at given temperature and pressure, instead of using Gibbs energy, it is more convenient to use the Helmholtz free energy approach in which molar volume and temperature are used as the independent variables. Heidemann and Khalil[8] and Michelsen and Heidemann[9] developed an improved algorithm that was considerably more rapid and more robust than its predecessors. In this test, the Heidemann–Khalil–Michelsen (HKM) algorithm was used.

In the HKM approach, the two restrictions of critical state for a multicomponent mixture can be written as

$$\det|Q| = 0$$

with elements

$$Q_{ij} = RTn_t \left(\frac{\partial \ln f_i}{\partial n_j} \right)_{T,V}$$

and

$$RTn_t^2 \sum_i \sum_j \sum_k \left(\frac{\partial^2 \ln f_i}{\partial n_j \partial n_k} \right)_{T,V} \Delta n_i \, \Delta n_j \, \Delta n_k = 0$$

where R = gas constant
T = temperature
V = total volume of system
n_i = moles of component i
Δn_i = change of moles of component i at $T_c + \Delta T$
n_t = total number of moles in system
f_i = fugacity of component i that can be calculated with EOS

By solving these two equations, two unknowns, critical temperature, T_c, and critical molar volume, v_c, can be obtained. The critical pressure, P_c, can then be calculated with the EOS. The strategy of the HKM algorithm is to iterate on T_c and v_c in a nested manner instead of performing iterations on both variables simultaneously as in a typical solution of multiple nonlinear equations. On the basis of an initial guess of v_c, the value of T_c can be obtained by iterating the first restriction. Closure of the second restriction is then checked, a new estimate for v_c is generated, and the iteration on T_c is carried out again. The advantage of this strategy is that it leads to convergence on the desired root much more often than by use of simultaneous iteration. Iteration on T_c and v_c by the secant method was satisfactory for most calculations in this study.

Figure 1 compares the calculated critical points with experimental data at different compositions for hexane–tetradecane mixture. Calculated critical points and experimental data for five binary mixtures containing CO_2 are compared in Fig. 2. As shown, the results obtained with the four equations of state are comparable, and the ALS equation always gives the best predictions. The average

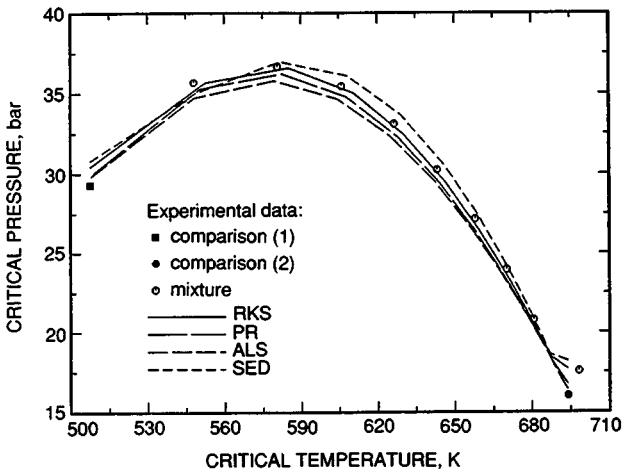

Fig. 1 Comparison between experimental data[10] and calculated critical temperatures and critical pressures of $C_6H_{14}(1)$–$C_{14}H_{30}(2)$ using the Redlich–Kwong–Soave (RKS), Peng–Robinson (PR), Adachi–Lu–Sugie (ALS), and Suresh–Elliott–Donohue (SED) equations of state.

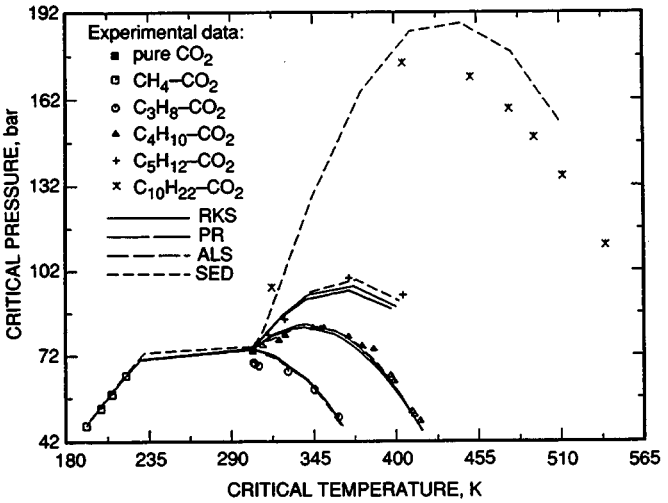

Fig. 2 Comparison between experimental data[10] and calculated critical temperatures and critical pressures of five binary mixtures containing CO_2 using the Redlich–Kwong–Soave (RKS), Peng–Robinson (PR), Adachi–Lu–Sugie (ALS), and Suresh–Elliott–Donohue (SED) equations of state.

percentage errors obtained from the calculations for the thirteen mixtures tested are given in Table 1.

In Fig. 2 calculations are presented only for the SED equation for the system decane–CO_2. Although these results are not good, the other equations (RKS, PR, and ALS) fail to predict the critical properties even qualitatively because the replusive terms used in these equations of state are based on the van der Waals theory, which assumes that the molecules are spherical. As shown in Table 1, the SED EOS gives better results for mixtures containing molecules that differ greatly in size.

Selection of EOS for the Statistical Studies

After consideration of the simplicity, accuracy, reliability, and availability of parameters of the eleven equations of state used in the preliminary tests, two equations of state were selected for the future statistically designed analysis.

TABLE 1

Average Percentage Errors Obtained from Mixture Critical Point Calculations with Four Cubic Equations of State*

	RKS		PR		ALS		SED	
System	E_{T_c}	E_{P_c}	E_{T_c}	E_{P_c}	E_{T_c}	E_{P_c}	E_{T_c}	E_{P_c}
CO_2–C_1	3.23	8.08	3.20	8.14	3.08	7.72	3.89	10.68
CO_2–C_3	2.60	5.55	2.42	5.39	2.49	5.46	2.48	5.52
CO_2–C_4	2.38	6.38	2.00	6.41	2.03	6.41	2.18	5.62
CO_2–C_5	2.42	6.54	2.15	6.22	2.14	6.17	2.53	5.65
CO_2–C_{10}							11.25	20.94
C_1–C_{10}							19.78	5.27
C_4–C_8	0.72	1.37	0.52	1.37	0.41	1.17	0.62	0.81
C_4–C_{10}	1.52	2.11	1.12	1.74	0.76	1.15	0.97	0.97
C_6–C_{10}	0.51	2.70	0.40	2.88	0.32	2.93	0.35	2.80
C_6–C_{14}	0.61	1.79	0.40	2.18	0.41	2.40	0.39	1.87
C_2–C_4–C_7	1.36	2.17	0.84	3.01	0.59	3.36	0.32	2.78
C_2–C_5–C_7	1.78	1.90	1.12	1.87	0.80	1.61	0.40	2.07
C_1–C_2–C_3–C_4–C_5–C_6	1.66	1.09	1.29	1.64	1.19	1.54	2.94	1.16

*RKS, Redlich–Kwong–Soave; PR, Peng–Robinson; ALS, Adachi–Lu–Sugie; SED, Suresh–Elliott–Donohue; T_c, critical temperature; P_c, critical pressure.

The accuracies of the equations of state tested were analyzed by generating an accuracy ranking for each EOS on the basis of the errors obtained from the calculations. For example, in the volume calculation, eleven equations of state were used. For the entire phase region of CO_2, the smallest error is obtained with the ALS equation and the largest error is given by the RK equation. Thus the error sequence numbers for the ALS equation and the RK equation are given as (1) and (11), respectively. Table 2 gives the accuracy rankings for the eleven equations used in the molar volume calculations for pure CO_2. Overall rankings of relative accuracies of the eleven equations of state also were made for molar volume calculations for pure alkanes, vapor-liquid equilibrium (VLE) calculations for mixtures and mixture critical point calculations. These are given in Table 3.

On the basis of the results in Table 3, the ALS equation is the most appropriate for the statistical studies. However, because the SED equation is the only cubic EOS tested that worked well for very large molecules, it should be more

TABLE 2

Accuracy Rankings for the Eleven Equations of State Used in the Volume Calculations for Pure CO_2*

Equation of State	Region 1	Region 2	Region 3	Region 4	Entire region
RK	(6)	(8)	(11)	(9)	(11)
RKS	(9)	(5)	(10)	(10)	(9)
RKT	(5)	(9)	(1)	(4)	(4)
PR	(3)	(3)	(6)	(2)	(3)
PRB	(4)	(4)	(2)	(11)	(5)
PT	(2)	(1)	(5)	(5)	(2)
ALS	(1)	(2)	(4)	(3)	(1)
SED	(10)	(6)	(9)	(8)	(8)
SPHCT(O)	(7)	(10)	(7)	(1)	(6)
SPHCT(M)	(11)	(7)	(8)	(6)	(7)
PACT	(8)	(11)	(3)	(7)	(10)

*RK, Redlich–Kwong; RKS, Redlich–Kwong–Soave; RKT; PR, Peng–Robinson; PRB; PT, Patel–Teja; ALS, Adachi–Lu–Sugie; SED, Suresh–Elliott–Donohue; SPHCT(O), Original Simplified-Perturbed-Soft-Chain Theory; SPHCT(M), Modified Simplified-Pertubed-Soft-Chain Theory; PACT, Perturbed-Anisotropic-Chain Theory; Region 1, supercritical region; Region 2, vapor phase in subcritical region; Region 3, liquid phase in subcritical region; Region 4, critical region.

TABLE 3

Overall Ranking of the Eleven Equations of State Studied in the Preliminary Tests*

Equation of State	Form	Number of parameters	Estimation of parameters	Pure alkanes (Cn ≤ 4)	Pure alkanes (Cn ≥ 4)	Mixtures	Mixture critical points
RK	c	2	cp	(11)	(10)	(9)	
RKS	c	2	cp	(9)	(9)	(7)	(4)
RKT	c	18	f	(5)			
PR	c	2	cp	(6)	(4)	(4)	(2)
PRB	c	3	cp	(3)	(3)	(3)	
PT	c	3	cp	(2)	(2)	(2)	
ALS	c	4	cp	(1)	(1)	(1)	(1)
SED	c	4	cp	(8)	(7)	(5)	(3)
SPHCT(O)	nc	4	f	(10)	(8)	(10)	
SPHCT(M)	nc	4	f	(9)	(6)	(8)	
PACT	nc	4	f	(4)	(5)	(6)	

*RK, Redlich–Kwong; RKS, Redlich–Kwong–Soave; RKT; PR, Peng–Robinson; PRB; PT, Patel–Teja; ALS, Adachi–Lu–Sugie; SED, Suresh–Elliott–Donohue; SPHCT(O), Original Simplified-Perturbed-Soft-Chain Theory; SPHCT(M), Modified Simplified-Pertubed-Soft-Chain Theory; PACT, Perturbed-Anisotropic-Chain Theory; c, cubic equation of state; nc, noncubic equation of state; cp, using critical properties; and f, fit experimental data.

reliable for EOR calculations. This EOS will be included in the statistical studies as well.

References

1. Y. Adachi, B. C.-Y. Lu, and H. Sugie, *Fluid Phase Equilibria*, 11: 29-48 (1983).
2. S. J. Suresh, J. R. Elliott, Jr., and M. D. Donohue, accepted by *Ind. Eng. Chem. Res.* (1989).
3. J. P. O'Connell, University of Virginia, Charlottesville, Va., personal communication, San Francisco, Calif., November 1989.
4. N. R. Nagarajan, Mobil Research and Development Corp., Dallas, Tex., personal communication, San Francisco, Calif., November 1989.
5. G. Soave, *Chem. Eng. Sci.*, 27: 1197-1203 (1972).
6. D. Y. Peng and D. B. Robinson, *AIChE J.*, 23: 137-144 (1977).
7. J. W. Gibbs, *The Scientific Papers of J. Willard Gibbs*, Vol. 1, Dover Publications, Inc., New York, 1961.
8. R. A. Heidemann and A. M. Khalil, *AIChE J.*, 26: 769-779 (1980).
9. M. L. Michelsen and R. A. Heidemann, *AIChE J.*, 27: 521-523 (1981).
10. C. P. Hicks and C. L. Young, *Chem. Rev.*, 75(2): 119-175 (1975).

GAS-MISCIBLE DISPLACEMENT

Cooperative Agreement DE-FC22-83FE60149, Project BE5A

National Institute for Petroleum and Energy Research
Bartlesville, Okla.

Contract Date: Oct. 1, 1983
Anticipated Completion: Sept. 30, 1990
Funding for FY 1990: $380,000

Principal Investigator:
Ting-Horng Chung

Project Manager:
Jerry F. Casteel
Bartlesville Project Office

Reporting Period: Jan. 1–Mar. 31, 1990

Objectives

The research of this project is designed to study (1) the gas foaming technology for gas mobility control and (2) the organic deposition problem in gas-miscible flooding. The objectives of this year's work are to: (1) develop a mathematical model that describes the adsorption and transport of foaming agents in reservoir rock and (2) develop a model that describes the deposition of organic materials under miscible conditions.

Summary of Technical Progress

Adsorption of Foaming Agents on Reservoir Rock

Adsorption is one of the important factors that determine the performance of foam for gas mobility control in the reservoir formation. In this quarter, the research was focused on the adsorption of anionic surfactants on Berea sand. Two anionic surfactants, sodium dodecyl sulfate (SDS) and Alipal CD-128 (nonadecyldiethoxy ammonium sulfate), were selected for this study. The SDS surfactant is isomerically pure (99+ %), whereas the Alipal CD-128 is a mixture that contains alcohols. Experiments conducted included (1) determining the adsorption isotherm for Alipal CD-128 on Berea sand, (2) determining the effects of salinity and alcohol on the adsorption of anionic surfactants, and (3) testing for SDS solution stability.

The equilibrium adsorption isotherm (75°F) for Alipal CD-128 surfactant on washed Berea sand has been determined for surfactant concentrations from 100 to 100,000 μmol/L (Fig. 1). The adsorption is small (in the range of 0.05 to 10 μmol/g), and the isotherm curve is similar to that of SDS surfactant, which was reported in the last quarter. At low concentrations (<1,000 μmol/L), the adsorption of surfactant increases slightly with surfactant concentration, and the adsorption obeys Henry's law. At higher concentrations, the adsorption increases rapidly with surfactant concentration and then reaches a plateau at surfactant concentrations higher than about 10,000 μmol/L.

The effect of salinity on adsorption is shown in Fig. 2 for the two anionic surfactants. As shown, the adsorption of

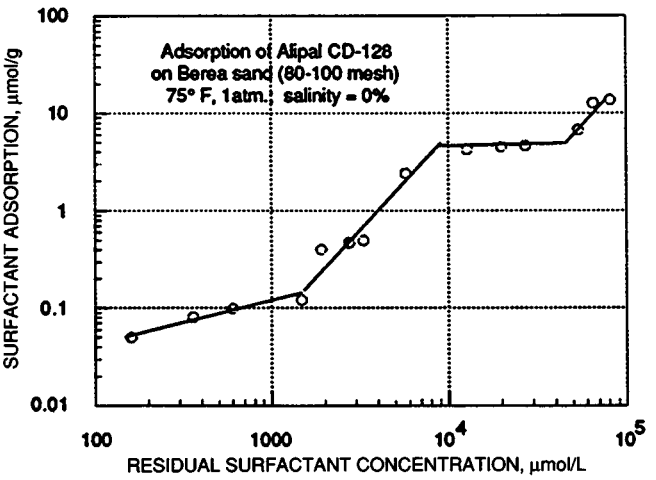

Fig. 1 Adsorption isotherm for Alipal CD-128 on Berea sand.

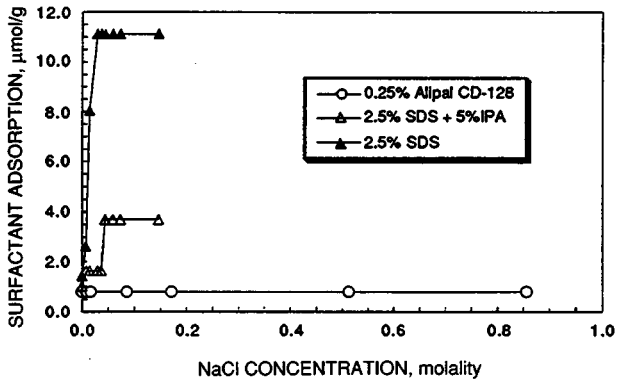

Fig. 2 Salinity effect of surfactant adsorption on Berea sand.

Alipal CD-128 is not sensitive to salinity, whereas the adsorption of SDS increases significantly with NaCl concentration. The figure also shows that the addition of isopropyl alcohol can mitigate the effect of salinity on surfactant adsorption. Precipitation of SDS surfactant was also observed as the NaCl concentration exceeded 3 wt %. Precipitation of SDS surfactant occurs at relatively low concentrations of divalent ions (<30 ppm Ca^{2+}). Figure 3 shows that the addition of isopropanol can increase tolerance to divalent ions and mitigate the precipitation problem.

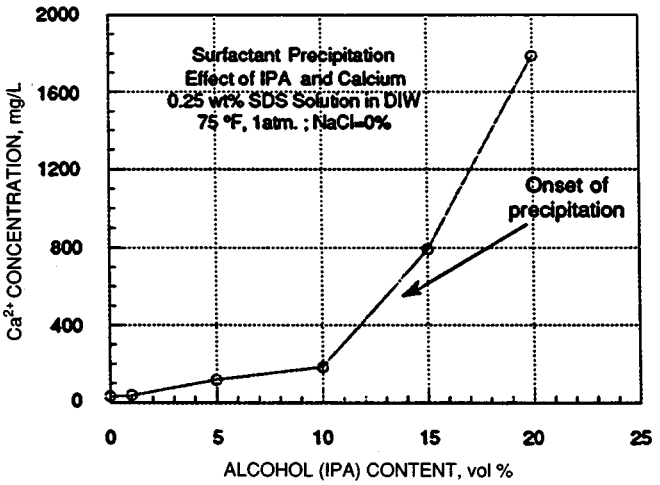

Fig. 3 Effect of alcohol on the minimum Ca^{+} concentration for surfactant precipitation.

Modeling Chemical Adsorption–Desorption and Transport in Porous Media

A general model for dynamic adsorption of chemical in porous media with stagnant volume (dead-end pores) was recently presented by Bidner and Vampa.[1] The model encompasses first-order reversible kinetic adsorption as well as dead-end pore volume and capacitance effects. The model can be reduced to the dispersion–capacitance model of Coats and Smith[2] and the dispersion–adsorption model reported in the last quarter. The transport phenomena of surfactant solution in porous media can be described by a set of differential equations.

$$D\frac{\partial^2 C}{\partial x^2} - \frac{q}{A\phi}\frac{\partial C}{\partial x} = f\left(\frac{\partial C}{\partial t} + \frac{A_s}{\phi}\frac{\partial C_s}{\partial t}\right) + k(C - C^*) \qquad (1)$$

$$k(C - C^*) = (1 - f)\left(\frac{\partial C^*}{\partial t} + \frac{A_s}{\phi}\frac{\partial C_s^*}{\partial t}\right) \qquad (2)$$

$$\frac{\partial C_s}{\partial t} = k_a(Q_s - C_s)\,C - k_d C_s \qquad (3)$$

$$\frac{\partial C_s^*}{\partial t} = k_a(Q_s - C_s^*)\,C^* - k_d C_s^* \qquad (4)$$

Boundary conditions:

1. At $x = 0,\ t > 0,$

$$vC_o = vC - D\frac{\partial C}{\partial x} \qquad (5)$$

2. At $x = L,\ t > 0,$

$$\frac{\partial C}{\partial x} = 0 \qquad (6)$$

where C = surfactant concentration in flow fluid
C^* = surfactant concentration in stagnant volume
C_s = surfactant adsorption on the solid surface
C_o = injected surfactant concentration
D = dispersion coefficient
q = volumetric flow rate
A = cross-section area
ϕ = porosity
f = fraction of pore space occupied by mobile fluid
A_s = solid interstitial area per unit volume
k = mass transfer coefficient
k_a = adsorption rate constant
k_d = desorption rate constant
Q_s = total adsorbent capacity
v = interstitial velocity

These coupled partial differential equations were solved numerically by finite differences of the Crank–Nicolson scheme and an iterative procedure. Computer coding has been completed and tested with reported data. The dead-volume effect on the surfactant transport in porous media was then studied with this model. Figure 4 is an example of the effect of dead volume on the effluent surfactant concentration. With the same conditions, Fig. 5 shows the con-

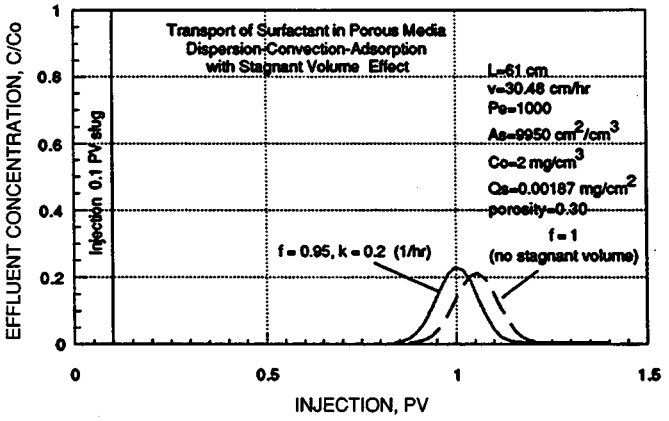

Fig. 4 Effect of stagnant volume on surfactant transport in porous media.

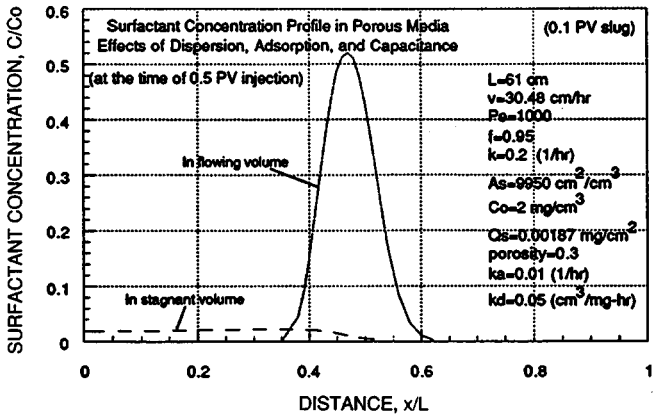

Fig. 5 Surfactant concentration profiles inside porous media after 0.5 PV injection.

centration profiles of the injected surfactant slug (0.1 PV) in porous media at the time of 0.5 PV injection.

Development of a Prediction Package for Asphaltene Precipitation

One of the problems in miscible flooding with gas is asphaltene instability, a problem that might result in asphaltene precipitation in the reservoir. The parameters that influence the precipitation include composition of the crude oil, pressure, temperature, and asphaltene properties. For a specific project, the conditions under which the deposition is likely to occur can be determined experimentally. However, experimental measurements can be expensive because a large number of experiments are required at reservoir conditions of pressure and temperature. Hence there is a need for a predictive model that can describe the behavior of asphaltenes in reservoir crude oils upon changes in pressure, temperature, or composition.

The principal objective of task 4 is to develop a predictive technique that can be used to answer the major questions of interest: "when" and "how much" asphaltene will precipitate under certain conditions.

The basic approach used in this study involves a vapor–liquid equilibrium (VLE) calculation of the total reservoir fluid to determine liquid phase composition (assuming no asphaltene precipitation) and an estimation of the amount of asphaltene precipitation from the liquid phase.

In the model, the VLE calculation is performed with the Soave–Redlich–Kwong (SRK) equation of state:

$$P = \frac{RT}{V - b} - \frac{a}{V(V + b)} \tag{7}$$

For VLE calculations, the composition of the C_7+ fractions was represented by a three-parameter gamma density distribution function. A generalized Laguerre–Gauss quadrature routine was used to generate effective heavy (asphaltene) components from the distribution function. Properties of these pseudo components were determined with the correlations proposed by Twu.[3] Molecular weights of the pseudo components were used as the independent variable in the distribution function and physical property correlation.

Once a vapor–liquid split has been calculated, the model will predict asphaltene precipitation using the Flory–Huggins solution theory,[4] which is defined by the following equation:

$$\phi_A = \exp\left\{\frac{V_A}{V_L}\left[1 - \frac{V_L}{V_A} - \frac{V_L}{RT}(\delta_A - \delta_L)\right]^2\right\} \tag{8}$$

where ϕ_A = volume fraction of asphaltene solution in the crude oil
V_A = molar volume of asphaltene
V_L = molar volume of asphaltene-free oil
δ_i = solubility parameter of component i

The solubility parameter (δ) was calculated from the Hildebrand's definition[5] as:

$$\delta_i = \left(\frac{\Delta H_i - RT}{V_i}\right)^{1/2} \tag{9}$$

where ΔH_i = heat of vaporization of component i at any temperature T
V_i = molar volume of component i
T = temperature
R = gas constant

In this work, the heat of vaporization at the normal boiling point was calculated with Kistyarowsky's equation[6]

$$(\Delta H)_{T_b} = T_b\,[8.75 + 4.571 \log (T_b)] \tag{10}$$

where $(\Delta H)_{T_b}$ is the heat of vaporization at normal boiling point (cal/g-mol) and T_b is the normal boiling point (K).

The heat of vaporization at any other temperature is then estimated with Theisen's correlation[6]

$$(\Delta H)_T = (\Delta H)_{T_b} \left(\frac{T_c - T}{T_c - T_b} \right)^{0.38} \quad (11)$$

where T_c is the critical temperature in Kelvin.

Computer coding of various subroutines for use in predicting asphaltene deposition from petroleum crude caused by changes in temperature, pressure, or composition of crude oil (the result of the injection of a miscible solvent such as CO_2) was completed during this quarter. Figure 6 illustrates the basic approach employed in the model. Debugging, testing, and modification of the code are under way.

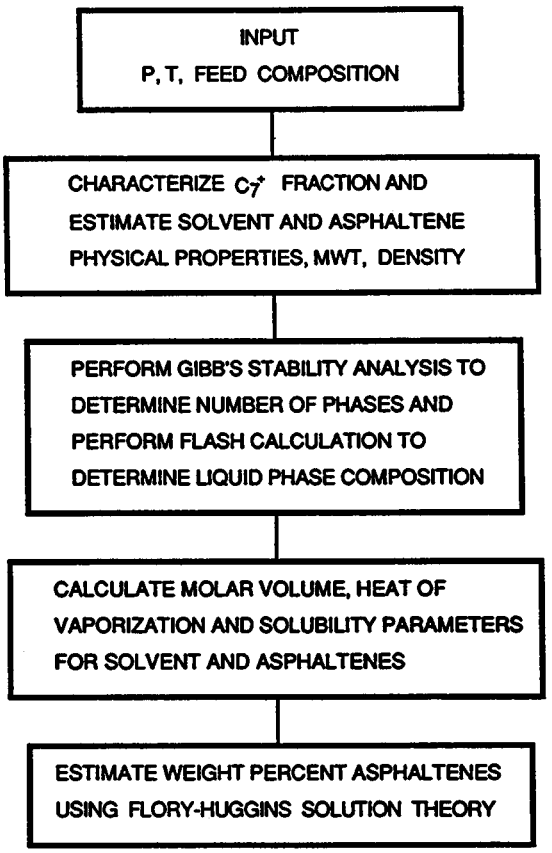

Fig. 6 Basic approach flowchart.

References

1. M. S. Bidner, and V. C. Vampa, A General Model for Convection–Dispersion–Dynamic Adsorption in Porous Media with Stagnant Volume, *J. Pet. Sci. Eng.*, 3:267 (1989).
2. K. H. Coats and B. D. Smith, Dead-End Pore Volume and Dispersion in Porous Media, *Soc. Pet. Eng. J.*, 73 (March 1964).
3. C. H. Twu, An Internally Consistent Correlation for Predicting the Critical Properties and Molecular Weights of Petroleum and Coal-Tar Liquids, *Fluid Phase Equilibria*, 137 (1984).
4. A. Hirschbeng, L. N. J. deJony, B. A. Schipper, and J. C. Meijer, Influence of Temperature and Pressure on Asphaltene Fluctuation, *Soc. Pet. Eng. J.*, 283 (June 1984).
5. J. M. Prausnitz, *Molecular Thermodynamics of Fluid Phase Equilibria*, Chap. 7, Prentice-Hall, Old Tappan, N.J., 1969.
6. W. R. Gambill, Determination of Heat of Vaporization, *Chem. Eng.*, 261 (December 1957).

DEVELOPMENT OF IMPROVED IMMISCIBLE GAS DISPLACEMENT METHODOLOGY

Cooperative Agreement DE-FC22-83FE60149, Project BE5B

National Institute for Petroleum and Energy Research
Bartlesville, Okla.

Contract Date: Oct. 1, 1983
Anticipated Completion: Sept. 30, 1990
Funding for FY 1990: $260,000

Principal Investigator:
Arden Strycker

Project Manager:
Jerry F. Casteel
Bartlesville Project Office

Reporting Period: Jan. 1–Mar. 31, 1990

Objective

The objective of this project is to develop methods for improving sweep efficiency and mobility control for gas flooding.

Summary of Technical Progress

Foam Flow in Porous Media

Effects of foam on gas injectivity were studied by means of radial flow experiments. A slug of foamer followed immediately by nitrogen gas injection produced even distribution of foam over an entire radial core. Results of the four experiments conducted will serve as baselines for those to be conducted next quarter to modify these effects by varying injection sequences and procedures. Both 5.75-in.-diameter unfired and 6-in.-diameter fired Berea sandstone cores were used; however, the 6-in.-diameter fired core is preferred because of its fewer repeatability problems.

The first experiment used an unfired Berea sandstone radial (cylindrical) core with an outer diameter of 5.75 in., an inside (wellbore) diameter of 0.25 in., and a thickness of

1.911 in. Flow was in the horizontal direction from the inner diameter to the outer. The 0.5 wt % NaCl brine was injected into the cleaned, evacuated core to determine its pore volume and then allowed to flow through to determine its liquid permeability. Even though the core's gas permeability to nitrogen was measured to be 254 mD, the liquid permeability to the brine declined from an initial value of 118 mD to a final value of 27 mD after injection of several pore volumes (PV). Then nitrogen gas was injected without stopping to displace the water to a residual saturation. Afterward, a 0.1-PV slug of foamer (consisting of 0.5 wt % active Alipal CD-128 surfactant in the same brine) was injected, followed by continuous nitrogen injection until a steady state was reached. Produced volumes of liquid and gas were monitored along with pressures at the four intermediate taps. Inlet pressure was held constant at 5 psig and outlet pressure was 0 psig; this allowed rates to vary as the effective permeability changed.

The second experiment used the same core, fluids, and conditions as the first with a different injection sequence. Brine was similarly injected into the evacuated core, followed by several pore volumes of foamer, to establish a 100% initial saturation of liquid foamer. Liquid permeability decreased from 118 mD for brine to a final 3.5 mD for foamer. Then nitrogen was injected to displace the foamer to residual water saturation and to reach a steady-state condition. A third experiment with the same core experienced such difficulties with initial liquid permeability reduction that it was terminated. The brine was a 0.5 wt % NaCl solution for all experiments.

In an attempt to alleviate the plugging problems encountered with the unfired core, a fired Berea sandstone radial core, which was prepared by drilling a 6-in. core from a block of Berea, slabbing it to the same thickness (1.911 in.), drilling a 0.125-in.-diameter injection wellbore in the center, and then firing it for 48 h at 1000°C to convert the clays to nonreactive minerals, was used for the fourth experiment. Its initial permeability to gas was not measured, but during the initial brine saturation procedure, the liquid permeability remained a nearly constant 185 mD. The fourth experiment was mostly a repeat of the first; only the different core was used. After many pore volumes of nitrogen had reduced the brine saturation to residual, a similar 0.1-PV slug of foamer was injected which was followed by continuous nitrogen injection to residual. Residual water saturation was assumed after water production ceased.

Results from tests 1 and 4, which used the same injection sequences and procedures in different cores, are compared in Figs. 1 to 4. Figure 1 shows the discrepancy between the ideal pressure distribution curve (calculated from Laplace's equation for steady-state flow) for a homogeneous core with 100% flowing liquid saturation and the experimental curve obtained in the first test flowing 100% brine. Plugging at the injector face increased the pressure differential across the first section of the core, and

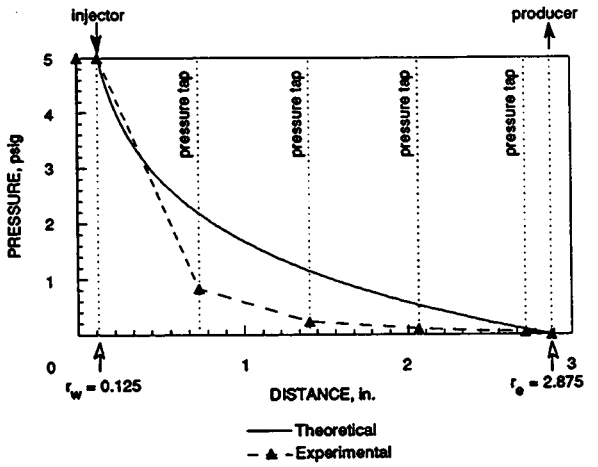

Fig. 1 Pressure distribution for first test, flowing brine at 100% brine saturation.

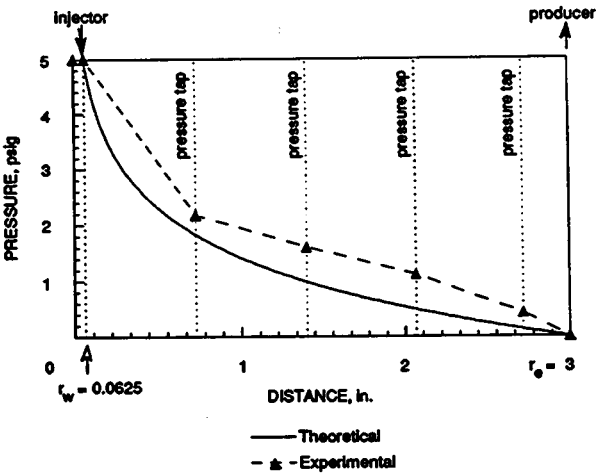

Fig. 2 Pressure distribution for fourth test, flowing brine at 100% brine saturation.

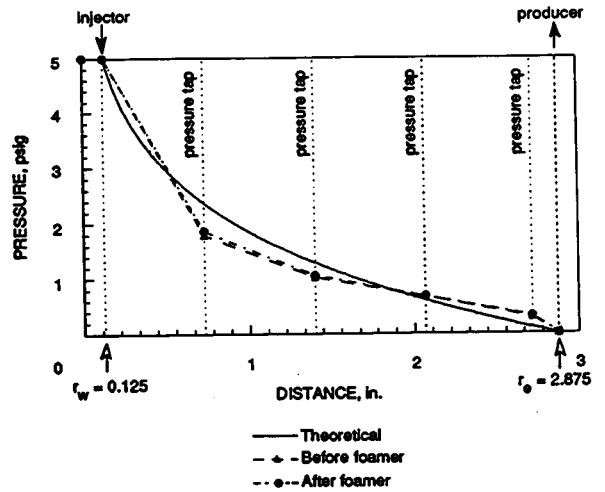

Fig. 3 Pressure distribution for first test, flowing gas at residual water saturation.

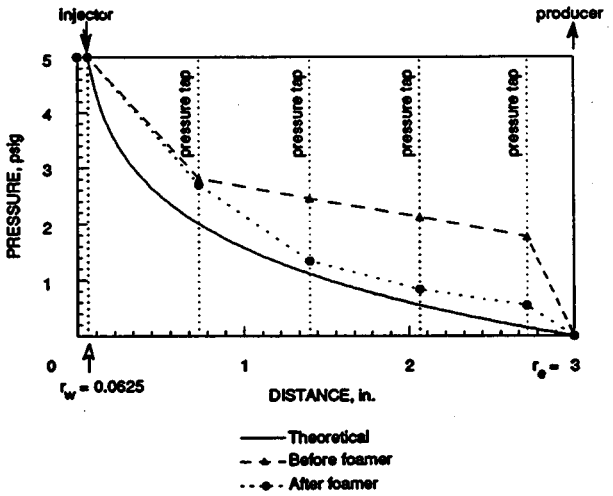

Fig. 4 Pressure distribution for fourth test, flow gas at residual water saturation.

thus the pressure dropped at the first intermediate pressure tap location below the theoretical value. Figure 2 shows a better match between the actual and theoretical 100% brine pressure distribution in the fourth experiment because of the elimination of plugging at the injector face. Some end effects or pressure measurement problems across the outlet section of the core, however, raised the entire curve and prevented a perfect match. From Fig. 3, the conclusion is drawn that injection of the foamer slug had no significant effect upon the pressure distribution of the gas. The plot compares gas flow at residual water saturation immediately before foamer injection to gas flow at residual water saturation after many pore volumes of injection to displace the foamer. A similar comparison for the fourth test (Fig. 4) shows that injection of the foamer corrected some end effect or measurement problem occurring at the outlet section. The final gas flow after injecting foamer and many pore volumes of gas was near the theoretical curve for both experiments, which means that the foam was formed evenly throughout the cores in both cases, and affected a uniform permeability reduction throughout the core. The permeability reduction was substantial in tests 1, 2, and 4. Tests to be conducted next quarter will attempt to evaluate different injection sequences and procedures to modify the permeability reduction profile.

Entrainers

The objective for this activity in evaluating carbon dioxide entrainers is to continue to study some of the more promising entrainer candidates and to improve the efficiency of laboratory procedures used in making these evaluations. A carbon dioxide (CO_2) entrainer is a cosolvent that enhances the solution properties of CO_2 in some way. For enhanced oil recovery (EOR) applications, an entrainer should enhance the solubility of crude oil in a gas phase and improve the mobility properties of the injected gas. Some researchers have found that the addition of minor amounts of certain materials to CO_2 selectively increases the solubility of another desired material. Work completed over the past 2 yr in this laboratory has shown that some entrainer materials increase the percentage of heavy ends contained in extracted crude oil. The objective of this task is to find a material as an entrainer that approaches these ideal properties for EOR applications.

For the entrainer technique development, it is essential to have a predictive model for the solubility of a high-molecular-weight compound (solid or liquid) in a gas at high pressure. An accurate predictive model could be used to quickly screen candidate entrainers and save time in conducting detailed experimental work. Considerable effort has been made by other researchers in modeling the supercritical extraction phenomena. Some progress has been made. This report summarizes currently available techniques in the prediction of solid or relatively nonvolatile liquid solubilities in a high-pressure gas. Thermodynamic models that have been applied to supercritical mixtures are separated into two approaches. One of these approaches is based on general phase equilibrium theory, and the other is based on fluctuation theory (Kirkwood–Buff solution theory).

The first approach is based on the thermodynamic relationship relating the fugacities (f_i) of components i in both equilibrium phases. For a binary solid–gas system, subscript 1 stands for the light (gaseous) component, and subscript 2 stands for the heavy (solid or nonvolatile liquid) component. The general equilibrium equation for component 2 is written as

$$f_2^s = f_2^v \tag{1}$$

where superscript s is the solid phase, superscript v is the vapor phase, and the solid phase is assumed to be pure. The solid-phase fugacity of component 2 is given by

$$f_2^s = P_2^{sat}\phi_2^{sat} \exp\left(\frac{v_2^s\left(P - P_2^{sat}\right)}{kT}\right) \tag{2}$$

where P_2^{sat} is the saturation (vapor) pressure of the pure solid, ϕ_2^{sat} is the fugacity coefficient at saturation pressure P_2^{sat}, and v_2^s is the solid molar volume, all at temperature T. The vapor-phase fugacity is

$$f_2^v = y_2\phi_2 P \tag{3}$$

If Eqs. 2 and 3 are substituted into Eq. 1, the solubility of the solid component in the gas phase at temperature T and pressure P is obtained.

$$y_2 = \frac{P_2^{sat}\phi_2^{sat}\exp\left[v_2^s\left(P - P_2^{sat}\right)/kT\right]}{\phi_2 P} \quad (4)$$

or

$$\ln(E) = \ln\left(\frac{y_2 P}{P_2^{sat}}\right) = -\ln\phi_2 + \frac{v_2^s}{kT}\left(P - P_2^{sat}\right) \quad (5)$$

The enhancement factor, E, is the correction factor for the ideal gas expression, which is a measure of the extent to which pressure enhances the solubility of the solid in the gas.[1] In Eq. 5, $\phi_2^{sat} = 1$ is assumed since the pure-solid vapor pressures of interest are very low.

For CO_2–hydrocarbon systems, the solubility of heavy component 2 in the vapor phase is given by[1]

$$y_2 = \frac{x_2\gamma_2 P_2^{sat}\phi_2^{sat}\exp\left(\int_{P_2^s}^{P}\frac{v_2^l dp}{kT}\right)}{P\phi_2} \quad (6)$$

where x_2 is the mole fraction of component 2 in the liquid phase and γ_2 is the activity coefficient for component 2, which is to account for the nonideality of the liquid mixture. Equation 6 can be simplified by setting $\phi_2^{sat} = 1$ and $\gamma_2 = 1$, where the pure solute vapor pressure is very low and the liquid phase is assumed to be an ideal solution. Introduction of these assumptions yields a simplified equation:

$$\ln(E) = \ln\left(\frac{y_2 P}{P_2^{sat}}\right) = \ln x_2 - \ln\phi_2 + \frac{Pv_2^l}{kT} \quad (7)$$

In Eqs. 4 to 7, the fugacity coefficient, ϕ_2, can be calculated from any accurate equation of state. However, most available equations of state are not accurate enough for the mixture properties in the critical region. Predicting the fugacity coefficient of the solute in the supercritical solvent from corresponding states theory based on critical properties of pure components is very difficult. Experimental data are usually required to determine the solute–solvent interaction constants in the equation of state; therefore Eqs. 4 to 7 are used only to model the experimental results.

The second approach in predicting phase behavior of entrainer type systems is based on the Kirkwood–Buff solution theory. The expression for the solubility of solid in gas phase at pressure P and temperature T is given as[2,3]

$$\ln(E) = \ln\left(\frac{y_2 P}{P_2^{sat}}\right) = \ln Z^0 - \alpha_{12}\ln\left(\frac{f^0}{\rho^0 kT}\right) + \left[v_2^s - \frac{1}{2}\left(V_{c,1} + V_{c,2}\right) + \alpha_{12}V_{c,1}\right]\frac{\left(P - P_2^{sat}\right)}{kT} \quad (8)$$

where superscript 0 is pure gas properties and subscript c is critical properties. Equation 8 involves only the solvent (gas) properties plus characterization parameters for the solute. For the application of Eq. 8, the molar volume of solute must be known at the respective values for P, T, and a scaling parameter, α_{12}, which is related to the Van der Waals attractive constant, a_{ij}.

$$\alpha_{12} = \frac{a_{12}}{a_{22}} \quad (9)$$

The parameter can also be estimated from the critical properties of both solvent and solute based on the conformal solution theory.[2]

$$\alpha_{12} = \frac{\left(V_{c,1} + V_{c,2}\right)}{2V_{c,1}}\left(\frac{T_{c,2}}{T_{c,1}}\right)^{1/2} \quad (10)$$

Since an accurate equation of state for CO_2 properties has been developed at the National Institute for Petroleum and Energy Research (NIPER), and since the critical property data for pure substances are available, Eq. 8 associated with Eq. 10 could be used to predict the solubility of high-molecular-weight compounds in supercritical CO_2. An example is given for the CO_2–naphthalene system in Fig. 5. As shown in Fig. 5, predictions were sensitive to

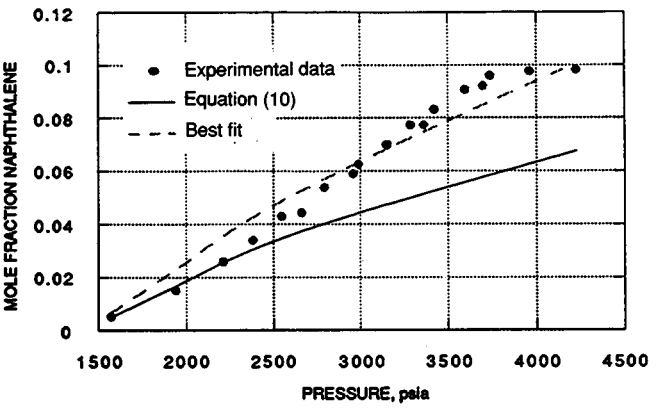

Fig. 5 Experimental and predicted solubilities for naphthalene in supercritical carbon dioxide at 140.7°F. Experimental data from reference 4; $\alpha_{12} = 4.23$ from eq. 10; $\alpha_{12} = 4.37$ from data regression.

the model parameter, α_{12}. With α_{12} estimated from Eq. 10, Eq. 8 adequately predicted the solute–solvent behavior for dilute solutions, but deviations from laboratory measurements increased with increasing solute concentration. Equation 8 associated with Eq. 10 underestimated the solubility of naphthalene in CO_2 at higher pressures. With α_{12} determined from data regression, Eq. 8 gives satisfactory results for the solubility over the full range of densities. A more accurate method of estimating the scaling parameter, α_{12}, is needed.

References

1. J. M. Prausnitz, R. N. Lichtenthaler, and E. Gomes de Azevedo, *Molecular Thermodynamics of Fluid-Phase Equilibria*, Prentice-Hall, Englewood Cliffs, N.J., 1986.
2. H. D. Cochran, L. L. Lee, and D. M. Pfund, Application of the Kirkwood–Buff Theory of Solutions to Dilute Supercritical Mixtures, *Fluid Phase Equilibria*, 34: 219 (1987).
3. D. M. Pfund, L. L. Lee, and H. D. Cochran, Application of the Kirkwood–Buff Theory of Solutions to Dilute Supercritical Mixtures II, The Excluded Volume and Local Composition Models, *Fluid Phase Equilibria*, 39: 161 (1988).

THERMAL RECOVERY—SUPPORTING RESEARCH

ELECTROMAGNETIC SENSING OF ENHANCED OIL RECOVERY

Lawrence Livermore National Laboratory
Livermore, Calif.

Contract Date: Oct. 1, 1984
Anticipated Completion: Sept. 30, 1990
Government Award: $388,000
(Current year)

Principal Investigators:
Michael Wilt
Phillip Harben

Project Manager:
Thomas B. Reid
Bartlesville Project Office

Reporting Period: Jan. 1–Mar. 31, 1990

Objective

The purpose of this project is to monitor in situ changes in the oil reservoir parameters during steam injection for enhanced oil recovery (EOR) by tomographic reconstruction of electromagnetic cross-borehole measurements.

The project goal is development of practical tools for monitoring the propagation of a steam front during an ongoing EOR operation. Cross-borehole electromagnetic induction is used to provide an image of an encroaching steam front. This technique is adapted to the hostile conditions in an oil field during EOR.

Summary of Technical Progress

During this quarter, laboratory studies of the electrical conductivity changes in petroleum reservoirs during steam injection were initiated. Development of a cross-borehole field system has continued with preparation of the system for a full-scale field test this summer. Additionally, the field data collected at South Belridge in 1989 have been interpreted and a paper has been submitted for a technical conference that summarizes this work.

Laboratory Studies

At present there are no adequate models describing the electrical conductivity changes that result from steam injection during EOR operations. Electrical conductivity data collected thus far came from computer simulations and some coarsely sampled field data. This lack of information means that accurate simulations of steam front imaging are not possible.

To help remedy this situation, laboratory measurements are being made of electrical conductivity in water- and petroleum-bearing sands during steam injection. This

project is being done in cooperation with the University of California, Berkeley, using their laboratory facilities. A graduate student is making the measurements and will be using the data as part of his master's thesis.

The initial stage of this project will involve one-dimensional studies where pure steam is injected into one end of a sandpack and the temperature, steam saturation, and electrical conductivity of the pack are monitored while the steam displaces the water (Fig. 1). These experiments are scheduled for April and May of 1990.

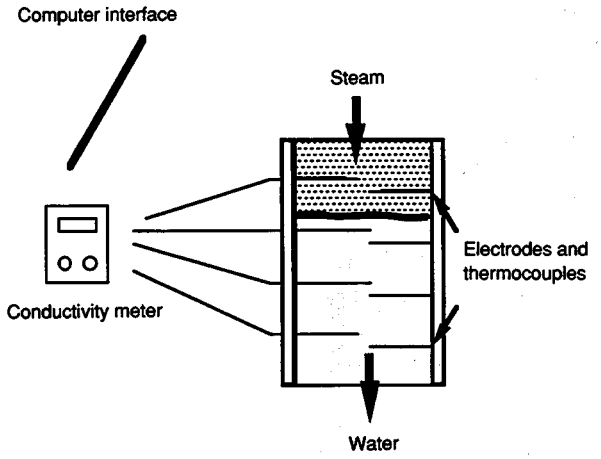

Fig. 1 Schematic diagram of the one-dimensional laboratory steam displacement cell.

In succeeding phases of the experiment, the water in the sands will be replaced by hydrocarbons and the quality of the steam (i.e., percentage of pure steam) is adjusted to correspond to actual EOR experiments. The final studies will be made in a two-dimensional cell where it is possible to study the steam override phenomena and the effects of inhomogeneous structure.

Field System Deployment at the Devine, Texas, Test Facility

In cooperation with the University of California and Lawrence Berkeley Laboratory, a field system for deployment at the SOHIO, Inc., test facility in Devine, Tex., is being prepared. This combined effort is partially funded by a consortium of oil and energy companies through a project initiated at the University of California. The field experiment is designed to test the feasibility of an audio-frequency cross-borehole electromagnetic (EM) system in an EOR environment where boreholes are spaced several hundred meters apart in high-conductivity sands and shales with injection zone at a depth of 500 m.

For the collection of high-quality data under these conditions, a more powerful version of the transmitter in which a high-permeability Mu-metal (obtained by the University) was used for the core was designed. The new transmitter has a moment of about three thousand, which is approximately 10 times more powerful than the present source. Incorporating this new source with the existing data acquisition system will provide a powerful, low-noise field system.

A computer-generated simulation of a cross-borehole experiment at the Devine site is displayed in Fig. 2. The figure shows the magnitude of the expected magnetic field in phase and out of phase (quad), with respect to the transmitter current, at a frequency of 540 Hz. The layered conductivity model was derived from electrical logs at the Devine site. The plot also displays the expected sensor noise level.

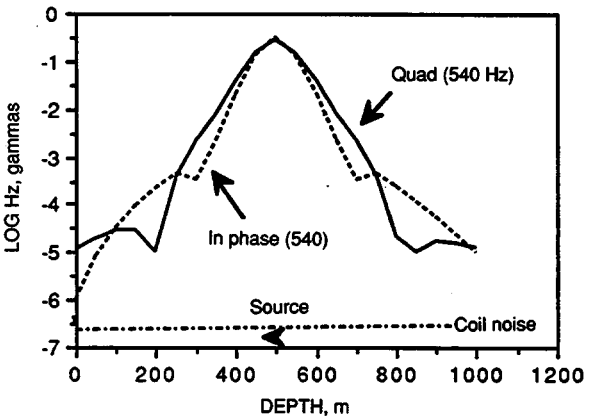

Fig. 2 Computer simulation of a cross-borehole electromagnetic profile for Devine, Texas. Source and receiver boreholes are separated by 200 m.

The field experiment is scheduled for late June or early July 1990 and will require about 10 field days. Data collected will be analyzed and interpreted at Lawrence Livermore National Laboratory (LLNL) and Lawrence Berkeley Laboratory (LBL).

Interpretation of Surface-to-Borehole Data at South Belridge

Surface-to-borehole field data collected at the Mobil, South Belridge field site last summer were interpreted, and the results are reported in a paper submitted to the Society of Exploration Geophysicists for their annual meeting.

Described in this paper is how data collected through steel casing can be interpreted in terms of the conductivity structure around the borehole. This is done by first measuring the attenuation and phase shift caused by the casing in free space and then subtracting this effect from the observed data. This procedure assumes that the two responses (i.e., casing and formation) are additive. This assumption is valid at frequencies up to several hundred hertz since the residual data can be fit to a layered model consistent with the known conductivity structure around the wellbore.

Annex IV Meeting—Caracas, Venezuela

The annual meeting of Annex IV of the agreement between the Department of Energy (DOE) and INTEVEP in

Venezuela was held in Caracas, Venezuela, Mar. 13–16. This annex concerns cooperative work between the two governments on thermal processes for EOR.

During this meeting, a 1-h presentation on the LLNL program for front tracking during EOR operations was given.

DEVELOPMENT OF METHODS FOR CONTROLLING PREMATURE OXYGEN BREAKTHROUGH DURING FIREFLOODING

Contract No. FG22-89BC14201

Union Carbide Corporation
Tonawanda, N.Y.

Contract Date: June 2, 1989
Anticipated Completion: Oct. 1, 1990
Government Award: $522,719

Principal Investigator:
C. J. Heim

Project Manager:
Thomas B. Reid
Bartlesville Project Office

Reporting Period: Jan. 1–Mar. 31, 1990

Objective

The objective of the program is to characterize the reservoir mechanisms that cause premature oxygen breakthrough and develop practical tools for controlling it. The focus will be on those conditions most likely to be encountered in reservoir depths of moderate to deep. Candidates include gas override, high-permeability streaks, and watered-out zones. Mitigation measures will be selected on the basis of the cost of implementation and their potential application to a wide range of specific problems.

This phase of the program consists of efforts to characterize the problem and develop possible solutions. Problem characterization focuses on obtaining first-hand information from operators of firefloods through a questionnaire and interviews. A literature search will be used to supplement operator information. Bench-scale screening tests will be performed to identify candidate mobility control techniques for use in physical and computer simulation models.

Summary of Technical Progress

Work continues on reviewing the literature identified as being pertinent to this project. Approximately 80% of the material received has been reviewed and summarized.

Seven oil companies agreed (one has decided not to participate since the last quarter) to participate in this study by providing specific information. As of this quarter, responses from three companies have been received. The additional two responses have reinforced earlier conclusions indicating that oxygen breakthrough was a significant problem for formations that have high permeability streaks running from injectors to producers. In addition, these operators have concluded that the flow of oxygen through watered-out zones (not enough fuel to support combustion) and also poor oxygen efficiency (caused by high injection rates) may have contributed to oxygen breakthrough. As in the previous studies, these problems have resulted in poor vertical sweep efficiency and thereby affect the economics of the process.

Fabrication and checkout of the test equipment has been completed. Figure 1 is a process and instrumentation diagram for laboratory apparatus used in the screening process. Figure 2 is a sectional drawing showing the internals and configuration of the apparatus.

Initial runs with a salt solution (sodium chloride) have indicated that precipitation can occur in specific zones as the result of rapid evaporation and that this precipitation causes a significant permeability reduction.

For the evaluation (quantification) of the effectiveness of blocking agents, a method was required that allows for the core (sandpack) to be analyzed on a sectional basis. This required the design and fabrication of a core sampler (Fig. 3). This equipment will remove the core in a manner that will allow sections to be isolated for further analysis [Energy Dispersive Spectrometry (EDS) and microscopic] and correlated to their original position in the tube (i.e., exact position from injection point, heat source, etc.).

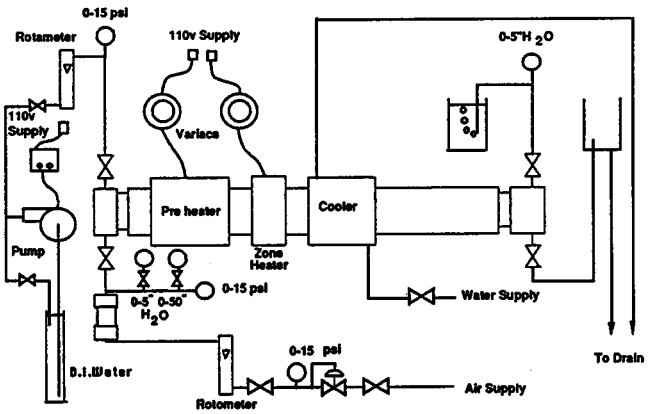

Fig. 1 Screening process laboratory apparatus—process and instrumentation diagram.

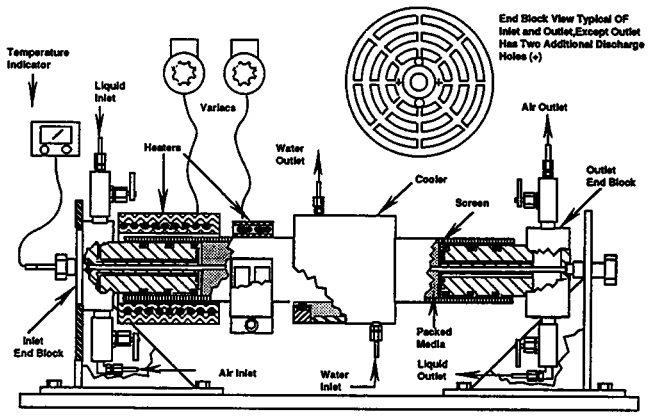

Fig. 2 Screening process laboratory apparatus—sectional view.

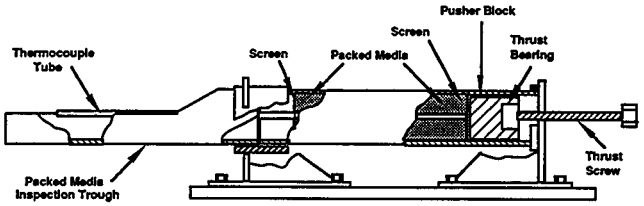

Fig. 3 Packed media removal and inspection apparatus.

In addition to the salt precipitation tests conducted, three other chemical systems are being considered as potential candidates.

1. *Carbon dioxide with predose of cations–anions.* Since an oxygen fireflood produces large quantities of relatively high-purity CO_2 and the gas reactant leaving the burn front has a high probability of flowing through the high permeability streak, this system may offer distinct advantages.

2. *Acid brine reactions.* Accounts have been described in the general literature where hydrofluoric acid has been used in well treatments as an acidizing agent. During these treatments, reactions with cations (Ca^{2+}, K^+, etc.) contained in the formation brines have caused precipitation and subsequent permeability reduction.

3. *Aerobic microorganism growth.* The use of a true (nonfacultative) aerobic microorganism has been suggested before; however, high reservoir temperature and pressure combined with a limited penetration depth posed severe limitations. Information from one operator who responded to the detailed questionnaire gave a reservoir temperature of 27°C (80°F), and recent literature references indicate the distance of microorganisms transported via groundwater in soils can be as high as 900 m from injection–infection point. This information combined with the possibility of oxygen reaching the producing wells via watered-out zones (i.e., no combustion occurring) led to the resumption of the investigation of this type of system. It is postulated that these microorganisms could be injected prior to a fireflood or from a producer into the reservoir via low-viscosity waterflood. The areas of high water saturation would receive the majority of the flow and thereby inoculate this region of the reservoir. If no oxygen reached this zone, the microorganisms would remain dormant. If oxygen were to flow through this zone, the dissolved oxygen level would increase in the water and thereby promote growth that would reduce the permeability of the zone in question.

These three systems will be tested in the next several months.

CHEMICAL ADDITIVES FOR IMPROVING STEAMFLOOD PERFORMANCE

Contract No. FG19-87BC14126

University of Southern California
Los Angeles, Calif.

Contract Date: Feb. 27, 1987
Anticipated Completion: Feb. 27, 1990
Government Award: $131,750
(Current year)

Principal Investigator:
Y. C. Yortsos

Project Manager:
Thomas B. Reid
Bartlesville Project Office

Reporting Period: Jan. 1–Mar. 31, 1990

Objectives

The broad objectives of the work to be performed under this contract are to select and evaluate various chemicals that may have the potential for increasing oil recovery from steamfloods at lower steam/oil ratios than those currently observed. For the accomplishment of these objectives, the work will include an assessment of classes of organic surfactants not previously studied as well as an extension of current work on inorganics. A major added research goal will be consideration of modifications in flooding procedures to improve steamflood performance. In accomplishing this, the completion of the thermal–chemical steam simulation model will provide a calculational procedure for assessing the various process modifications. The work with numerical simulators will be combined with further adaption of physical models to study these processes.

Summary of Technical Progress

A technical paper on steady-state, concurrent vapor–liquid flow that addresses saturation and temperature profiles, end effects, and the effects of parameters in relative permeability experiments was completed. The numerical simulation of phase change processes in the presence of temperature gradients is under way with the use of network models. Investigations of mechanisms in thermal recovery in naturally fractured reservoirs have started, and the study of parallel flow in fully developed fingers is near completion.

Experimental research continued with the assembly of Hele–Shaw apparatus for the study of steam injection and of a long Hele–Shaw cell for the study of parallel flows. Glass micromodels of various patterns were developed for use in pore-level observation of steam displacement mechanisms. In the area of steam additives, further experiments on the mechanism of foam generation and propagation were conducted. The use of a prefoamer enhanced foam flow considerably, although the foam texture within the porous medium soon adapts to and becomes controlled by the pore structure.

Vapor–Liquid Flow

Work in the area of vapor–liquid flow in porous media continued. The theoretical and experimental research carried out is summarized. Considerable progress has been made on the theoretical aspects. The study on steady-state, concurrent, vapor–liquid flow was completed after investigation of the generalized end effects, construction of the temperature–saturation trajectories, and performance of a parameter sensitivity analysis. This work is the sequel of a recent study in countercurrent flow.[1] Saturation and temperature responses to a capillary (permeability) heterogeneity are plotted in Fig. 1. The profiles follow in general the features of a previous study,[2] although the temperature response is novel. Figure 2 shows saturation–temperature trajectories for steam–water in a homogeneous core. Such trajectories unify the various flow regimes that may develop (e.g., evaporation in situ[3] or steam–water injection).[4] Finally, Fig. 3 portrays the inlet liquid saturation and the corresponding error estimate (deviation from a flat profile) as a function of the rate parameter R_m. Here R_m denotes a macroscopic capillary number

$$R_m = \frac{m_i L v_l}{\sigma (k)^{1/2}}$$

where m_i = mass injection rate
k = core permeability
L = core length
v_L = liquid kinematic viscosity
σ = surface tension

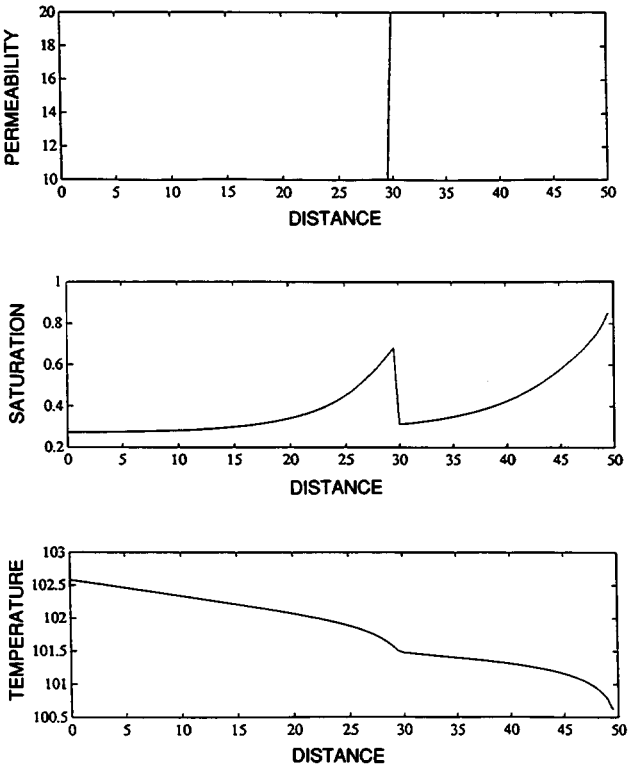

Fig. 1 Capillary heterogeneity: saturation and temperature response for a step increase in permeability.

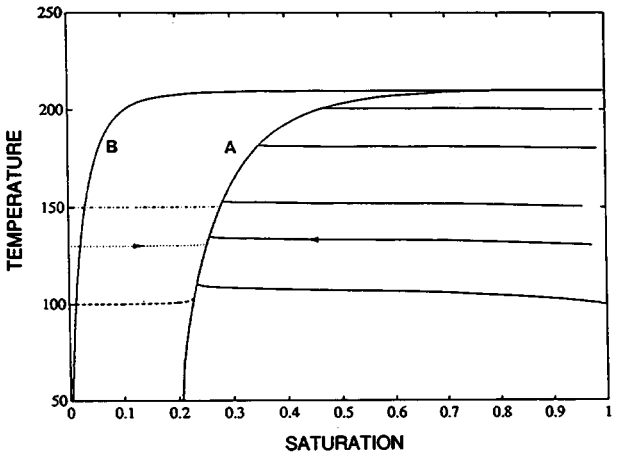

Fig. 2 Phase portrait and saturation–temperature trajectories for steam–water in a homogeneous core. Arrow indicates upstream direction.

The existence of a plateau region is important with regard to steady-state vapor–liquid relative permeability experiments.[4] See reference 5 for a detailed analysis.

In parallel, an investigation has started that will contribute to the understanding of finite size and temperature gradient effects on liquid-to-vapor phase change in porous media. One approach is to simulate the process with network models, across which a prescribed temperature difference is applied. This study would extend previous

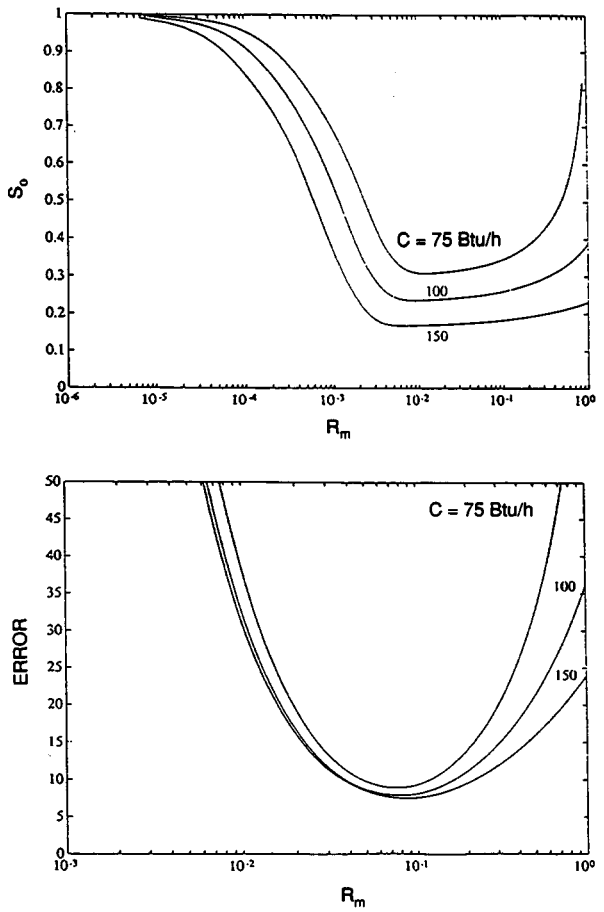

Fig. 3 Sensitivity of inlet saturation (S_o) and of error estimate to the rate parameter (R_m). Effect of heat injection rate C (Btu/h).

work on nucleation and phase change[6] to account for temperature gradients. The ultimate objective is the direct application to steam–water relative permeabilities, whereas boiling processes in porous media, in general, would also benefit from the results obtained. This work is currently in progress. In a separate project, an investigation of the modeling of thermal processes in naturally fractured systems is under way. At present, efforts include further understanding of block-to-block mechanisms and the proper representation of the fracture network. The analysis previously undertaken[5] will be a useful application in such systems.

Finally, a theoretical project on the motion of lateral interfaces in fully developed fingers is almost complete. This phenomenon has been considered in the context of the simpler Hele–Shaw flows, where a nonlinear (but small amplitude) analysis of the finger interface has been carried out. It was found that, in the limit of large capillary number, where capillary effects are negligible, a dispersive wave motion is possible, the dynamics of which are governed by the coupled set of the KdV and the Airy equations. Interestingly, the wave motion is nondispersive for the Saffman–Taylor finger. Analytical and numerical solutions of the problem that allow the effects of the mobility ratio and of the finger size to be investigated have been developed. This research is near completion.

On the experimental side, work has focused on the construction of the experimental apparatus for the study of steam displacement processes in Hele–Shaw cells and in micromodels. An important limitation of steam injection processes in Hele–Shaw cells is lateral heat loss. Experimentation with a thermal insulation design that will allow operation under adiabatic conditions is currently under way. The apparatus is currently being tested, and plans are to start running experiments in the next quarter. In parallel, glass micromodels of various patterns that would allow the pore-level study of steam displacement processes have been made. Finally, a long and narrow Hele–Shaw cell has been assembled to study the wave motion of fully developed fingers and, more generally, of parallel flows. The objective is to test the theoretical predictions described previously. Experiments are currently being conducted.

Chemical Additives

The study of incubation phenomena associated with foam generation and propagation continued. Several experiments were conducted to study the effect of injecting pregenerated foam into a porous medium. The mechanism of foam propagation in the porous medium was also studied.

Experiments were conducted under conditions similar to those reported in previous reports. Upon injection of gas, the pressure in the first section of the core increased immediately (Fig. 4). A delayed response was observed in the other sections of the core: section 2, then 3 and 4. The pressure drop in the effluent section of the core was higher than that in section 3, possibly the result of an end effect. Within 25 pore volumes (PV) a steady pressure drop was reached throughout the core. The foam propagated as a front through the core. After foam flow was initiated with the

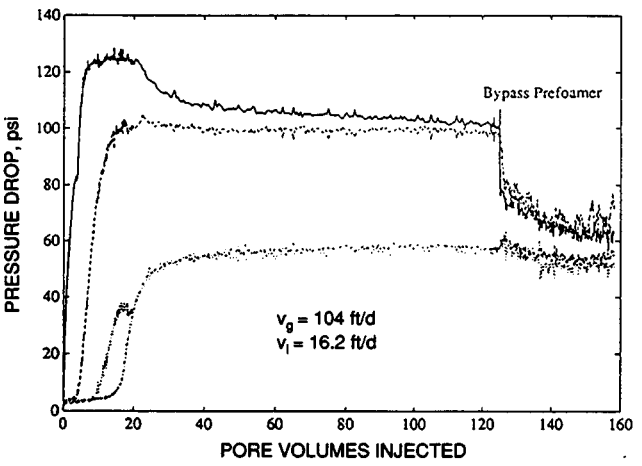

Fig. 4 Pressure drop history in Berea sandstone during simultaneous surfactant and gas injection (with prefoamer).

prefoamer, the bypass line was opened and the fluids were mixed in the tubing before entering the core. At steady state, after the prefoamer was bypassed, the first two sections of the core showed pressure drops comparable with the last two sections. This indicated that the effect of the prefoamer does not extend too far and certainly not beyond the first two sections.

The same experiment was repeated without a prefoamer (Fig. 5). It took more than 50 PV of injection before the pressure responses stabilized, more than twice as many pore volumes as with a prefoamer. The prefoamer was put in line for a brief time period. However, the bypass line was soon reopened because pressures were excessively high. As the liquid velocity was dropped by a factor of 2, the pressure drop also collapsed by a factor of 2, which indicated Darcy flow for the liquid phase. The early time plot (Fig. 6) shows that the pressure drop increased first in the second section of the core, which indicates that fluids travel a certain distance before lamellae form and propagate. Foam started generating in the first section only after foam propagated through sections 3 and 4. As soon as the prefoamer was turned on, the first pressure tap experienced a sudden increase in pressure (Fig. 7). The pressure in the second section of the core increased as well, although to a lesser degree, whereas the effect on the third and fourth sections of the core was minimal. Bypassing the prefoamer caused a drop in pressure in all the sections, most significantly in the upper end.

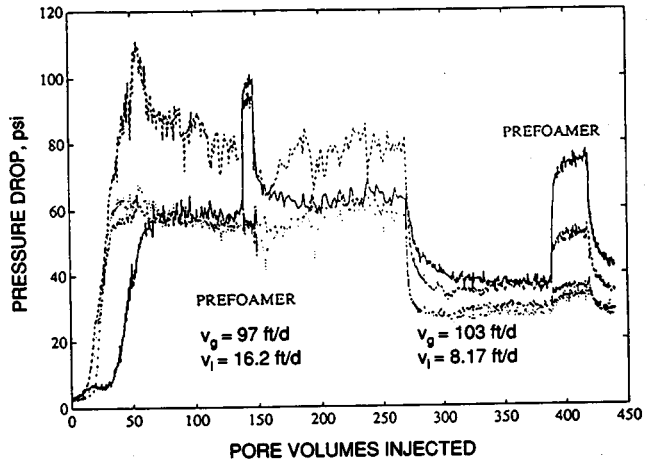

Fig. 5 Pressure drop history in Berea sandstone during simultaneous surfactant and gas injection (without prefoamer).

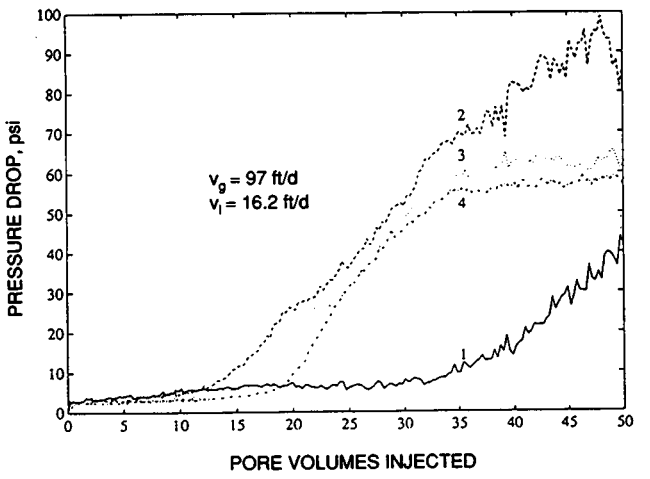

Fig. 6 Pressure drop history in Berea sandstone during simultaneous surfactant and gas injection (without prefoamer, early time). Curves 1, 2, 3, and 4 correspond to consecutive core sections (upstream to downstream).

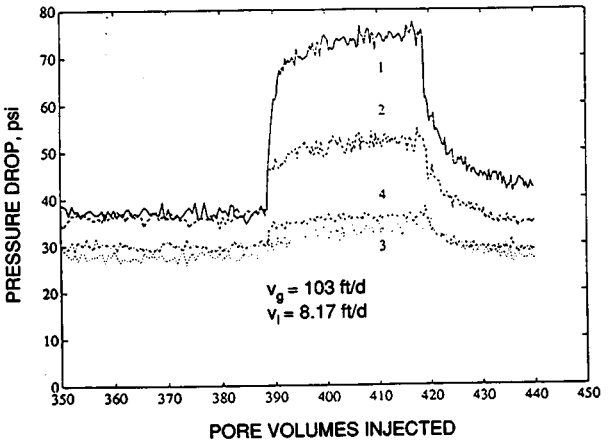

Fig. 7 Effect of prefoamer in Berea sandstone during simultaneous surfactant and gas injection. Curves 1, 2, 3, and 4 correspond to consecutive core sections (upstream to downstream).

On the basis of these results, the conclusion can be reached that the use of a prefoamer enhances foam flow by generating a foam front that propagates in the porous medium. Also, the effect of pregenerating a foam before injection does not extend too far from the inlet end of the core.

References

1. C. Satik, M. Parlar, and Y. C. Yortsos, A Study of Steady-State Steam–Water Counterflow in Porous Media, *Int. J. Heat Mass Transfer*, (accepted) (1990).
2. Y. C. Yortsos and J. Chang, Capillary Effects in Steady-State Flow in Heterogeneous Cores, *Transp. Porous Media* (in press) (1990).
3. F. G. Miller, Steady Flow of Two-Phase Single-Component Fluids Through Porous Media, *Trans. AIME*, 192: 205 (1951).
4. J. M. Sanchez and R. S. Schechter, paper SPE 16967 presented at the 62nd Annual SPE Fall Meeting, Dallas, Tex., 1987.
5. M. Parlar, M. Zeybek, and Y. C. Yortsos, paper SPE 20054 presented at the SPE California Regional Meeting, Ventura, Calif., 1990.
6. Y. C. Yortsos and M. Parlar, paper SPE 19697 presented at the 64th Annual SPE Fall Meeting, San Antonio, Tex., 1989.

CHARACTERIZATION OF THE GRAVITY DRAINAGE PHENOMENA THROUGH NUMERICAL AND PHYSICAL SIMULATION

Contract No. DE-AC22-90BC14472

Western Research Institute
Laramie, Wyo.

Contract Date: Jan. 1, 1990
Anticipated Completion: Jan. 10, 1992
Government Award: $299,986

Principal Investigator:
Palmer Vaughn

Project Manager:
Robert E. Lemmon
Bartlesville Project Office

Reporting Period: Jan. 1–Mar. 31, 1990

Objective

The objective of this project is to provide a predictive model for the gravity drainage mechanism and to verify the model by performing one- and three-dimensional physical simulations. The model will be used to evaluate well pattern geometries on gravity drainage flow patterns and the effects of natural fracture orientations of these systems. The predicted production rates from these models will aid in the evaluation of initial drilling and the use of horizontal, slant, or vertical wells and in oil mining.

Summary of Technical Progress

A conceptual model has been developed which describes the gravity drainage of heavy oil through a porous reservoir. The gravity drainage phenomena is characterized by the fact that part of the boundary defining the fluid system is a free surface. A free surface is a fluid surface in equilibrium with the atmosphere rather than a rigid boundary. It is therefore a streamline along which pressure is uniform or saturation is at an irreducible level.

Prior to the development of the conceptual model, an extensive review of the gravity drainage and associated moving boundary problem literature was analyzed. The conceptual model, reformulation, and solution approach resulted from the literature study.

This review revealed that oil gravity drainage is best described by consideration of two-phase flow (oil and water or gas). The model's geometry is that of two-dimensional flow consisting of a radial description of areal extent and a Cartesian representation of the vertical movement. In this formulation the free surface boundary is a function of both time and radial position. Finite difference techniques are used to discretize the reservoir. Thus the reservoir is numerically divided into a grid pattern.

Except for the free surface, the reservoir is assumed to be surrounded by an impervious formation so that the transmissivities normal to the impervious boundaries are zero. Wells are specified by point sinks in the particular grid blocks in which they occur. Flow rate or wellbore pressure is specified. The definition of a free surface provides two additional boundary conditions: one of which is required to determine the pressure distribution and the other is required for the specification of the free surface location and shape. These conditions are: (a) the pressure gradient normal to the free surface is zero and (b) the pressure along the free surface is constant.

The solution of the gravity drainage problem is most amendable to a transformation of the natural coordinate system to one of body-fitted coordinates. This transformation allows the moving boundary to become fixed for all time. The attractions of working in a fixed region are partly offset by the increased complexity of the transformed partial differential equations that govern the flow.

THERMAL PROCESSES FOR LIGHT OIL RECOVERY

Cooperative Agreement DE-FC22-83FE60149, Project BE11A

National Institute for Petroleum and Energy Research
Bartlesville, Okla.

Contract Date: Oct. 1, 1983
Anticipated Completion: Sept. 30, 1990
Funding for FY 1990: $300,000

Principal Investigator:
David K. Olsen

Project Manager:
Thomas B. Reid
Bartlesville Project Office

Reporting Period: Jan. 1–Mar. 31, 1990

Objectives

The objectives of this project are to improve the understanding of the basic mechanisms responsible for the

improvement of light oil production using steam and to use that understanding for accelerating development of this production technology. Specifically for FY90, the objectives are to: (1) support the U.S. Department of Energy (DOE) in its cooperative effort with Venezuela in thermal technology transfer by participating in the Annex IV meetings; (2) determine the potential of oil recovery by steamflooding previously waterflooded light oil reservoirs that are oil wet rather than water wet; (3) correlate capillary pressure experimental results obtained from high-temperature centrifuge data with two-phase relative permeability experiments performed at high temperatures and design an empirical model that will be useful in existing numerical simulators that describe this behavior for use in steamflood projects; (4) investigate the use of novel steam diverters for steamflooding of light oils; and (5) design a scaled, two-dimensional (2-D) steamflood physical model with the capability to model various steamflooding conditions.

Summary of Technical Progress

Participation in Annex IV Meeting

A presentation and technical review of research conducted under project BE11A were presented to the DOE and the Ministry of Energy and Mines of the Republic of Venezuela on March 13–14, 1990, at INTEVEP Headquarters in Los Teques, Venezuela. The presentation included research on capillary pressures, wettability at high temperatures, effects of wettability on steamflood recovery of light oil, and the results of the National Institute for Petroleum and Energy Research (NIPER) scaling study to design a new multi-dimensional steamflood physical model.

Capillary Pressure and Wettability at High Temperature

Two papers have been prepared for presentation at the UNITAR Heavy Oil and Tar Sands meeting scheduled for February 1991 in Caracas, Venezuela. The first paper, "Effects of Elevated Temperatures on Capillary Pressure and Wettability," by M. E. Crocker, P. S. Sarathi, and D. K. Olsen, summarizes the NIPER work in this area over the past year. The second paper, "Evaluation of Artificially Wetted Surfaces for Use in Laboratory Steamflood Experiments," by D. K. Olsen and M. E. Crocker, summarizes the study of the stability of silylated consolidated and unconsolidated media and their use in steamflood oil displacement experiments.

Light Oil Steamflood Experiments

Most light oil reservoirs are waterflooded after primary production. To investigate the potential for oil production after waterflooding via steam, a series of steamfloods was conducted on water-wet porous media in 1989 to study the effect of oil composition.[1] To investigate the effect of wettability on steamflood oil recovery, a similar series of experiments in the 2-D model was conducted during the first quarter of FY90 using crushed Berea sandstone of different wettabilities (intermediate wettability or strongly water wet). This study used New London crude oil (32° API) and the 2-D model was waterflooded before steamflooding.[2]

The series of experiments was expanded this quarter to incorporate strongly oil-wet porous media (crushed quartz sand that had been silylated), uncrushed quartz sand that had been silylated to yield a surface of intermediate wettability, and untreated quartz sand that was strongly water wet. The effects of wettability are illustrated by oil production and decline curves in Figs. 1 through 4. The oil-wet quartz sand yielded a high initial and high waterflood residual oil saturation (Figs. 1 and 4). Quartz sands of intermediate

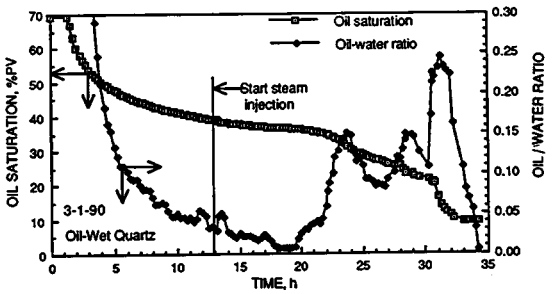

Fig. 1 Oil production from a two-dimensional model packed with strongly oil-wet quartz sandpacks.

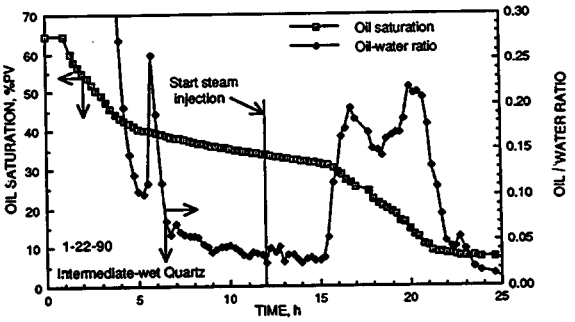

Fig. 2 Oil production from a two-dimensional model packed with intermediate-wet quartz sandpacks.

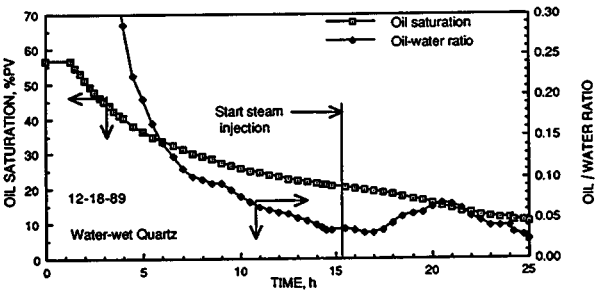

Fig. 3 Oil production from a two-dimensional model packed with water-wet quartz sandpack.

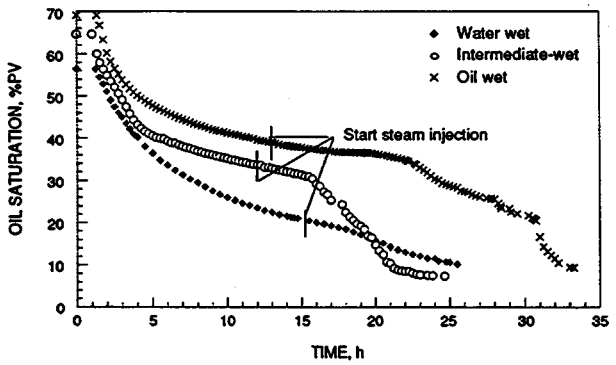

Fig. 4 Comparison of oil production from waterflood followed by a steamflood in oil-wet, intermediate-wet, and water-wet two-dimensional quartz sandpacks.

wettability showed lower initial and intermediate waterflood residual oil saturation but were steamflooded to a low residual oil saturation (Figs. 2 and 4). Water-wet quartz sand resulted in the lowest initial oil saturation, the lowest oil saturation after waterflood, and very little oil to be produced by steamflooding (Figs. 3 and 4). In each experiment, waterfloods were conducted until the water cut was greater than 97% before the start of steam injection. The oil saturation continued to drop as steam was injected and the water, sand, and oil were heated. The oil/water ratio abruptly increased just before steam breakthrough in the cases of intermediate and oil-wet sands. The most significant oil production was seen in those sandpacks which were more oil wet. The oil-wet quartz sandpack experienced mechanical failure of the backpressure system soon after steam injection started (hours 15 to 19, and again at hour 26). Steam injection had to be greatly reduced, and the model began to cool. The 7-h delay in steam breakthrough affected the oil/water ratio. The oil saturation decline curve for the oil-wet sands was not as sharply decreasing as expected, compared with intermediate wet sands. This experiment is being repeated to confirm this result. Oil analysis from these experiments and replotted production curves based on energy (Btu/h) injected into the model will be included in a status report on this project. Comparison of the oil saturation profiles of the sandpacks (Fig. 4) indicates that waterflooding recovers more oil from sands that are more water wet. These results indicate that oil recovery by steamflooding of oil-wet sands looks promising.

References

1. A. Strycker, *Thermal Recovery of Light Crude Oils Using Steam—A Laboratory Study Using a Two-Dimensional Physical Model,* DOE Report NIPER-347, June 1988.
2. D. K. Olsen, National Institute for Petroleum and Energy Research, *Quarterly Technical Report for Oct. 1–Dec. 31, 1989,* DOE Report NIPER-463, Vol. II, p. 64, February 1990.

THERMAL PROCESSES FOR HEAVY OIL RECOVERY

Cooperative Agreement DE-FC22-83FE60149, Project BE11B

National Institute for Petroleum and Energy Research
Bartlesville, Okla.

Contract Date: Oct. 1, 1983
Anticipated Completion: Sept. 30, 1990
Funding for FY 1990: $200,000

Principal Investigator:
David K. Olsen

Project Manager:
Thomas B. Reid
Bartlesville Project Office

Reporting Period: Jan. 1–Mar. 31, 1990

Objectives

The objectives of this project are to improve the understanding of the basic mechanisms responsible for the improvement of heavy oil production with steam and to use that understanding for further development of this production method. The FY90 objectives are to: (1) investigate the effectiveness of mobility control and diverting agents in diverting steam from a zone of high permeability to a zone of lower permeability; (2) compare the predicted values obtained with the numerical simulator with laboratory-measured values of steamflood performance; and (3) compile and write a summary on the operation of steamfloods.

Summary of Technical Progress

Steamflood Field Equipment and Operation

Interviews were held with operators of thermal enhanced oil recovery (EOR) projects, and California cyclic steam and steamdrive operations were visited to compile information for a status report on field equipment and operations. This analysis of field operations will help document thermal operations and identify areas for future research. In California, many major and independent operators have gone to great lengths to make their thermal steam generation and delivery to the formation face cost-effective by implementing cogeneration (generation of electricity and steam). Cogeneration with natural gas is providing electricity for use on leases and for possible sales and

allows operators to comply with air quality standards, thus permitting continued thermal oil production operations. Analyses by several operators indicate that costs of steam produced by cogeneration are lower than those of steam produced by large conventional tube type steam generators. These older generators are being replaced because their operating costs are high and because of necessary additions and uses of pollution-control devices to meet ever stricter air quality regulations. The use of natural gas as a fuel is quickly replacing high-sulfur lease crude in attempts to meet air quality standards. A status report is being written for this task. It will contain sections on water quality, steam generation, steam transport and injection, steam quality, insulated tubulars, gravel packing, sand control, and production surface and monitoring equipment.

Steamflood Experiments

One of the major difficulties with steam is its poor sweep efficiency in displacing viscous crude oil. This project has been evaluating surfactants as steam diverters or mobility-control agents to increase the sweep efficiency of the process. Last year, the two-dimensional (2-D) model was altered to include multilayers to simulate multiple sand zones, each with different permeabilities. Altering the flow of steam into zones not originally contacted by steam has been the goal of this research. Several 2-D steamflood runs will be made using low-pH alkaline chemicals added to reduce surfactant requirements. These formulations are expected to accelerate the propagation of the foam front.

Part of the 2-D steamflood model data-collection system was upgraded to include new thermocouples and software for operating the system, controlling pressure, monitoring temperature, and steam-generator control. Steamfloods on heavy oil will incorporate internal insulation into the 2-D model to reduce heat loss. These suggested modifications originate from the scaling study conducted under a complementary project that analyzed the current 2-D model and its operation. A new multidimensional physical model is being designed for construction in FY91.

MECHANISMS OF MOBILITY CONTROL WITH FOAMS

Contract No. DE-AC03-76SF00098

Lawrence Berkeley Laboratory
University of California
Berkeley, Calif.

Contract Date: Oct. 1, 1985
Anticipated Completion: Sept 30, 1990
Government Award: $300,000
(Current year)

Principal Investigators:
K. S. Udell
C. J. Radke

Project Manager:
Thomas B. Reid
Bartlesville Project Office

Reporting Period: Jan. 1–Mar. 31, 1990

Objective

Foam is a promising fluid for achieving mobility control in a variety of underground processes, including enhanced oil recovery by steam, CO_2, N_2, or light hydrocarbon flooding. Because of its dispersed nature, foam exhibits low flow mobilities that may possibly overcome gravity override and viscous fingering through the permeable streaks always present in underground porous media.

From the outset of foam studies in porous media, it was recognized that a very important factor controlling foam mobility is the bubble-size distribution, or equivalently, the foam texture. In spite of this recognition, relatively little work has been directed toward incorporating bubble size into models of foam flow. In the September 1989 quarterly progress report, bubble sizes measured at the inlet and outlet of a 0.8-μm^2 Berea sandstone core were presented. Here a simple population-balance model to explain that data for steady foam flow is outlined.

Summary of Technical Progress

A modified form of Darcy's law is written to describe foam flow in a strongly water-wetting porous medium:

$$\underset{\sim g}{U} = - \frac{k\, k_{rgF}}{\mu_e} \nabla P_g \qquad (1)$$

where U_g = flowing foam superficial velocity
P_g = gas pressure
k = absolute permeability
k_{rgF} = relative permeability of the flowing foam (k_{rgF} is the usual relative permeability of the non-wetting phase but evaluated at the flowing gas saturation, S_F. Since S_F may be small as a result of large amounts of trapped gas, k_{rgF} may also be quite small)
μ_e = effective or apparent viscosity

Equation 1 is useful only insofar as μ_e is a known function. The most important property of μ_e is that it increases with increasing texture so that smaller bubbles produce larger flow resistances. Both experimental and theoretical evidence to date suggest the following form for μ_e (Ref. 1–3):

$$\frac{\mu_e - \mu_g}{\mu} = A\, n_F\, D_b^3 \left(\frac{\sigma}{\mu U_g}\right)^{1/3} \qquad (2)$$

where μ = liquid viscosity
μ_g = gas viscosity
D_b = characteristic pore-body diameter
σ = equilibrium surface tension
n_F = local bubble density
A = scaling coefficient

For fixed liquid and flowing gas saturations and for a fixed surfactant type and concentration, A is a constant.[1,2] Equation 2 teaches that the viscous resistance of flowing foam is linearly proportional to bubble density, ostensibly because most of the hydrodynamic resistance of the bubbles is localized near the lamellae.[1,2] It also teaches that flowing foam is shear thinning. Typical values for μ_e in this work and in that of Persoff et al. (Figs. 10 and 11 of Ref. 4) range approximately from 10 to 100 mPa·s.

It is necessary to quantify the bubble texture to proceed. As in Eq. 2, let $n_F(X)$ denote the mean bubble density, or the number of bubbles per available flowing volume, as a function of axial position, x, along the linear core. A steady-state population balance on the average flowing bubble size then reads:[3,5,6]

$$\frac{d(n_F U_g)}{dx} = r_g - r_c \qquad (3)$$

where r_g and r_c are the rates of bubble generation and coalescence, respectively, per unit bed volume.

For constant surfactant concentrations, constant gas and liquid saturations, and at a fixed liquid velocity, the coalescence rate is written as:

$$r_c = k_{-1}\, U_g^n\, n_F \qquad (4)$$

where k_{-1} is a coalescence rate constant. Equation 4 is motivated by the idea that foam lamellae disappear in proportion to their flux into termination sites, $n_F U_g$. In addition, higher gas velocities lead to a higher probability of breakage because the stretched, vulnerable lamellae do not have sufficient time for healing from the surrounding foamer solution.[7] In other words, the limiting capillary pressure for the onset of coalescence is a function of gas velocity.[8] Hence the power index n in Eq. 4 should be somewhat larger but close to unity. The coalescence rate constant depends strongly on the surfactant type and concentration with weak surfactants and low concentrations making k_{-1} quite large, possibly large enough to prevent any steady foam in the medium.

The foam generation rate by snap-off should be independent of texture as long as the bubble size does not fall to quite a low value.[3] Constant liquid velocity and saturation is written as:

$$r_g = k_1 U_g^m \qquad (5)$$

where k_1 is a generation rate constant, and the power index m should not be large. The generation rate constant should not depend on the surfactant formulation.[9,10] Equation 5 is valid only when the critical velocity or pressure gradient necessary to initiate snap-off is exceeded, [3,11] otherwise $k_1 \equiv 0$ (Ref. 3).

In addition to describing bubble-density evolution by Eq. 3, a statement is required about overall mass conservation of the gas phase. For an ideal gas, this statement reduces to

$$P_g U_g = P_{gL} U_{gL} \qquad (6)$$

where P_{gL} and U_{gL} are the gas pressure and gas velocity, respectively, at the core exit.

Equations 1 to 6 reduce to two, first-order, coupled, and nonlinear ordinary differential equations describing the pressure and bubble concentration profiles. They are solved numerically subject to a fixed inlet texture and a known outlet pressure.[12] These conditions correspond to the experimental procedures used here.

Figures 1 and 2 compare typical measured and theoretical bubble density and pressure profiles both for pregenerated (closed symbols) and in situ (open symbols) produced strong foam. Parameter-fitting procedures and additional profile data are given elsewhere.[12] Solid lines follow the population-balance model, whereas dashed lines obey the local-equilibrium approximation. Generally, measured and predicted textures are always in good agreement. Predicted pressure profiles, however, tend to overestimate the in situ generated foam behavior and to underestimate the pregenerated foam behavior. In particular, the predicted sharp rise in pressure near the inlet upon injection of a fine-textured foam is never seen experimentally. Possibly some foam collapse may take place in the inlet distribution channels as the pregenerated bubbles attempt to enter the sandstone medium. Also, small errors in measuring these

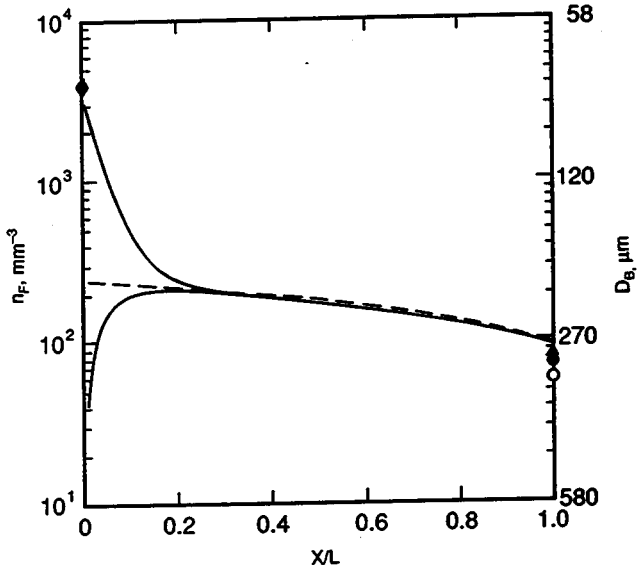

Fig. 1 Bubble density profiles for pregenerated (♦●) and in situ generated (○) foam flow experiments: U = 0.91 m/d and f_g = 0.70. Model predictions (—) and the local-equilibrium approximation (– – –) are shown.

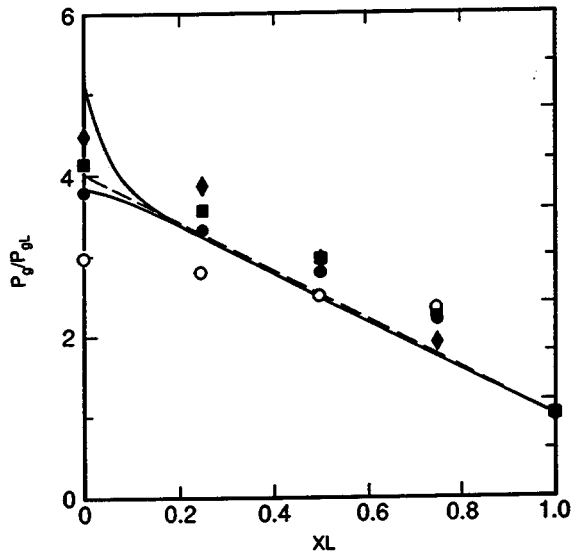

Fig. 2 Dimensionless pressure profiles for pregenerated (♦■●) and in situ generated (○) foam flow experiments: U = 0.91 m/d and f_g = 0.70. Model predictions (—) and the local-equilibrium approximation (– – –) are shown.

fine bubble sizes result in rather large changes in n_F. In view of the scatter typically seen in repeated foam flow experiments (the various solid symbols in Figs. 1 and 2), the model predictions are adequate but not sterling. The population-balance approach has merit as the measured textures and predicted foam-flow behavior are consistent.

Nomenclature

A	effective viscosity scaling coefficient (dimensionless)
D_b	average pore-body diameter (m)
D_B	average bubble diameter (m)
f_g	gas fractional flow (dimensionless)
k	absolute permeability (m^2)
k_{rgF}	relative permeability to flowing foam (dimensionless)
k_1	generation rate constant [$(cm/s)^{2/3}$ mm^{-3}]
k_{-1}	coalescence rate constant (m^{-1})
L	core length (m)
m	generation rate gas-velocity order (dimensionless)
n	coalescence rate gas-velocity order (dimensionless)
n_F	local bubble density (m^{-3})
P_g	gas-phase pressure (Pa)
P_{gL}	exit gas-phase pressure (Pa)
r_c	rate of coalescence (m^{-3} s^{-1})
r_g	rate of generation (m^{-3} s^{-1})
S_F	flowing foam saturation (dimensionless)
U	total superficial velocity (m/day)
U_g	gas superficial velocity (m/day)
U_{gL}	gas exit superficial velocity (m/day)
x	axial distance along core (m)

Greek

μ	liquid viscosity (mPa·s)
μ_e	effective foam viscosity (mPa·s)
μ_g	gas viscosity (mPa·s)
σ	equilibrium surface tension (N/m)

References

1. G. J. Hirasaki and J. B. Lawson, Mechanism of Foam Flow in Porous Media: Apparent Viscosity in Smooth Capillaries, *Soc. Pet. Eng. J.*, 25(2): 176-190 (April 1985).
2. G. M. Ginley and C. J. Radke, Influence of Soluble Surfactants on the Flow of Long Bubbles Through a Cylindrical Capillary, in *Oil-Field Chemistry; Enhanced Recovery and Production Stimulation*, J. K. Borchardt and T. F. Yen (Eds.), ACS Symposium Series 396, American Chemical Society, Washington, D.C., Chapter 26, 481-501 (1989).
3. F. Friedmann, W. H. Chen, and P. A. Gauglitz, *Experimental and Simulation Study of High-Temperature Foam Displacement in Porous Media*, paper SPE/DOE 17357, presented at the 1988 SPE/DOE Enhanced Oil Recovery Symposium, Tulsa, Okla., Apr. 17–20.
4. P. Persoff, C. J. Radke, K. Pruess, S. M. Benson, and P. A. Witherspoon, *A Laboratory Investigation of Foam Flow in Sandstone at Elevated Pressure*, paper SPE 18781, presented at the 1989 SPE California Regional Meeting, Bakersfield, Calif., Apr. 5–7.
5. A. H. Falls, G. J Hirasaki, T. W. Patzek, P. A. Gauglitz, D. D. Miller, and T. Ratulowski, Development of a Mechanistic Foam Simulator: The Population Balance and Generation by Snap-Off, *SPE Reservoir Eng.*, 3(3): 844-892 (August 1988).
6. T. W. Patzek, Description of Foam Flow in Porous Media by the Population Balance Method, *Surfactant-Based Mobility Control*, D. H. Smith (Ed.), ACS Symposium Series, Vol. 373, pp. 326-341, 1988.
7. A. I. Jiménez and C. J. Radke, Dynamic Stability of Foam Lamellae Flowing Through a Periodically Constricted Pore, in

Oil-Field Chemistry; Enhanced Recovery and Production Stimulation, J. K. Borchardt and T. F. Yen (Eds.), ACS Symposium Series 396, American Chemical Society, Washington, D.C., Chapter 25, 461-479 (1989).
8. Z. I. Khatib, G. J. Hirasaki, and A. H. Falls, Effects of Capillary Pressure on Coalescence and Phase Mobilities in Foams Flowing Through Porous Media, *SPE Reservoir Eng.*, 919-926 (August 1988).
9. P. A. Gauglitz, C. M. St. Laurent, and C. J. Radke, An Experimental Investigation of Gas-Bubble Breakup in Constricted Square Capillaries, *J. Pet. Technol.*, 39(9): 1137-1146 (September 1987).
10. T. C. Ransohoff, P. A. Gauglitz, and C. J. Radke, Snap-Off of Gas Bubbles in Smoothly Constricted Noncircular Capillaries, *AIChE J.*, 753-765 (May 1987).
11. T. C. Ransohoff and C. J. Radke, Mechanisms of Foam Generation in Glass-Bead Packs, *SPE Reservoir Eng.*, 3(3): 573-585 (May 1988).
12. R. A. Ettinger, *Flow Resistance of Foam in Berea Sandstone,* M. S. thesis, University of California, Berkeley, 1990.

INNOVATIVE DRILLING COMPLETION SYSTEM

Contract No. DE-AC22-89BC14203

Petrolphysics, Inc.
San Francisco, Calif.

Contract Date: Sept. 25, 1989
Anticipated Completion: Sept. 30, 1990
Government Award: $276,159

Principal Investigator:
R. Wayne Dickinson

Project Manager:
Thomas B. Reid
Bartlesville Project Office

Reporting Period: Jan. 1–Mar. 31, 1990

Objective

The objective of this project is to demonstrate the applicability of the Petrolphysics Ultrashort Radius Radial System (URRS) to thermal operations in the relatively shallow heavy oil formations of the Southern San Joaquin Valley in California.

The project has been divided into four tasks: (1) geological review and selection of the well location, (2) drilling and completion of the horizontal radials, (3) injection of steam and production of the well, and (4) preparation of the final report on the project.

Summary of Technical Progress

During the current quarter, task 1 was completed, and approximately 60% of task 2 was completed.

Geological Review and Well Site Selection

Task 1 was completed and a topical report documenting the work was prepared. A candidate well was selected and designated as RI-53. The well site was located in Union Oil Company's Bremer Fee lease in the Midway Sunset field in the southern San Joaquin Valley in California.

Three considerations were taken into account in the final selection of the RI-53 location. First, the well was located in close proximity to other steam injectors and oil producers, which can provide meaningful baseline data for comparative analysis. Second, RI-53 was drilled as part of an ongoing drilling program, which minimized Union Oil Company's exposure to unnecessary drilling costs. Third, the well was capable of becoming a full-time steam injector well once the well was produced for one cycle. By being able to revert back to steam injection status once the project was completed, the overall cost of the project would be reduced.

Summary of Drilling and Completion of the Horizontal Radials

The vertical portion of RI-53 was drilled to a depth of 1250 ft. A 7-in., 23-lb casing was then run to 870 ft. The well was then cemented with a class "G" cement. The well was then "plugged back" to 1060 ft, which left an open interval from 870 to 1060 ft.

The interval from 870 to 900 ft was underreamed to a diameter of 24 in. When the underreaming was completed, a caliper survey of the underreamed zone was made. This survey provided an accurate profile of the wellbore in the zone of interest.

The preceding operations were performed from Mar. 28 to Mar. 31, 1990.

Horizontal radial placement operations using the URRS in RI-53 began on Apr. 9, 1990.

The first radial was placed at an elevation of 884 ft. The initial azimuth orientation of this radial was N7W. The radial was placed to a horizontal distance of 74 ft into the formation. This radial was positionally logged and completed with Petrolphysics' gravel-packing technology.

The second radial was placed at 884 ft. The radial's initial orientation was S80W. This radial was placed 106 ft into the formation and was also completed with Petrolphysics gravel-packing technology.

The first radial was completed on Apr. 11, 1990, and the second radial was completed on Apr. 13, 1990.

A subsequent quarterly report will give the details of the final two radials placed in RI-53 as well as the vertical completion of the well. Additionally, preliminary steam injection and oil production information should be available.

Additional detailed information on both task 1 and task 2 can be found in their respective topical reports, which have previously been submitted to the U.S. Department of Energy.

GEOSCIENCE TECHNOLOGY

PETROLEUM GEOCHEMISTRY

Lawrence Livermore National Laboratory
Livermore, Calif.

Contract Date: Oct. 1, 1987
Anticipated Completion: Sept. 30, 1990
Government Award: $197,000
(Current year)

Principal Investigator:
Alan K. Burnham

Project Manager:
Robert E. Lemmon
Bartlesville Project Office

Reporting Period: Jan. 1–Mar. 31, 1990

Objectives

The purpose of this project is to develop and test an improved chemical kinetic model of petroleum generation, expulsion, and destruction. Laboratory pyrolysis is used in conjunction with literature data to develop models. The model will include equation-of-state calculations to predict the amount and compositions of gaseous and liquid phases. Geological modeling will be used to derive thermal histories in petroleum-generating basins. These histories will be used in the chemical kinetic model to generate predictions to be compared with geochemical evidence. One part of the work will be in collaboration with INTEVEP, as described in ANNEX XII of the implementing agreement between the Department of Energy (DOE) and the Ministry of Energy and Mines of Venezuela.

Summary of Technical Progress

During this period, work continued on the refinement of time–temperature history models for wells in the Maracaibo Basin using the commercial basin analysis software, BasinMod. Technology transfer activities included helping Platte River Associates upgrade the organic chemistry modeling capabilities of BasinMod in return for free use of the software. This provides a quick and convenient means to transfer the developments in chemical kinetic modeling of the research community to the general petroleum exploration community. In addition to this software upgrade, two papers were finalized and submitted to journals. One paper[1] is designed to acquaint geochemists and geologists in the petroleum community with the concepts of distributed activation energies in chemical kinetic modeling. It includes a short FORTRAN program listing to illustrate the technique and will be published in the American Association of Petroleum Geologists (AAPG) computer applications journal *Geobyte*. The other paper,[2] which will be published in the *AAPG Bulletin*, describes and illustrates the use of the simplified model of vitrinite

maturation. The intent with both of these publications, and with interactions with Platte River, is to disseminate developments in chemical kinetic modeling to the wider community of petroleum geologists actively engaged in exploration and not just to the more specialized community of organic geochemists.

During the last quarter, BasinMod was used to develop time–temperature histories for wells in the Maracaibo Basin to check those previously provided by INTEVEP. Previous INTEVEP thermal history models used a simpler geothermal gradient approach, where gradients were estimated from bottom hole temperatures. In the INTEVEP models, the regional gradients were adjusted to account for higher local gradients observed in the thick Colon and La Luna shales. With BasinMod, the change in gradient is successfully modeled by using lower values of thermal conductivity in the Colon and La Luna formations and a constant value of regional heat flow of about 40 to 45 mW/m.^{2} A regionally consistent set of lithological physical parameters and heat flow values that produce thermal histories consistent with vitrinite reflectance profiles in about 15 wells were determined. These parameters were then used to develop thermal histories for about 15 additional wells for which INTEVEP has not determined thermal histories. These additional wells, from which INTEVEP has provided oil and extract chemical data, are crucial for comparison of calculated and measured characteristics of hydrocarbon generation.

References

1. J. J. Sweeney, BASINMAT: FORTRAN Program Calculates Oil and Gas Generation Using a Distribution of Discrete Activation Energies, *Geobyte*, 37–43 (April 1990).
2. J. J. Sweeney and A. K. Burnham, Evaluation of a Simple Model of Vitrinite Reflectance Based on Chemical Kinetics, *AAPG Bulletin*, 74: 1559-1570 (1990).

ADVANCED SEISMIC GEODIAGNOSTICS— BOREHOLE ACOUSTIC SOURCE

Los Alamos National Laboratory
Los Alamos, N. Mex.

Contract Date: Mar. 1, 1988
Anticipated Completion: Sept. 30, 1990
Government Award: $197,000

Principal Investigators:
James N. Albright
R. Hanold

Project Manager:
Robert E. Lemmon
Bartlesville Project Office

Reporting Period: Jan. 1–Mar. 31, 1990

Objectives

The objectives of this project are to (1) improve oil reservoir characterization techniques by interwell tomographic imaging of producing horizons, (2) investigate the design of a totally new downhole acoustic source that will permit interwell seismic surveying between oil wells with much larger separation distances, and (3) evaluate the performance of a Department of Energy (DOE) borehole receiver developed for interwell seismic surveying in the environment of a producing oil field.

Summary of Technical Progress

Design of a Chemically Powered, Seismic Source for Crosswell Seismic Surveying

The Los Alamos National Laboratory is developing a borehole seismic source based on explosives manufactured in small quantities within the source while in use. For any borehole source to be adopted for widespread use in the oil industry, the source must have the following characteristics: high seismic frequency, high energy, high firing rate, and low cost of operation. The tool is being designed for use with standard seven-conductor wirelines that will provide hoisting and telemetry channels for operation of the tool. The tool will enable a nominal quantity of 10,000 shots to be fired during one trip in the wellbore.

The requirements for the explosive source are not simultaneously met by any other borehole source under development. High energy and firing rates are required if a source is to be used economically in oil fields having commonly encountered well spacings. A unique feature of the design is the fact that the energy for the source will come from chemicals contained in reservoirs in the tool; this provides a combination of high energy and firing rate that will far exceed that possible for sources powered through conventional wirelines. Another unique tool design feature is that the two liquid chemicals, which are mixed in the tool to produce an insensitive explosive, are classified, respectively, as a flammable solvent and organic base by the Department of Transportation. Ensuring product safety is a major part of this development effort. Tool operation should be inherently safe. At no time should explosives

exist aboveground, or at any instant, only a few grams should be present in the tool. When not immediately used, the few grams of explosive should ideally self-desensitize.

Progress during the second quarter included an analysis that focused on understanding how energy is converted to mechanical energy for initiation of the sensitized explosive mixture. Understanding how energy is partitioned and conserved will provide insights for increasing energy conversion efficiency. High energy conversion efficiency is required to minimize the volume in the tool occupied by the capacitor and associated electronics that provide the energy for initiation.

Analyses were also begun on the circuits for charging the capacitor in the tool and for discharging the capacitor in accordance with the requirements for initiation of the sensitized explosive mixture. The results of these analyses are needed for interfacing this seismic source with commercial wirelines and for specifying the electrical requirements for the initiation system. A standard seven-conductor well logging cable can easily handle the electrical power requirements for repetitively charging the initiation system capacitor at a rate of one pulse per second.

Progress during this quarter also included a preliminary layout of the mechanism that will transport the explosive mixture from the mixing device to the site of initiation in the tool.

AN EXPERIMENTAL AND THEORETICAL STUDY TO RELATE UNCOMMON ROCK–FLUID PROPERTIES TO OIL RECOVERY

Contract No. AC22-89BC14477

Pennsylvania State University
University Park, Pa.

Contract Date: Sept. 21, 1989
Anticipated Completion: Aug. 31, 1992
Government Award: $260,221

Principal Investigators:
Turgay Ertekin
Robert W. Watson

Project Manager:
Robert E. Lemmon
Bartlesville Project Office

Reporting Period: Jan. 1–Mar. 31, 1990

Objectives

The overall objectives of the project are to:

1. Develop a better understanding of some important but not really well-investigated rock properties, such as tortuosity, wettability, pore-size distribution, surface area, wettability, and neck–throat average rock size, and develop a better insight on capillary pressure variation with respect to wettability and pore geometry of Berea sandstone, limestone, and dolomite.

2. Develop a relationship between oil recovery at breakthrough and wettability and surface areas of the rocks and develop correlations between oil recovery at infinite water/oil ratio and wettability and surface area of these different porous media. Additionally, variations of average irreducible water saturation and average residual oil saturation with respect to wettability will be investigated.

3. Improve the understanding of fluid flow in porous media under conditions of secondary and tertiary recovery through the laboratory study of the performance of enhanced recovery methods, such as waterflooding.

Summary of Technical Progress

Amott's method for determining average wettability indices was applied to Berea sandstone cores. So that a more accurate average wettability index could be determined for each waterflooded rock, 524 core plugs were extracted from the waterflooded cores. The mean wettability of the reservoir was functionally related to the amount of hydrophobic or hydrophilic surface area present in each core sample. The wettability of Berea sandstone core plugs ranged from a minimum value of +0.45 to a maximum value of +1.00 or absolute water wettability. Wettability variations of the less permeable rocks were more pronounced. This was attributed to the relative abundance of shaley streaks in the tighter cores and led to the conclusion that, with respect to the plugs tested, the wettability is heterogeneous or "Dalmatian" with some parts of the surface area being water wet and others being oil wet.

The analysis of data collected during these experiments indicated the following with respect to the effect of wettability on Berea sandstone cores:

1. Wettability controlled fluid distribution.

2. Average wettability index was directly proportional to average irreducible water saturation and inversely proportional to average residual oil saturation.

3. Oil recovery at breakthrough and ultimate oil recovery were higher for the strongly water-wet system.

4. Statistical analysis indicated that the oil recovery at breakthrough and oil recovery at an infinite water/oil ratio were directly proportional to wettability.

Furthermore, analyses indicate that frequency distribution of the wettability indices is skewed to the left since the overall median of the distribution is higher than the mean. Furthermore, the frequency distribution of the average wettability indices is exponential. The conclusion predicated on these observations is that the wettability of Berea sandstone rocks is heterogeneous with hydrophilic dominance. The test of rock heterogeneity in terms of the analysis of variance of the wettability (Table 1) indicates

that a high coefficient of variability is characteristic of the lower permeability cores in which bedding planes perpendicular to the core radius are apparent. The presence of these bedding planes enhances the heterogeneity of the less permeable Berea sandstone cores and consequently increases the standard deviation of the average wettability index determined as an arithmetic average of the wettability index for the eight core plugs shown in Table 2. The hetero-

TABLE 1

Test of Rock Heterogeneity in Terms of Analysis of Variance of Wettability Index*

	Coefficient of variability, %			F-test, dimensionless		
Core No.	Top layer	Medium layer	Bottom layer	Calculated F	Table F	Decision
2	5.57	4.70	1.88	1.89	3.47	Accept H_o
4	2.10	2.14	2.13	0.26	3.47	Accept H_o
5	2.49	4.30	3.02	1.24	3.47	Accept H_o
6	3.85	1.81	4.02	0.65	3.47	Accept H_o
7	3.36	3.76	1.78	2.34	3.47	Accept H_o
8	2.90	1.68	3.66	4.62	3.47	Reject H_o
9	3.58	3.67	4.22	0.42	3.47	Accept H_o
10	2.39	2.18	2.75	0.54	3.47	Accept H_o
11	2.26	2.10	1.99	0.98	3.47	Accept H_o
12	1.86	2.01	2.02	0.54	3.47	Accept H_o
13	1.44	1.80	1.63	1.80	3.47	Accept H_o
14	3.17	2.47	2.42	0.14	3.47	Accept H_o
15	4.56	4.20	2.94	0.90	3.47	Accept H_o
16	5.38	3.01	6.54	0.44	3.47	Accept H_o
17	7.33	9.03	5.60	1.03	3.47	Accept H_o
18	14.45	9.56	14.22	0.06	3.47	Accept H_o
19	5.86	4.57	17.08	2.70	3.47	Accept H_o
20	18.09	13.96	15.21	0.04	3.47	Reject H_o
21	1.86	2.62	2.60	6.16	3.47	Accept H_o
22	9.08	1.69	2.61	1.18	3.47	Accept H_o

*H_o: $\mu_1 = \mu_2 = \mu_3$; H_a: not all μ's are equal; $F = (MSB/MSE) < f(\alpha, df\ factor, dfE)$.

TABLE 2

Average Wettability Index*

Core No.	Top layer	Standard deviation, %	Medium layer	Standard deviation, %	Bottom layer	Standard deviation, %
1	0.836	6.49	0.807	9.11	0.813	4.23
2	0.935	5.21	0.954	4.48	0.975	1.83
3	0.971	1.59	0.971	1.59	0.958	2.16
4	0.965	2.03	0.958	2.05	0.961	2.05
5	0.923	2.30	0.901	3.88	0.921	2.78
6	0.937	3.61	0.954	1.73	0.941	3.79
7	0.897	3.01	0.895	3.36	0.922	1.64
8	0.929	2.69	0.969	1.63	0.956	3.50
9	0.936	3.35	0.952	3.49	0.941	3.97
10	0.958	2.29	0.961	2.10	0.969	2.67
11	0.963	2.17	0.972	2.04	0.959	1.43
12	0.959	1.79	0.966	1.94	0.969	1.96
13	0.977	1.40	0.962	1.73	0.967	1.58
14	0.952	3.02	0.955	2.36	0.959	2.32
15	0.929	4.24	0.930	3.91	0.951	2.79
16	0.933	5.02	0.941	2.83	0.919	6.01
17	0.711	5.21	0.749	6.77	0.737	4.13
18	0.887	12.82	0.906	8.67	0.893	2.70
19	0.858	5.03	0.857	3.92	0.910	6.45
20	0.767	13.87	0.776	10.83	0.784	11.92
21	0.907	1.70	0.890	2.33	0.935	2.43
22	0.934	8.48	0.974	1.65	0.958	2.50

*Average wettability is based on arithmetic average over eight sandstone core plugs.

geneity of the plug samples was examined through statistical hypothesis testing of the equality of means for three layers in each core. The F-test was then implemented to compare the mean square between the wettability values and their mean square for error.

NATURAL RESOURCES INFORMATION SYSTEM FOR THE STATE OF OKLAHOMA

Contract No. DE-FG22-89BC14483
Oklahoma Geological Survey
University of Oklahoma
Norman, Okla.

Contract Date: June 22, 1989
Anticipated Completion: June 21, 1992
Total Project Cost: $1,261,547

Principal Investigator:
Charles J. Mankin

Project Manager:
R. Michael Ray
Bartlesville Project Office

Reporting Period: Jan. 1–Mar. 31, 1990

Objective

The objective of this research program is to continue developing, editing, maintaining, utilizing, and making publicly available the Natural Resources Information System (NRIS) for the state of Oklahoma. The Oklahoma Geological Survey, working with Geological Information Systems at the University of Oklahoma, has undertaken the construction of this information system in response to the need for a computerized, centrally located library containing accurate, detailed information on the state's natural resources. Particular emphasis during this phase of development is being placed on computerizing information related to the energy needs of the nation, specifically oil and gas.

Summary of Technical Progress

The Oil and Gas Production Subsystem

The Oil and Gas Production (OGP) subsystem is composed of three major files: a Lease File, a Field File, and a County File. The Lease File contains production and formation records based on data obtained from the Oklahoma Tax Commission (OTC); data elements include lease name and number, location information, formations data, and monthly production totals. The Field File contains historical and current records for all 5086 active and inactive Oklahoma oil and gas fields, as identified by the Oklahoma Nomenclature Committee (ONC); data elements on this file include field identification data, consolidation histories when relevant, discovery data, location information (county, section/township/range, and quarter/quarter section data), and monthly production aggregated (by location) from the records maintained on the Lease File. The County File has monthly oil and gas production data aggregated by county.

Processing for the OGP subsystem primarily consists of processing monthly computer tapes received from the OTC to update production totals for all three files and to add new records to the Lease Master File. At the beginning of this quarter, monthly production was on file for the period January 1983 through July 1989. New records for the Field Master File are added by manually coding and keying the results of ONC meetings. The process of reconciling the Lease and Field Master Files is accomplished through combined computerized and manual efforts.

As reported previously, a primary thrust for the OGP subsystem must be toward enhancing the files through ongoing quality assurance efforts. Although the estimated error rate in the production input tapes received from the OTC is rather low, the sheer volume of data processed from these tapes creates many errors on the Lease File. One result of these errors in the OTC source tapes is the significant number of production records that are added to the file with invalid "Producing Unit Numbers" (PUNs), commonly called "no-master" records. A series of computerized and manual processes have been developed to research company reporting patterns as part of the effort to allocate the no-master production to the appropriate leases. Significant efforts also are required to detect and resolve cases in which a monthly production total is unreasonably large for a lease; these usually are caused by decimal problems in the production reports or by the allocation of production to the wrong lease.

The foremost goal of the OGP subsystem processing during this quarter has been to prepare the data for the upcoming May data release. The August through November source data received from the OTC were added to the files. Approximately 875,000 records, representing about 135,000 unique PUNs, are on the Lease File. About 85,000 of these PUNs had production reported. Quality assurance efforts in preparation of the data release included resolving no-master records as well as detecting and resolving cases in which monthly lease production totals were unreasonably large.

Table 1 gives an overview of the progress and current status of production data quality assurance efforts by region and county. Although 4250 no-master records have been resolved this year, another 2503 have been added through the processing of new OTC tapes; therefore, about 6700

TABLE 1

Progress and Current Status of Production Quality Assurance Efforts

Progress Summary May 1989–March 1990

	Counts of "No-Master" Records				Cumulative quality assurance transactions since October 1988
	Starting total, May 1989	Number added February–November tapes	Number resolved	Ending total, March 1990	
North central					
047 Garfield	292	52	122	222	1002
053 Grant	154	26	53	127	341
071 Kay	114	99	81	132	595
073 Kingfisher	331	57	100	288	1219
081 Lincoln	123	39	33	129	211
083 Logan	141	53	37	157	334
103 Noble	145	16	33	128	362
109 Oklahoma	302	36	170	168	972
119 Payne	106	33	75	64	319
Region subtotal	1708	411	704	1415	5355
Northeast					
001 Adair	2	4	4	2	7
035 Craig	3	0	2	1	4
037 Creek	264	49	77	236	507
097 Mayes	1	0	0	1	0
101 Muskogee	64	0	36	28	121
105 Nowata	60	6	44	22	97
107 Okfuskee	120	24	76	68	434
111 Okmulgee	170	18	49	139	325
113 Osage	115	31	40	106	152
115 Ottawa	1	1	2	0	2
117 Pawnee	160	17	118	59	383
131 Rogers	50	16	52	14	134
135 Sequoyah	12	2	10	4	28
143 Tulsa	72	13	38	47	212
145 Wagoner	47	4	13	38	66
147 Washington	76	8	38	46	148
Region subtotal	1217	193	599	811	2620
Northwest					
003 Alfalfa	162	41	103	100	422
007 Beaver	319	89	208	200	1696
025 Cimarron	37	16	35	18	223
043 Dewey	157	78	53	182	508
045 Ellis	144	53	51	146	304
059 Harper	254	77	72	259	718
093 Major	334	88	232	190	1554
139 Texas	185	192	132	245	1599
151 Woods	72	34	30	76	220
153 Woodward	95	32	24	103	176
Region subtotal	1759	700	940	1519	7420
Southeast					
005 Atoka	4	2	3	3	22
013 Bryan	14	0	0	14	0
Southeast (cont'd.)					
023 Choctaw	0	0	0	0	0
027 Cleveland	52	7	31	28	121
029 Coal	17	11	12	16	79
049 Garvin	246	47	107	186	742
061 Haskell	108	41	38	111	273
063 Hughes	160	48	115	93	482
069 Johnston	1	0	1	0	3
077 Latimer	148	64	105	107	877
079 Le Flore	84	30	26	88	548
087 McClain	133	22	32	123	132
089 McCurtain	0	1	1	0	3
091 McIntosh	45	–3	38	4	302
095 Marshall	25	5	7	23	60
099 Murray	28	2	2	28	5
121 Pittsburg	197	93	111	179	853
123 Pontotoc	61	8	31	38	1252
125 Pottawatomie	105	42	37	110	361
127 Pushmataha	1	0	1	0	2
133 Seminole	106	12	27	91	179
Region subtotal	1535	432	725	1242	6296
Southwest					
009 Beckham	139	64	103	100	747
011 Blaine	133	49	24	158	476
015 Caddo	268	86	193	161	1358
017 Canadian	264	54	169	149	1058
019 Carter	215	87	152	150	987
031 Comanche	38	3	6	35	104
033 Cotton	21	17	3	35	5
039 Custer	234	87	80	241	729
051 Grady	284	73	188	169	976
055 Greer	57	9	33	33	91
057 Harmon	0	1	0	1	0
065 Jackson	2	1	1	2	4
067 Jefferson	34	4	7	31	48
075 Kiowa	17	5	1	21	3
085 Love	82	14	37	59	116
129 Roger Mills	184	128	201	111	1585
137 Stephens	181	62	68	175	965
141 Tillman	3	0	0	3	1
149 Washita	86	23	16	93	284
Region subtotal	2242	767	1282	1727	9537
Grand total	8461	2503	4250	6714	31228

problem records remain on the Lease File. The bar chart in Fig. 1 provides a little more perspective on the resolution rates. For all data years except 1989, consistent progress has been made on reducing the number of no-master records since last May. For 1989, however, new OTC tapes have been processed throughout the year; this has resulted in a tremendous increase in the number of 1989 no-master records. With the exception of the 1989 data, the number of no-master records has been reduced by nearly 50%. Since production quality assurance efforts began in October 1988, over 31,000 transactions have been generated to correct no-master and other types of production data problems. Significant progress has been made this year in developing and refining both computerized and manual processes to perform the production quality assurance tasks; therefore, the resolution rates are expected to improve for future data releases.

A second goal of the OGP subsystem work involves quality assurance efforts to "assign" leases to fields and derive field production totals from those lease assignments. These lease assignments are based on the official field outlines as designated by the ONC. Some areas exist in which significant field extension drilling has taken place, but the ONC has had insufficient resources to update the field boundaries accordingly; therefore, almost 25% of the state's production is not allocated to any field(s) in the OGP subsystem. Table 2 provides more detailed information about the current status of unassigned production by region

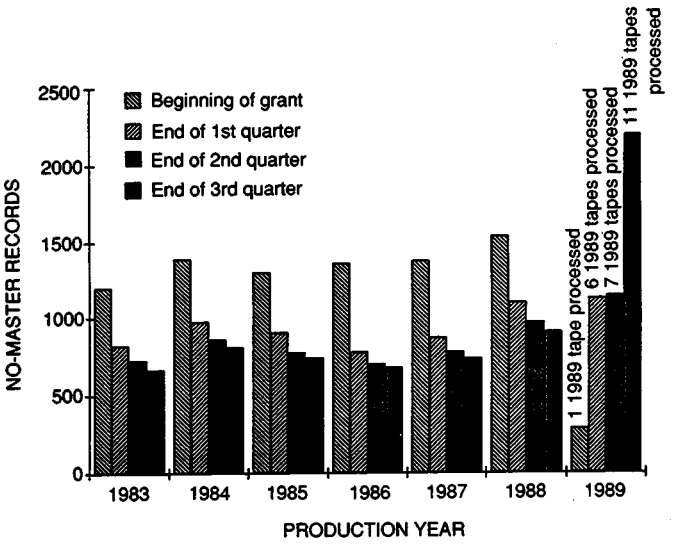

Fig. 1 Change in the no-master record totals.

and county. A series of information packages for selected areas is being developed to assist the ONC in updating their field outlines. The packages consist of maps and lists that depict producing leases located outside current field boundaries; those areas with the largest amount of "unassigned" production are receiving the highest priority. The first of these packages was presented at the January 1990 ONC meeting, and more are planned for their next meeting; so far these packages are being well received by the Committee.

Quality assurance efforts regarding the formations data comprise a third goal. During this quarter, further progress was made in developing a prototype system for formations editing and code assignments. The effort assigned to this task will be increased in the coming months, with the plan to fully implement the system in the coming year. As reported previously, with significant ongoing quality assurance efforts required for the OGP subsystem, the decision was made to hire an individual to be assigned

TABLE 2

Unassigned Production* by Region and County

	Gas production (annual average),† Mmcf			Liquid production (annual average),† Mbbl		
	Total	Unassigned	Percent	Total	Unassigned	Percent
North central						
047 Garfield	52,067	7,951	15	2,682	457	17
053 Grant	16,638	11,500	69	2,718	1,656	61
071 Kay	3,117	231	7	1,446	88	6
073 Kingfisher	63,687	21,690	34	4,542	1,186	26
081 Lincoln	11,333	6,612	58	1,558	579	37
083 Logan	20,999	9,186	44	2,151	1,116	52
103 Noble	9,391	3,310	35	3,289	1,112	34
109 Oklahoma	25,582	17,819	70	3,548	2,090	59
119 Payne	5,010	1,072	21	2,090	431	21
Regional subtotal	207,824	79,371	38	24,024	8,714	36
Northeast						
001 Adair	0	0	0	0	0	0
035 Craig	34	20	60	6	4	71
037 Creek	8,273	2,955	36	5,891	800	14
097 Mayes	2	2	100	33	33	100
101 Muskogee	1,378	798	58	293	45	15
105 Nowata	732	387	53	476	155	33
107 Okfuskee	6,469	3,252	50	1,051	417	40
111 Okmulgee	6,852	1,866	27	1,352	314	23
113 Osage	8,223	3,298	40	8,173	1,272	16
115 Ottawa	0	0	0	0	0	0
117 Pawnee	7,658	6,125	80	2,746	1,848	67
131 Rogers	380	355	93	151	80	53
135 Sequoyah	2,172	1,782	82	0	0	0
143 Tulsa	1,310	459	35	872	98	11
145 Wagoner	806	478	59	289	122	42
147 Washington	1,181	603	51	799	67	8
Region subtotal	45,471	22,379	49	22,133	5,255	24

(Table 2 continued on next page.)

TABLE 2 (Continued)

	Gas production (annual average),† Mmcf			Liquid production (annual average),† Mbbl		
	Total	Unassigned	Percent	Total	Unassigned	Percent
Northwest						
003 Alfalfa	15,026	754	5	962	50	5
007 Beaver	84,798	32,341	38	3,041	1,699	56
025 Cimarron	11,910	4,033	34	648	374	58
043 Dewey	64,128	20,828	32	2,568	1,483	58
045 Ellis	35,166	2,731	8	1,203	200	17
059 Harper	50,067	7,071	14	392	170	43
093 Major	84,734	14,486	17	4,291	1,058	25
139 Texas	101,362	14,815	15	4,104	1,381	34
151 Woods	27,655	368	1	536	3	1
153 Woodward	30,557	851	3	470	13	13
Region subtotal	505,404	98,276	19	18,214	6,430	35
Southeast						
005 Atoka	281	218	78	2	0	25
013 Bryan	1,706	13	1	100	0	0
023 Choctaw	(3)	(3)	0	0	0	0
027 Cleveland	6,401	2,841	44	2,294	818	36
029 Coal	4,697	40	1	195	0	0
049 Garvin	43,835	6,184	14	7,022	1,243	18
061 Haskell	35,416	15,645	44	0	0	0
063 Hughes	13,427	8,113	60	1,266	595	47
069 Johnston	5	0	0	0	0	0
077 Latimer	73,245	11,544	16	0	0	0
079 Le Flore	21,053	11,769	56	0	0	0
087 McClain	23,033	5,160	22	3,757	1,280	34
089 McCurtain	0	0	0	0	0	0
091 McIntosh	8,058	6,307	78	6	5	88
095 Marshall	6,019	118	2	342	3	1
099 Murray	440	32	7	1,597	518	32
121 Pittsburg	62,977	20,378	32	0	0	0
123 Pontotoc	1,299	87	7	4,639	53	1
125 Pottawatomie	6,381	4,963	78	4,485	1,989	44
127 Pushmataha	0	0	0	0	0	0
133 Seminole	3,712	1,217	33	4,334	623	14
Region subtotal	311,984	94,626	30	30,040	7,129	24
Southwest						
009 Beckham	78,230	3,494	4	1,134	103	9
011 Blaine	92,865	18,216	20	1,305	550	42
015 Caddo	106,901	5,090	5	4,037	198	5
017 Canadian	109,259	46,216	42	3,036	2,034	67
019 Carter	18,167	5,477	30	14,159	1,150	8
031 Comanche	9,909	3,591	36	309	198	64
033 Cotton	345	61	18	392	57	14
039 Custer	127,269	18,405	14	2,383	413	17
051 Grady	110,586	41,355	37	7,405	1,874	25
055 Greer	248	51	20	14	2	14
057 Harmon	0	0	0	74	0	0
065 Jackson	0	0	0	108	25	23
067 Jefferson	390	339	87	1,146	797	70
075 Kiowa	226	42	19	111	42	38
085 Love	4,409	1,367	31	1,722	1,172	68
129 Roger Mills	148,766	15,992	11	1,087	65	6
137 Stephens	43,133	7,804	18	11,583	873	8
141 Tillman	0	0	0	129	78	61
149 Washita	62,613	11,211	18	788	104	13
Region subtotal	913,317	178,711	20	50,920	9,736	19
Grand total	1,983,999	473,363	24	145,331	37,265	26

*Production not assigned to any field.

†Annual averages based on January 1983–November 1989 production (as of 3/21/90).

primarily to OGP quality assurance. That position was filled early in February with an individual who brings to the project geological training as well as mapping experience at the mainframe level in an industry environment.

Progress has also been made on a fourth goal, the development of mapping applications. An agreement with Phillips Petroleum Company to obtain their Digital Land Grid Oklahoma Database was finalized in late January; latitude and longitude coordinates contained in the database will be added to the NRIS files within the next few months. Prior to obtaining the Phillips system, a variety of mapping applications were pursued using SAS software. Although several SAS-generated maps have been produced based on calculated coordinates, the accuracy problems encountered with this method should be alleviated once the Phillips system is fully operational. Two new graphics terminals and a controller were installed this quarter.

The Well History File

The Well History File contains historical and current completion records for oil and gas wells reported to the Oklahoma Corporation Commission on Form 1002-A. At the start of the quarter, the Well History File contained 60,165 records for the Ouachita Mountains uplift and Arkoma basin areas and the Anadarko basin area. On a special project basis, supplemental data (where available) are added to the file from well logs, scout tickets, and core and sample documentation. Data elements on this file include demographic items (e.g., API well number, lease name and well number, location information, elevations, and dates of significant activities for the well), formation items (e.g., formation names, completion and test data, and depths and perforations), and reference information (e.g., for drilling samples, core samples, and well logs).

In addition to the standard Well History File processing, special activities are being undertaken to enhance the supplemental data on the file. Work is under way on a parallel track within the NRIS Project to organize and computerize information from the OGS core and sample libraries and from the Ardmore Sample Cut Library. Through computer and manual reconciliation processes, relevant data are being added to the Well History File. As other data sources become available, they will be reviewed as a cost-effective means to add supplemental information to the well records.

A large portion of the Well History File work involves photocopying the completion reports for use in coding prior to data entry. All new completion reports are copied as soon as they are received from the Oklahoma Corporation Commission; the originals are filed in the Oklahoma Geological Survey's Well Log Library. Completion reports for areas of the state that have already been (or are being) worked are entered into the processing stream immediately. The others are filed for future processing. All historical completion reports are checked out of the Well Log Library and copied at the rate of about 8,000 to 12,000 forms per month; approximately 30% of these historical completion reports have now been copied.

Presently, well records are being prescanned, keyed, and edited for the following southwestern counties: Jackson, Tillman, Comanche, Cotton, Stephens, and Carter. More than 13,000 well records were added to the file this quarter. As of Mar. 21, 1989, there were 73,432 records on file. The Well History File progress is shown below by NRIS Regional Division.

Area of coverage	Start of grant	Start of quarter	Current
Southeast Region	27,385	28,380	32,496
Southwest Region	9,284	19,310	27,597
Northeast Region	6,768	7,492	8,351
Northwest Region	4,735	4,836	4,837
North Central Region	138	147	151
Total number of well records	48,310	60,165	73,432

The current status of county coverage and the total record counts by county are displayed in Figs. 2 and 3. An additional 7200 well completion reports have been keyed but not yet verified for accuracy through the redundant keying (rekeying) process. As data entry operators gain further experience, this backlog of unverified data is being depleted. Also, the recent installation of the new data entry network is greatly facilitating the data entry effort.

Thus far, supplemental data have been added to a total of 3413 records for the Ouachita Mountains area in southeastern Oklahoma. Efforts to key and verify data on approximately 30,000 sample records obtained from the Ardmore Sample Library were also completed. As previously reported, a computer matching process is being developed to add these supplemental data, as well as the core data that have been computerized for the OGS Core and Sample Library, to the well records.

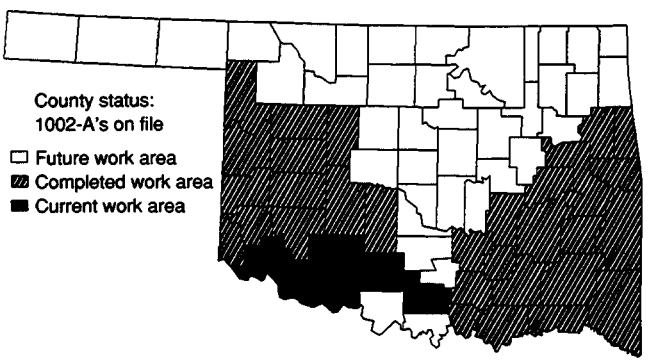

Fig. 2 Status of well history database project. County coverage as of Mar. 21, 1990.

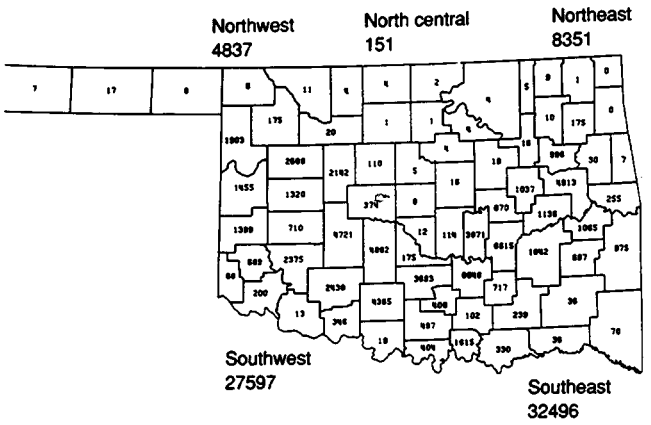

Fig. 3 Status of well history database project.

Public Data Release

Response to the release of NRIS data is increasing as word spreads about the availability of the data. Largely, this response continues to be internal among the geologists of the OGS and the University's School of Geology. A large project based on gas production data was completed in January which assisted a pipeline company in deciding where to expand its operations. (This work has resulted in a followup order based on the more recent production data.) Another project involved a retrieval of records on wells drilled or completed since 1970 that penetrated the Arbuckle formation. Still another involved a retrieval of field and discovery well data for 10 fields in eastern Oklahoma.

Plans are under way to display Wilburton field data as part of the OGS booth at this year's American Association of Petroleum Geologists (AAPG) convention in June. Included in the display will be a map depicting the Wilburton field outline within Pittsburg and Latimer counties, a line graph showing 1983–1989 Wilburton oil and gas production by formation, and a map showing the well locations within one township of the Wilburton field. It is hoped that the AAPG convention and display, as well as the addition of mappable coordinates to the files, will combine to generate greater interest in the NRIS data.

DEVELOPMENT OF NUCLEAR MAGNETIC RESONANCE IMAGING/SPECTROSCOPY FOR IMPROVED PETROLEUM RECOVERY

Contract No. FG07-89BC14446

Texas A&M University
College Station, Tex.

Contract Date: Sept. 15, 1989
Anticipated Completion: Dec. 15, 1992
Government Award: $290,000
(Current year)

Principal Investigators:
A. T. Watson
R. W. Flumerfelt
J. W. Jennings
M. P. Walsh

Project Manager:
Edith Allison
Bartlesville Project Office

Reporting Period: Jan. 1–Mar. 31, 1990

Objectives

The overall objectives are to develop and apply nuclear magnetic resonance imaging (NMRI) and computerized tomographic (CT) X-ray scanning methods for determining rock fluid and petrophysical properties and for fundamental studies of multiphase flow behavior in porous media. Specific objectives are to: (1) develop NMRI procedures for measuring porosity, permeability, pore-size distribution, capillary pressure, and wetting characteristics; (2) apply imaging methods for improved methods of determining two- and three-phase relative permeability functions; (3) apply NMRI for development of a better understanding of dispersed phase displacement processes; and (4) apply imaging methods to develop a better understanding of saturation distributions and fingering during miscible displacements. The objectives have been organized into four subtasks. Progress reports from each subtask are provided.

Summary of Technical Progress

The Development of NMRI and CT Scanning for the Determination of Rock–Fluid and Petrophysical Properties

Over the past quarter, activities were slowed down, primarily because of the move of the CT scan and nuclear magnetic resonance imaging (NMRI) instruments to the new facility. In addition, both instruments have had hardware problems; this resulted in little scan activity for the quarter. These problems are being resolved, and a much higher level of activity is expected over the next two quarters. Weekly seminars, held jointly with the Geophysics Department, have been helpful in obtaining a better understanding of the use of imaging and image analysis for rock characterization.

A fairly complete set of core samples now exists in the library. These samples cover various rock types, sandstones and limestones (with both microcrystalline and fracture–vugular porosity). As the project continues, this library will be expanded. Suitable end caps for 4-in. core samples have been constructed. These end caps are placed on the 4-in.-diameter by 1-ft-long core samples, and the entire end cap/core sample assembly is coated with fiberglass cloth–epoxy. This results in a very easily reproduced flow cell for conducting the saturation profile experiments. A device for measuring the slice thickness profile of the computer assisted tomography (CAT) scan has also been constructed. This device will provide information on the slice profile of the beam produced by the CAT scan and will be useful in improving the resolution of the data produced by the CAT scan.

The procedure for conducting the porosity and porosity profile tests has been developed for the NMRI instrument. This procedure involves placing a rock sample, saturated with water, in the NMRI along with an appropriate sample of agarose–copper sulfate gel. The agarose–copper sulfate gel standard is picked to have the same T_1 and T_2 relaxation times as the water in the rock sample. This results in a method of getting an accurate proton count in the rock sample, which provides a means of obtaining porosity. Samples have been prepared for porosity determination on the NMRI with this method.

Development of NMRI and CT Scanning for Characterizing Conventional Multiphase Displacement Processes

A sequence of immiscible displacement experiments was conducted with NMR imaging to determine the transient saturation distributions. One-dimensional (1-D) images were taken during the transient phases of the displacement experiments and two- and three-dimensional (2-D and 3-D) images were taken during the steady-state phases. Deuterium oxide (D_2O) and *n*-octadecene were used as fluids with a limestone core sample. The primary imbibition displacement was analyzed to determine the saturation distributions that correspond to a sequence of times during the experiment. Several profiles are shown in Fig. 1. The saturation was estimated to ± 0.015 saturation units with a resolution of 0.566 mm for the experiment. The details of this work are available in a manuscript presented at the American Institute of Chemical Engineers (AIChE) 1990 Spring National Meeting in Orlando, Fla.[1] In the next quarter, the other sequences of the displacement experiments will be analyzed. Also, 2-D and 3-D images that were acquired during steady-state phases of the displacement experiments will be analyzed.

Existing computer software has been modified so that relative permeability and capillary pressure functions can be estimated simultaneously with saturation profiles and pressure data collected at the inlet and exit of the core sample as well as at positions along the core. The program has been tested. Accurate estimates of relative permeability and capillary pressure functions can be obtained from data collected in displacement experiments. A flow system is being constructed to actually carry out the displacement experiments.

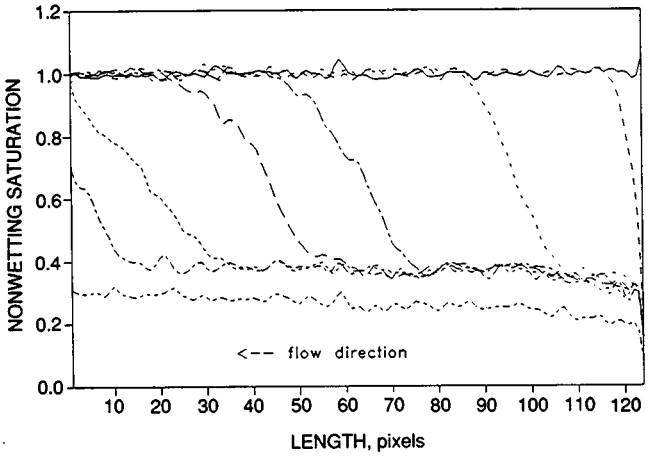

Fig. 1 Nonwetting fluid saturation profiles.

Several modifications are being made to the experimental arrangements used to demonstrate the ability to image saturation distributions, as discussed previously in this report. Syringe pumps will be used in place of the chromatography pumps used in the previous experiment. These pumps will provide uniform, pulse-free flow. An epoxy cast, rather than a Hassler cell, will be used for the core holder. This will allow the insertion of pressure taps at several positions along the core. A cast has been built for plotting the core samples, and the process of calibrating pressure transducers and setting up real-time data monitoring for the pressure taps is in progress. Saturation profiles will be imaged during the experiment, as demonstrated in the previous displacement experiment.

Development of NMRI and CT Scanning for Characterizing Dispersed Phase Processes

The tasks performed during the period were: (1) spin-lattice relaxation time (T_1) characterization of the wettability of water-wet (uncoated) and oil-wet (coated with silicone compound) glass beads, (2) static capillary pressure measurements with nondispersed phase (water–gas) and dispersed phase (foam) systems, (3) design of a dynamic foam displacement apparatus for investigating the mobility relations with dispersed phase systems, and (4) modification of 1-D foam flow network model to allow both drainage and imbibition capillary and threshold pressure curve predictions.

Long-term nonequilibrium effects observed in the T_1 measurements appeared to be the result of adsorption effects, paramagnetic contamination, and reactions on the glass–water interface (ion-exchange and hydration). For the

prevention of the inconsistency in measurements of T_1, future tests will be performed immediately after the glass beads are prepared. Several Plexiglas cells to be placed in the NMRI system have been fabricated with coated or uncoated beads. The existing commercial radio-frequency (r-f) coil generates a weak r-f magnetic field (H_1) that results in inaccuracies in the measurement in $T_{1\rho}$. A new r-f coil was constructed to alleviate these problems. Revisions are under way for observing free induction decay (FID) and T_1 to verify its applicability for spectroscopy. The completion of coils and cells support the first task.

Multicycle static capillary pressure measurements were partially completed for dispersed and nondispersed phase systems. The results show that capillary pressure behavior for dispersed phase systems is quite different from that for nondispersed phase systems. Although only two drainage–imbibition cycles are required to reach invariant capillary pressure behavior with the nondispersed systems, additional cycles are required for dispersed phase systems, with each successive cycle producing lower and lower saturations. Invariant capillary pressure curves are obtained after six cycles, and the final drainage and imbibition curves show minimal hysteresis and small differences between the irreducible and residual saturations. In general, these end saturations are well below those for nondispersed phase systems; the imbibition value is particularly depressed. A paper related to this study was presented at the 1990 SPE California Regional Meeting.[2] The successful measurement of multicycle capillary pressures is covered in the second task.

In connection with task 3, a dynamic foam displacement apparatus was designed which consists of the main flowing cell, a foam generator, liquid and gas probes, foam texture viewing cells, and pumping systems. The construction of the main cell and probes are under way.

A 1-D network model for predicting both capillary and threshold pressures for dispersed and nondispersed phase systems was developed. The predicted drainage–imbibition capillary pressure curves provide insights into the effects of pore structure characteristics, bubble size, lamella density, and continuous phase pressure gradients on phase saturations. The predicted threshold pressure curves indicate the effects of such variables on the fraction of the pore space available for flow. Two papers that relate to these studies were presented, one at the 1990 SPE California Regional Meeting[3] and one at the 1990 AIChE Spring National Meeting.[4]

Miscible Displacement Studies

An additional graduate student was added to the project to begin the simulation work. The purpose of the simulation work will be to: (1) provide a theoretical analysis of the fingering observed in the flow tests, (2) provide insight into scaling the laboratory results to field conditions, and (3) guide future experimental displacement tests. The first phase of the simulation work will be to design and test a multidimensional flow model.

The experimental work testing the flow system continues. During this quarter the CAT scan apparatus was moved to the new Petroleum Engineering Building, and operational problems have delayed the completion of the unit mobility ratio flow test.

References

1. S. Mandava, C. M. Edwards, and A. T. Watson, *NMR Imaging of Saturation During Immiscible Displacements*, presented at AIChE 1990 Spring National Meeting, Orlando, Fla., Mar. 18–22, 1990.
2. H.-L. Chen, paper SPE 20069, presented at the 1990 SPE California Regional Meeting, Ventura, Calif., Apr. 4–6, 1990.
3. R. W. Flumerfelt, paper SPE 20066, presented at the 1990 SPE California Regional Meeting, Ventura, Calif., Apr. 4–6, 1990.
4. R. W. Flumerfelt, paper presented at the AIChE 1990 Spring National Meeting, Orlando, Fla., Mar. 18–22, 1990.

GEOPHYSICAL AND TRANSPORT PROPERTIES OF RESERVOIR ROCKS

Contract No. DE-AC22-89BC14475

University of California
Berkeley, Calif.

Contract Date: Sept. 22, 1989
Anticipated Completion: Sept. 30, 1992
FY 1990 Project Cost: $137,000

Principal Investigator:
Neville G. W. Cook

Project Manager:
Robert E. Lemmon
Bartlesville Project Office

Reporting Period: Jan. 1–Mar. 31, 1990

Objectives

The definition of reservoir characteristics, such as porosity, permeability, and fluid content, on the scale of meters, is the key to planning and control of successful enhanced oil recovery (EOR) operations. Equations relating seismic and electrical properties to pore topology and mineral–fluid interactions are needed to invert geophysical images for reservoir management. Both the geophysical and transport properties of reservoir rocks are determined by pore topology and the physics and chemistry of mineral–fluid and fluid–fluid interactions. The objective of this

research is to gain a better understanding, through analysis and experiment, of how fluids in pores affect the geophysical and transport properties of reservoir rocks.

Summary of Technical Progress

During this quarter work was carried out in three activities: one-dimensional (1-D) percolation tests using Wood's method, analysis of percolated structures by scanning electron microscopy (SEM) and first-order analytical techniques, and measurement of seismic properties of sandstone samples saturated with a variety of fluids. The percolation tests provide quantitative data needed to relate pore topology to fluid-flow properties. Seismic measurements provide data to evaluate the relative effects of pore structures, in particular, thin cracks as opposed to more equidimensional pores, on wave propagation. Accomplishments this quarter in each of the three activities are summarized.

One-Dimensional Percolation

With apparatus designed last quarter for 1-D percolation experiments using Wood's metal, tests were carried out at various capillary pressures on Berea sandstone and Indiana limestone. The results are summarized in Table 1.

TABLE 1

One-Dimensional Percolation Data

Rock	Capillary pressure, atm	Time allowed to reach final capillary pressure, min	Saturation, %	Minimum pore size, μm
Berea sandstone	0.88	15	46	9
	0.85	24	50.5	9.4
	0.67	81	39.5	12
Indiana limestone	1.0	29	7.5	8

The saturation of the sample percolated at a capillary pressure of 0.88 atm was 46%, which is in fair agreement with previously obtained two-dimensional (2-D) partial saturation data. The experiment was repeated at a capillary pressure of 0.85 atm, and the sample was quenched as soon as the first trace of Wood's metal percolated through. The sample was 50% saturated. The results also indicated that there is still some time dependence of percolation.

With sufficient time, percolation in Berea sandstone can be achieved at a capillary pressure of 0.67 atm, which indicates that there is a connected path with throats greater than 12 mm running along the entire length of the core. The sample was 39.5% saturated. However, when the experiment was repeated at the same capillary pressure on a slightly longer sample (1.942 in. in length compared to 1.8 in.), critical percolation of Wood's metal could not be obtained even after waiting for several hours. However, upon increasing the capillary pressure to 0.85 atm, rapid percolation occurred.

The percolation results, in combination with the SEM analysis, indicate that in Berea sandstone the distribution of pores and throats is more or less uniform throughout the sample. Thus, rather than a single path of least resistance, the nonwetting phase moves as a front through the sample.

The 1-D percolation through limestone was very slow. Wood's metal percolated through the sample at 1.0 atm capillary pressure after about 29 min. The saturation of the sample was 7.5%, which was much lower than the 2-D saturation at the same capillary pressure. In limestone, Wood's metal apparently does not percolate as a front. The percolating cluster quickly becomes very tenuous in the form of twined ribbons distributed somewhat nonuniformly, which gives rise to apparently three or four levels of correlation lengths over the sample.

Image Analysis

A collage of SEM micrographs for Indiana limestone was obtained and a representative 2-D section of 43.5 cm^2 (on the photograph), representing 11.9 mm^2 at actual scale, was selected for image analysis. The void space was subdivided in classes defined by the pore size diameter. The void diameter at any point was defined as the diameter of the largest sphere that contains the point and remains wholly within the pore space. The porosity from the 2-D section was calculated to be 14.6%, slightly higher than the bulk porosity measured gravimetrically at 14%. As a first-order approximation, permeability was estimated by means of the Kozeny–Carman equation (this theory represents the porous medium by an assemblage of tortuous capillary tubes).

The Kozeny–Carman equation for permeability is

$$k = \frac{\phi R_H^2}{cT^2} \qquad (1)$$

where k = intrinsic permeability
ϕ = porosity
R_H = hydraulic radius
c = shape factor (≈ 2 for circular tubes)
T = tortuosity [$\approx (2)^{1/2}$]

The main assumptions underlying this equation are:

- Flow obeys Darcy's law.
- Tortuosity is constant.
- The flow channels are equal in size.

The Kozeny–Carman equation was applied to every class size as if all detected pores in the 2-D section were of that size. Permeability was calculated to be ≈610 mD if all the pores are considered to be of the smallest detected size ($\approx 38 \times 10^{-3}$ mm). Hence the Kozeny–Carman equation overpredicts permeability for limestone by at least a factor of ten. This result is not surprising if the fact that the smaller constrictions in the larger paths through the material control permeability (also, the size of the connections are more important than connectivity itself) is considered. From this simple capillaric model, it becomes clear that no simple correlation between porosity and permeability exists and that an involved correlation exists between structure and permeability. The next step is to consider a serial-branching model of the pore space to take into account the convergent–divergent nature of the flow channels and the fact that channels may branch and reconnect again. A network model such as this will provide insight into how topological parameters control fluid flow.

Actual observations from pore casts and stereo micrographs of Indiana limestone seem to indicate the presence of a clustered structure with total porosity distributed among intergroup and intragroup components. If such a grouping arrangement of grains exists, the flow channels surrounding the grain groups will be larger than those passing through the groups and between individual grains.

Seismic Measurements

A study of the energy dissipation processes that produce seismic wave attenuation in fluid-saturated (and partially saturated) reservoir rock was begun with measurements on Berea sandstone and Indiana limestone. Tests have also been performed on alundum (Al_2O_3), an artificial (i.e., man-made) porous material. Measurements on artificial porous materials will be included in this study to help identify attenuation mechanisms that may be specific to sedimentary rock. The artificial materials selected for testing include Al_2O_3 and sintered glass beads. These artificial materials were selected for use in this study because they have single-component solid phases and well-sintered contacts that do not contain clay. Thus it may be possible to use these artificial materials to isolate seismic energy dissipation processes associated with grain contacts and clay.

A recipe for sintering glass beads was developed. Glass beads are poured into a cylindrical carbon mold and placed in an oven. By carefully monitoring the temperature of the glass, specimens with any level of sintering can be created. The level of sintering is determined by viewing the bead contacts under a SEM. Both well-sintered and poorly sintered specimens for 75- to 150-μm diameter glass beads have been created.

A number of fluids have been selected according to their viscosity, surface tension, polar nature, and reaction with clay. Among these are distilled water, brine, glycerol, silicone oil, decane, and paraffin. Two low-melting-point solids will be used to partially saturate the pore spaces and grain contacts. These solids will be melted and allowed to solidify in place. Wood's metal is nonmelting in its liquid state and will only occupy the large pores. Sulfur is a wetting fluid and will be used to solidify the grain contacts. Stiffening of pores and grain contacts will help identify where the losses of seismic energy occur. Selection of a wide range of fluids with well-characterized chemical and physical properties will allow the isolation and identification of the microchemical, microphysical, and micromechanical processes that control the dissipation of seismic energy.

Aluminum standards were calibrated frequently to assure repeatability. Sandstone specimens were cut from the same core and then ground so that their ends were flat and parallel. Prior to testing, the specimens were placed in an oven at 120°C for at least 12 h. Specimens that were tested saturated were vacuum-saturated with the fluid and then weighed to determine the quantity of fluid in the specimen.

The specimens are loaded in a carefully aligned load frame. Transducers are coupled to the specimen via a thin disk of lead foil. Seismic measurements of P and S waves transmitted through sandstone cores were made by applying a square wave pulse 500 V in amplitude and 640 nsec in width to the transducer placed on the top of the specimen. The resonance frequencies of the piezoelectric crystals in the transducer are 1 MHz. The transmitted wave is received by an identical transducer located on the bottom of the sandstone core, digitized, and then displayed and stored on an IBM AT computer.

Preliminary results have been obtained for 5.1-cm-diameter by 4.3-cm-long cores of Berea sandstone (~20% porosity). The peak-to-peak amplitudes of both P and S waves were measured as a function of the load on the specimen for an oven-dried sandstone specimen and sandstone specimens saturated with distilled water, glycerol (1000 cP), and silicone oil (1000 centistokes). The results are shown in Figs. 1 and 2. The P- and S-wave amplitudes for a specimen load of 5.5 MPa show a large variation

$$A_p^{dry} > (84\%)\, A_p^{silicone} > (55\%)\, A_p^{water} > (29\%)\, A_p^{glycerol}$$

$$A_s^{dry} > (40\%)\, A_s^{silicone} > (20\%)\, A_s^{glycerol} > (10\%)\, A_s^{water}$$

where the values in parentheses indicate the percentage of the peak-to-peak amplitude for the oven-dried specimen.

These results confirm previous work that found large changes in amplitude for fluids of similar viscosity but different chemistry (i.e., glycerol and silicone oil). These results demonstrate that seismic wave amplitudes are very sensitive to changes in the chemistry of saturating fluid and not just its physical properties. Although the difference between the largest and smallest travel times is 9% for the P wave and 15% for the S wave, the difference between the largest and smallest peak-to-peak amplitude measurements

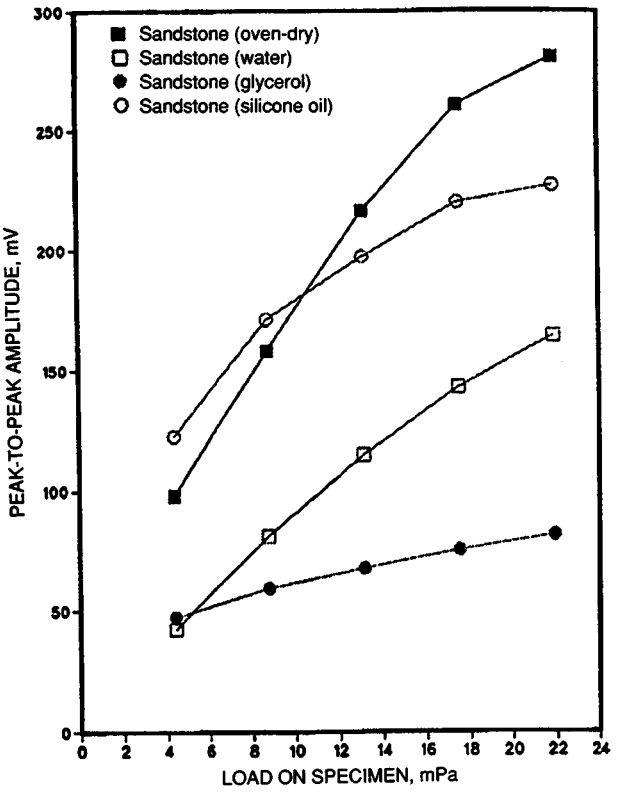

Fig. 1 P-wave peak-to-peak amplitude as a function of the applied load for Berea sandstone (dry and fluid saturated).

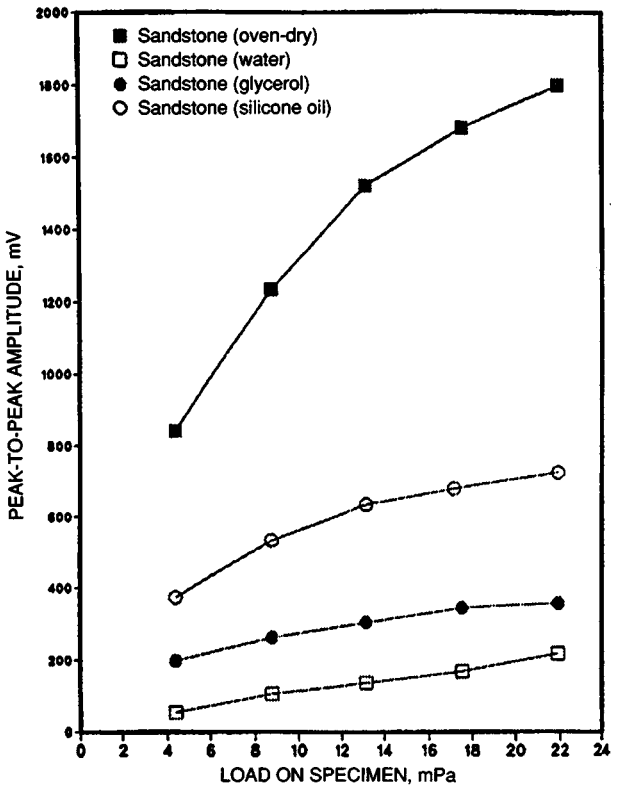

Fig. 2 S-wave peak-to-peak amplitude as a function of the applied load for Berea sandstone (dry and fluid saturated).

is 71% for the P wave and 90% for the S wave. These results clearly demonstrate that amplitudes are much more sensitive to changes that result from the addition of fluid to sandstone.

Future research will investigate the effects of clay and grain contacts on seismic wave attenuation. A set of experiments is being planned for glass beads. Glass bead specimens with the same dimensions as those of the rock specimens have been manufactured using the process described in the beginning of this report. Tests are also being planned for sandstone and limestone. These tests will be performed with and without confining pressure. The judicious selection of saturating fluids will aid in isolation and identification of the physical and chemical processes that control seismic attenuation.

IN SITU STRESS AND FRACTURE PERMEABILITY: A COOPERATIVE DOE–INDUSTRY RESEARCH PROGRAM

Sandia National Laboratories
Albuquerque, N. Mex.

Contract Date: Oct. 1, 1986
Anticipated Completion: Sept. 30, 1990
Funding for FY 1990: $200,000

Principal Investigators:
David A. Northrop
Lawrence W. Teufel

Project Manager:
Edith Allison
Bartlesville Project Office

Reporting Period: Jan. 1–Mar. 31, 1990

Objective

This is a cooperative Department of Energy (DOE)–industry research program between Sandia National Laboratories and Phillips Petroleum Company to study and understand the interrelationships among in situ stresses, natural fractures, and reservoir permeabilities. There are three different but coupled tasks: (1) measurements of in situ stresses in the reservoir and adjacent formations, (2) laboratory deformation and permeability measurements in fractured and intact reservoir rock, and (3) characterization of the natural fracture system in the reservoir. The primary

focus is the Ekofisk oil field in the Norwegian sector of the North Sea.

Summary of Technical Progress

The Ekofisk field is the largest of nine chalk reservoirs in the southern part of the Norwegian sector of the North Sea. Almost 20 yr of petroleum production of the Ekofisk field has resulted in a 21-MPa (or more) reduction in reservoir pore pressure. The decline in pore pressure has led to an increase in the fraction of the overburden load that must be supported by the structurally weak chalk matrix, which, in turn, has caused significant reservoir compaction and seafloor subsidence.

The reservoir contains a natural fracture system that forms the primary conductive path for produced hydrocarbons and injected fluids. Numerical models suggest that deformation as a result of compaction and subsidence can alter the in situ stress state. Changes in stress state could affect reservoir permeability and productivity because the deformation and conductivity of natural fractures are strongly stress dependent.

In Situ Stress Measurements in the Ekofisk Field

Hydraulic fractures have been used to measure the minimum horizontal stress magnitudes at different locations across the Ekofisk field. The minimum horizontal stress magnitude was determined from the closure stress derived from shut-in pressure data after the initial cool down phase of a hydraulic fracture stimulation. In this phase, 28 to 55 m^3 of seawater is pumped into the well to break down the formation, and then the well is shut in before the main acid treatment. Fracture treatments were made in selected perforated zones in the Ekofisk formation, Tor formation, and simultaneously in both formations. The perforated zones were short, discontinuous intervals of less than 15 m, and the gross vertical height of all the perforated zones that were fractured ranged from 39 to 151 m.

Over 60 hydraulic fracture stimulations have been made in the Ekofisk field over its nearly 20-yr production history. Unfortunately, the procedures used in these stimulations and the quality of most of the pressure–time records prior to 1985 were not sufficient to estimate stress magnitude. Twenty-three wells have been analyzed that had good hydraulic fracture pressure–time records during the cool-down phase of the stimulation and were stimulated since 1985.

The minimum stress magnitude is not uniform across the field, ranging from 33.8 to 46.6 MPa, compared to an average overburden stress of 62 MPa. (The overburden stress is assumed to be a principal stress and is calculated from gravitational loading.) In general, the lowest magnitudes of the minimum horizontal stress were at the crest and on the west flank and the highest magnitudes were on the north and south flanks.

Pore pressure is also not uniform across the field and varies with time or degree of depletion (i.e., pore pressure measured in 1985 is usually greater than that measured in 1990). Pore pressure has also been affected by the waterflood (e.g., the Ekofisk formation in the K-23 well has been repressurized by nearby injection wells). Pore pressure measurements are based on well tests made in selected zones in the Ekofisk formation, Tor formation, and commingled tests in both formations.

Variations in the minimum horizontal stress and pore pressure across the reservoir are illustrated by two traverses (Figs. 1 to 3). The locations of wells on these two traverses are shown in Fig. 1. The minimum stress and pore pressure for nine wells of a north-south traverse along the west flank of the reservoir are shown in Fig. 2. Magnitudes of the minimum stress range from 33.8 to 46.6 MPa. The highest magnitudes of the minimum stress are on the northwest and south flanks. Pore pressure in the Tor formation ranges from 26.2 to 35.2 MPa. The highest pore pressure is on the northwest flank. The high pore pressure in the A-13a well on the south flank is because the measurements were made in 1985 and the pressure decline is not as large as more recently completed wells on this traverse.

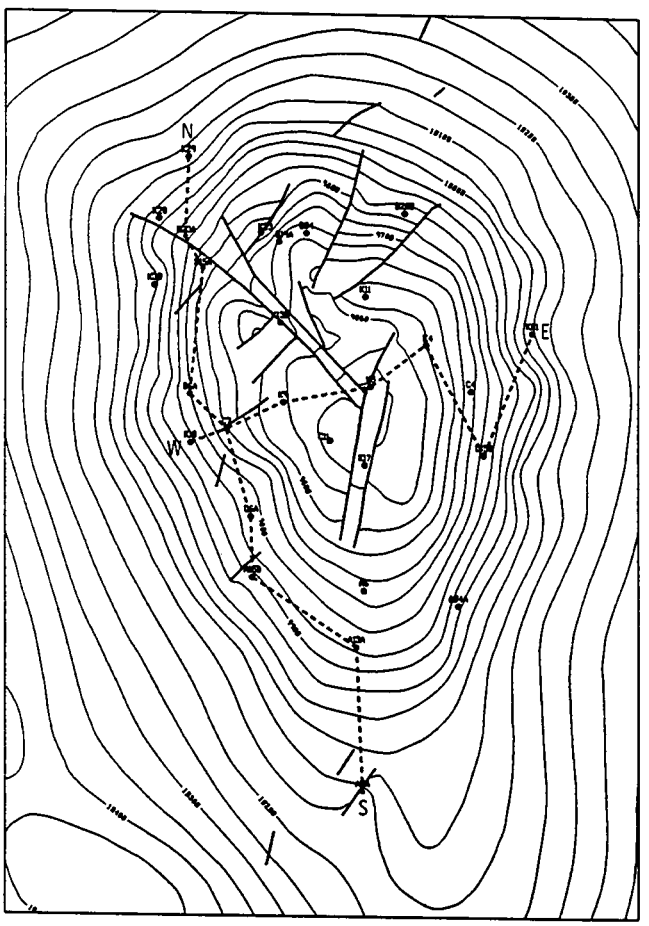

Fig. 1 Structure contour map for top of the Ekofisk formation showing the location of wells along a north-south traverse on the west flank and a west-east traverse across the crest of the Ekofisk field.

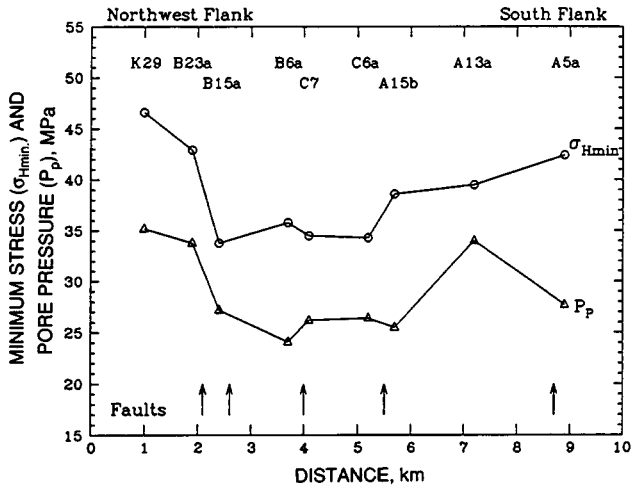

Fig. 2 Plot of minimum horizontal stress and pore pressure in nine wells located on a north-south traverse on the west flank of the Ekofisk field. Arrows indicate the location of faults along the traverse.

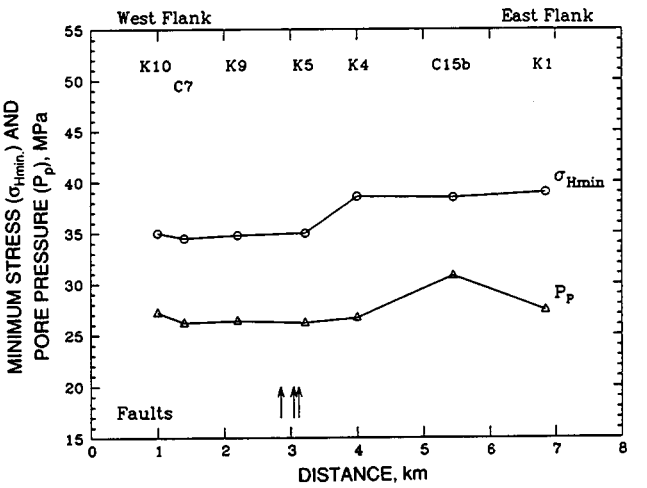

Fig. 3 Plot of minimum horizontal stress and pore pressure in seven wells located on an west-east traverse across the crest of the Ekofisk field. Arrows indicate the location of faults along the traverse.

Along the north-south traverse, a normal fault is crossed on the northwest flank between wells B-23a and B-15a. The B-23a well is on the downthrown side of the fault. A major contrast in the minimum stress magnitude and pore pressure exists between the wells and across the fault. In the B-23a well, the minimum stress and pore pressure in the Tor formation are greater than those in the B-15a well by 9.1 MPa and 6.6 MPa, respectively. This is the first direct evidence that a fault can act as a partial seal in the reservoir. (Both wells were completed and stimulated within 4 months of one another, and therefore the stress and pore pressure difference is not the result of depletion.) Several other faults are crossed along this traverse, but wells on either side of these faults do not show any significant stress contrasts and differences in pore pressure.

The minimum horizontal stress and pore pressure for seven wells of a west-east traverse across the crest of the field are shown in Fig. 3. On the west flank and crest, the minimum stress is about 35 MPa. On the east flank, the stresses are about 3 to 4 MPa higher. Pore pressure in the Tor formation ranges from 26.2 to 30.8 MPa. Several faults are crossed along this traverse. No significant stress contrasts or differences in pore pressure are found in wells on either side of these faults.

Distribution of Natural Fractures in the Ekofisk Field

Phillips Petroleum Company has been analyzing the distribution and orientations of fractures in the Ekofisk field. Fracture orientations were measured by two methods: (1) from oriented core and (2) from the formation microscanner (FMS) logs. Tectonic fractures can be identified on FMS images with confidence, and these show that a strong NNE-SSW fracture trend is present. Fractures with this trend form a conjugate set and dip to the west and to the east. This NNE-SSW fracture trend is parallel to the trend of major faults that have been mapped from seismic data in the northwest quadrant of the field. Fractures with this orientation are assumed to be genetically related to this faulting, that is, they developed at the same time and in response to the same stresses as the faults. These fractures and faults, which are geometrically similar features, differing only in scale, are not genetically associated with the Ekofisk structure itself. Their location and orientation are not affected by position on the dome. Their orientation is relatively constant, and they are predominant in the northwest part of the field. They are subordinate or absent on the east and southeast flanks of the dome.

On the east flank of the dome the tectonic fractures trend approximately east-west, and on the southeast flank the fractures trend northwest-southeast. Again, these fractures form a conjugate set of shear fractures dipping to the north and south. They are interpreted as being part of radial fracture trend that is genetically related to the dome. Radially oriented fractures also form subordinate trends in several other wells on the north and northwest flanks of the dome.

The Ekofisk field is therefore cut by two generations of fractures. One set trends NNE-SSW throughout the field but is concentrated in the northwest part of the field. These fractures are thought to have resulted from an episode of regional tectonic faulting that probably cuts the pre-Cretaceous rocks in this area as a result of late Paleozoic and early Mesozoic extension of the North Sea basin and formation of the Central Graben. The second set of fractures cutting the field are genetically related to doming and developed under a radial and tangential stress system.

CHARACTERIZATION OF FACIES AND PERMEABILITY PATTERNS IN CARBONATE RESERVOIRS BASED ON OUTCROP ANALOGS

Contract No. AC22-89BC14470

Bureau of Economic Geology
University of Texas
Austin, Tex.

Contract Date: Sept. 21, 1989
Anticipated Completion: Sept. 20, 1991
Government Award: $134,713

Principal Investigator:
C. Kerans

Project Manager:
Robert E. Lemmon
Bartlesville Project Office

Reporting Period: Jan. 1–Mar. 31, 1990

Objectives

The primary objective of this research has been to develop better methods for describing the three-dimensional (3-D) geometry of carbonate reservoir flow units as related to conventional or enhanced recovery of oil. Detailed characterization of geologic facies and rock permeability in reservoir-scale outcrops of the Permian San Andres Formation in the Guadalupe Mountains of New Mexico has provided the key database. Improved techniques for estimating permeability on the basis of geologic description will be developed with emerging geostatistical techniques and reservoir flow simulation experiments. Methodologies developed from outcrop studies will ultimately be tested in an operating reservoir in the Permian Basin to improve strategies for recovery of remaining mobile and residual oil.

Most San Andres and Grayburg reservoirs are composed of a lower, predominantly subtidal, part and an upper, predominantly shallow subtidal to intertidal, part. Distribution of the remaining mobile oil between these two intervals must be resolved on a reservoir-by-reservoir basis, but detailed analysis of several reservoirs indicates that more than 50% of the remaining resource lies in the geologically and petrophysically less well understood subtidal parts (typically the lower two-thirds of the oil column).

Geologic studies in the first quarter of this study defined an inclined flow-unit geometry in the equivalent subtidal strata in the San Andres outcrop. These subtidal strata, referred to as outer ramp clinoforms, are made up of interstratified peloid–fusulinid wackestone/packstones and crinoid–fusulinid–peloid packstone/grainstones in upward-shallowing cycles 10 to 30 ft thick.

Key tasks for the second quarter were to develop a quantitative geologic framework for the inclined flow-unit geometry and to collect core-plug data from the geologic units to be used in describing flow characteristics.

Quantitative Geologic Framework

Seven detailed geologic sections were measured and plotted on a photomosaic geologic base map. Sections were taken at 200-ft sampling distances along east-northeast- and east-southeast-trending canyon walls forming panels of a 3-D grid 1300 ft on a side, which approximates a 20-acre five-spot pattern. Each section covered 100 ft of vertical section and contained eight clinoform depositional units, seven of which were continuous through all sections (Fig. 1). Depositional units are upward-coarsening cycles

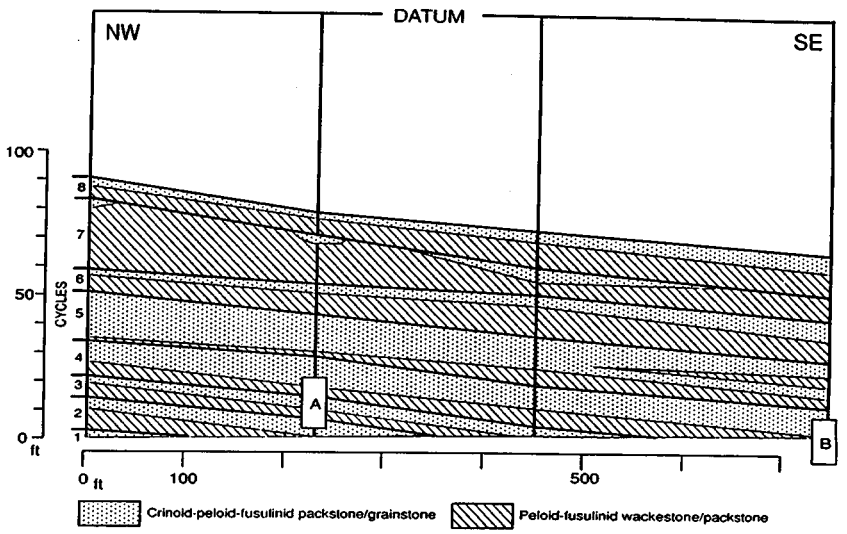

Fig. 1 Geologic cross section of the north wall of Irabarne Tank Canyon showing the continuity of facies within the depositional units (cycles) and the position of the core-plug sample grids within this geologic framework. The datum from which the sections are hung marks a horizontal surface or time-line during deposition. The E-SE dip of the fusulinid cycles shown in the section marks the depositional dip of these facies.

grading from fusulinid–peloid wackestone to fusulinid–peloid–crinoid packstone/grainstone. Depositional dip on the clinoform units is 1 to 2°.

Petrophysical Sampling

The core-plug sampling procedure was designed to determine the vertical and lateral variability of porosity and permeability within geologically defined units at a scale of less than 1000 ft. Two sampling localities (localities A and B) about 700 ft apart laterally and in overlapping depositional units were selected. A total of 105 permeability plugs (1 to 2 in. long, 0.5 in. across) were collected from the two sampling locations with a portable coring drill. Ninety-two samples have been prepared and sent for standard porosity–permeability analysis.

At locality A, 57 samples were collected on a 20 × 20 ft grid pattern containing four vertical transects spaced 5 ft apart laterally, and each was sampled at 1-ft vertical increments where possible (Fig. 2, locality A). The samples were spread across parts of three moldic fusulinid wackestone to fusulinid grainstone depositional units (units 2, 3, and 4). At locality B, 34 samples were collected from two 20-ft vertical sections spaced 10 ft apart laterally and sampled at 1-ft increments over portions of the same three depositional units (Fig. 2, locality B). Nine samples were also collected at locality B from a 1-ft square to characterize small-scale porosity and permeability variability.

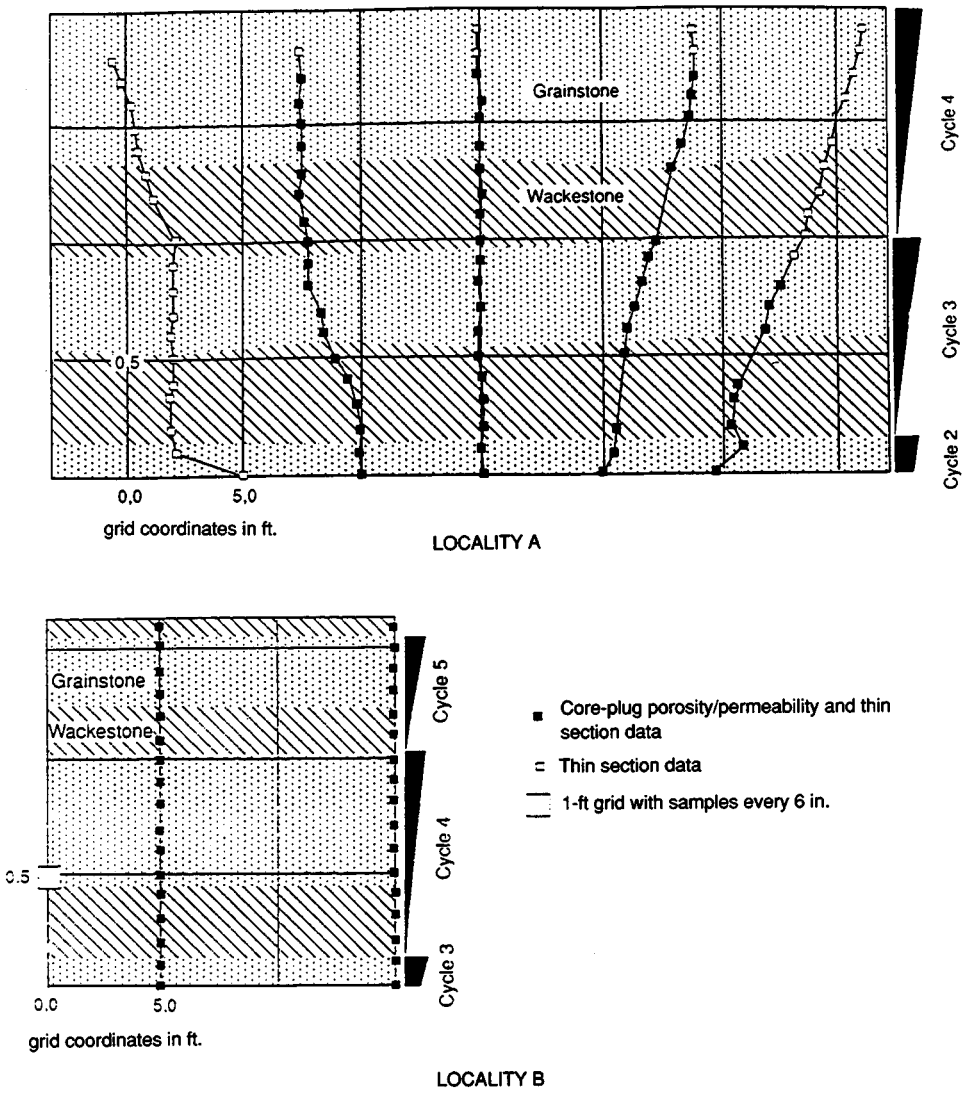

Fig. 2 Sampling grids for core plugs.

IMAGING TECHNIQUES APPLIED TO THE STUDY OF FLUIDS IN POROUS MEDIA

Cooperative Agreement DE-FC22-83FE60149, Project BE12

National Institute for Petroleum and Energy Research
Bartlesville, Okla.

Contract Date: Oct. 1, 1987
Anticipated Completion: Sept. 30, 1990
Funding for FY 1990: $395,000

Principal Investigator:
Liviu Tomutsa

Project Manager:
Robert E. Lemmon
Bartlesville Project Office

Reporting Period: Jan. 1–Mar. 31, 1990

Objectives

The objectives of this project are: (1) to develop and use new imaging techniques for measurements of pore geometries and fluid distributions in reservoir rocks at scales varying from a pore to a whole core and (2) to study the effect of microscopic-scale heterogeneities on oil trapping in core-size rock samples.

Summary of Technical Progress

A low-pressure (<200 psi) coreflooding experimental setup has been installed in the computerized tomography (CT) room. It allows the control and monitoring of fluid inlet pressures and rates and fluid production rates without interfering with CT scanning. Positioning devices for both epoxied slabs ($10 \times 5 \times 2$ cm) and a low-pressure coreholder for 2-in.-diameter cores (up to 8 in. long) have been designed and built. They allow CT scanning along the direction of flow with a minimum of artifacts.

Because of beam hardening, an attenuation cupping effect occurs when scanning rock samples, with X-ray attenuation increasing from the center toward the periphery of samples. By surrounding samples with attenuating materials (tagged fluids, sand, or rock) such that the shape of the entire volume scanned approaches cylindrical symmetry, the cupping is reduced, but the noise present in the image is increased as the result of the weakening of the X-ray beam reaching the detectors. This causes an uncertainty in the values of the attenuation for each image voxel. The average voxel uncertainty was determined by subtracting images taken of the same sample. Because odd and even scans are taken by the movement of the gantry in opposite directions and a certain slack is present in the mechanical drive, two consecutive images are slightly displaced. Thus errors as a result of this slight misalignment can be avoided by subtracting odd images from odd images and even from even. An average voxel uncertainty of 5 Hounsfield units was obtained. For a brine tagged with 20% NaI in a 30% porosity rock, this value corresponds to a 2.5% uncertainty in saturations computed from CT images. By recalibrating the CT scanner for the higher density present in quartz and with improvements in the selection of the attenuating materials surrounding the core, this number should be reduced further.

The processing of files downloaded from the CT scanner has been improved by adding a menu-driven interface that allows quick access of the programs to be used with these files, such as file conversion, porosity calculation, saturation calculation, and false color. The hardware has been improved by bringing the upgraded version of the image processing package to fully operational status by adding an 80 megabyte (MB) hard disk, a 3 MB RAM disk, and a better Analog RGB color monitor to the AT system dedicated to processing CT images.

Measurement of Fluid Distributions by Computerized Tomography Scanning

Effects of heterogeneities on fluid flow and oil trapping were studied by performing floods on a $10 \times 5 \times 2$ cm slab of heterogeneous Shannon sandstone (Fig. 1). On the CT scan of the dry slab, a central zone of higher porosity and permeability (darker color) and peripheral zones of lower permeability (lighter colors) can be observed. At the lower part of the sample, the lighter coloring indicates tighter rock plus shale streaks. These heterogeneities control the front fingering both during the drainage process (oil displacing the brine) and imbibition (brine displacing oil).

Figure 2 shows four progressive steps during a flood in which brine (white) displaces mineral oil tagged with 40%

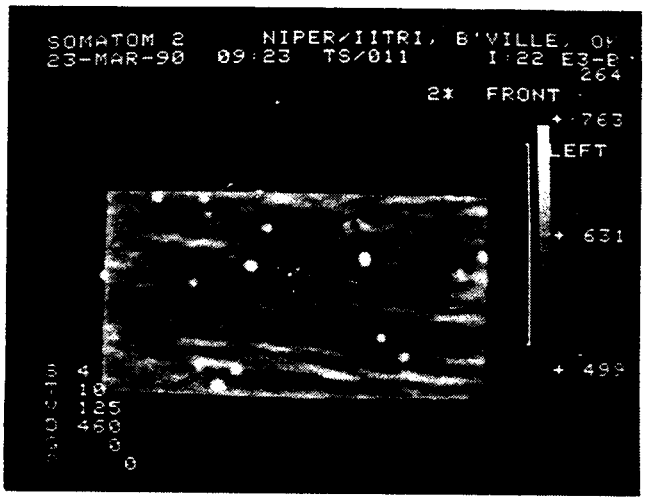

Fig. 1 Computerized tomography scan of Shannon sandstone slab.

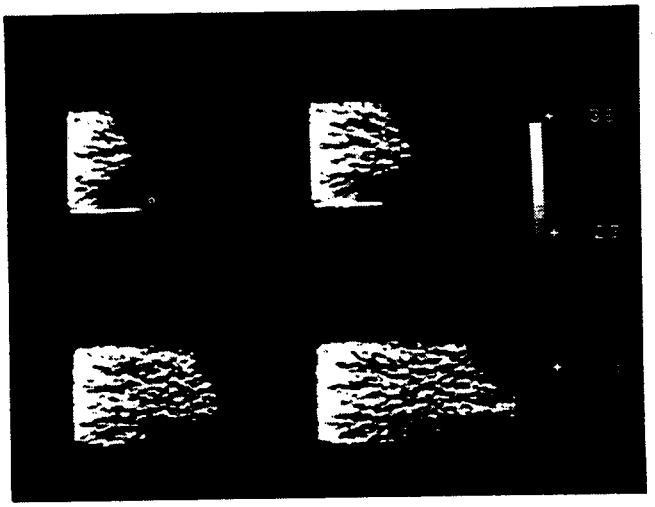

Fig. 2 Front advancement during waterflooding of Shannon sandstone slab.

1-bromododecane (black). The effect of various rock permeabilities on the front advancement can be seen. The viscosity of the brine and the mineral were 1.006 and 30 cP, respectively. The four images represent (from top left to lower right) a succession of 0.09, 0.16, 0.22, and 0.28 PV of brine injected. The respective elapsed times from the start of the flood were 735, 1035, 1335, and 1635 s, respectively. This corresponds to a front advancement speed of approximately 17 ft/d.

The volumetric monitoring of the oil and brine produced allowed the computation of average oil and brine saturations during the flood. The average saturations calculated from CT scans agreed within 1% with those calculated from volumetric measurements (Table 1).

TABLE 1

Average Oil Saturation Changes During Waterflooding, Shannon Outcrop Core

Volumetric values, %	Computerized tomography (CT) values, %	Difference between CT and volumetric oil
6.2	7.5	1.3
7.5	7.9	0.4
8.6	9.3	0.7
9.4	10.1	0.7
11.0	11.4	0.4
12.3	12.6	0.3
13.7	13.7	0.0
15.0	15.4	0.4
16.3	16.0	–0.3
17.4	17.5	0.1
18.8	18.1	–0.7
20.1	21.7	0.6
23.0	22.4	–0.6
23.8	23.8	0.0
24.9	26.1	1.2

The core saturated with isopropyl alcohol (IPA) was dried with nitrogen gas. Two distinct stages of IPA saturation distributions have been observed in the CT scans. In the first stage (parts a and b of Fig. 3), fingering controlled by rock heterogeneity reaches the outlet almost instantaneously. The region behind the front (white) represents saturations in the 50 to 80% range, whereas ahead of the front (gray), the rock is fully saturated (100%) with IPA.

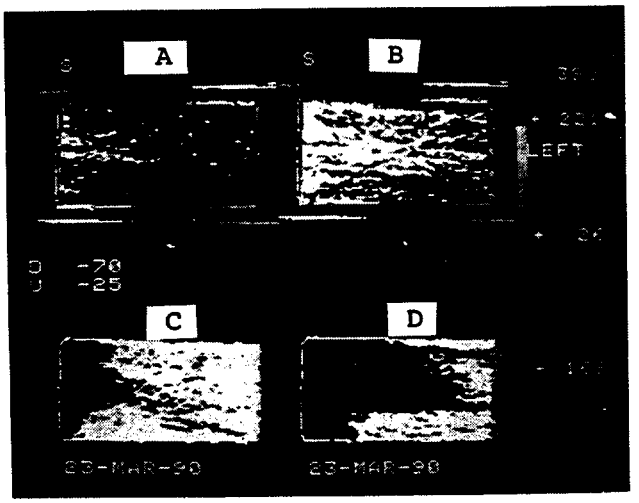

Fig. 3 Drying of Shannon sandstone slab saturated with isopropyl alcohol.

In the second stage, another front appears (parts c and d of Fig. 3) with the fingering of the front not as pronounced as previously but nevertheless also controlled by rock heterogeneity. The region behind this front (black) is dry rock, whereas ahead of it, the white region is partially saturated. The four images (from top left to bottom right) have been taken at 30, 150, 3000 and 4800 s from the beginning of the nitrogen flow. After 3 h of flow, the average IPA saturation in the rock was reduced to 2%. The core was completely dry after allowing the gas to flow overnight, with a total of 3×10^6 cm^3 of nitrogen having flowed through the system.

NMRI Research

The three-dimensional (3-D)-projection reconstruction software, both for controlling the image acquisition using the PC/AT and for processing the resulting data file on the MICROVAX, has been improved in several areas and is working very well. The major bottleneck is the long time required for transferring data files to the MICROVAX and processing the data to display the image. For an image data file acquired at $128 \times 128 \times 128$ pixel resolution (16 megabytes), the total turnaround time required has been as long as 40 h. This long time is required because program runs on the MICROVAX in batch mode at low priority and central processing unit time is shared with

other users. A benchmark program (Sieve of Eratosthenes) used on several types of computers, including the MICROVAX and a 20-MHz 386 computer, demonstrated that a 386 computer was five times as fast as the MICROVAX even without sharing the VAX on batch priority. This indicates an improvement in data processing speed of 15 to 20 times by going to a dedicated 20-MHz 386 computer. A 20-MHz 386 DTK computer with a Lahey F77 32-bit FORTRAN compiler is being evaluated to see if the speed of computation on the 3-D-reconstruction software will demonstrate the improvement indicated by the benchmark tests.

With the developments in the 3-D reconstruction and image display software essentially complete, nuclear magnetic resonance imaging work this quarter has focused on increasing the resolution of the system down to 25 μm on samples prepared from polymer microspheres. These microspheres have a nominal size distribution of 100 to 500 μm diameter. Several beadpacks have been prepared and saturated with water using Teflon plugs inside a 15-mm nuclear magnetic resonance tube (12.5-mm inside diameter) and a 4-mm tube (2.7-mm inside diameter). Images have been acquired at 128 × 128 × 128 pixel resolution. The images show water between the microspheres of the 12.5-mm-diameter beadpack with a resolution of about 120 μm. Each slice is about 200 μm thick. Size-grading of the polymer microspheres revealed that the actual diameter of the microspheres ranged from 130 to 900 μm. The microspheres have since been sieved and graded into six size ranges: 750 to 900, 700 to 800, 530 to 700, 300 to 500, 200 to 350, and 130 to 250 μm. A small sample holder was made of Teflon with a 2.7-mm inside diameter and a beadpack made using the 300- to 500-μm microspheres. Images have also been taken of the 2.7-mm-diameter beadpack with a resolution of about 30 μm. Figure 4 shows one of the 128 adjacent slices of the 2.7-mm-diameter beadpack. The slice is about 40 μm thick. The circular outlines of the microspheres are clearly evident, and the nearly uniform size of the graded microspheres is shown.

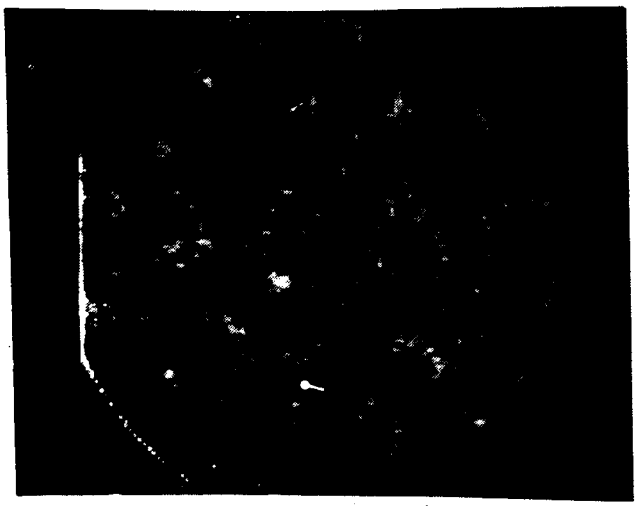

Fig. 4 Nuclear magnetic resonance image high-resolution scan of 300- to 500-μm sphere pack.

Micromodel Studies

The objective for micromodel studies during FY90 is to observe the effect of small-scale heterogeneities on fluid flow distribution. This work will involve using the same techniques as those developed in FY89 but with different rock samples. Previous research at NIPER and elsewhere was evaluated to aid in the design of these experiments. Video tapes prepared in FY89 were briefly reviewed to understand the scope and limitations of various micromodels used.

On the basis of the review of earlier research, it seemed appropriate to use a layered rock sample and make two or three micromodels from it with varying orientation of the layers. The focus of these experiments will be to study the effect of layering on transient displacement behavior. The work in this direction has begun, and a suitable layered rock slab has been selected and CT scanned. Workable cutting strategies that will allow cutting thick sections (2 to 3 mm) without damaging layers are being sought.

LABORATORY MODELING AND FIELD DEVELOPMENT OF BOREHOLE SEISMIC IMAGING TECHNIQUES USING SEISMIC WAVEFIELD MEASUREMENT

Contract No. DE-AC22-89BC14478

Colorado School of Mines
Golden, Colo.

Contract Date: Sept. 25, 1989
Anticipated Completion: Sept. 25, 1992
Funding for FY 1990: $160,337

Principal Investigator:
A. H. Balch

Project Manager:
Robert E. Lemmon
Bartlesville Project Office

Reporting Period: Jan. 1–Mar. 31, 1990

Objective

The objective of the research program is to develop processing, imaging, and interpretation techniques for the

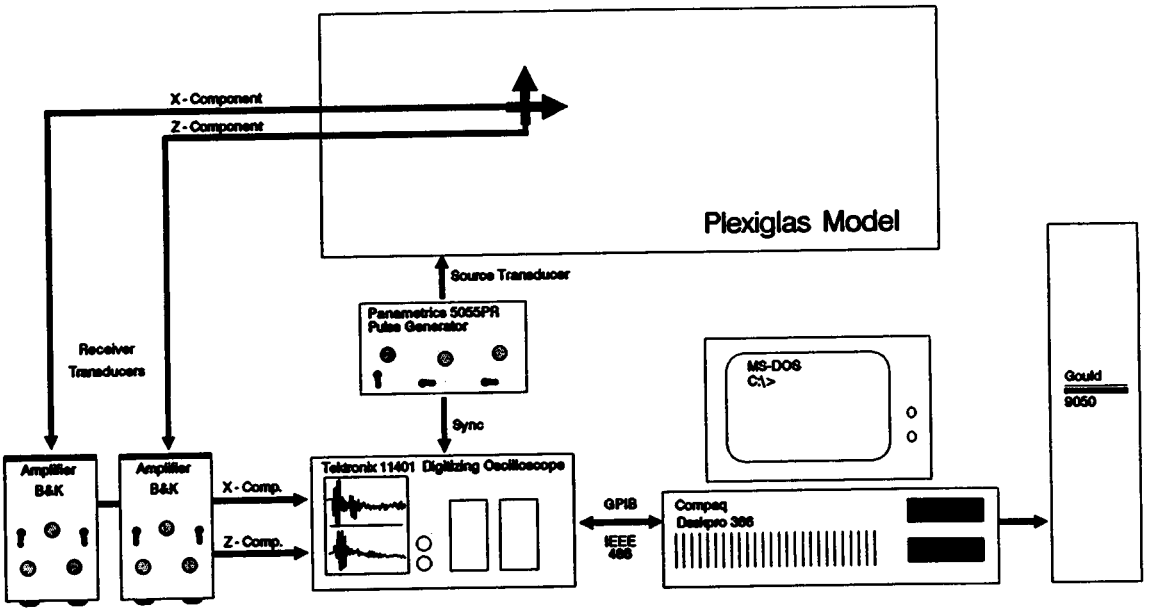

Fig. 1 Block diagram of the laboratory cross-borehole modeling system.

use of crosswell seismic data to acquire a higher resolution image of hydrocarbon-bearing formations and to aid the extraction (i.e., hydrocarbon production) process. This program consists of three overlapping activities: (1) use of physical acoustic models to study crosswell seismic phenomena and develop processing (imaging) and interpretation procedures; (2) field test and demonstration of the crosswell procedure in a controlled, known, geological environment; and (3) test of the procedure in an actual oil and/or gas field.

Summary of Technical Progress

Acoustic Modeling

The "Tunnel" Model. During the previous report period a cross-hole acoustic model was built. Figure 1 is a schematic of the laboratory setup for this modeling experiment. Figure 2 is a diagram of the model itself. The primary interest is in imaging reflectors (or diffractors) using reflected (or diffracted) seismic events. Typical source–receiver ray paths, associated with five such events, are shown in Fig. 2. Note that all four reflection modes (p–p, p–s, s–p, and s–s) are possible, a wide range of dip angles is involved, both forward-scattered and backscattered events are considered, and both horizontal and vertical components of motion are recorded. In Fig. 3, a typical vertical component "common source gather" is illustrated. It represents the vertical component recordings at 256 receiver locations for one source location. A total of 33 such gathers was produced. Several coherent events are identified. In Fig. 4, a typical p-wave-only common source gather is shown. It was obtained by combining the

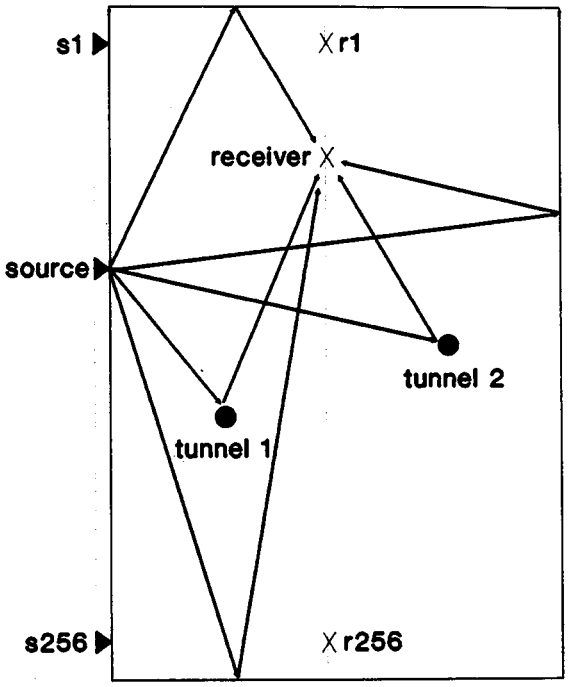

Fig. 2 Typical ray path diagram for the constant velocity plexiglas model shown in Fig. 1. Source and receiver lines are indicated. The rays represent all four modes of reflection: p–p, p–s, s–p, s–s. Note that two reflectors and one "tunnel" are located in the region between the boreholes, whereas one reflector and one "tunnel" are located outside the region between the boreholes.

horizontal and vertical component data for the same gather; a method described by Dankbaar was used.[1] A similar s-wave only data set was generated for each gather. This operation was carried out for all 33 common source gathers.

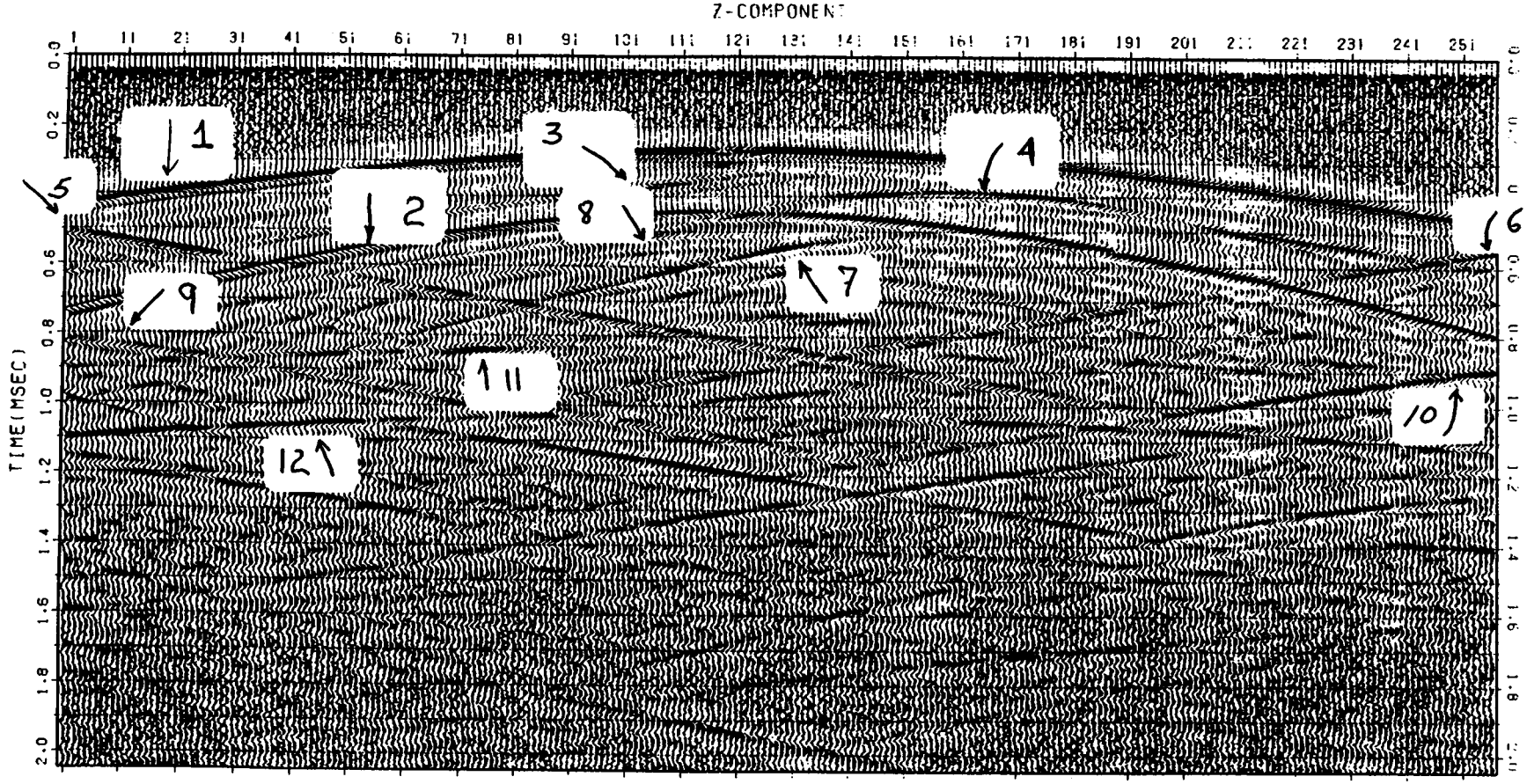

Fig. 3 Common source point gather of raw data, vertical Z component. The source was at location 121 approximately 30 in. from the top of the model. Several coherent events are identified as follows: (1) direct p arrival, (2) direct s arrival, (3) p diffraction from left-hand tunnel, (4) p to s converted diffraction from left-hand tunnel, (5) p reflection from top of model, (6) p reflection from bottom of model, (7) s diffraction from left-hand tunnel, (8) p diffraction from right-hand tunnel, (9) s–p converted reflection from top of model, (10) s–p converted reflection from bottom of model, (11) p reflection from right-hand side, and (12) s reflection from right-hand side.

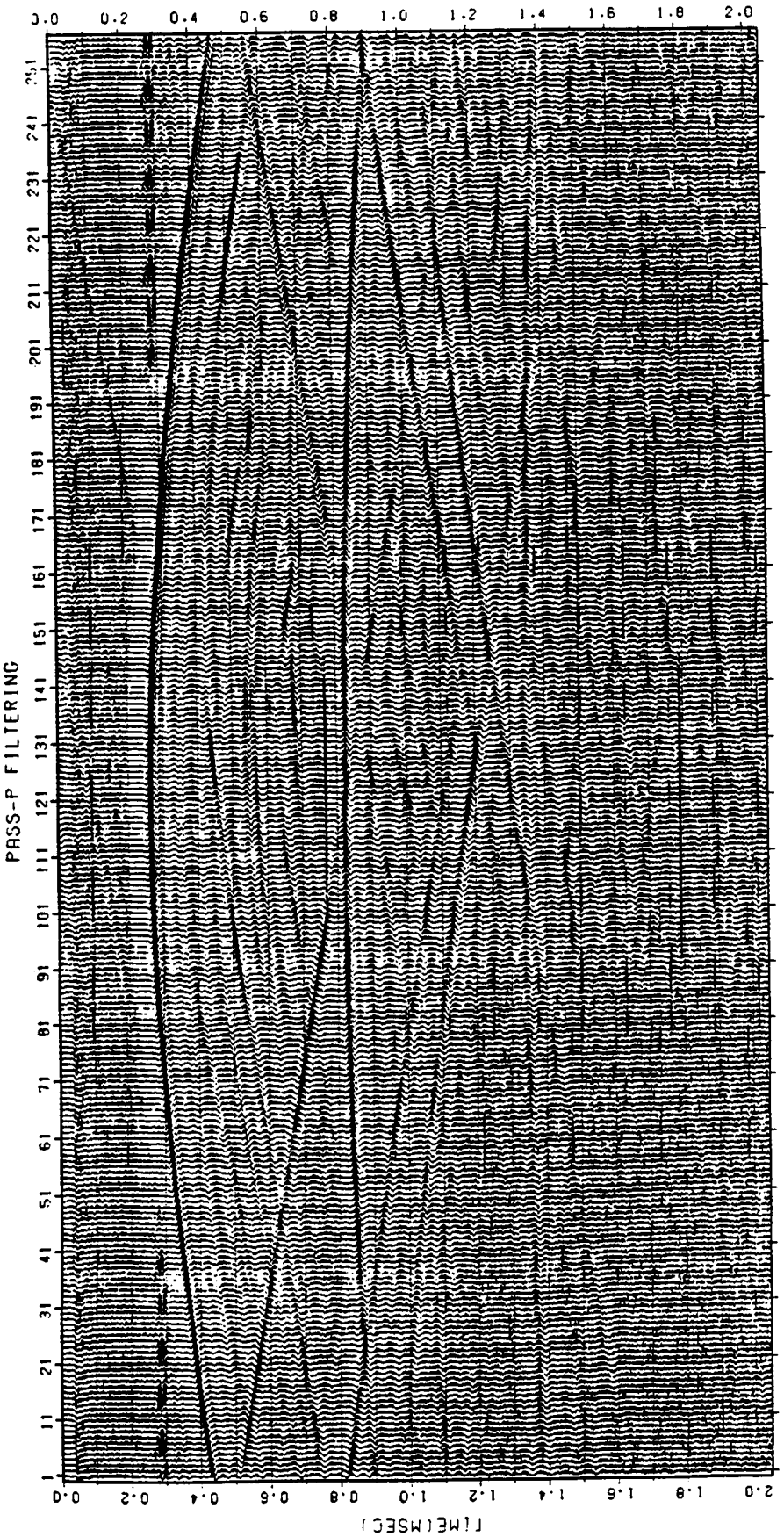

Fig. 4 Common source point gather of the data in Fig. 3 after extraction of p-waves.

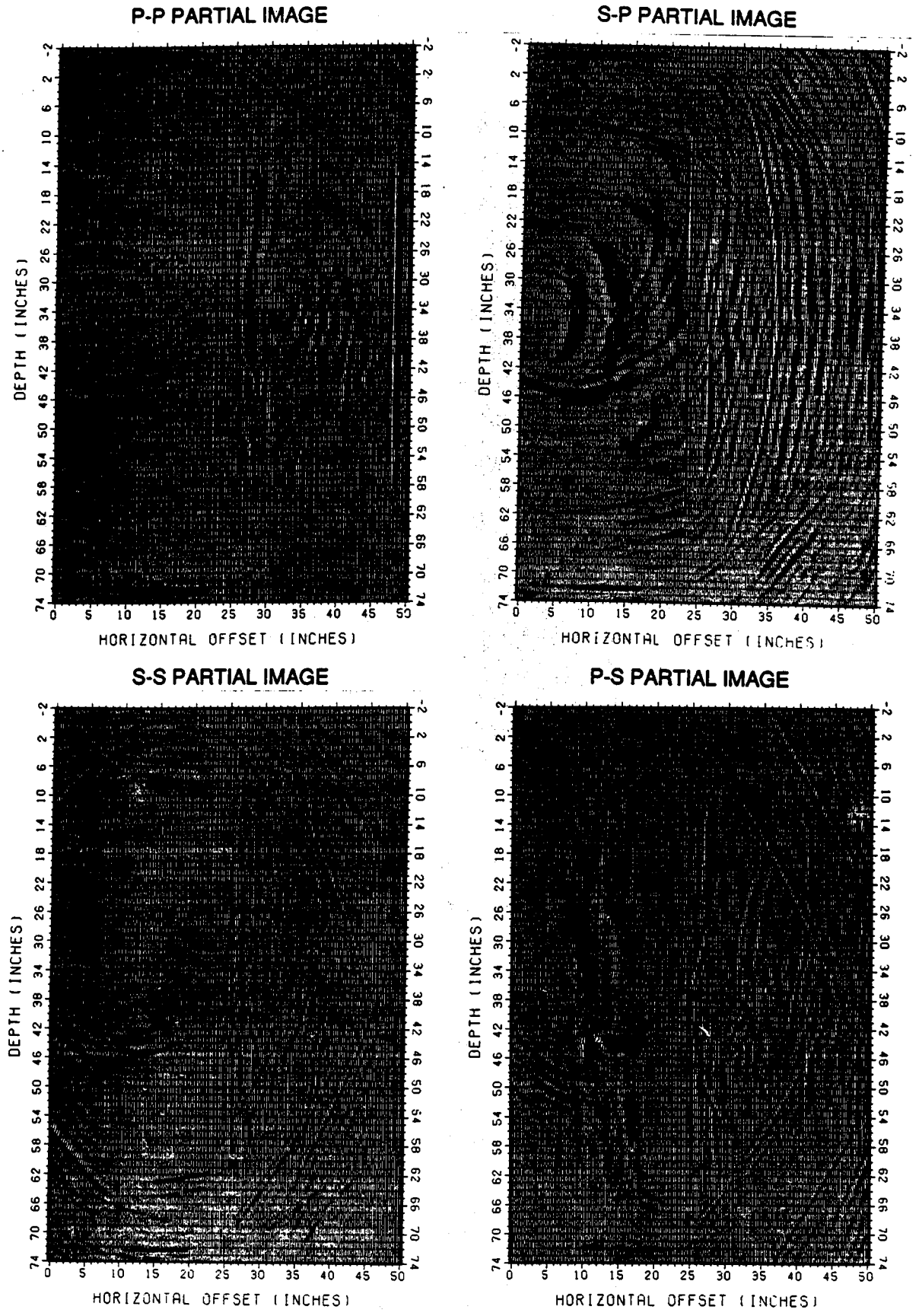

Fig. 5 Set of four partial images resulting from migrating, or imaging, a single common source gather. The common source gather input data were obtained from the model shown in Figs. 1 and 2. Artifacts are unavoidable and are the result of imaging of wrong modes and imaging in the wrong image space.

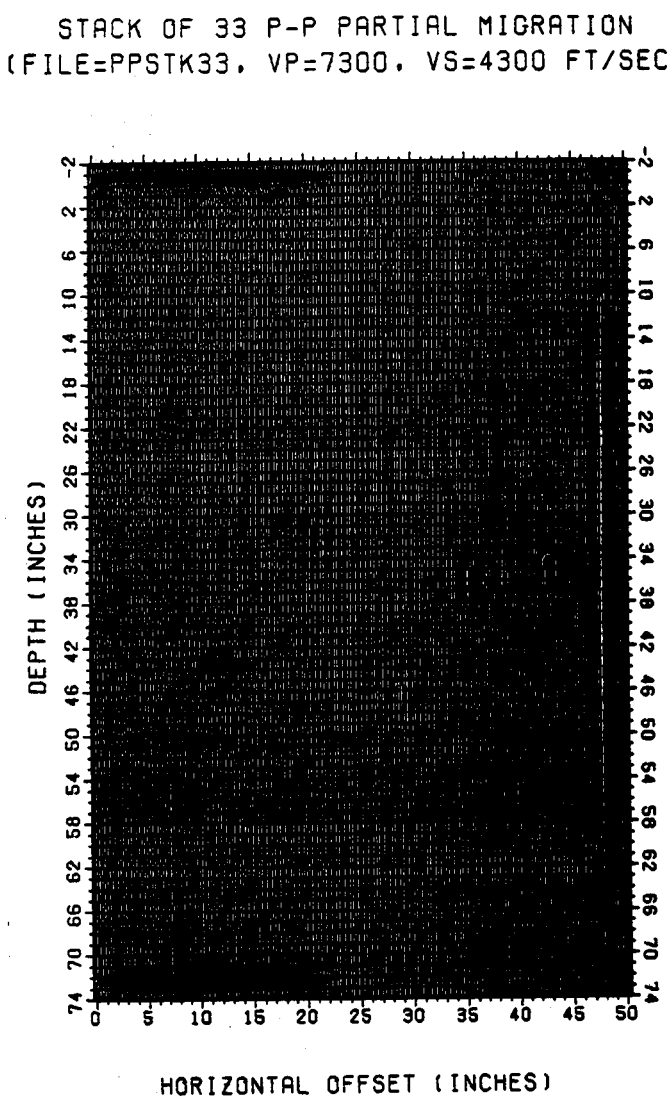

Fig. 6 Final stacked p–p image of the model shown in Fig. 2, based on 33 common source gathers. All three edges and both tunnels show clearly and in their proper size and location. Edge images are created only along those portions of the edge which reflect source energy into the receiver array (or " borehole").

After mode separation, the common source gathers were "inverse Q deconvolved." In migration, or imaging, considerable simplification is obtained by assuming a nonattenuating medium. The inverse Q deconvolution produces an estimate of the data sets that would have been obtained if the medium had been nonattenuating.

The process of prestack reverse-time migration was then performed on all 66 mode-separated, deconvolved gathers. There are four reflection modes; the operation was done for each mode on each gather. A typical result is shown in Fig. 5. These images are called partial images. Since the wave field was measured only along a part of the boundary surrounding the medium, it can only be partially reconstructed within the medium. As a result, images of the reflectors can only be partially constructed.

The next step was to combine (or "stack") all 33 partial images, for each reflection mode, into composite images. Figure 6 shows the final image for the p–p reflection, and Fig. 7 shows the results for all four reflection modes.

The final stacked images, particularly the p–p images, are a good representation of the reflecting horizons. Compare Figs. 6 and 7 with Fig. 2.

A successful test of the ability of the reverse-time imaging algorithm to image forward-scattered and back-scattered reflections, multimode reflections, and reflectors with 0 to 90° of dip was completed.

The Stratigraphic Trap Model. The attempt to image the tunnel model, by prestack migration of the "cross-borehole" model data, is considered successful. The next step was to design and build a more nearly realistic physical model of an actual oil field. The Peoria field, in eastern Colorado, was selected as the prototype, after a review of several possibilities. The Peoria field was selected because its geology is fairly well-known, it is typical of many "point-bar" stratigraphic trap oil reservoirs, and there is a real possibility of doing a test survey at Peoria field during the last stage of the investigation.

A simplified geologic cross section of a portion of the Peoria field is shown in Fig. 8. Hydrocarbons are entrapped in the J sandstone, where it pinches out between the boreholes.

The physical model to represent the configuration is shown in Fig. 9. It is a two-phase model (Plexiglas and Lexan) scaled approximately 100 : 1. This model will be constructed during the third quarter.

Computer Development

During the quarter considerable effort was made to adapt the Landmark seismic workstation to the seismic cross-borehole imaging problem. This system, on loan from Landmark Graphics, runs on an IBM R/T workstation. The raw digitized model data and the imaged results were reformatted and made compatible to the Landmark. Then the extensive Landmark graphics packages were used to display the imaged results in color. This turns out to be an effective way to display the reflectors.

In addition, the reverse-time migration procedure uses a finite-difference solution to the wave equation to back project the reflected energy. The solution can be displayed, time step by time step, on the Landmark. This gives the observer a motion-picture effect, which allows the wave field to be observed as it appears to develop and travel within the medium. This technique is very useful in identifying coherent events on the data set. It gives considerable insight into how the migration algorithm actually works.

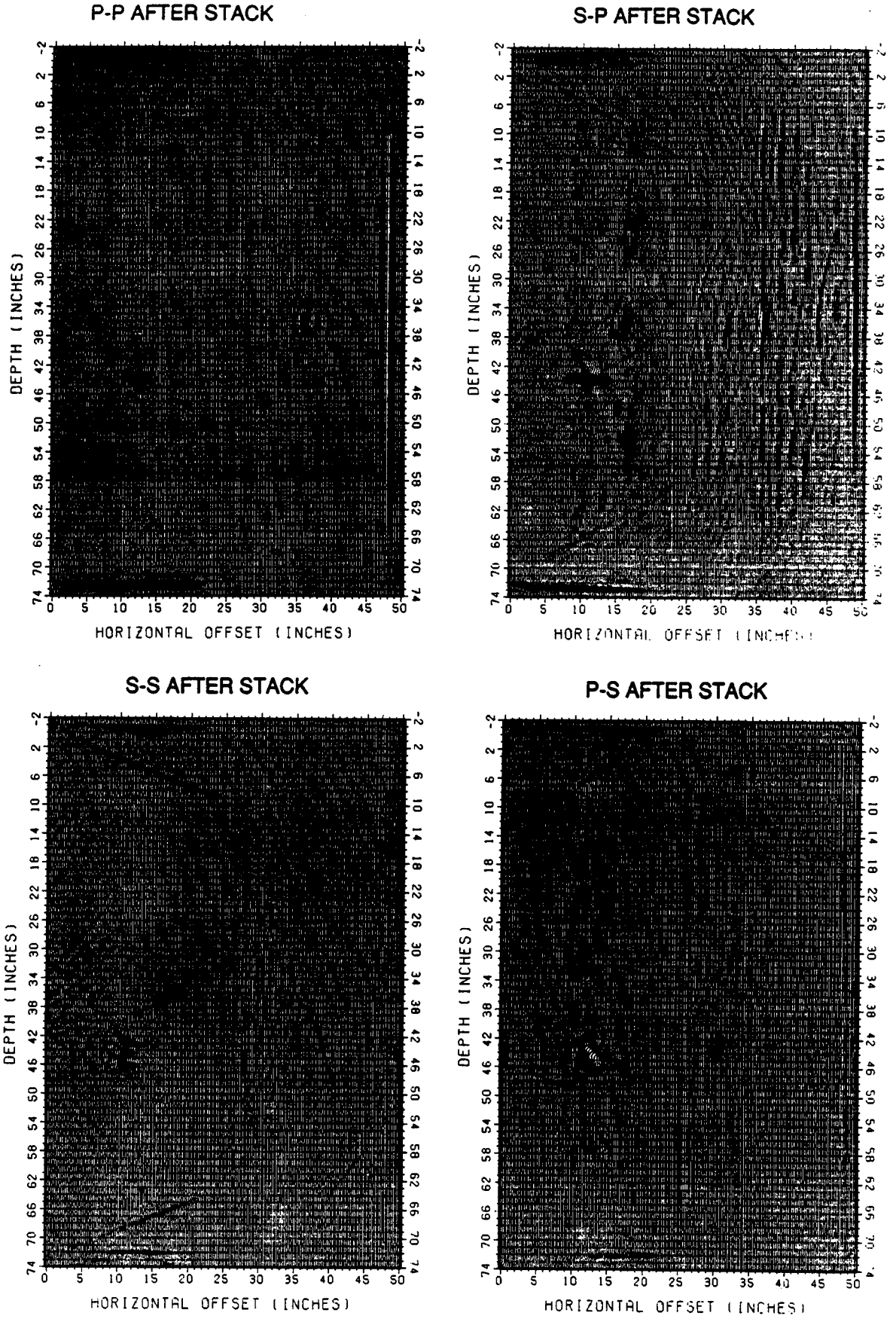

Fig. 7 Final stacked images of the physical model shown in Fig. 1, based on 33 cross-borehole common source gathers. All four reflected/diffracted modes have been imaged: p–p, p–s, s–s, s–p.

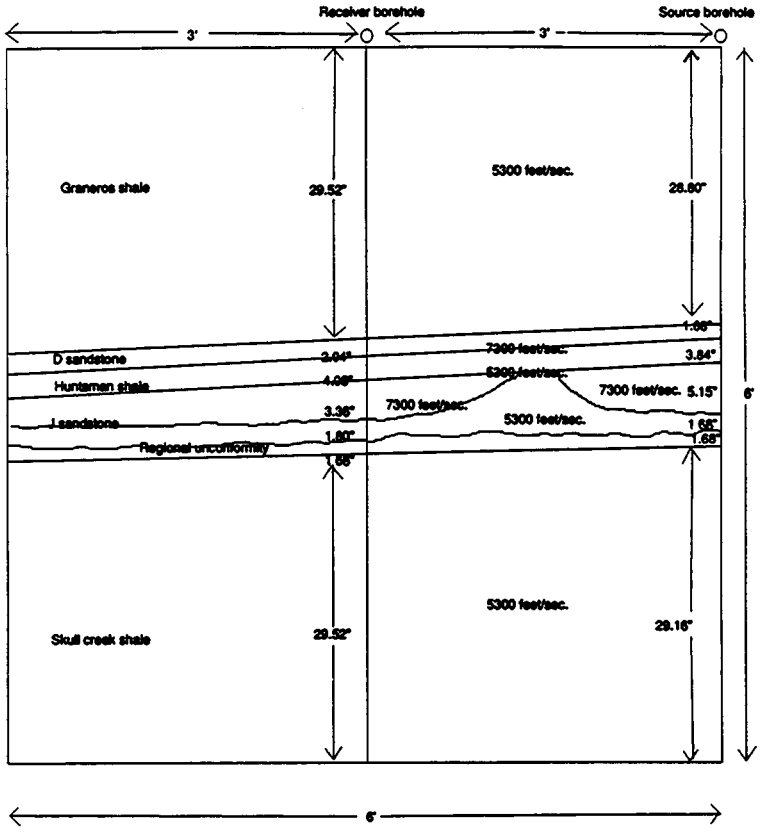

Fig. 8 Simplified geologic model of the Peoria field in Colorado. Note the (productive) "J" sand pinchout beneath the Huntsman shale.

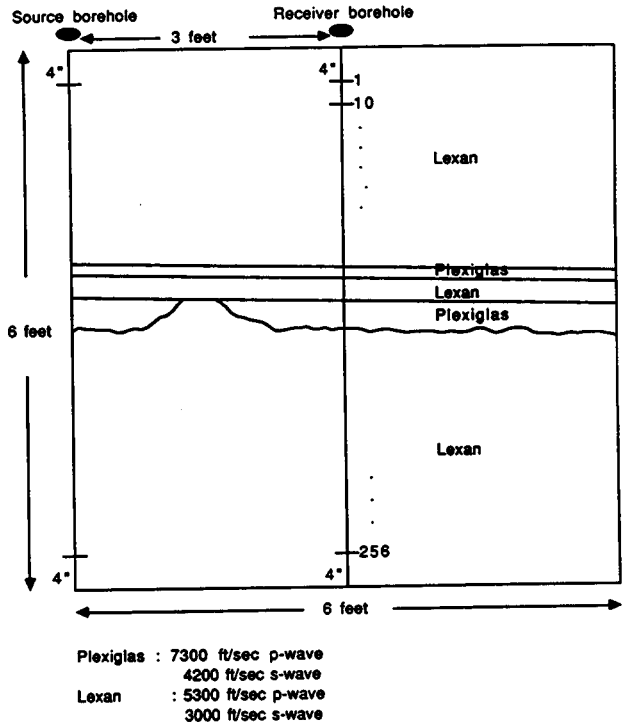

Fig. 9 Actual physical geologic model of the Peoria field based on the geologic model shown in Fig. 8.

Reference

1. S. W. M. Dankbaar, Vertical Seismic Profiling—Separation of P- and S-Waves, *Geophys. Prospect.*, 35: 803-814 (1987).

RESOURCE ASSESSMENT TECHNOLOGY

CHARACTERIZATION OF RESERVOIR ROCKS AND FLUIDS BY SURFACE ELECTROMAGNETIC TRANSIENT METHODS

Contract No. AC22-90BC14476

Blackhawk Geosciences, Inc.
Golden, Colo.

Contract Date: Feb. 15, 1990
Anticipated Completion: Mar. 15, 1992
Government Award: $273,623

Principal Investigator:
Pieter Hoekstra

Project Manager:
Robert E. Lemmon
Bartlesville Project Office

Reporting Period: Jan. 1–Mar. 31, 1990

Objective

The objective of this project is to enhance the resolution capabilities of two-dimensional (2-D) subsurface imagery using surface-based transient electromagnetic (TEM) data to enhance reservoir characteristics.

Summary of Technical Progress

Approximately two years elapsed between the submission of the research proposal to the U.S. Department of Energy (DOE) and the award of the contract. During those two years several significant events occurred that have an impact on the manner in which the research under this contract is conducted. The major events follow.

The changed relations between the Union of Soviet Socialist Republics (USSR) and the United States allowed several Soviet scientists prominent in the fields of electromagnetic geophysical prospecting to visit the United States, and some have taken permanent residence here. Particularly in theoretical aspects of electromagnetic geophysics, Soviet scientists maintained a leading role over several decades. Specific interactions include:

Dr. M. S. Zhdanov, Professor at the University of Moscow and a prominent research scientist in electromagnetic imaging, visited Golden, Colo., in the fall of 1989. He lectured at the Colorado School of Mines, and the principal investigators of subject research contract had several discussions with Dr. Zhdanov. The knowledge gained from those discourses directly affects the proposed research effort.

Dr. Leonty Tabarovsky (previously Chief Research Associate of the Institute of Geology and Geophysics of the Siberian Branch of the USSR Academy of Sciences, Novosibersk, USSR) has been granted permanent residence status in the United States. He is now domiciled in Golden,

Colo., and he has accepted permanent employment with Interpex Ltd., a principal subcontractor for subject DOE work. Dr. Tabarovsky is one of the foremost scientists in the world in theoretical electromagnetic geophysics. His publication list is extensive.

During the two years that elapsed between proposal and award of subject contract, the principal investigators conducted several time domain electromagnetic surveys at the Savannah River Site (SRS) and at the Waste Isolation Pilot Plant (WIPP). Testing several algorithms for data processing was part of the work effort. The knowledge gained from those investigations influences the work under this contract.

To allow events discussed to fully impact the conduct of this DOE research proposal, a topical report was written to describe the state of the art of 2.5D forward modeling and imaging of time domain electromagnetic data. This topical report will properly reflect the recent interaction with Soviet scientists. It will contain recommendations about directions to proceed, fully taking into account the knowledge gained.

Other activities concluded during the period of performance of this report were the issuance of two subcontracting agreements with the coprincipal investigators under this subject research contract, Interpex Limited and James Consulting Services, Inc.

CHARACTERIZATION OF SANDSTONE HETEROGENEITY IN CARBONIFEROUS RESERVOIRS FOR INCREASED RECOVERY OF OIL AND GAS FROM FORELAND BASINS

Contract No. FG07-90BC14448

Geological Survey of Alabama
Tuscaloosa, Ala.

Contract Date: Feb. 20, 1990
Anticipated Completion: May 30, 1990
Government Award: $175,000
(Current year)

Principal Investigator:
Ernest A. Mancini

Project Manager:
Chandra M. Nautiyal
Bartlesville Project Office

Reporting Period: Jan. 1–Mar. 31, 1990

Objectives

The objectives of this project are to augment the National Reservoir Database Tertiary Oil Recovery Information System (TORIS), to develop models of reservoir heterogeneity, and to identify resources that are producible at reasonable cost. If these objectives are accomplished, the recovery of oil and gas from Carboniferous siliciclastic reservoirs in the Black Warrior basin of Alabama and Mississippi should increase. The objectives will be achieved through detailed geological, engineering, and geostatistical investigations of Carboniferous reservoir sandstone throughout the basin. These investigations will be used to develop and to test geological and mathematical models for predicting the effect of reservoir heterogeneity on the recovery of oil and gas.

Summary of Technical Progress

Geological Studies

A primary understanding of reservoir heterogeneity may be obtained by direct observation of the geometry and primary stratification of sandstone bodies in outcrop. The quartzose-sandstone lithofacies comprises quartzarenite and sublitharenite bodies that are interspersed throughout the Carboniferous strata of the eastern and midcontinental United States; the lithofacies provides the principal siliciclastic oil and gas reservoirs of the Carboniferous in this region. In the Black Warrior basin, quartzose sandstone crops out in the Chesterian (Upper Mississippian) Pride Mountain and Hartselle Formations and the New Riverian (Lower Pennsylvanian) Pottsville Formation.

Chesterian Quartzose Sandstone

In the Mississippian System, the quartzose-sandstone lithofacies occurs in a thick, regional carbonate sequence. The oldest occurrence of the lithofacies is in Osagian rocks (Fort Payne Formation) on the Cumberland Saddle of the Cincinnati arch in south-central Kentucky. By Chesterian time, however, the lithofacies was widespread in parts of the Appalachian, Illinois, and Black Warrior basins. In each of these basins, interpretation of sediment sources and depositional environments is controversial, although most investigators accept an origin involving sedimentation in marginal-to-shallow open-marine depositional systems. For a better understanding of the origin and reservoir characteristics of Chesterian quartzose sandstone in the Black Warrior basin, several exposures of the Pride Mountain Formation and the Hartselle Sandstone (Fig. 1) were described and measured near the towns of Huntsville and Hartselle, Ala. (Fig. 2), along the northeast margin of the Black Warrior basin.

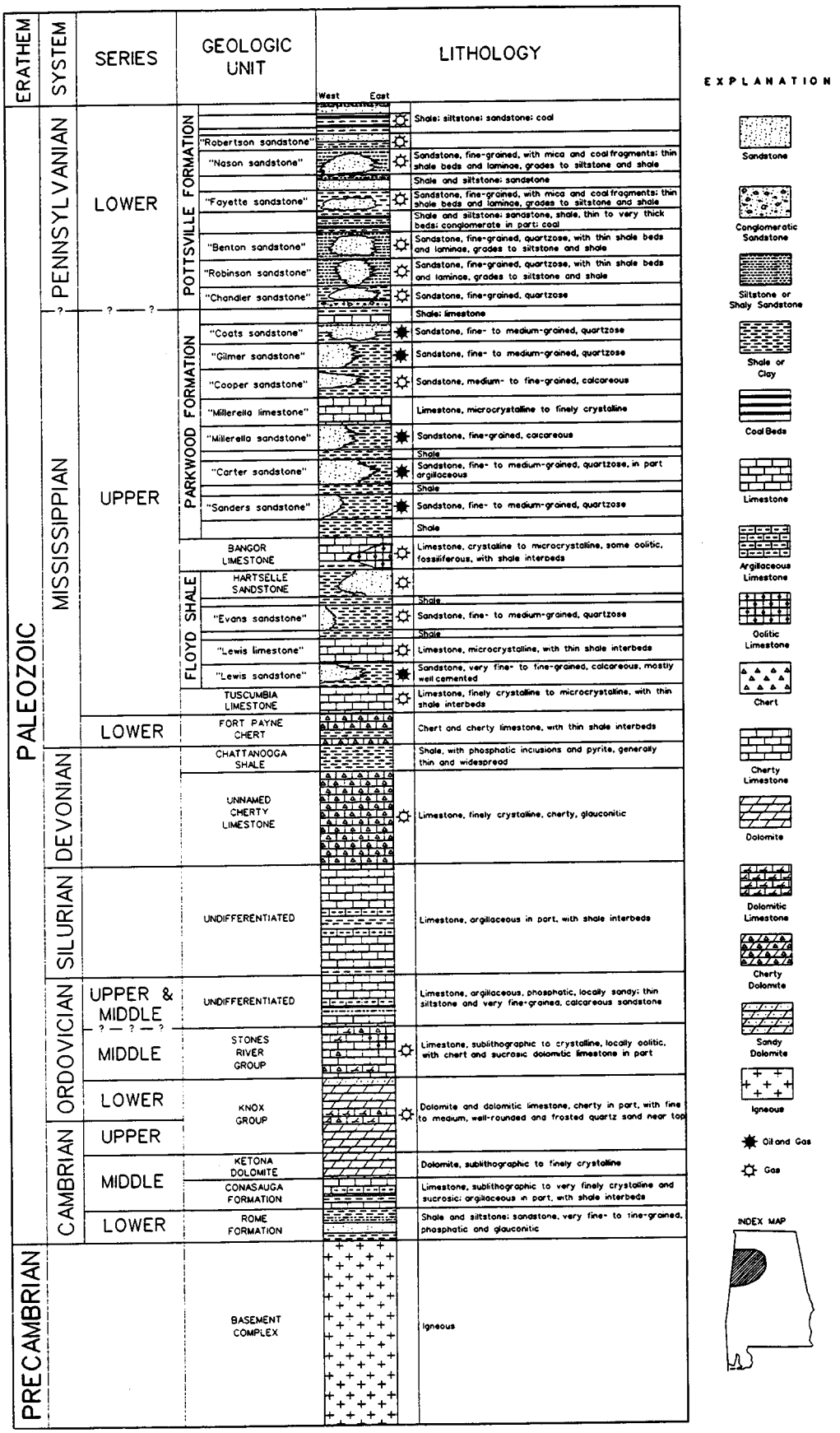

Fig. 1 Generalized stratigraphy of oil- and gas-bearing units in the Black Warrior basin.

Fig. 2 Index map of locations mentioned in this report.

East of Huntsville (Fig. 2), the Pride Mountain Formation is thin or absent and the Hartselle Sandstone is discontinuous. The thickest sandstone (21 ft) occurs in a body only a few hundred feet wide that is encased in carbonate. The sandstone is a pure, white, fine-grained quartzarenite that sharply overlies crossbedded calcarenite of the Monteagle Limestone. The sandstone contains fossilized logs at the base and tangential and planar crossbeds with possible herringbone structures. However, vertical exposure makes measurement of crossbed orientation difficult. Map geometry of the sandstone body suggests that the sandstone is scoured into the Monteagle Limestone and is overlain evenly by the Bangor Limestone, although the upper contact of the Hartselle is not exposed.

Throughout the remainder of the Huntsville area, the Hartselle generally forms a mixed carbonate–siliciclastic blanket sandstone. The sandstone is generally fine grained and varies from light gray to light brownish gray; thickness typically varies from 3 to 15 ft, but the sandstone is locally absent. It sharply and evenly overlies subjacent strata and contains abundant trough, planar-tangential, and planar-tabular crossbeds. Foresets are generally composed of alternating skeletal calcarenite and arenaceous calcarenite laminae that stand out in strong relief. Some crossbeds have sigmoidal topsets, and crossbed orientation is roughly bipolar.

Just east of Huntsville, at Monte Sano State Park, approximately 4 ft of the Pride Mountain Formation is exposed. The Pride Mountain is composed mainly of greenish clay shale and contains scarce lenses of dark gray ostracodal biosparite. The shale is separated from the blanket sandstone of the Hartselle by two broad scour-and-fill structures. One scour-and-fill structure contains arenaceous calcarenite with low-angle (dip <15°) crossbeds and platy shale chips. The other scour-and-fill structure truncates the east margin of the previous one and also contains low-angle crossbeds. However, the latter structure contains abundant *Pentremites* (blastoid) calyces as well as echinoderm ossicles, articulate brachiopods (mainly spiriferids), and comminuted fenestrate bryozoans.

Near Hartselle (Fig. 2), the Pride Mountain is composed mainly of soft clay shale that expands when wet. The shale is approximately 100 ft thick. The contact with the Hartselle is poorly exposed but appears to be gradational at most localities. The Hartselle in this area is generally composed of the fine-grained, yellowish-brown quartzose sandstone. The main part of the sandstone is 23 ft thick, has a blanket geometry, and contains abundant tangential and planar crossbeds. The lower part of the unit is extremely friable, whereas the upper part is fairly well indurated. Bedsets are generally thinner than 1 ft, are variably continuous, have strongly undulatory bounding surfaces, and commonly contain lenses of current-ripple-drift cross laminae. Additionally, the bedsets are commonly capped by wave ripples and are separated by thin, burrowed, clay–shale laminae.

In most exposures near Hartselle, the friable blanket sandstone is overlain sharply by interbedded shale and sandstone with wavy and lenticular bedding. This unit is generally less than 12 ft thick, and the sandstone contains wave ripples and abundant burrows and trails. Near the top of the Hartselle, wavy and lenticular shale and sandstone coarsens upward into a facies containing numerous thick sandstone lenses. The lenses are separated by shale and sandstone similar to that below and are imbricated. Trough crossbeds dip southeast in the direction of lens imbrication, and wave ripples are superimposed on many of the foresets. Throughout the Hartselle area, the top of the sandstone is not exposed.

On the basis of proximity to a cratonic calcarenite facies, the Hartselle near Huntsville is interpreted to be a series of sandstone bodies that formed at the margin of the Monteagle carbonate sandbank. Bipolar paleocurrents suggest that scour-and-fill structures represent tidal-channel fills and that blanket-sandstone bodies represent bank-margin tidal shoals. In the Hartselle area, however, thick Pride Mountain Shale below the Hartselle suggests progradation into the foreland basin, although the direction of that

progradation is unclear. The thick blanket sandstone is lithologically similar to shoreface or inner-shelf deposits, whereas the shaley, lensoid sandstone is suggestive of deeper water sedimentation, perhaps in the transition zone between storm and fair-weather wave base. Imbrication of the sandstone lenses and superimposition of wave ripples on foresets suggests that shelf or lagoonal bars migrated in response to strong storm-related currents, such as geostrophic flows.

Primary controls on sandstone heterogeneity near Huntsville appear to be blanket vs. channel sandstone-body geometry and carbonate content. Pure quartzose sandstone is restricted to channel fills and may thus have high permeability but limited lateral continuity. In contrast, carbonate-rich sandstone may have limited permeability owing to secondary cementation. However, the blanket sandstone has much greater lateral continuity than the channel sandstone. Near Hartselle, heterogeneity may be related to sandstone-body geometry and cementation. Friable sandstone is probably the most permeable, whereas well indurated sandstone suggests occlusion of porosity by secondary cementation. Clay shale may provide excellent sealing beds for Hartselle reservoirs, particularly the blanket sandstone, but the outcrop-scale lensoid geometry of many beds may indicate locally restricted reservoir continuity.

New Riverian Quartzose Sandstone

Quartzose sandstone occurs in Lower Pennsylvanian (New Riverian) rocks in a series of entrenched fluvial–estuarine belts extending from the Appalachian basin of Ohio, Kentucky, and Tennessee and passes into a widespread, marginal- to open-marine blanket-sandstone facies in the Black Warrior basin of Alabama. Whereas Chesterian quartzose sandstone occurs in a major carbonate sequence, New Riverian quartzose sandstone occurs in a major coal-bearing siliciclastic sequence. This regional change in facies characteristics has been interpreted to reflect a combination of eastern North America drifting from the trade wind belt into the equatorial rainy belt and the onset of the Alleghanian orogeny.

Numerous sections of quartzose sandstone have been measured from the Mary Lee cycle of the upper Pottsville Formation near Carbon Hill, Ala. (Fig. 2). Mary Lee quartzose sandstone is the highest stratigraphic occurrence of the facies in the outcrops of the Black Warrior basin and is geographically the least restricted. The sandstone underlies the Mary Lee coal group, which is the principal mining and coalbed degasification target in Alabama. Moreover, the Mary Lee quartzose sandstone is known in the nearby subsurface to the driller as the Robertson Sand (Fig. 1), which has produced economic quantities of pipeline gas.

Examination of outcrops indicates that the Mary Lee quartzose sandstone occurs as a tripartite series of stacked sandstone lenses overlying mudstone. Surface and subsurface mapping indicates that the bodies have an elongate geometry and are oriented southwest. At the base of the bodies is a conglomeratic lag zone containing abundant mudstone, siderite, and coal pebbles. The lags are pebble supported and have quartzose sandstone matrix; they are generally 1 ft thick and are even and continuous throughout each exposure.

The main part of the sandstone bodies is homogeneous quartzose sandstone containing abundant trough, planar-tangential, and planar-tabular crossbeds. Reactivation surfaces and sigmoidal topsets are abundant, and some crossbedding is overturned. Bedsets are generally 1 to 4 ft thick and are separated by dipping bounding surfaces; the crossbeds dip unimodally southwest in the direction of the bounding surfaces, and some of the surfaces are burrowed. In many outcrops, the bounding surfaces define larger scale foresets that are as thick as 25 ft and dip as steeply as 12°.

At the top of the bodies is low-angle trough crossbedding (dip <15°) that commonly contains superimposed wave ripples, current ripples, and burrows. Bedsets are generally less than 1 ft thick, and cosets contain as many as 15 bedsets. Dip of the trough crossbeds is generally perpendicular to the major foresets below. At most exposures, the troughs dip southeast, although northwest-dipping crossbeds predominate at a few localities.

The upper contact of the Mary Lee quartzose sandstone is exposed in several coal mines in the Carbon Hill area. The top of the sandstone is root worked, and abundant *Stigmaria* root systems are exposed. Thick coal is thickest and is mined in swales between the lenses, and some of the swales have 30 ft of topographic relief and are approximately 150 ft wide.

The even, continuous nature of the conglomeratic lags at the base of the bodies coupled with the topographic relief at the top suggests that the sandstone bodies were built up above the substrate. The internal stratification and elongate, lens-like geometry of the bodies suggests that they originated as either tidal or storm sand waves and ridges in open-shelf environments. However, the low-angle trough crossbeds with wave ripples indicates reworking of the megaforms by storm surge–ebb currents in shoreface environments. Ultimately, the sand waves and ridges were exposed and thereby provided topographic low that evidently facilitated accumulation of thick peat. In the Okefenokee Swamp of Georgia, thick, low-ash peat is presently forming between exposed Pleistocene beach ridges.

Aside from pebble lags, the Mary Lee quartzose sandstone is, for the most part, lithologically homogeneous. The primary sedimentologic control on reservoir heterogeneity, therefore, apparently is the lensoid nature of the sandstone bodies. An important aspect of the Mary Lee quartzose sandstone is the close association with thick coal of sufficient rank to have generated methane thermally. Hence, close association with a methane source rock suggests that upper Pottsville quartzose sandstone may be a more viable source of pipeline gas than previously thought. For example, well logs in upper Pottsville quartzose sandstone consistently show crossing of the neutron–porosity

and density–porosity curves. Crossing of the curves suggests that producible gas may exist in quartzose sandstone that has been drilled but not completed.

Future Work

Field investigation of sedimentologic controls on reservoir heterogeneity will continue. Emphasis will be placed on measuring sections of the Hartselle Sandstone along the northern and southeastern margins of the Black Warrior basin. Data collection from outcrops of the Mary Lee quartzose sandstone will be completed, and sections will be measured from some of the stratigraphically lower Pottsville sandstone units.

Subsurface investigation also will continue during the next quarter. Investigation will emphasize development of a regional network of well-log cross sections to refine the stratigraphic framework of Carboniferous reservoir sandstone in the Black Warrior basin. These cross sections will use lithologic data from gamma-density logs, induction logs, and mud logs.

ESTABLISHMENT OF AN OIL AND GAS DATABASE FOR INCREASED RECOVERY AND CHARACTERIZATION OF OIL AND GAS CARBONATE RESERVOIR HETEROGENEITY

Contract No. FG22-89BC14425

Geological Survey of Alabama
Tuscaloosa, Ala.

Contract Date: Apr. 19, 1989
Anticipated Completion: Apr. 18, 1992
Government Award: $240,000
(Current year)

Principal Investigator:
Ernest A. Mancini

Project Manager:
Chandra Nautiyal
Bartlesville Project Office

Reporting Period: Jan. 1–Mar. 31, 1990

Objective

The objective of this project is to augment the National Reservoir Tertiary Oil Recovery Information System (TORIS) Database and to increase understanding of geologic heterogeneities that affect the recoveries of oil and gas from carbonate reservoirs in Alabama and to identify those resources which are producible at moderate cost. This objective will be achieved through detailed geological, geostatistical, and engineering characterization of typical Jurassic Smackover Formation hydrocarbon reservoirs in selected productive fields in Alabama. The results of these studies will be used to develop and test mathematical models for prediction of the effects of reservoir heterogeneities in hydrocarbon production.

Summary of Technical Progress

Geological Studies

Geological characterization of a petroleum reservoir requires the definition of the lithofacies within the geologic unit comprising the reservoir. This is achieved primarily through examination and analysis of geophysical well logs, core material, well cuttings, and well test data from wells penetrating the reservoir within a field. From these data, reservoir heterogeneities, such as lateral and vertical changes in lithology, porosity, permeability, and diagenetic overprint, can be recognized and used to produce maps, cross sections, graphs, and other graphic representations to aid in interpretation of the geologic parameters that affect the reservoir.

Geological research this quarter has focused on descriptions of core material and petrographic thin sections from reservoirs producing from Smackover Formation in southwestern Alabama, computer entry of pertinent data, and generation of maps and cross sections. This research will result in a comprehensive characterization of all Smackover fields in the state.

All Smackover cores housed at the Geological Survey of Alabama have been inventoried and their condition and coverage evaluated. These data have been organized into computer databases that are updated regularly. More than 20 whole cores have been slabbed to facilitate description. At present, cores from eight Smackover fields (Bucatunna Creek, Chappell Hill, Chatom, Gin Creek, Hatter's Pond, North Choctaw Ridge, Toxey, and West Barrytown) have been described, and graphic summaries of the core descriptions have been integrated with other data to generate reservoir characterizations for these fields. Depositional and diagenetic sequences have been interpreted and summarized for each core. Thin-section studies have been made on five of the eight fields listed, in order to supplement and extend interpretations made from core descriptions. Sixty-two thin sections have been described, and 156 have been selected but not yet made. A comprehensive record, in the form of an annotated file of 35-mm color slides, is being compiled from all thin sections examined. Paragenetic sequences have

been reconstructed for each of the eight fields, and point counts have been used to estimate the relative proportions of different particle- and pore-types making up the reservoirs. This type of analysis and description will be carried out on all 46 Smackover fields for which core material currently is available.

Geophysical log suites for all 70 Smackover fields in Alabama were studied, and a type log for each field has been selected to be digitized. Digitization of these type logs is in progress. In addition, well-log data have been used to construct structure maps and structural cross sections for all 70 Smackover fields in Alabama. These maps and cross sections, which were generated by computer drafting techniques, are under review. Oil samples from six Alabama Smackover fields were sent to the U.S. Geological Survey in Denver for geochemical analysis. Twenty-one other samples have been selected and will be shipped in April. These analyses will further enhance the existing geochemical database for Smackover oils in Alabama. All available commercial core-analysis data (porosity and permeability) for Smackover reservoirs have been identified, and these data have been entered into a computerized database. These data will be used for statistical analyses and to generate Dykstra–Parsons coefficients for the Smackover fields.

Another area of concentration during this reporting period has been the synthesis and evaluation of data generated during earlier phases of the study and collection of additional information on rock properties associated with specific reservoirs in order to produce a relative ranking of reservoir heterogeneity. The Smackover reservoirs at Chappell Hill, Chatom, Chunchula, Copeland, Fanny Church, North Choctaw Ridge, Stave Creek, Sugar Ridge, Vocation, and West Bend fields have been studied in detail. The following data have been compiled for each of these 10 fields:

1. Tabulated porosity and permeability data for all wells for which core analyses are available.
2. Porosity and permeability vs. depth plots for all wells for which core analyses are available.
3. Representative detailed cross sections through each field showing distribution of potential reservoir.
4. Statistical analysis (e.g., mean, standard deviation, skewness, kurtosis, etc.) of the porosity and permeability of potential reservoir for each reservoir interval in each field and for each field as a whole.
5. Porosity and permeability (arithmetic and log) histograms of the potential reservoir in each field.
6. Porosity and permeability (arithmetic and log) histograms of the potential reservoir for each reservoir interval in each field.
7. Porosity–permeability cross plots of the potential reservoir in each field.
8. Porosity–permeability cross plots of the potential reservoir for each reservoir interval in each field.
9. Histograms of potential reservoir interval thickness for each reservoir in each field.
10. Histograms of nonreservoir interval thickness for each reservoir in each field.

These data were synthesized and used to define a series of measures of reservoir heterogeneity. The data presently are being assessed in order to rank the fields in terms of their relative vertical heterogeneities.

In order to assess the lateral heterogeneities of the reservoirs, reservoir continuity between individual wells was calculated for each of the 21 individual reservoirs. Continuity vs. distance plots were prepared for each reservoir. The plots are presently being evaluated as measures of lateral heterogeneity.

Engineering Analysis

During this reporting period, work has progressed on porosity and permeability testing of core samples from Smackover fields. Test procedures for these analyses were outlined in previous quarterly reports. To date, porosity and permeability analyses have been performed on 132 core plugs from selected Smackover fields in the study area. These data have been entered into a computerized database and are being used to supplement data derived from commercial sources. In addition, a computer spreadsheet-based method for calculating Dykstra–Parsons coefficients from permeability data was developed during this reporting period.

Work is continuing on digitization and analysis of geophysical well logs from selected fields. A complete suite of logs from 89 wells has been digitized to date. Porosities and water saturations at 2-ft intervals have been calculated through the Smackover for these wells.

Geostatistical Analysis

The emphasis during this quarter was on stochastic modeling and simulation of porosity distribution. Methods of stochastic modeling and simulation have become more sophisticated in recent years. The present work has gone beyond previous studies in three ways: (1) the intent to develop a continuous (as opposed to discrete) model; (2) application to carbonate reservoirs (Smackover Formation), which generally are more complex than clastic reservoirs; and (3) the simulation is conditional—that is, measured data points are honored. Some details on conditional stochastic simulation are outlined below.

Porosity distribution is described by an autocovariance function C(d) giving the degree of correlation between two points separated by a distance d. A self-similar (or fractal) structure is one for which C(d) has a power law form,

$$C(d) = d^{2H-2}$$

for some "fractal index" H (related to the fractal dimension of the system). The simulations will begin with this

simple form but can be easily generalized to an arbitrary correlation function C(d), chosen to more accurately describe a real system.

Here, "simulation" refers to the generation of a porosity graph (a mathematical function relating porosity to spatial coordinates) given certain statistical information about the system. This statistical information includes the mean porosity. If a large number of graphs are generated, the mean porosity of the total should match the assumed mean, although any one specific graph may not. The novel aspect of the present project is that it will use an exact hierarchical method for simulation, which should be more efficient and should allow simulations of much larger systems.

As mentioned, conditional simulation (generation of a porosity distribution of which some locations are known beforehand) is being used in this study. For example, in a graph of porosity vs. depth in a reservoir, porosity values can be measured wherever wells have already been drilled. The inclusion of actual values in the simulation changes the statistical distribution of porosity in the unknown regions (interwell regions). Where the porosity has been found to be higher than average, the mean porosity in the simulations will also be higher than average. Previous conditional simulation work has not been hierarchical; i.e., only the finest scale subdivision has been considered. Most of the computational effort in nonhierarchical simulations is expended computing correlations between fine details of structure at widely separated pairs of points. In the real system, only coarse-grained properties are significantly correlated with distant locations; this fact is difficult to include in the nonhierarchical approach.

In the hierarchical approach taken here, the lack of correlation of fine-scale structures at distance points is utilized by using differences (i.e., a discrete gradient of the simulated function, rather than the function itself) as working variables. The hierarchical approach allows the use of known physical and geometrical properties of the system to simplify the calculation.

National Reservoir (TORIS) Database

Data from all Smackover fields in Alabama have been entered into the TORIS database. Augmentation and refinement of these data will continue throughout the project.

RESEARCH ON IMPROVED AND ENHANCED OIL RECOVERY IN ILLINOIS THROUGH RESERVOIR CHARACTERIZATION

Contract No. DE-FG22-89BC14250

Illinois Department of Energy and Natural Resources
Springfield, Ill.

Contract Date: June 28, 1989
Anticipated Completion: June 27, 1993

Total Project Cost:

DOE	$2429
Contractor	4398
Total	$6827

Principal Investigator:
D. F. Oltz

Project Manager:
R. Michael Ray
Bartlesville Project Office

Reporting Period: Jan. 1–Mar. 31, 1990

Objective

This project will provide information that can be used to maximize hydrocarbon production, minimize formation damage, and stimulate new and increased production in Illinois. Twelve project tasks are designed to examine in detail the selected subsurface oil reservoirs of Illinois, which will increase knowledge of reservoir components and behavior and aid development of methodologies having potential to increase the amount of recovered oil. Information to be provided includes: assessment of hydrocarbon resources, including an estimate of unrecovered mobile oil; characterization of hydrocarbon reservoirs; and the description of methods that will improve hydrocarbon extractive technology. Methods of analysis of reservoir complexities include subsurface mapping using logs, core analyses, clay identification, petrographic thin sections, and predictive computer modeling.

First-year funding supports tasks 1 to 6 and 10 (Fig. 1). Figure 2 outlines the management scheme for the project.

Summary of Technical Progress

Task 1: Planning and Prioritization

In-house data have been evaluated. Existing data sets, including core analyses, samples (including cores and core

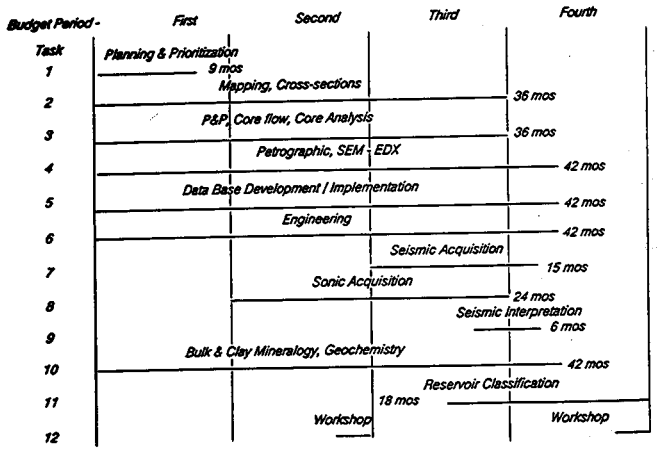

Fig. 1 Performance schedule for project period.

"biscuits"), engineering test results, wireline logs, and other pertinent data housed in the Illinois State Geological Survey (ISGS) or potentially available from industry, have been identified. Standard operating procedures have been produced. The program will focus on two reservoirs: the Mississippian Cypress and the Valmeyeran Aux Vases, two of the most prolific hydrocarbon reservoirs in the Illinois Basin. Improving the recovery efficiency from these reservoirs may add new reserves. The results of task 1 show the depositional "plays" for various producing zones in those two reservoirs.

Task 2: Subsurface Geologic Mapping

Cypress Formation

This clastic reservoir is the most prolific in the Illinois Basin and has been a primary target of exploration for 90 yr. Several environments are believed to be reflected by Cypress sandstones, which suggests that reservoir heterogeneity is an important factor in recovery efficiency. Only limited information is currently available to explain any of its important reservoir characteristics.

Aux Vases Formation

The Aux Vases Formation is primarily sandstone, although it interfingers with and grades into limestone

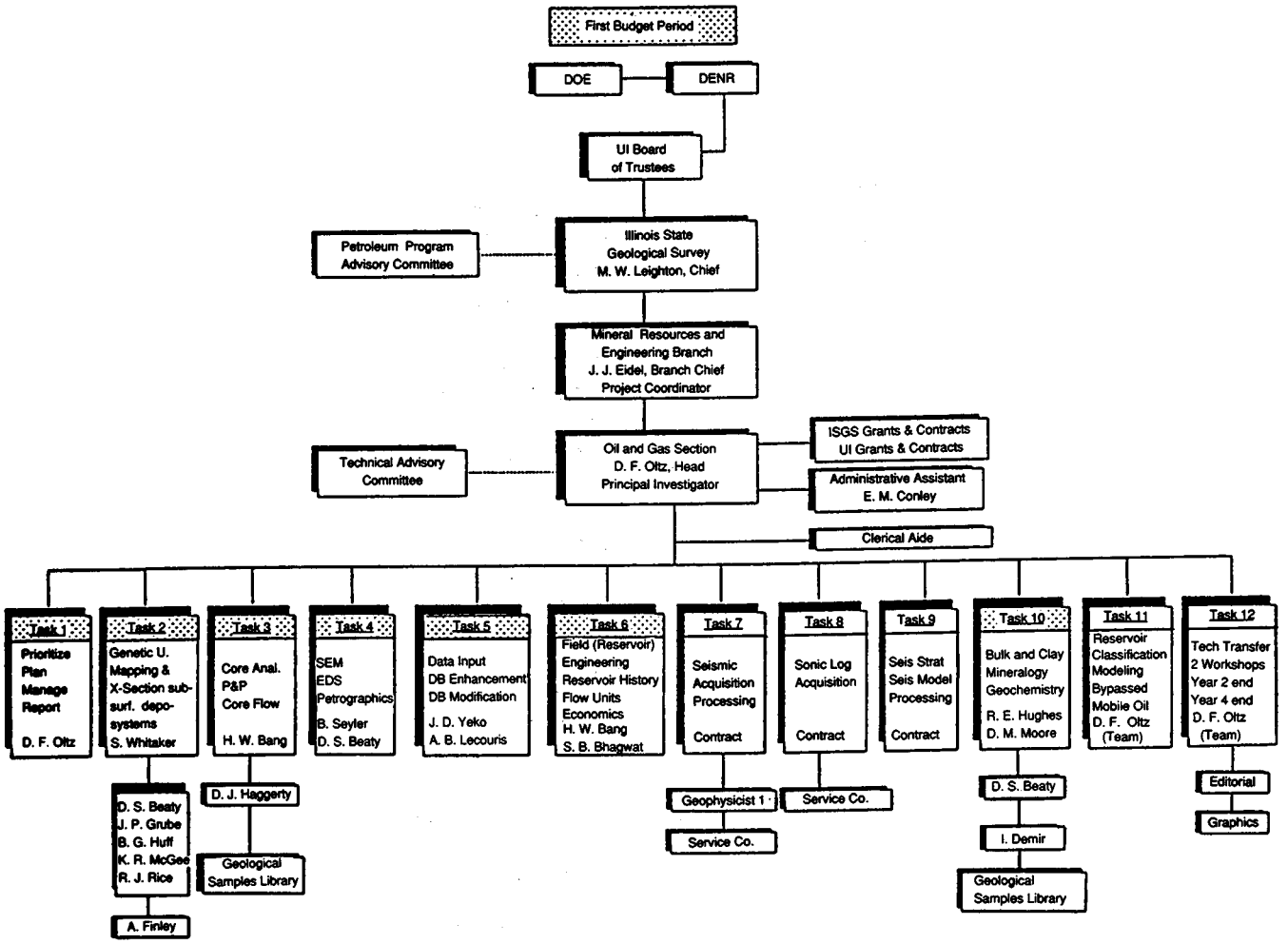

Fig. 2 Research on improved and enhanced oil recovery in Illinois through reservoir characterization.

and sandy dolomite along the eastern third of the Illinois Basin. In the last 50 yr, it has become an increasingly important reservoir as fracturing techniques have improved. Preliminary studies have revealed that sandstones within the Aux Vases contain varying amounts of authigenic clays, which commonly affect resistivity readings on wireline logs and production characteristics.

There are two subtasks under task 2: (1) regional studies and (2) pool (or field) studies. Both studies are in progress. Selected updates to field studies follow.

Bartelso field. The field, located in T1N-R3W, Sections 4, 5, 8, and 9, Clinton County, was discovered in 1936 when Cypress production was established on a small domal structure at a depth of 985 ft. Three years later, oil was discovered in Silurian reef rocks at a depth of about 2400 ft. Cumulative production has totaled over 4.3 million bbl of oil.

Cypress production is related to a combination structure/stratigraphic trap from four distinct Cypress sands draped over the Silurian reef. Cypress production occurs mainly from the uppermost sands, although commingled production makes precise figures impossible to determine. Three waterfloods were initiated in the middle 1950s with a secondary oil recovery of over 1 million bbl of oil. Only one waterflood is currently in operation. The lower Cypress sands represent a more fluvial environment; they shift to a more marine environment in the upper sands.

Electric logs were correlated and cross sections were generated to help define the compartmentalization of the Cypress sands. Net sand isopach maps were made of the upper three sands with the help of electric logs and sample tops from scout tickets. Structure maps on the important pay sands have been made for the purpose of reservoir engineering modeling.

The study has shown the existence of four distinct Cypress sands separated by marine transgressive shales. Each sand, in turn, contains several smaller shale layers which, in some cases, further compartmentalize the trap. The lowest sand has log characteristics and local distribution typical of a fluvial sequence. The middle two sands seem to represent a transitional phase with characteristics of originally fluvial sands that have been reworked by marine or tidal currents. The uppermost sand has log characteristics and a distribution that strongly indicate offshore marine bar deposition.

Preliminary findings indicate that oil recovery is being influenced by compartmentalization within the Cypress reservoir. Detailed mapping will need to be completed before any additional secondary or future tertiary recovery methods are initiated to optimize drainage from this reservoir.

Energy field. Energy oil field produces only from the Aux Vases Sandstone, is moderately complex in geometry and lithology, and was the target of a promising but unsuccessful waterflood project. Recent development of the field has revealed primary production problems in the Aux Vases. Core that has been and will be provided to the ISGS from the field may give insights into the cause, prevention, and remedy of this presumed formation damage.

The field is located in T9S-R2E, Section 4, Williamson County and was discovered with the completion of the Eovaldi–Fairchild No. 1 well in June 1968. The well was drilled to a depth of 2442 ft and initially produced 15 bbl of oil per day from the Aux Vases Sandstone. The productive zone was hydraulically fractured in October 1968, and production increased to 40 bbl of oil and 40 bbl of water per day. Within 1 yr, eight oil wells had been drilled, and the average daily production for the field was approximately 150 bbl of oil per day. In 1988, Budmark Oil drilled an extension well and began to develop the northwest quarter of the section. To date, six new oil wells have been drilled, and development is continuing with the Morgan Coal No. 5 to be spudded in early 1990. The field has produced 250,000 bbl and currently produces about 50 bbl of oil per day.

The structure on top of the St. Genevieve and Joppa Limestones consists of a broad, northward-sloping ramp. The oil field is located on a terrace along the ramp, but oil productive wells and high initial potentials are not associated directly with structural highs. Stratigraphic controls are dominant over structural factors in controlling oil accumulation.

Locally the Aux Vases Sandstone consists of a basal limestone (Joppa Limestone) overlain by interfingering deposits of sand and shale. Mapping for this project has shown that the Aux Vases reservoir rocks in this field are a northwest–southeast trending bar or channel sand deposit about one-half mile wide. The sand rests on top of the basal lime and laterally pinches out into shale. The length of the reservoir has not been determined as control wells are lacking to the southeast and northwest of the field.

Data available from the older part of the field are primarily in the form of old electric logs. Cuttings from the discovery well and a piece of core from the confirmation well have been collected and examined. The newer wells all have induction logs as well as porosity and gamma-ray logs. Data from these logs have been entered on the VAX computer and structure contour, isopach, and three-dimensional (3-D) maps on several horizons have been prepared. A fence diagram prepared by hand graphically illustrates the spatial limits and attitude of the reservoir.

In January 1990, the Oil and Gas Section was contacted by a petroleum engineer with Budmark Oil regarding production declines for wells in the field. Wells that had been treated with mud cleaning acid (MCA) had declined from around 30 bbl of oil and little water to 1 to 2 bbl of oil and 10 bbl of water. A well not treated with MCA had maintained a high-oil, low-water production. At a meeting with the President of Budmark Oil, sample core from the field from one of the problem wells was received for analysis. Chips were taken for scanning electron microscope (SEM), thin section, and clay analysis. Plugs

are to be taken for core flow experiments to attempt to define what is causing the production decline and to see what, if any, remedial action can be taken to restore production in the wells. Early SEM work shows that the sand grains in the reservoir rock are coated with chlorite and illite and have the potential to react with the acid and cause formation damage.

King field. This field, T35-R3E, was discovered in 1942 and has a cumulative production of over 4 million bbl of oil. Good wells have initial potential of over 150 bbl of oil per day and have a cumulative production of over 100,000 bbl.

A number of structural and stratigraphic cross sections and several structure and isopach maps have been generated. The primary reservoir in the field, the Aux Vases Sandstone, has three different facies: (1) channel sands, (2) marine bar sands, and (3) limestone facies. The different sand bodies do not seem to be in communication and therefore have different water levels. The field is a combination structural–stratigraphic trap. The structural crest of the field contains a dry hole.

Early indications from thin sections, X-ray diffraction (XRD), and SEM are that the reservoir facies is a well-sorted, fine-grained sand exhibiting quartz overgrowths and containing both chlorite and illite clays. Microporosity has developed because of the dissolution of feldspar grains.

Additional data are currently being compiled and should be integrated within the next month.

Mattoon field. Mattoon field, located in southwest Coles County, Ill., is a 6680-acre anticlinal trap that was discovered in February 1939. Less than half the total 667 completions are active today. Principal production is from the Mississippian-aged Cypress, Aux Vases, and Rosiclare sands. More recently, completions have been made from several Lower Mississippian and Devonian-aged intervals. Cumulative production from Mattoon field was 21,595,417 bbl of oil as of October 1989 with a daily field production of 298 bbl of oil. These figures do not include Mattoon North or Mattoon South production.

Mattoon field is defined by a North–South anticlinal trap, approximately 9 miles long and $^1/_2$ mile wide. From this field 223 electric logs have been annotated and correlated in an effort to establish a field-wide stratigraphic framework and to define the overall geometry, lateral continuity, and correlative sequence stratigraphy within the Cypress and Aux Vases clastic intervals. To date, 57 logs have been incorporated within 5 East–West Stratigraphic cross sections that are oriented perpendicular to the main field axis. These cross sections include the stratigraphic interval from the Glen Dean through the Rosiclare Formations; the datum is the top of the Barlow Lime. The remaining 166 annotated and correlated well logs will be incorporated into 10 stratigraphic cross sections that will augment the genetic delineation and distribution of clastic intervals within the Cypress and Aux Vases Formation intervals.

Thirty-two cores from the Cypress and 11 cores from the Aux Vases were spotted on Mattoon field base maps and are being used in conjunction with structural and isopach mapping for lithofacies reconstruction and interpretation of environments of deposition.

Oakdale field. Oakdale oil field, located in T2S-R4E, Sections 11, 12, and 14, Jefferson County, Ill., lies within the Fairfield subbasin of the Illinois Basin. The Aux Vases Sandstone is the primary reservoir at Oakdale with minor commingled production from oolitic carbonate reservoirs in the underlying St. Genevieve Limestone. Approximately 928,210 bbl of oil has been produced by both primary and secondary waterflood methods. The field was discovered in 1956, and initial waterflood operations began in 1964. Today, two wells continue to produce from the Aux Vases at Oakdale. One of the remaining producers drilled in 1982 targeted the McClosky but was completed in the Aux Vases despite its location within formerly waterflooded acreage. The well has produced nearly 8,000 bbl of oil with a large water cut.

As presently understood, the field is comprised of two discrete sand bodies: a small four-well productive zone in the northeast separated by shaley sands from the larger pool in the southwest. Altogether, 31 wells have produced from the Aux Vases at Oakdale. The dimensions of the larger pool (in the southwest) are approximately $^1/_4$ to $^1/_2$ mile wide (two to four 10-acre well locations) by $1^1/_2$ miles long (twelve 10-acre well locations). The field lies upon a relative structural high located upon a structural "nose" evident on a map of the structure at the top of the Karnak Member of the St. Genevieve Limestone, a prominent marker bed immediately below the Aux Vases Formation. Regional dip is to the southwest.

Interpretation of logs and cross sections shows that the Aux Vases at Oakdale commonly consists of three basic units: a lower shaley sandstone and sandy limestone unit, a middle limestone or multiple limestone unit (sometimes referred to as the Joppa Limestone), and a reservoir sand consisting of thick (up to 39 ft) clean sandstone. The reservoir sandstone may be subdivided into two sand subunits where a thin shaley spontaneous potential (SP) deflection is present, which suggests that the sands are stacked. These upper Aux Vases reservoir sands appear to grade laterally into nonreservoir shaley sand and limestone toward the western and eastern field margins. The middle Aux Vases (Joppa) Limestone may lose continuity across the field, and limestone becomes the more dominant lithology along the eastern margin of the field.

Sedimentary features noted from cores are fine-grained sandstones containing abundant clay laminae associated with high-angle cross beds and a single scour or cut-and-fill structure. It is not possible to detect whether cross bedding is uni- or bi-directional. Increased cementation in the core and plugs is apparently due to calcite cementation and corresponds to a log response of slightly increased resistivity. Conventional core analysis measured permeability as

high as 850 mD and porosity in the range of 20 to 26% in producing zones. High porosity measurements do not necessarily correspond to high permeability measurements.

The presence of cross-bedded sandstones, a scour feature, and maps of elongate northeast-southeast, narrow, meandering field geometry and orientation suggests that the environment of deposition of the reservoir sandstone at Oakdale was a subaqueous tidal channel. The channel may cut into underlying limestones, as evidenced by poor correlation of limes across the field. Reworking of sandstones by storm, tidal currents, or meandering of the channel may be responsible for relatively wider portions of clean sand in the field.

Stewardson field. The Stewardson field is located on the north-central flank of the Illinois Basin in southeastern Shelby County, Ill., Sections 22 and 27, T10N-R5E. Data for 60 wells in the field study area were compiled and electric log tops picked for the formations of interest between the Barlow Limestone and the St. Genevieve Limestone. There have been 33 productive wells from the Aux Vases Sandstone, 3 from commingled Aux Vases and Spar Mt. sandstone, and 1 from the Spar Mountain. Currently, there are 13 wells producing in the field. A production history of the field has been compiled and illustrated. As of October 1989, the field has accumulated 1,079,269 bbl of oil since its discovery in April 1939.

Preliminary structure maps have been prepared of the Barlow Limestone, Renault Limestone, Aux Vases Sandstone, and St. Genevieve Limestone. Two isopach maps illustrating paleostructure and two isopach maps of the Aux Vases Sandstone using 25 and 50% SP deflection were also prepared. Correlation of two North–South and two East–West stratigraphic cross sections with 28 wells is near completion. Within the Aux Vases Formation, 5 sandstone intervals separated by 2 to 10 ft of shale and/or limestone have been identified and correlated for the 33 wells in the field. A cross section is being correlated, starting from the Stewardson field in the east through the Mode and Clarksburg fields and ending in the Lakewood field approximately 18 miles to the west.

Thin sections are being prepared from sample cuttings of a portion of the Aux Vases for three wells that were productive in the field. Thin sections of two nonproductive Aux Vases wells are being prepared from core. These wells are located approximately 4 miles southwest and 7 miles west of the Stewardson field. Core from the field has been obtained from Doran Oil Properties. Field work was necessary to determine from which wells the cores came and from what depth, since this information is not known. Brine and oil from three wells in the field have been sampled and are being analyzed for geochemical characterization.

The three operators of the field have been contacted. Doran Oil Properties has been very helpful in providing core analysis, core, and access to their leases for oil and brine sampling. Belden Trust has no additional completion, production, or coring information in their files. The third operator of the field has been contacted and has said he will send any core analysis that he has in his files.

Tamaroa field. Tamaroa field in Perry County, Ill., T4-5S, R1W, produces from four separate Mississippian Cypress sandstone pools and one Ordovician Trenton carbonate pool. Each of the pools was discovered about a decade apart beginning in 1942, with the southernmost pool being discovered in 1971. This study focuses on the geology of the Cypress sandstones with emphasis on the potential for improved and enhanced oil recovery from these reservoirs.

Approximately 820,000 bbl of 27 to 31 gravity oil have been produced from these marine bar-type reservoirs. These bars are typically less than 10 ft thick, $^1/_4$ to $^1/_2$ mile wide, and less than 2 miles long. They trend northeast–southwest and commonly stack vertically up to four separate bar cycles. Shales 1 to 10 ft thick separate the bar facies. Structural folding associated with the Du Quoin Monocline assists in trapping hydrocarbons in these lenticular Cypress sandstones. Drilling depth to the Cypress is approximately 1,150 ft.

Gamma-ray and SP log character as well as core data indicate that many of these bars are internally complex; they consist of sands separated by shale or clayey partings. Porosity and permeability, particularly in the vertical plane, are significantly affected by these reservoir heterogeneities. Isopach and structural mapping, aided by computer modeling, are currently in progress to define as much detail about these reservoirs as is possible from available data.

Typical porosities for these very fine to fine-grained reservoirs range from 17 to 23% with a mean of 21%. Permeabilities range from 100 mD to 200 mD for the better portions of these reservoirs. Analyses by XRD indicate that the productive sandstones are relatively clean (clay free) with minor amounts of calcite, chlorite, and kaolin. Thin-section analyses support these data and also show considerable quartz overgrowths and sutured grains. Therefore, although porosity appears to be sufficient for good reservoir development, pore throats, and therefore permeability, are restricted by secondary quartz. The lack of clay appears to have allowed for significant quartz cementing within these Cypress sandstones.

Two waterflood projects were initiated in two separate pools in 1961 and 1962. The waterfloods used five and seven wells, including injection wells. Over 210,000 bbl of oil were produced from these projects with 150,000 bbl attributed to four producers in one project. Nitro-fracking and minor hydraulic fracking are the only reported stimulation these wells initially received. Cypress formation water was used exclusively in one project, whereas 10% fresh water was added to produced water in the other project. Both projects are now plugged and abandoned (P&A).

Only one lease in the southernmost portion of the field is producing from the Cypress. Recoverable reserves may

exist in the unflooded portions of these pools and possibly from infield and offset locations.

Zeigler field. The Zeigler field was discovered in 1963 by Gallagher Drilling Company, the sole operator. It has produced over 2 million bbl from 26 wells in the Aux Vases Sandstone. The field has recently been expanded by the discovery of the Gallagher Mac No. 1 and Mac No. 2. Data from these recent discoveries and from the older portion of the fields provided by Gallagher include core analysis reports and production by well. These data have made a detailed reservoir study possible.

To date, preliminary cross sections have been constructed and stratigraphic tops have been picked on 150 wells in the Zeigler field and adjacent areas. These data have been computerized. Isopach maps of Aux Vases Sandstone were generated with the Zycor mapping software package on the GeoQuest workstation. Structure maps on the St. Genevieve Limestone, Renault Limestone, and Beech Creek "Barlow" Limestones show that Zeigler field is a stratigraphic trap.

Five cores from closely spaced wells were studied on a macroscopic scale. Sedimentary structures, lithologies, grain size, sorting, etc., were compared with electric log characteristics, including spontaneous potential, gamma ray, and resistivities. These logs were digitized using the Arc/Info software on the Prime and transferred to the GeoQuest Workstation for display purposes. Porosity and permeability data provided by Gallagher Drilling Company were integrated with log analyses and core description.

Preliminary analysis of data suggests that deposition of Aux Vases Sandstone contains very good reservoir qualities: porosity is in the 26% range, permeability ranges from 240 to 700 mD. High-angle cross bedding coincides with deposition of point bars within tidal channels incised into tidal flats, or offshore tidal bars deposited on top of an offshore shelf green, very fine grained, rippled-bedded calcareous sandstone. This lower green sand facies is more tightly cemented, with porosity ranging from 12% to less than 1% and poor permeability commonly less than 1 mD. Other poor reservoir quality lithologies include tidal flat deposits composed of red–green shales, siltstones, and very fine grained sandstones containing tidal couplets and mud cracks.

XRD-bulk and clay mineralogy analyses have been completed on samples from the Mac No. 2 well. These analyses show large amounts of quartz and feldspars and lesser amounts of chlorite and illite clays in good reservoir quality sandstones. Preliminary SEM-Energy Dispersive Spectrometry (EDS) work shows chlorite and illite clays coating most sand grains. They are commonly so prevalent that they are the cementing agent for these friable sandstone facies. These clays may also be responsible for the erroneously high S_w calculations typical of the Aux Vases Sandstones as a result of extremely low resistivities even in excellent wells producing no water. These clays are capable of creating formation damage if not properly treated.

Additional petrographic, XRD, SEM-EDS analyses are being completed for this field. Gallagher Drilling Company has donated five more cores from their most recently drilled wells.

Tasks 3 and 6: Engineering Laboratory

The permeameter and core-flooding apparatus are being calibrated.

Task 4: Petrographic and SEM Studies

The petrographic and SEM studies are on schedule.

Task 5: Database Manager

The ISGS database manager is being interfaced with project requirements. Project data are currently being added to mapping files.

Task 10: Bulk and Clay Mineralogy, Geochemistry

Standard preparation procedures have been adopted; initial interpretations are under way. Field brine sampling is under way; analytical results are beginning to be reported. These data are expected to be used for predictive geochemical modeling.

Technology Transfer

The initial Meeting of the Petroleum Advisory Committee (PAC) and the Technical Advisory Committee (TAC) was held in Champaign, Ill., on Mar. 1, 1990. The seven members of PAC and twelve members of TAC reviewed the project goals, heard presentations on several projects, visited the core facility, and toured the major laboratories involved in the project. The final hours of the day were spent in committee deliberations designed to provide a forum for input into the project.

A suite of microfiche containing information on the oil and gas wells in Illinois was purchased and transferred to the offices of the Illinois Oil and Gas Association in Mt. Vernon, Ill., for use by the industry.

The project was presented at the Mt. Carmel, Ill., "Oil Appreciation Day," Jan. 30, 1990.

DEPOSITIONAL SEQUENCE ANALYSIS AND SEDIMENTOLOGIC MODELING FOR IMPROVED PREDICTION OF PENNSYLVANIAN RESERVOIRS

Contract No. DE-FG07-90BC14434

Kansas Geological Survey
Lawrence, Kans.

Contract Date: Feb. 1, 1990
Anticipated Completion: Apr. 30, 1993
Government Award: $173,479
(Current year)

Principal Investigator:
W. Lynn Watney

Project Manager:
Chandra Nautiyal
Bartlesville Project Office

Reporting Period: Jan. 1–Mar. 31, 1990

Objectives

Research during the first year of this project will include field screening and analogue identification and depositional sequence characterization. Objectives of the first-quarter activities include: (1) isolate stratigraphic interval, (2) target oil fields for development and application of concepts and methods of sequence stratigraphy, (3) select near-surface and surface analogues in eastern Kansas, and (4) supplement and develop regional databases.

Summary of Technical Progress

Isolate Stratigraphic Interval

The upper Pennsylvanian (Missourian) Lansing–Kansas City groups were selected to be the focus of this study for several reasons. The stratigraphic interval is a major petroleum-producing unit in Kansas. The interval produces from over 8100 wells in Kansas and has contributed a substantial amount of oil and gas production (Fig. 1). The Lansing–Kansas City group contains a dozen potential reservoir units. Multiple pays are common in many fields in western Kansas and are often difficult to operate. Reservoirs are usually solution gas driven with recoveries of less than 20% original oil in place (OOIP). Waterflooding is commonly inefficient and reflects only a fraction of the primary oil recovered. Many Lansing–Kansas City fields are approaching a critical stage where producing rates are much diminished and the economic limit is imminent. Near-surface and surface analogues to Lansing–Kansas City reservoirs can be analyzed in detail in three dimensions using existing well-log control, coring, and surface expo-

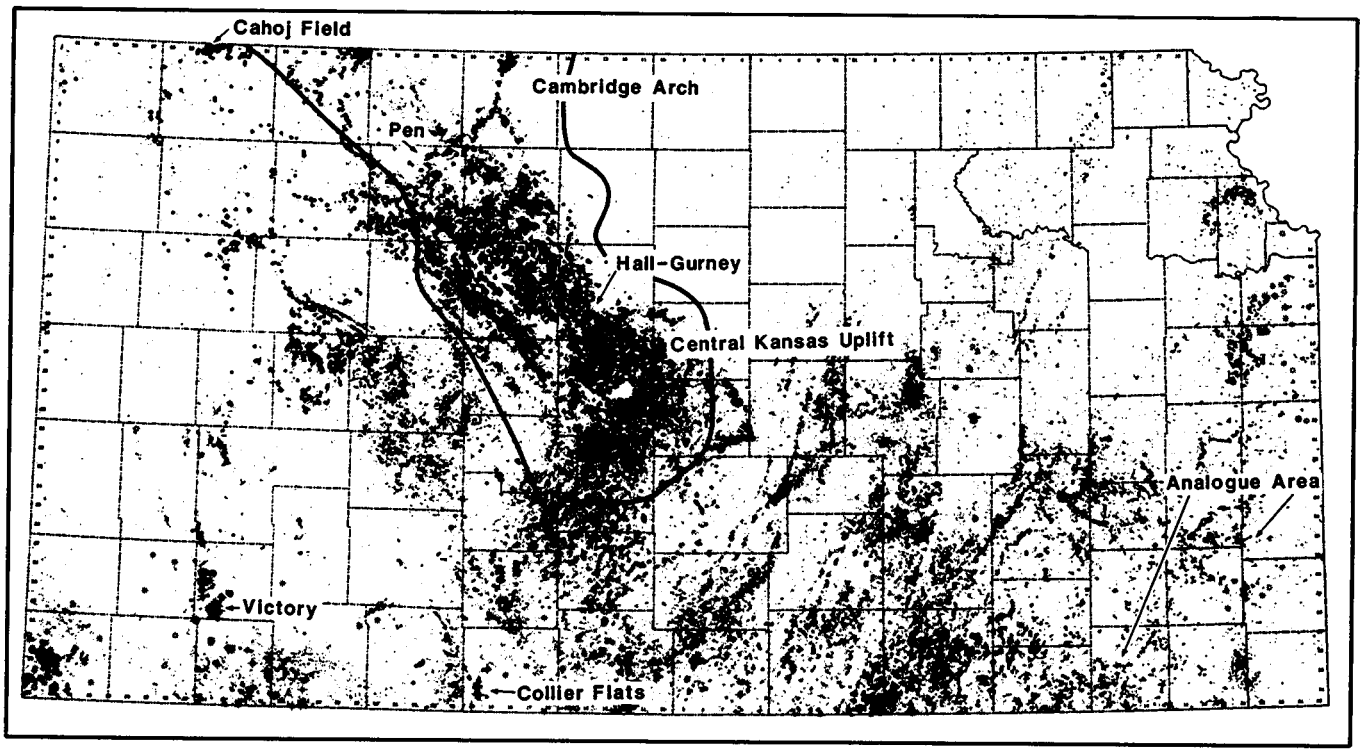

Fig. 1 Wells penetrating and producing from the Lansing–Kansas City reservoir in Kansas. Gray circles are wells penetrating the interval but not producing. Black dots are oil wells, and black spoked circles are gas wells producing from the Lansing–Kansas City reservoir. Central Kansas uplift and Cambridge arch are outlined. Cahoj, Pen, Victory, and Collier Flats fields and analogue sites in southeastern Kansas are located on this map. The largest Lansing–Kansas City field in the Midcontinent is Hall–Gurney.

sures in eastern Kansas which can then be tied to the subsurface in producing areas of western Kansas for direct comparison.

Target Oil Fields for Development and Application of Concepts and Methods of Sequence Stratigraphy

Screening criteria for field selection were more precisely defined and fields were designated for continued study. The field studies are being coordinated with staff and students in the Department of Geology and the Tertiary Oil Recovery Project (TORP) at the University of Kansas in order to encourage collaboration where possible in geology and engineering. The screening criteria developed for field selection are listed in Table 1.

TABLE 1

Screening Criteria for Field Selection

1. Fields produce from Lansing–Kansas City reservoirs.
2. Fields are representative of varied paleogeographic shelf settings.
3. Cores are available (including information on S_o, S_w, S_{or}, K, relative permeability curves).
4. Availability of modern log suites:
   a. Gamma ray (correlation and shale log).
   b. Compensated neutron and density, sonic, resistivity (lithology, porosity, and fluid content).
   c. Gamma-ray spectrolog (characterization of depositional sequences).
5. Production history and tests are available:
   a. Monthly lease and well data on oil, gas, and water production.
   b. Bottom hole pressure information vs. time per well, by well and lease.
   c. Well completion information (perforation, well treatment).
   d. Production tests (transient tests, tracer tests, injection profiles).
6. Operator cooperation.
7. Problems encountered in production; potential for addressing problems using geologic modeling.

Four fields have been selected for continued study. They represent both the upper (northern) shelf and lower (southern) shelf settings based on paleographic interpretation (Fig. 2). The character of Lansing–Kansas City strata varies markedly across this shelf.[1] Through a systematic comparison of these fields in different paleoshelf and structural settings, the effects of varying depositional environment, structure, and diagenesis on reservoir development can be evaluated. These reservoirs have a complex porosity development.[2,3] Pen and Cahoj fields represent the northern paleoshelf and are associated with prolific producing areas on the Central Kansas uplift and Cambridge arch (Figs. 1 and 2). Victory and Collier Flats fields, which represent the lower, southern shelf, have been chosen for further study. Fields in this area are more isolated and are located off the major uplifts.

Pen field, located in Graham County, Kans., (S17, T65, R22W) has been recently developed (discovered 1985). Thirty-six wells have been completed in the field. It contains multiple skeletal grainstone, oolitic grainstone, and vuggy, micritic carbonate reservoirs. Fifteen wells were cored and modern logs were run; this has provided an exceptional geologic database. An initial geologic study has begun through other funding.

The Cahoj field area in Rawlins County (T1S, R34W) is a large established producing area discovered in 1959. Sixty-one wells are now producing from Cahoj field with cumulative production in excess of 7.5 million barrels. Five cores, including a long, continuous core through the Lansing–Kansas City reservoir, provide acceptable geologic control. Previous studies indicate that steps toward developing a more comprehensive reservoir model are warranted. Recent drilling has provided modern logging suites. It produced from twelve zones, including grainstones and vuggy micritic carbonates in the Lansing–Kansas City reservoir from patchy areas within the field. Together with multizone completions, this field presents a complex situation for improved oil recovery. The field area is now operated by independents.

The Victory field in Haskell County (S33, T30S, R33W), discovered in 1960, has 86 producing wells. Four Lansing–Kansas City diagenetically altered oolitic grainstone reservoirs comprise the major production. Over 10 million barrels of oil have been produced from this field, which is located on the lower (southern) shelf. A continuous core through the Lansing–Kansas City reservoir and three short cores are available and have been described and sampled. Thin sections need to be made for petrographic study. Modern well log suites are available from recent drilling. A spectral gamma-ray log has been digitized and analyzed using cross plots and Fourier analysis of uranium, potassium, and thorium data for recognition of stratal sequences and genetic units.[2,3]

Collier Flats field in Comanche County (T33S and T34S, R20W), discovered in 1970, has 48 producing wells from primarily an oolitic grainstone reservoir of the Swope Limestone (Kansas City Group). Cumulative production exceeds 1.6 million barrels. The field, which has 11 cores from the Swope, is located on the far lower shelf. Most wells include a modern suite of logs. The field provides the opportunity to examine the effects of heterogeneity on production from one major producing reservoir. The field will also serve as a control site for geologic modeling on the lower shelf. Collier Flats is operated by several independents.

Stages of work in all the field studies will consist of geologic characterization, geologic modeling, and evaluation of field performance. Engineering reservoir modeling by the TORP is planned for the Pen field, which will be partly supported by this grant.

Geologic characterization of Pen field will continue during the second quarter. The use of Cahoj and Victory fields will be further appraised during the second quarter. The geologic characterization of Collier Flats field, which will begin the third quarter, will extend for one year.

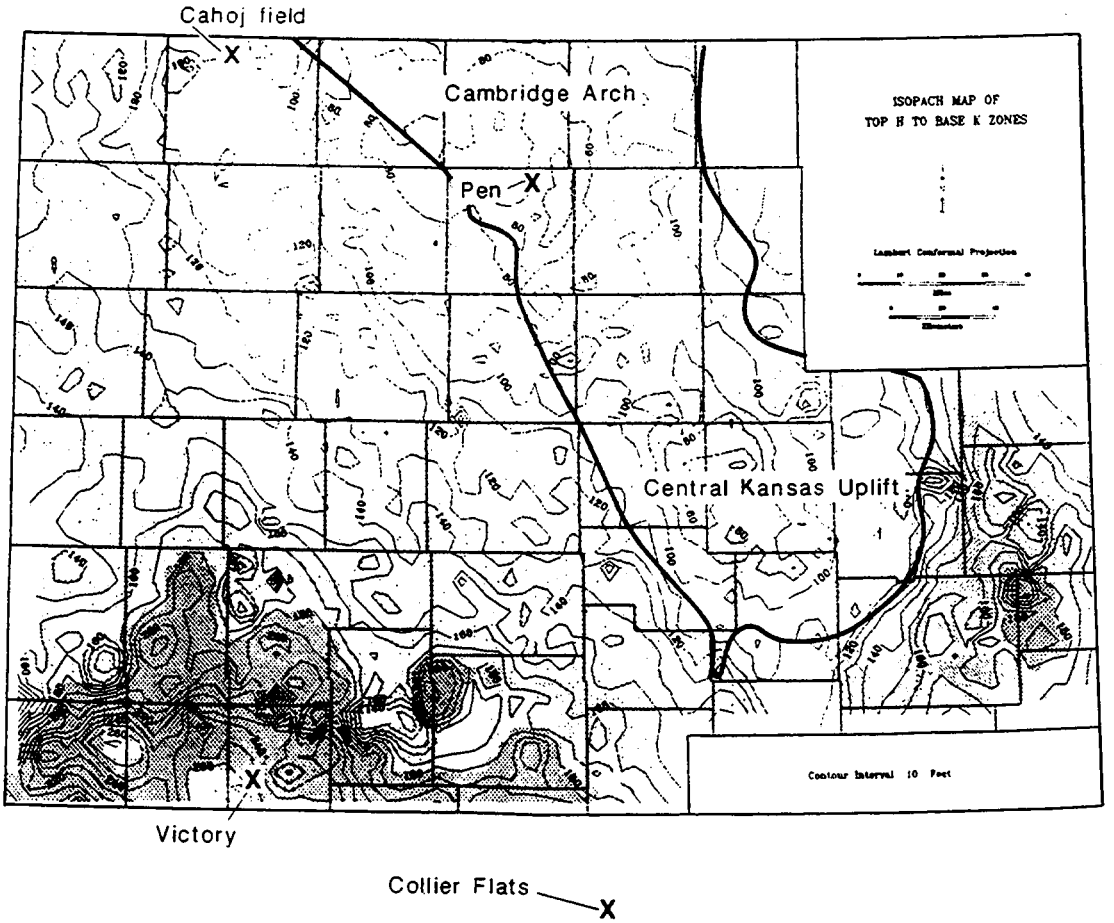

Fig. 2 Isopach map of four cycles in the Kansas City group, including zones that are important producers in all four fields. Collier flats field is south of presently mapped area. Thin areas on upper shelf coincide with cycle characteristics that indicate higher paleoshelf settings. Fields are representative of these contrasting shelf settings.

Geologic modeling will include both three-dimensional (3-D) graphic modeling and eventually simulation modeling of the stratal architecture. Stratamodel™, a 3-D graphics modeling package, has been licensed to the Kansas Geological Survey for use on the graphic workstation. The Kansas Geological Survey will also become a beta test site for SEDPAK™, a geologic simulation package developed at the University of South Carolina for the graphic workstation environment. The latter package will be used to develop simulation models tailored to these reservoirs. Workstation hardware and software will be made operable during the second quarter.

Selection of Near-Surface and Surface Analogues in Eastern Kansas

Drum Limestone Analogue

The Drum Limestone analogue represents the outcrop and near-surface portion of the reservoir characterization study. The objective of this analogue and others is to establish a more rigorous understanding of the nature of reservoir heterogeneity and apply the results to similar types and ages of reservoir rocks in western Kansas. The Drum Limestone is equivalent to the I-zone in western Kansas, which is producing in the Pen field. The Drum is mostly an ooid grainstone or fossiliferous packstone–wackestone, the former is a major reservoir type in the fields selected in western Kansas. The Drum is well exposed along the outcrop belt in Montgomery County and in quarries near Independence, Kans. (Fig. 1). In this area, the Drum changes from several feet to more than 65 ft in thickness along a shallow-to-deep water (paleoslope) traverse of several miles to several 10's of miles. Subsurface well log data reveal similar trends in the Drum Limestone throughout the Independence, Kans., area.

The outcrop and near-subsurface study of the Drum is being conducted by the Kansas Geological Survey. Sixteen stratigraphic sections have been measured and sampled, and thorough field reconnaissance of the Drum Limestone outcrops in Montgomery County has been conducted to date. Well logs throughout the county are being correlated. Isopach maps of the Drum and underlying Cherryvale Formation strata have been constructed for the local Independence area. An isopach map of the Drum Limestone and underlying intervals to the Dennis Limestone is being constructed for the entire Montgomery County area to

evaluate the influence of preexisting paleotopography on Drum deposition. Rock samples have been slabbed and thin sections are being made for petrographic study. Several cores of the Drum Limestone near Independence, Kans., at Amoco (Tulsa, Okla.) have been examined and logged. These cores are available for continued study.

On the basis of well log data, outcrop data, and the generation of isopach maps, several areas were identified for additional coring and well log data acquisition. Four wells are scheduled to be drilled by the Kansas Geological Survey in August 1990.

A high-resolution seismic line along a shallow-to-deeper water (paleo dip) transect of the Drum Limestone adjacent to the outcrop belt near Independence will be acquired by Kansas Geological Survey in the second quarter. The seismic data will be used to delineate the geometric and internal stratigraphic characteristics of the Drum and encasing strata and to identify bounding surfaces of different stratal units. The initial seismic line will determine the usefulness of high-resolution data for important characterization and correlation of the Drum Limestone and other stratigraphic horizons in the near subsurface. Processing of the seismic data should be well under way during the second quarter of 1990, and initial results will be compared with the available surface and subsurface data that will have been acquired by that time. The seismic line will be taken in the area which has available subsurface well log data and which will be the site of two cores drilled in August 1990.

Field work, including stratigraphic section measuring and sampling, will continue. Petrographic studies of samples and thin sections will be conducted to supplement field descriptions. Thin sections will continue to be made in the second quarter. Additional well log data throughout the Montgomery County area will be correlated, and isopach maps of Drum and underlying strata will continue to be generated.

Hertha, Swope, and Dennis Analogues

The formations in the lower Kansas City group, Hertha, Swope, and Dennis, are excellent reservoirs (L, K, and J zones) in western Kansas; four fields have been selected for further analysis. The units in eastern Kansas are exposed and are represented in the near subsurface through extensive drilling. The Hertha Limestone contains phylloid-algal banks, and the Swope and Dennis formations include porous oolitic and bioclastic carbonates. The goals of this project are to understand the regional and local controls (e.g., eustatic, tectonic, and depositional) on the distribution of these reservoir facies where abundant lithologic and subsurface information is available to constrain and test resultant models. The application of sequence-stratigraphic concepts and quantitative simulation modeling is especially important in this study. Results will be applied to reservoir studies in western Kansas.

This study began with the mapping of an approximately 18,000-square-mile area that extends from surface exposures of these rocks to a distance of 50 miles to the west into the subsurface. The area mapped runs from Kansas City on the north to the Oklahoma line on the south. A set of isopach maps and cross sections based on about 700 surface and subsurface control points was prepared. Eight cores were obtained at selected sites in southeastern Kansas near and at the outcrop, which is located where reservoir-type facies and their lateral equivalents are developed. Additional strategically defined coring is planned to determine changes in lithofacies and stratal geometries. At least 20 outcrops were examined, and preliminary descriptions of both surface exposures and cores were made.

A short (few hundred feet) high-resolution seismic profile was obtained to evaluate usefulness in imaging this strata. The results suggest that this technique may be useful in further resolution of stratal geometries; if so, seismic studies will be an important component of this analogue investigation.

The quantitative modeling portion of this study has progressed significantly during the quarter. A prototype version of a two-dimensional stratigraphic computer simulation model and two supporting programs were written during a six-week period in February and March. The model runs on a VGA or EGA color IBM-compatible microcomputer (286, 386-based CPU preferred). This model reasonably replicates known stratigraphic geometries and lithofacies at the scale of individual reservoir-bearing cycles. As it is developed, the model will be used to understand the quantitative interaction of processes interpreted from the rocks.

Efforts to develop more precise and accurate interpretations of lithofacies for improved quantitative modeling are ongoing through all these studies. The black shales are important, but enigmatic strata in the Lansing–Kansas City depositional sequences. Their interpretations are critical to quantitative modeling.

Goals for the second quarter include: (1) prepare and give poster session of simulation model of lower Missourian strata (at the San Francisco meeting of the American Association of Petroleum Geologists);[4] (2) select site and contact landowners for six cores to be obtained during late July and August 1990; (3) begin detailed description and sampling of existing cores; and (4) continue to refine computer model, including incorporation of algorithms to deposit siliciclastics.

Supplement and Develop Regional Databases

Regional databases are being developed to: (1) establish a regional stratigraphic and structural framework linking analogue sites with fields and field studies with each other, (2) establish data sets to constrain interpretations of regional controls that influenced sedimentation and diagenesis in western Kansas suitable for modeling, (3) compare lease performance of Lansing–Kansas City reservoirs on a regional basis to discern trends and patterns,

and (4) integrate information to extend results of field studies to other Lansing–Kansas City reservoirs.

Regional digital databases of facies, thickness, and porosity of H, I, J, and K zones have been previously prepared covering in excess of 72,000 square miles in western Kansas. Integrated multivariate statistical analysis of this data set is under way to ascertain spatial patterns. A manuscript is in preparation, and presentations are planned in June.[5,6]

Six regional stratigraphic cross sections depicting strata from pre-Cretaceous to basement are in preparation. An east-west cross section extending from the outcrop and near-surface study area on the east to western Kansas (Hodgeman County) is nearly complete.

Structural mapping of the Precambrian basement is being revised and placed on a digital base for the State of Kansas. Reactivation of basement weaknesses appears to have controlled the location of many of the producing structures as well as to have governed patterns of shelf, basin, and uplift development throughout the Phanerozoic. Integration of basement configuration with basement composition, geochronology, and magnetic and gravity data should provide a much improved basis to delimit local (field-scale) and regional structural patterns. Areas in the central portion of the state have been completed and are ready to be digitized. Because of very limited subsurface control, structural maps of south-central Kansas have been constructed on the Arbuckle Group that immediately overlies the basement. From this stratigraphic level, a map of the estimated basement structure will be constructed.

Mapping of Precambrian structure on the Central Kansas uplift is complete, and base maps of the remainder of western Kansas are being plotted for manual structural mapping of the Arbuckle Group. All mapping is being done at the scale of 1:125,000. These maps will be digitized for regional compilation and computer reproduction at a larger scale. Preliminary results of this project[7] will be presented at the 9th International Conference on Basement Tectonics at Canberra, Australia, in July 1990.

Goals for the second quarter are to complete the regional cross sections, to extend the digital Lansing–Kansas City database to include the area of Collier Flats field, and to complete the basement maps.

Develop Options for Technology Transfer

The next Midcontinent American Association of Petroleum Geologists meeting will be held in Wichita in September 1991. Plans are to include the Drum Limestone analogue study as a field trip. A Pen field workshop will demonstrate an example of integrated geological-engineering studies on integrated petroleum reservoir characterization.

A book on the topic of sedimentary modeling will be published by the Kansas Geological Survey in early 1991. The book is a follow-up to a symposium held in Lawrence, Kans., in October 1989.[8] Compilation and editing of papers will continue during the second quarter. This book involves current modeling efforts of other researchers which will be useful in the ongoing development of models.

References

1. W. L. Watney, J. A. French, and E. K. Franseen, *Sequence Stratigraphic Interpretations and Modeling of Cyclothems*, Kansas Geological Society Guidebook, Lawrence, Kans. (1989).
2. W. L. Watney, J. E. Anderson, and J. C. Wong, Porosity Advisor—An Expert System Used as an Aid in Interpreting the Origin of Porosity in Carbonate Rocks, in *Microcomputer Applications in Geology II*, J. T. Hanley and D. F. Merriam (Eds.), pp. 275-288, Pergamon Press, Elmsford, N.Y., 1990.
3. W. L. Watney, J. H. Doveton, J. A. French, and D. R. Collins, Petrophysical Characterization of Upper Pennsylvanian Depositional Sequences in Western Kansas, *Geol. Soc. Am., Abstr. Programs*, 22(1): 32 (1990).
4. J. A. French, Jr. and W. L. Watney, Computer Modeling of Midcontinent Cyclothems and Its Application in the Prediction of Hydrocarbon Reservoirs (abstract), *Am. Assoc. Pet. Geol. Bull.* (in press).
5. J. Harff, J. C. Davis, L. Watney, G. Bohling, and J. C. Wong, Regionalization of the Western Kansas Shelf Based on Stratigraphic Data from Wells (abstract), *Am. Assoc. Pet. Geol. Bull.* (in press).
6. W. L. Watney, J. Harff, J. Davis, J. Wong, and G. Bohling, *Controls on Petroleum Accumulation in Upper Pennsylvanian Cyclic Shelf Carbonates in Western Kansas, U.S.A. as Interpreted from Space Modeling and Multivariate Techniques* (abstract), presented at the Symposium on Computerized Basin Analysis of the Prognosis of Energy and Mineral Resources, Academy of Sciences of the GDR, Gustrow, GDR.
7. D. L. Baars, *Conjugate Basement Rift Zones in Kansas, Midcontinent U.S.A.*, presented at the Ninth International Conference on Basement Tectonics, Canberra, Australia, July 1990.
8. E. K. Franseen and W. L. Watney (Eds.), *Sedimentary Modeling: Computer Simulation of Depositional Sequences*, Kansas Geological Survey, Subsurface Geology Series 12, Lawrence, Kans. (1989).

GEODIAGNOSTICS FOR RESERVOIR HETEROGENEITIES AND PROCESS MAPPING

Sandia National Laboratories
Albuquerque, N. Mex.

Contract Date: Oct 1, 1987
Anticipated Completion: Sept. 30, 1993
Funding for FY 1990: $285,000

Principal Investigator:
David A. Northrop

Project Manager:
Robert E. Lemmon
Bartlesville Project Office

Reporting Period: Jan. 1–Mar. 31, 1990

Objective

The long-range objective is to improve the efficiency of oil recovery by better definition of reservoir heterogeneities and mapping of enhanced oil recovery (EOR) processes through the development of advanced geodiagnostics systems. This project provides an EOR perspective for the diagnostic systems development. FY90 tasks include: (1) quantify and understand the resistivity changes associated with the passage of a steamflood, (2) define realistic electrical steamflood models for physical simulation and numerical modeling, (3) apply geostatistical techniques to incorporate heterogeneous reservoir geology in the interpretation of geodiagnostic data, and (4) critically examine current electrical measurement and interpretation techniques.

Summary of Technical Progress

Field data showing how formation resistivity changes during steamflooding is being gathered and analyzed for reservoirs with different characteristics: Kern River, a field where clay effects are very important, and Elk Hills, a field where salinity change is important. Data from these analyses and other examples of EOR resistivity changes found in the literature are summarized in Table 1.

During this quarter, information was gathered from published sources and discussions with major oil companies which suggests that Kern River steamflood resistivity changes are representative of a large number of heavy-oil steamfloods. It was previously thought that data from the Kern River field would be exceptional because of its low salinity and high residual water saturation. However, resistivity change depends on the change in these properties, not their absolute values, and in this respect the Kern River field is apparently typical. This is fortunate because most of the published field examples of steamflood resistivity change located to date are from the Kern River field.

The analysis of resistivity changes at Elk Hills has been completed and will be reported in "Field Examples of Electrical Resistivity Changes During Steamflooding," to be presented at the annual SPE meeting in September. The analysis showed that shales tend to increase the effect of temperature on resistivity change over that predicted by Arps' law.

Several of the papers presented at the Society of Geophysicists (SEG) symposium on Borehole Geophysics held February 1990 in Tucson, Ariz., included forward modeling of electrical techniques for mapping steamfloods.

TABLE 1

Field Examples of Resistivity Change as a Result of EOR Processes*

Field	Ref.	Technique	Oil (°API) gravity and viscosity	Initial resistivity, Ω-m	Resistivity ratio†			Salinity	Temperature, °C	Saturation, %	Clay conductivity
					Cold condensate	Hot condensate	Steam				
Steamfloods											
Kern River, Calif.			~14°API								
Kern Pilot	1	‡	4.0 Pa·s	~27	1.0	~0.38	0.38 ± 0.2	NC	38 → 127	50 → ~60	>90%
Kern "A" Pilot	1	‡			1.0	~0.38	0.38 ± 0.2				
Canfield	2	‡			Results similar to above						
San Joaquin	2	‡			Results similar to above						
Green and Whittier	2	‡			Results similar to above						
Section 33	2	‡			Results similar to above						
Elk Hills, Calif.	3	‡	27°API 0.007 Pa·s	2 to 16		0.37	0.53	high → low	25 → 132	35 → 60	
Charco Redondo, Tex.	4	§	18°API 0.095Pa·s	U	~3.8	~2.6	~2.6 to 0.75	high → low	28 → 160	66 → U	U
Surfactant–Polymer Flood											
Salem Unit, Ill.	5	¶		6 to 10	to 17	NA	NA	**	NC	~70 → ~84	U
Waterflood–Polymer Flood											
Tar Springs, Ill.	6	¶		5 to 10	8 or 9	NA	NA	1/10††	NC	NC	U
					9 to 20	NA	NA	≤1/10 ††	NC	U	U
Firefloods											
South Belridge, Calif.	7			U	Postburn resistivity >200 Ω-m						
Fry Comb. Test, Ill.	8			U	Postburn resistivity >200 Ω-m						
CO_2 Flood											
U	9			~30	pre ~5	CO_2 ~2	post ~10				

*NA, not applicable; NC, no significant change; U, not given in references.
†Zone resistivity divided by resistivity before process began.
‡Resistivity determined by open-hole well logs taken before and after passage of the steamfront.
§Resistance of cemented-in electrodes measured as a function of time as steamfront passed.
¶Resistivity determined by periodic logging of fiberglass-cased wells.
**Injection of fresh water (lake water) followed by field brine (117,000 ppm) into a 30,000 → 60,000 ppm formation water.
††Preflood water had a resistivity 10 times original formation water; polymer flood was even greater.

The resistivity contrasts assumed in these papers are much higher than the values determined by work at Sandia.[3] The effect of assuming high resistivity contrasts on the conclusions of the forward modeling papers is not evident. The data in Table 1 provide realistic steamflood resistivity data that can be used for forward modeling of electrical techniques to determine if the techniques can be used for mapping steamfloods.

Examples of published field data showing resistivity changes during nonthermal EOR processes were also found. These include surfactant–polymer, waterflood–polymer, fireflood, and CO_2 flood. These examples have been included in Table 1 to show that the electrical geodiagnostic techniques currently being developed for steamflooding will be applicable to other EOR processes.

Work was started on examining the uniqueness of inversions of frequency-domain surface-base electromagnetic soundings. A fundamental question that needs to be answered is whether the nonunique resistivity inversions commonly discussed are the result of (1) poor inversion algorithms, (2) noisy or incomplete data, or (3) more than one mathematical solution to the inversion problem. This question was addressed by comparing forward models of downward moving plane waves and a three-layered earth. The calculations address the inversion of frequency-dependent data to get the resistivity structure of a laterally homogeneous earth. Two distinctly different subsurface resistivity structures were found to give the same complex surface impedance to better than 0.05%. Regardless of which of the three preceding possibilities results in the nonuniqueness of the inversion, very different resistivity structures can be obtained starting from measured data sets that are within expected noise levels of each other. That is, the nonuniqueness is of practical significance, and apparently the last of the three possibilities is true: more than one mathematical solution exists to the inversion problem. Future work will consider what happens when spatially dependent and pre- and poststeamflooding data are inverted together as a data set to try to determine resistivity change.

Previous work has shown how the relationships used to interpret well logs can be used to understand steamflood resistivity changes at the wellbore scale (centimeters). Geophysical techniques for mapping thermal recovery processes, such as cross-borehole tomography, measure at a reservoir scale (hundred meters). The inversion of such measurements, or forward modeling to predict the results of such measurements, describes the in situ resistivity at an intermediate scale (ten meters). Because of geologic variability and heterogeneities, the electrical characteristics of the wellbore and intermediate scales are not necessarily the same. As a result, electrical geodiagnostic measurements can produce pictures of the process that are technically accurate, but their relationship to the fundamental geology or fluid distributions is unclear. Work has begun on identification of ways to understand the scaling or averaging between the wellbore and intermediate scales.

References

1. C. G. Bursell and G. M. Pittman, Performance of Steam Displacement in the Kern River Field, *J. Pet. Technol.* (August 1975).
2. G. R. Greaser and R. A. Shore, *Steamflood Performance in the Kern River Field,* paper SPE 8834, 1st SPE/DOE EOR Symposium (April 1980).
3. A. J. Mansure and R. F. Meldau, *Steam-Zone Electrical Characteristics for Geodiagnostic Evaluation of Steamflood Performance,* paper SPE 18797, presented at the California Regional SPE Meeting, Bakersfield, Calif., April 5–6, 1989.
4. R. H. Widmyer, C. E. Howard, M. F. Fontaine, and S. Haynes, Jr., The Charco Redondo Thermal Recovery Pilot, *J. Pet. Technol.* (December 1977).
5. R. H. Widmyer, D. B. Williams, and J. W. Ware, Performance Evaluation of the Salem Unit Surfactant/Polymer Pilot, *J. Pet. Technol.* (September 1988).
6. J. E. Richardson, Monitoring Flood Profiles with Induction Logs, *J. Pet. Technol.*, 31(1): 19-24 (January 1979).
7. C. F. Gates and H. J. Ramey, Jr., Field Results of South Belridge Thermal Recovery Experiment, *Petroleum Transactions AIME,* V213 (1958).
8. B. E. Hilton, C. H. Cotterell, H. Surkalo, and W. L. Kinney, Logging Observation Wells in an In Situ Combustion Test, *Trans. SPWLA* (1966).
9. E. C. Thomas, et al., The Scope and Perspective of ROS Measurement and Flood Monitoring, *J. Pet. Technol.*, 1398-1406 (November 1987).

CHARACTERIZATION AND MODIFICATION OF FLUID CONDUCTIVITY IN HETEROGENEOUS RESERVOIRS TO IMPROVE SWEEP EFFICIENCY

Contract No. AC22-89BC14474

University of Michigan
Ann Arbor, Mich.

Contract Date: Sept. 26, 1989
Anticipated Completion: Aug. 30, 1992
Government Award: $112,000
(Current year)

Principal Investigator:
H. Scott Fogler

Project Manager:
Robert E. Lemmon
Bartlesville Project Office

Reporting Period: Jan. 1–Mar. 31, 1990

Objective

The objective of this work is to develop effective flow-diverting techniques through experimentation; neutron

imaging will be used for flow characterization before and after treatment. Theoretical modeling will be used to identify the important parameters that govern the process of diverting fluids.

Summary of Technical Progress

The work during this quarter may be broken into three phases. Each phase involved preliminary experiments with a cross-linking foam. A stable three-component foaming solution was formulated in the first phase. In the second phase, linear corefloods were performed with the solution from phase one to demonstrate the effect of foam stabilized by a cross-linked structure on the apparent permeability of water. The third phase consisted of visual experiments of foam floods.

Formulation of the Experimental System

The goal of the work performed in this quarter was to demonstrate the effectiveness of a foam stabilized by a cross-linked structure on the relative permeability of porous media. A high molecular weight polyacrylamide/chromium nitrate [PAA/Cr(III)] system was used for cross-linking. This system was chosen because it has been extensively studied and it is a commonly used system in oil field applications.[1-4] It was necessary to find a surfactant that may be used in conjunction with the polymer–chromium system. Anionic surfactants cannot be used because the surfactant forms an ion pair with the Cr(III) and effectively removes both components from the solution. Therefore, either cationic or nonionic surfactants must be used. The cationic surfactant hexadecyl cetylpyridinium chloride (CPC) was chosen because it was stable in a polymer solution at PAA/CPC weight ratios of 10 or more. If the ratio drops below 10, then there is enough CPC to interact with the anionic polymer and cause it to come out of solution. The mixture of 10,000-ppm PAA:1000-ppm CPC:1000-ppm Cr(III) formed a gel just like the 10,000-ppm PAA:1000-ppm Cr(III) in bulk tests, which indicates no interference from the surfactants. A high-quality, fine-textured foam was created when the solution was stirred vigorously in a beaker. The foam remained for several hours before it collapsed as the result of gravity drainage; this indicates good stability.

Linear Corefloods

The experiments performed during this phase were to demonstrate the effectiveness of polymer gels, aqueous surfactant foams, and a cross-linked surfactant foam on reducing the water permeability of a ceramic core. A schematic of the experimental apparatus is shown in Fig. 1. The ceramic core is held in a simple Hassler cell. The injected fluid is displaced from a floating piston accumulator into the core by an FDS-210 pump. The gas mixes with the liquid stream just before it reaches the core. The inlet

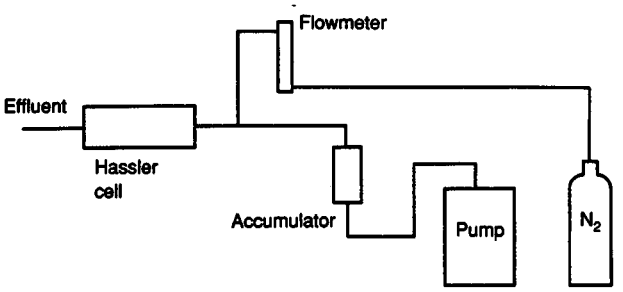

Fig. 1 Schematic of experimental apparatus.

pressure is measured on a series of Bourdon tube gages, and the effluent stream is collected in a beaker.

The general procedure was as follows. First, the ceramic core was cut to a length of 1 in., saturated with deionized water, put in the Hassler cell, and a 1000-psig overburden was applied. Next, the initial permeability to water was measured. After the permeability was measured, the PAA/CPC solution was mixed with the appropriate amount of Cr(III). This solution was quickly transferred into the floating piston accumulator, and injection commenced immediately. In corefloods that involved foam, the gas was simultaneously injected with the PAA/CPC/Cr(III) solution. The time required for injection of the polymer solution was very short, so there was little gelation of the solution during this period. The initial permeability of all the cores was approximately 10 to 15 darcys.

The basic corefloods performed were: (1) an aqueous surfactant foam flood, followed by a waterflood; (2) a polymer solution flood that was shut in to allow cross-linking, followed by a waterflood; and (3) a polymer foam flood that was shut in to allow cross-linking, followed by a waterflood. The conditions of the experiments are shown in Table 1.

The surfactant foam did not hold up well when the waterflood was initiated. Within several injected pore volumes of water, a substantial amount of the permeability had been restored. This is in agreement with many literature sources. [5-9]

The polymer gel experiments were conducted at two chromium concentrations (see Table 1). The post shut-in resistance factor due to the cross-linked gel increased with increasing chromium ion concentration. This agrees with the fact that the greater availability of the Cr(III) ion allowed more intermolecular cross-links to form, and hence a more elastic material was formed.[10,11] An indication that the gels formed with low Cr(III) concentrations were weak was the fact they were displaced from the core to a high extent relative to strong gels during the waterflood.

The foam stabilized by the cross-linked polymer demonstrated a relatively long-term persistence during a waterflood (Table 1). This presents the interesting possibility of being able to use the advantages of a foamed diverting agent during a waterflood.

TABLE 1

Summary of Resistance Factors (K_o/K) of Preliminary Corefloods*

Injected fluid	Shut-in time	$\left(\frac{K_o}{K}\right)_{maximum}$	$\left(\frac{K_o}{K}\right)_{after\ 24\ h}$	Gas flow rate, mL/min
1,000 ppm CPC	–	355	2	10
10,000 ppm PAA 1,000 ppm CPC 500 ppm Cr(III)	3 d	450	450	–
10,000 ppm PAA 1,000 ppm CPC 1,000 ppm Cr(III)	3 d	41,700	41,700	–
10,000 ppm PAA 1,000 ppm CPC 400 ppm Cr(III)	5 d	681	300	10
10,000 ppm PAA 1,000 ppm CPC 1,000 ppm Cr(III)	5 d	1,870	1,340	10
10,000 ppm PAA 1,000 ppm CPC 1,000 ppm Cr(III)	3 d	2,990	2,090	5

*CPC, hexadecyl cetylpyridinium chloride; PAA, polyacrylamide; Cr(III), chromium nitrate.

The aforementioned experiments were preliminary in nature and consequently were marked by several failed experiments. However, the information learned from these experiments is very valuable since it helps in the design of reliable experiments. Two major improvements were made as the result of information learned from the failures. Initially, the injected polymer solution was held in an aluminum floating piston accumulator. The injection fluids are at a pH of approximately 4.0 to 4.5. At this pH the aluminum is slightly soluble. The increase in the multivalent ion concentration increased the gelation rate and created a strongly adsorbed polymer slime around the insides of the accumulator. For the alleviation of this problem, a small accumulator with all plastic wetted parts, which performed perfectly in subsequent corefloods, was designed and built. Additionally, the system was refitted with Peek tubing. Another troublesome area was the method of preparing the core to be shut in the Hassler cell to undergo cross-linking. The coreface, feed, and effluent lines had to be cleaned immediately after injection of the polymer to prevent plugging. The removal of the distribution caps to clean the coreface caused a vacuum that pulled some of the fluid out of the core. This problem will be negated once controlled experiments are started with a Temco Hassler cell that has a different configuration.

Visual Studies

The third phase of preliminary experiments was a series of visual experiments designed to show the mechanism of how the fluid phase flows through a cross-linked foam.

A schematic of the apparatus is shown in Fig. 2. The sandpack was made from Ottawa sand (20 to 30 mesh). The sand was packed into a 25-cm-long by 2.5-cm-dia. polycarbonate tube. A 1-cm-dia. glass rod was inserted in the center of the sandpack to reduce the pore volume. The liquid is displaced with a syringe pump. The gas flow enters the liquid stream before entering the sandpack. A stereomicroscope equipped with a Javelin CCTV camera was used to transfer the image of the experiment to a Sony Trinitron high-resolution monitor. The experiments were recorded on a Panasonic high-density videocassette recorder (VCR).

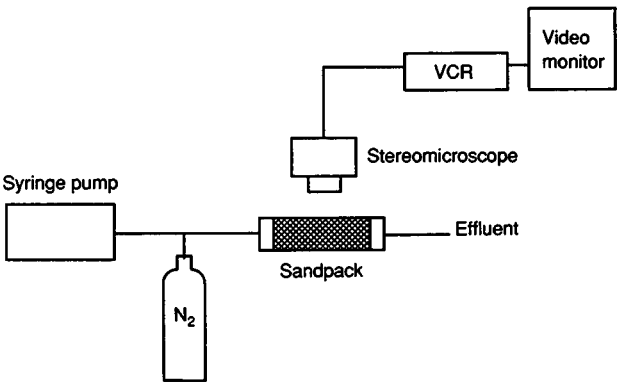

Fig. 2 Schematic of visual experiment apparatus.

One interesting observation made from the visual studies with the cross-linked foam was that during the waterflood the lamellas increased in thickness considerably. The flow within the lamellas entrained the bubbles of nitrogen that had previously been held in place by the lamellas. Interestingly, there was no coalescence of the bubbles. The entrainment of noncoalescing bubbles resulted in the flow of the bubble trains through the sandpack. The bubbles would often jam at the pore throats and thus plug a particular flow path. As time went on, dominant flow paths were developed where no bubbles could become trapped. Other areas simply accumulated trapped bubbles. These accumulated trapped bubbles diverted the flow to the dominant flow paths.

References

1. T. S. Young, J. A. Hunt, D. W. Green, and G. P. Willhite, Study of Cr(III)/Polyacrylamide Gels by Swelling Measurement and Equilibrium Dialysis, *SPE Reservoir Eng.*, 4(3): 348-356 (August 1989).
2. J. A. Hunt, T. Young, D. W. Green, and G. P. Willhite, A Study of Cr(III)–Polyacrylamide Reaction Kinetics by Equilibrium Dialysis, *AIChE J.*, 35(2) (February 1989).
3. R. K. Bhaskar, J. A. Stinson, G. P. Willhite, and J. L. Thiele, The Effects of Shear History on the Gelation of Polyacrylamide/Chromium(VI)/Thiourea Solutions, *SPE Reservoir Eng.* (November 1988).
4. R. K. Prud'homme, J. T. Uhl, J. P. Poinsatte, and F. Halverson, Rheological Monitoring of the Formation of Polyacrylamide/Cr(III) Gels, *Soc. Pet. Eng. J.* (1983).

5. D. G. Huh, T. D. Cochrane, and F. S. Kovarik, The Effect of Microscopic Heterogeneity on CO_2–Foam Mobility: Part 1—Mechanistic Study, *J. Pet. Technol.* (August 1989).
6. R. W. Burley, C. W. Nutt, and M. Gh. Bayat, Studies of Foam Displacement by Foam in Porous Media, *Chem. Eng. Res. Des.*, 62 (March 1984).
7. G. G. Bernard and L. W. Holm, The Effect of Foam on Permeability of Porous Media Gas, *Soc. Pet. Eng. J.* (September 1964).
8. G. G. Bernard, L. W. Holm, and W. L. Jacobs, The Effect of Foam on Trapped Gas Saturation and on Permeability of Porous Media Water, *Soc. Pet. Eng. J.* (December 1965).
9. L. W. Holm, The Mechanism of Gas and Liquid Flow Through Porous Media in the Presence of Foam, *Soc. Pet. Eng. J.* (December 1968).
10. G. P. Willhite, D. W. Green, J. L. Thiele, T. Young, and K. B. Mertes, *Investigation of the Application of Gelled Polymer Systems for Permeability Modification in Petroleum Reservoirs*, Report DOE/BC/10843-10, The University of Kansas, Lawrence, Kans., November 1988.
11. G. P. Willhite, *Investigation of the Application of Gelled Polymer Systems for Permeability Modification in Petroleum Reservoirs*, Report DOE/BC/10843-5, The University of Kansas, Lawrence, Kans., November 1987.

CHARACTERIZATION OF OIL AND GAS RESERVOIR HETEROGENEITY

Contract No. FG22-89BC14403

University of Texas
Austin, Tex.

Contract Date: September 1988
Anticipated Completion: September 1991
Government Award: $235,000
(Current year)

Principal Investigator:
William Fisher

Project Manager:
Chandra Nautiyal
Bartlesville Project Office

Reporting Period: Jan. 1–Mar. 31, 1990

Objectives

Progress in the fourth quarter of research funded under the auspices of Memorandum of Understanding Annex I is summarized for seven main subtask areas. These subtask areas are: (1) definition of the distribution of carbonate sandbar facies for Grayburg reservoirs, (2) definition of three-dimensional geometry of carbonate sand bodies, (3) analysis of engineering and petrophysical attributes of reservoir flow units, (4) development and testing of extended conventional oil recovery strategies, (5) characterization of gas reservoirs, (6) geologic and engineering characterization of generic gas reservoir types, and (7) refinement of exploitation strategies. Key areas of progress for the quarter concern subtasks 3 and 6.

Summary of Technical Progress

Subtask 3

The objective of this subtask is to conduct geological, petrophysical, and engineering studies of a subsurface Grayburg reservoir in which major production is from a sandbar facies similar to that being examined on the outcrop. Detailed correlation from the outcrop to the Foster field, on the eastern side of the Central Basin Platform, has documented the equivalence of these two sites.

Detailed examination of cores from the ARCO North Foster Unit is complete, and a facies section has been constructed across the unit to demonstrate the changes in the rock characteristics from the area of lower production to the west to the area of higher production to the east. This increase in production to the east parallels the increase in grain-dominated, highly altered, vertically structured pellet grainstone–packstone facies.

Because of the small area encompassed by the ARCO North Foster Unit, cores from neighboring units are now being examined to better establish trends to the facies and scales of major depositional features recognized in the ARCO unit. Several cores have been logged from the Johnson Grayburg Unit to the north, and the general facies patterns recognized in the ARCO unit have been documented in the Johnson unit. However, major changes in thickness of low-permeability siltstones have been recorded from these cores; these siltstone thickness changes in the Johnson unit are similar to those described from the outcrop as channel fills. Delineation of the scale and trend of the channel fills on the outcrop will aid in the mapping of these low-permeability features in the reservoir. Published engineering studies report anhydrite barriers to production in the Johnson unit. The anhydrite barriers have not yet been documented in the cores studied thus far.

Negotiations are now under way with Conoco personnel to obtain cores, production data, and test data from wells in a Conoco unit that actually lies within the ARCO unit. The Conoco cores will fill a large gap in the existing facies cross section.

Subtask 6

Subtask 6, geologic and engineering characterization of generic gas reservoir types, continued to focus on the application of detailed outcrop information from the Ferron Sandstone to deltaic gas reservoirs on the Gulf Coast. Mapping of reservoir analogs was initiated in November when seven sections through sandstone member 5 were

measured in detail. Activities during the fourth quarter centered on statistical treatment of the permeability data gathered from the outcrop and from hand-sample blocks of key facies returned to the laboratory for further analysis. These samples were collected to test the accuracy and precision of the Mechanical Field Permeameter (MFP).

Results of Reconnaissance Outcrop Sampling

Core samples with permeabilities determined by conventional gas permeability were used as test standards to verify minipermeameter accuracy. Corresponding hand samples were measured to determine accuracy under field conditions. Obvious surface effects, such as fractures and vugs that would affect tip seal quality, were avoided.

A plot of conventionally measured permeabilities against MFP permeabilities of corresponding hand samples displays a significant positive departure from the expected 1:1 correlation over the lower permeability range of 1 to 50 mD (Fig. 1). Constant positive departure from the expected value over the lower permeability range indicates that the variation is the result of inadequate tip seal quality (gas leakage) rather than local permeability variation of hand samples. Application of a sealant (toothpaste or petroleum jelly) to the injection tip corrected the variation.

A series of repeatability measurements were performed over the range of 1 to 300 mD. For measurements greater than 10 to 20 mD, the results are in close agreement with a maximum deviation less than 5% for any measured value. However, at values less than 10 mD, precision rapidly decreases. This conclusion is similar to that reached by Goggin.[1]

More than 700 measurements were made with the MFP on outcrop and hand samples of fluvial–deltaic sandstones. On the Ferron Sandstone, e..st-central Utah, measurements were taken every foot along seven closely spaced (40 to 240 ft) vertical transects across the outcrop. Detailed (0.25- to 1.0-in. grid spacing) MFP measurements were also made on hand samples of representative stratification types to examine fine-scale permeability variations.

From a comparison of permeability distributions (F- and T-tests), it was determined that fluvial–deltaic sandstones contain four basic patterns of permeability variability. A larger scale pattern corresponds to variations between facies, between subunits, and between beds. A smaller scale pattern corresponds to variations within beds. Among facies, the distributary channel contains the most dissimilar permeability distribution. Statistically different permeability distributions occur between the distributary channel and all other facies: fluvial, transgressive, and shoreface. At the subunit scale, permeability variation was significant between the upper and lower distributary channel and shoreface units, respectively. Within the distributary channel facies, permeability distributions vary according to stratification type. At the bed-to-bed scale, permeability distributions within the contorted and trough-cross-bedded units were statistically different from those in the horizontal- and ripple-laminated

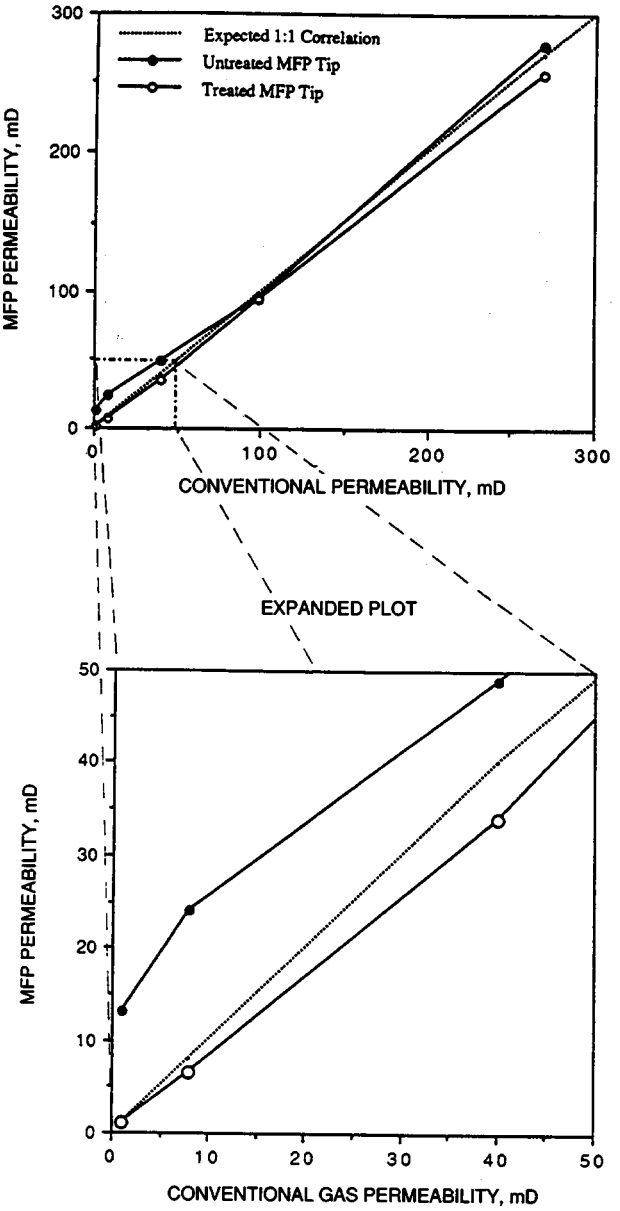

Fig. 1 Cross plot of MFP permeability against conventional gas permeability.

units. Within the shoreface facies, permeability distributions vary according to subunits and stratification type. Substantial variability was noted within individual bedded units. Small-scale permeability variation approximates larger scale variation for shoreface, bioturbated, and trough-cross-bedded hand samples.

Hand samples displayed marked spatial permeability anisotropy. Strong spatial correlation of permeability exists parallel to bedding within the trough-cross-bedded, ripple-laminated, and horizontal-laminated sandstones. However, in the bioturbated sample, permeability data are clustered with no preferred direction of spatial correlation.

Detailed permeability measurements were taken parallel and perpendicular to paleoflow direction, as well as verti-

cally to bedding, to assess directional permeability anisotropy within hand samples. In general, mean permeabilities were greatest parallel to paleoflow direction and least perpendicular to bedding. Comparison of mean permeabilities (T-test) indicates that directional differences are not statistically significant up to a 0.30 confidence limit.

Comparison Between Surface and Subsurface Samples

It is critical in reservoir characterization studies that outcrop measurements of overall permeability variation and spatial correlation be representative of subsurface deposits and not reversed by weathering processes. Goggin et al.[2] and Kittridge and Lake[3] concluded from field studies of the Page Sandstone and San Andres Formation, respectively, that outcrop and subsurface permeability variation and spatial correlation agree well.

Stalkup and Ebanks[4] compared permeability of rocks from the Ferron outcrop with similar rocks in the same stratigraphic unit in a nearby well. Mean permeabilities were greater and permeability variation less among and within lithofacies from outcrop compared with subsurface samples. However, the direction of change in subsurface lithofacies is preserved in analog surface lithofacies. Furthermore, the vertical arrangement of statistically different permeabilities is similar in the two situations.

References

1. D. J. Goggin, *Geologically Sensible Modelling of the Spatial Distribution of Permeability in Eolian Deposits: Page Sandstone (Jurassic), Northern Arizona,* Ph.D. dissertation, The University of Texas at Austin, 1988.
2. D. J. Goggin, M. A. Chandler, G. Kocurek, and L. W. Lake, Permeability Transects in Eolian Sands and Their Use in Generating Random Permeability Fields, SPE paper 19586, in *Proceedings of the 64th Annual Technical Conference and Exhibition of the Society of Petroleum Engineers, San Antonio, Tex., Oct. 8–11, 1989,* pp. 149-163.
3. M. G. Kittridge and L. W. Lake, Outcrop-Subsurface Comparisons of Heterogeneity in the San Andres Formation, SPE paper 19596, in *Proceedings of the 64th Annual Technical Conference and Exhibition of the Society of Petroleum Engineers, San Antonio, Tex., Oct. 8–11, 1989,* pp. 259-273.
4. F. I. Stalkup and W. J. Ebanks, Permeability Variation in a Sandstone Barrier Island–Tidal Channel Delta Complex, Ferron Sandstone (Lower Cretaceous), Central Utah, SPE paper 15532, in *Proceedings of the 61st Annual Technical Conference and Exhibition of the Society of Petroleum Engineers, New Orleans, La., Oct. 5–8, 1986,* pp. 1-13.

RESERVOIR CHARACTERIZATION AND ENHANCED OIL RECOVERY RESEARCH

Contract No. DE-FG22-89BC14251

University of Texas at Austin
Austin, Tex.

Contract Date: Sept. 1, 1989
Anticipated Completion: Aug. 31, 1990
Government Award: $580,000
(Current year)

Principal Investigators:
Gary A. Pope
Larry W. Lake
Robert S. Schechter

Project Manager:
Jerry F. Casteel
Bartlesville Project Office

Reporting Period: Jan. 1–Mar. 31, 1990

Objective

The objective of this project is to increase the understanding of enhanced oil recovery (EOR) processes as they relate to realistic reservoir settings for increased efficiencies and decreased risks in known reservoirs in Texas. The primary activities include:

1. Systematic reservoir characterizations.
2. Modeling and scaleup of chemical flooding techniques.
3. Gaining a broader understanding and providing fundamental information on CO_2–surfactant phase behavior.

Summary of Technical Progress

Systematic Procedure for Reservoir Characterization

Development of an Averaging Procedure for Relative Permeability that Accounts for Both "Continuity" and "Crossbedding"

This work is largely complete.[1] The development of a new procedure for deriving effective or pseudo relative permeabilities for viscously dominated flow in crossbedded sands also makes use of the observation that crossbedding, as represented through a tensorial permeability, can be accurately represented by isotropic permeabilities that have been corrected for the crossbedding. This observation, which was extensively validated with detailed simulation, means that the Hearn technique can be applied to this geologically complicated flow without significant error. Although the method was derived specifically for eolian sequences, the procedure should be valid for any crossbedded sand.

The effective relative permeabilities were applied to a viscously dominated, highly detailed simulation of a miscible displacement through a portion of the Page Sandstone outcrop using the effective properties' results in a reduction in the number of finite element nodes from more than 11,000 to 36 with essentially the same recovery function. Since this displacement was miscible, the effective relative permeabilities incorporate the details of the underlying geology almost exclusively.

Quantification of Existing Taxonomy Through the Use of Correlation, Fractal Representation, and Nonlinear Dynamic Statistical Procedures

Work in the past quarter has centered on methods to separate the effects of fluid from heterogeneity in realistic displacements. To this end, the project has focused on the scaling laws of a waterflood in a homogeneous medium.

During this period a rigorous mathematical procedure for determining the dimensionless groups that govern this immiscible displacement was developed and applied. There are five such groups: a mobility ratio, an aspect ratio, a capillary number, a gravity number, and a dimensionless dip angle. The gravity number, in particular, is interesting because there have been more than 10 such numbers reported in the literature, none of which are identical with the number derived from the procedure. With simulation, the parameter space between recovery and these dimensionless groups was explored, and the insight obtained will be used to extend the scaling ideas to flow through heterogeneous media.

Use of Geochemical Flow Modeling to Determine the Geometric Patterns in Porosity and Permeability that Result from Diagenetic Processes

One avenue of attack for this problem is a fundamental study of reactive flow in the presence of a combination of reactions both in and out of local thermodynamic equilibrium. For reactions out of local equilibrium, a solution was found to a reactive problem for flow through a tube with the intent of using these insights to broaden the work to flow through permeable media. The results of the tube model are to be used in a network simulation to identify circumstances when dissolution or precipitation (calcification) would occur. Thus far, both instabilities and damping in network reactive flow have been generated.

Modeling and Scaleup of Chemical Flooding

Measure the In Situ Behavior of Gels Formed While Flowing in Permeable Media

Until now, this project has not focused on simulations of reservoir treatments. Recently, the scope of work was enlarged to include simulation work of conformance control treatments with UTCHEM. A gel option added to UTCHEM by Hortes[2] several years ago was later modified and used by Garver[3] to simulate coreflood. The use of UTCHEM to simulate a gel treatment in a producing well using the radial option is illustrated.

One of the questions to be studied in the future with UTCHEM is the effect of zone isolation on conformance treatments. This is an issue Seright et al.[4] has addressed with analytical models, and they made many interesting observations.[4,5,6] The use of simulation to study this and related issues has a number of advantages since less severe assumptions about the reservoir, chemistry, fluids, and treatment process are required compared with the analytical approach.

Only one example (for general illustrative purposes) is given in this report. The gellants are the same as those used in Garver's experiments.[3] After polymer and Cr^{3+} have been injected for 5 d, the well is shut in for 3 d and then produced for 20 d. The reservoir consists of two equal-thickness, noncommunicating layers with a ten-to-one permeability contrast. The oil cut before the gel treatment is 0.2831. The results after the gel treatment are plotted in Figs. 1 to 5. Figures 1 to 4 show the polymer concentration, chromium concentration, gel concentration, and oil saturation, respectively, just before shut-in vs. radial distance into the reservoir for each layer. Figure 5 shows the producing cuts for the first 20 d after the treatment.

The oil cut first decreases because of the flushing effect of the injected gellants and then gradually increases until it exceeds the initial oil cut before treatment. The oil cut at 20 d is about 0.4. Thus this treatment has been at least a partial success, even though the gellants were injected without zonal isolation and even though the gel has not propagated very far into the reservoir even in the high-permeability layer (Fig. 3). Note that a simulated tracer has gone about 50 ft into the high-permeability layer compared with only 15 ft for the gel. This is due, in part, to gel retention. This result is probably optimistic, however, because for simplicity no Cr^{3+} retention was simulated, even though Garver[3] showed that in Berea cores it can be very significant. A part of the plan is to include the effects of this retention and also pH in subsequent simulations and to study the effects of crossflow and other reservoir characteristics, zonal isolation, gel chemistry, and the size of the gel treatment.

CO_2–Surfactant Phase Behavior

CO_2–Surfactant–Water Interactions

Alcohol-free microemulsions. Microemulsions often "require" added alcohols to achieve the desired stability and needed solvency to qualify as oil recovery candidates.

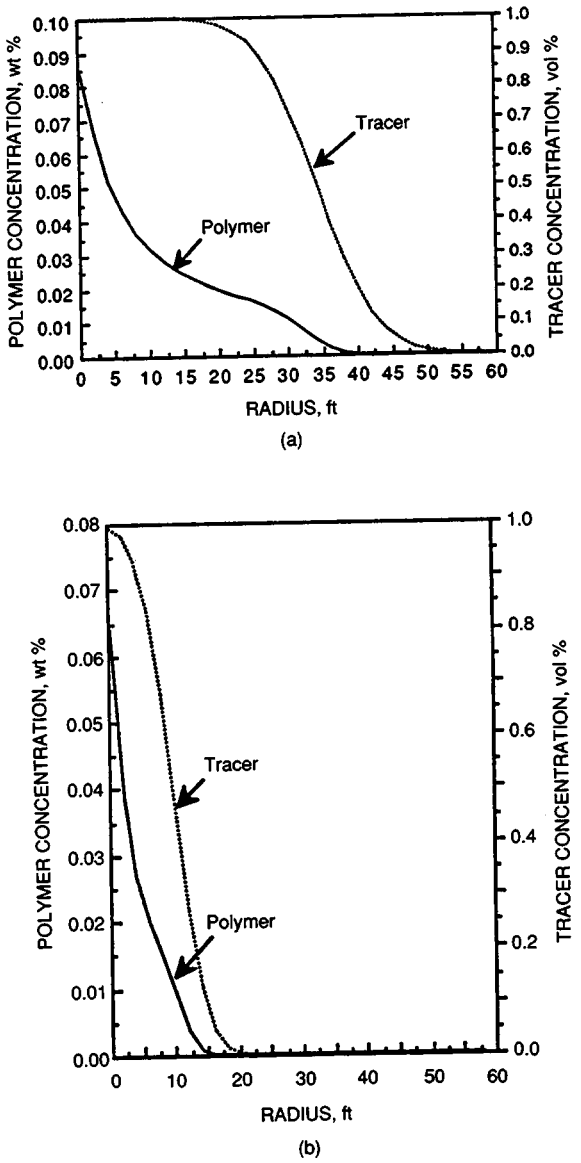

Fig. 1 Polymer and tracer concentration profiles for the high-permeability (a) and low-permeability (b) layers just before shut-in.

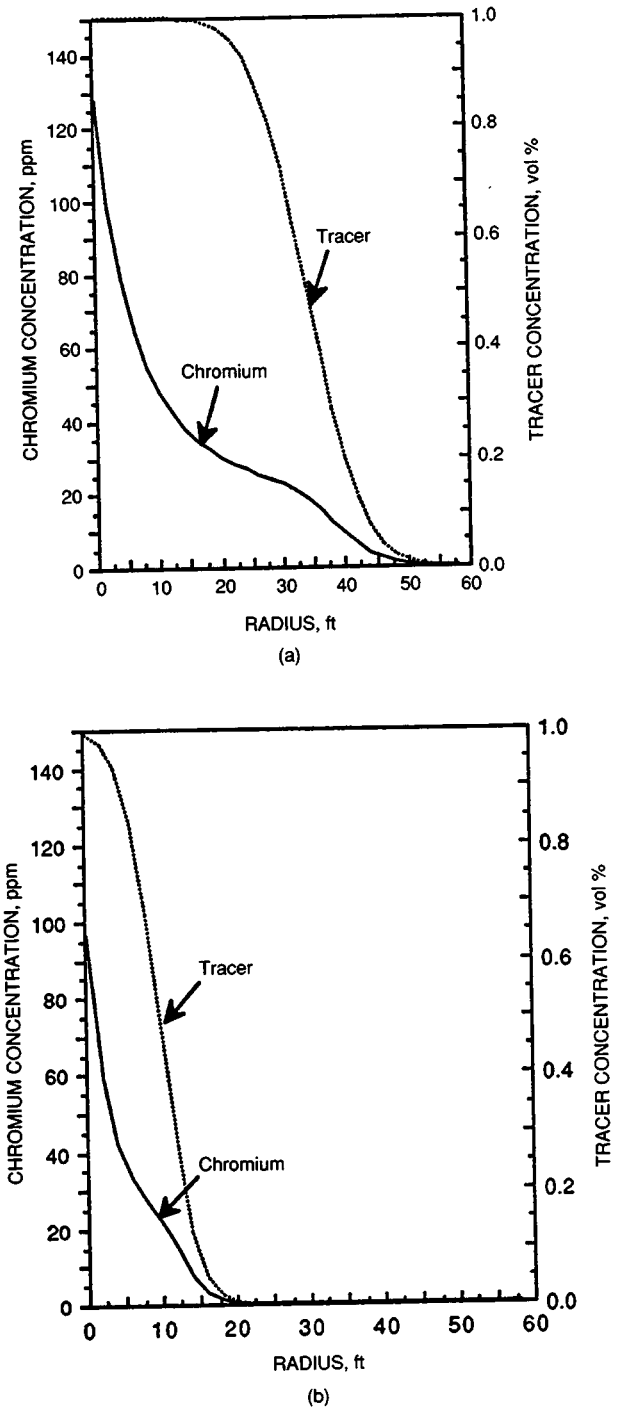

Fig. 2 Chromium and tracer concentration profiles in the high-permeability (a) and low-permeability (b) layers just before shut-in.

Most microemulsions that have been studied include alcohols. A study of alcohol-free microemulsions using three surfactants has just been concluded. These are sodium paradihexyl benzene sulfonate ($C_6\phi C_6$), sodium 2-3-dimethyl-5-dodecyl benzene sulfonate ($C_{12}\phi 2CH_3$), and sodium 7-(paraphenyl sulfonate)-7-methyl pentadecane ($C_{16}V\phi$). Under certain conditions of temperature and salinity, three-phase microemulsions with octane can be formed.

The submicroscopic structures of these alcohol-free microemulsions have been studied using quasilinear light scattering in the Winsor II region (essentially water-in-oil microemulsions). The conclusions are that the second virial coefficient characterizing the interaction between drops depends on the surfactant structure but is apparently not related uniquely to either the drop size or the salt concentration contained within the drop. The virial coefficients were all negative, which indicates an attractive interactive force, and this force seemed to increase with surfactant chain length, which is contrary to expectation.

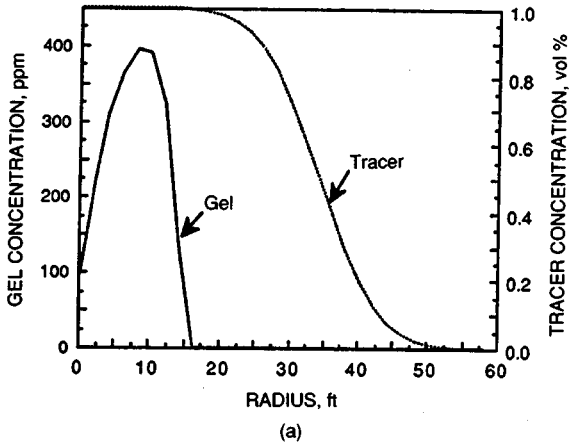

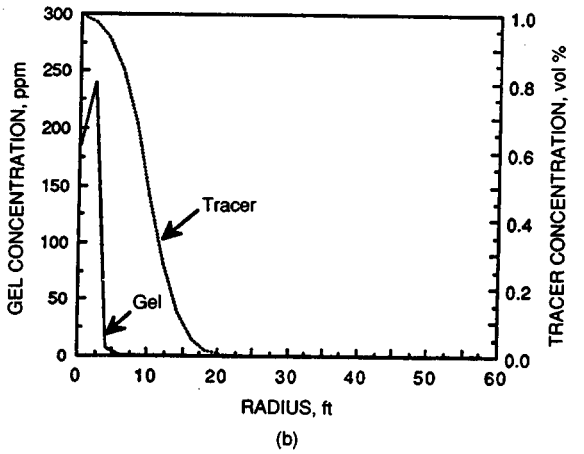

Fig. 3 Gel and tracer concentration profiles for the high-permeability (a) and low-permeability (b) layers just before shut-in.

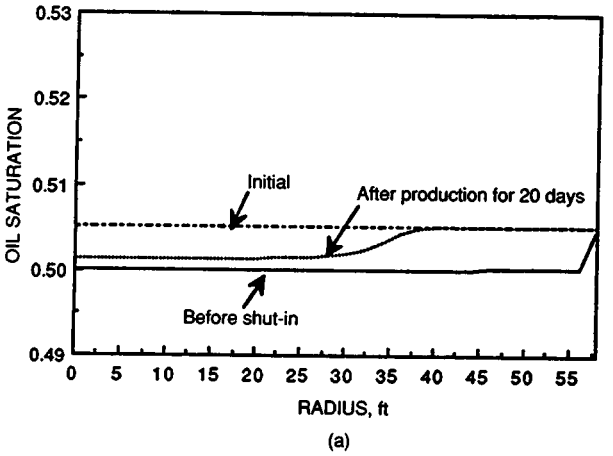

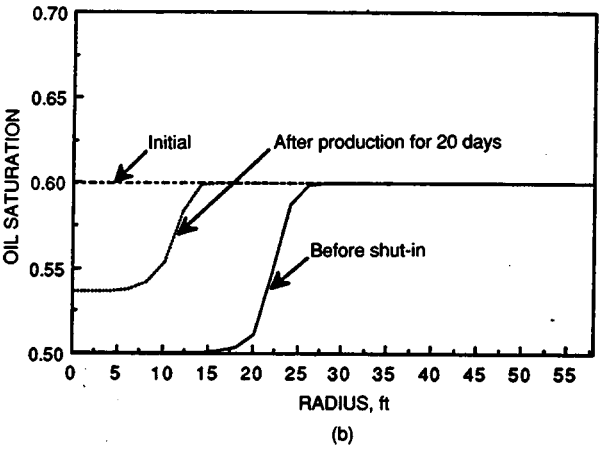

Fig. 4 Oil saturation profiles for the high-permeability (a) and low-permeability (b) layers at the beginning of gel injection, before shut-in and after production for 20 days.

References

1. E. Kasap and L. W. Lake, *Dynamic Effective Relative Permeabilities for Crossbedded Flow Units,* paper SPE/DOE 20179 presented at the SPE/DOE Seventh Symposium on Enhanced Oil Recovery, Tulsa, Okla., Apr. 22–25, 1990.
2. E. Hortes, *Development of a Reservoir Model for Gel Treatment,* Center for Enhanced Oil and Gas Recovery Research, Report No. 87-3, University of Texas, Austin, 1987.
3. F. J. Garver, *The Competition for Chromium Between Xanthan Biopolymer and Resident Clays in Sandstones,* paper SPE 19632 presented at the 64th Annual Technical Conference of the SPE, San Antonio, Tex., October 1989.
4. R. S. Seright, F. S. Kovarik, and F. D. Martin, *Fluid Diversion and Sweep Improvement with Chemical Gels in Oil Recovery Processes,* Quarterly Technical Progress Report, New Mexico Petroleum Recovery Research Center, New Mexico Institute of Mining and Technology, Socorro, N. Mex., August 1989.

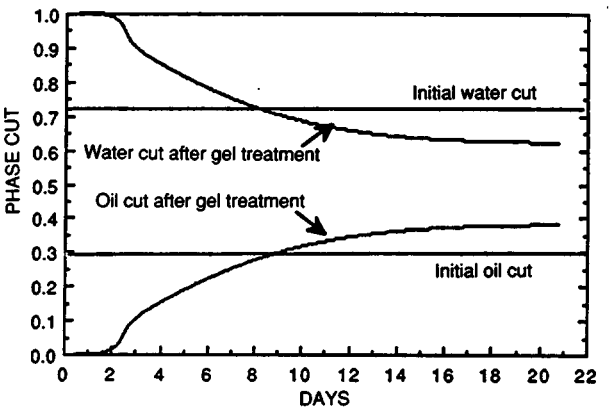

Fig. 5 Production history after the gel treatment.

5. R. S. Seright, *An Examination of Flow-Profile Changes for Field Applications of Gel Treatments in Injection Wells*, Quarterly Technical Progress Report, New Mexico Recovery Research Center, New Mexico Institute of Mining and Technology, Socorro, N. Mex., October 1989.

6. R. S. Seright, *Impact of a Water Post-Flush on Gel Placement in Injection Wells*, Quarterly Technical Progress Report, New Mexico Recovery Research Center, New Mexico Institute of Mining and Technology, Socorro, N. Mex., September 1989.

ANALYSIS OF RESERVOIR HETEROGENEITIES DUE TO SHALLOWING-UPWARD CYCLES IN CARBONATE ROCKS OF THE PENNSYLVANIAN WAHOO LIMESTONE OF NORTHEASTERN ALASKA

Contract No. AC22-89BC14471

University of Alaska
Fairbanks, Alaska

Contract Date: Sept. 29, 1989
Anticipated Completion: Dec. 31, 1992
Government Award: $149,935

Principal Investigator:
Keith F. Watts

Project Manager:
Robert E. Lemmon
Bartlesville Project Office

Reporting Period: Jan. 1–Mar. 31, 1990

Objectives

The primary objective of the project is to develop an integrated database to characterize reservoir heterogeneities resulting from numerous small-scale shallowing-upward cycles comprising the Pennsylvanian Wahoo Limestone of northeastern Alaska. A computerized database system is being developed to document information on carbonate petrology, diagenesis, and biostratigraphy derived from the analyses of thousands of samples systematically collected from over 20 stratigraphic sections in the Arctic National Wildlife Refuge (ANWR). Lateral and vertical variations in the complex mosaic of carbonate facies comprising the Wahoo Limestone will be determined.

A correlation scheme, with distinct marker beds and cyclic stratigraphy, will allow the interpretation of the depositional history and paleogeographic evolution of the region and the development of predictive facies models and paleogeographic maps. Biostratigraphic data, provided by the University of Montreal (algae and foraminifera) and the U.S. Geological Survey (conodonts), will provide two independent means of correlation. Exposure surfaces and associated variations in cement stratigraphy analyzed at the University of Kansas will be considered when these correlations are refined.

The ultimate goals are to construct sea-level curves modeling the carbonate cycles and to determine the use of cyclic stratigraphy as a means of correlation. In the later stages of the project, the relationship between cyclic stratigraphy and reservoir properties in correlative rocks at the Lisburne oil field will be examined, and the use of cyclic stratigraphy for regional correlations will be tested. The detailed analysis of the Wahoo Limestone will provide a basis for interpreting correlative rocks in the adjacent subsurface of the coastal plain of ANWR, a potential hydrocarbon lease–sale area. In a broader sense, this work will provide an excellent example of carbonate shallowing-upward cycles that typify carbonate sediments. If the cyclicity resulted from global (eustatic) sea-level fluctuations, these sea-level curves may be applicable to cyclic Pennsylvanian rocks elsewhere.

Summary of Technical Progress

Computerized Database

During the second quarter of this project, significant progress has been made in developing a computerized database system for petrographic data from the Lisburne Group. With a 4th Dimension database program on a MAC IIx computer, a menu-driven data-input structure modeled after a standardized data entry form has been established (Table 1). In addition, another data entry form (Table 2) was established to capture data previously collected by a graduate student working on the project. An advantage of 4th Dimension is its ability to have multiple data entry modes (even in different languages), which allows it to accommodate a variety of data sheets used by different researchers. Additional data entry formats are being developed to allow easy input of existing data previously collected by other researchers. In the future, the standardized entry form (Table 1) will be used to record petrographic descriptions to increase consistency and maximize the power of the database system. Both formats can be output as report forms, which allows computerized data to be checked against the original data sheets, to serve as a permanent record (hard copy), and future researchers to check the original analyses for consistency and make changes if necessary.

The strength of the computerized database is its ability to search for selected characteristics and illustrate variations

in lithology or composition in a stratigraphic sequence. For example, the lithologic cycles (shallowing-upward parasequences) that characterize the upper Wahoo Limestone are dramatically illustrated by the graph that shows variations in content of ooids and peloids in the Plunge Creek stratigraphic section (Fig. 1). The cycles indicate the repeated southward progradation of ooid shoals and peloidal lagoons following rapid northward transgression at the base of each parasequence. Such plots generated by 4th Dimension will provide an objective means of checking the consistency of the paleoenvironmental interpretations and of quantifying the nature of lithologic cycles (parasequences).

TABLE 1

Standardized Data Sheet for Petrographic Data Recorded in the Computer Database

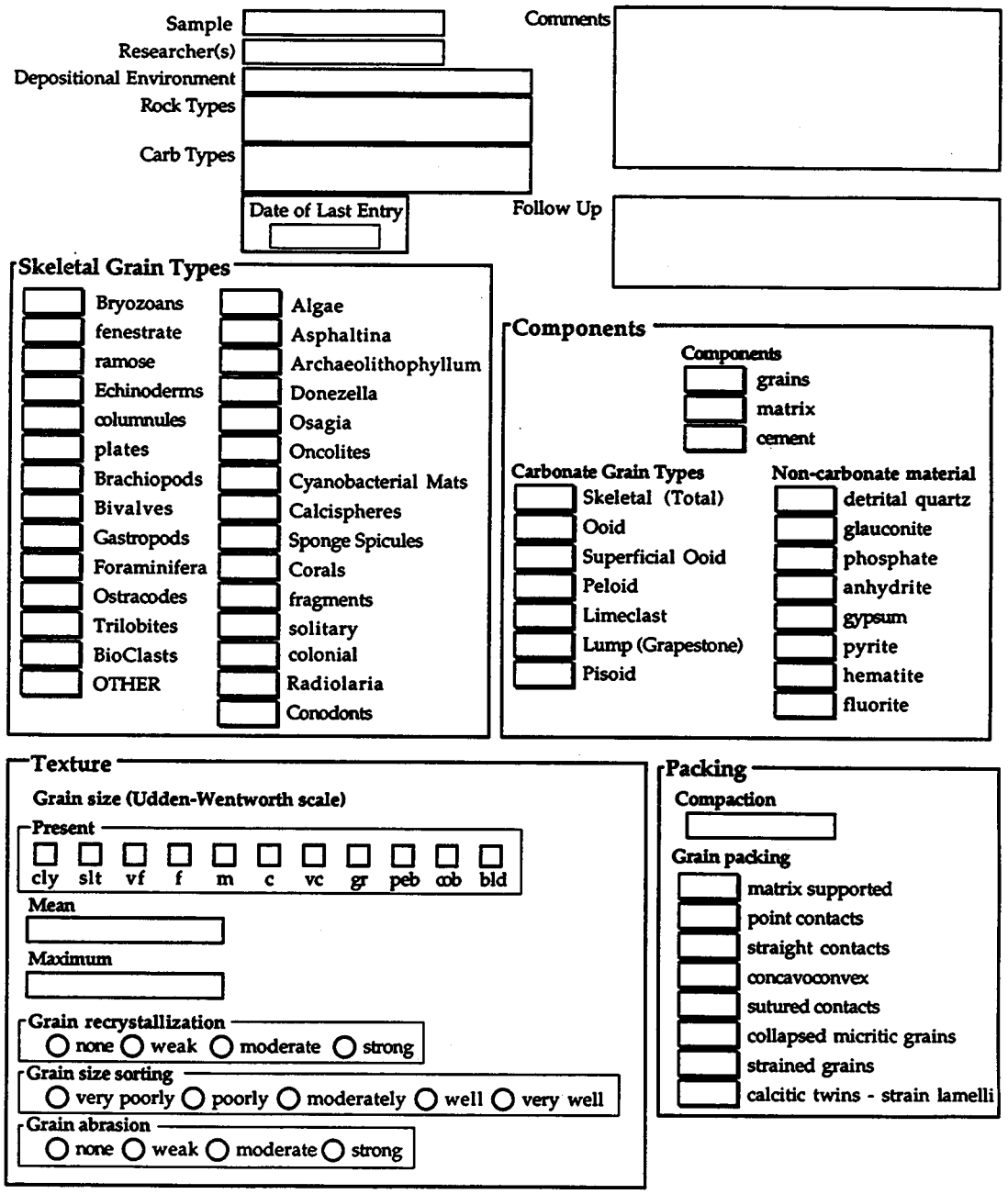

A C M R 0 - Abundant (>50%), Common (10-50%), Minor (1-10%), Rare (<1%), 0 (none), E (Exact number from point count)

(Table 1 continued on next page.)

TABLE 1 (Continued)

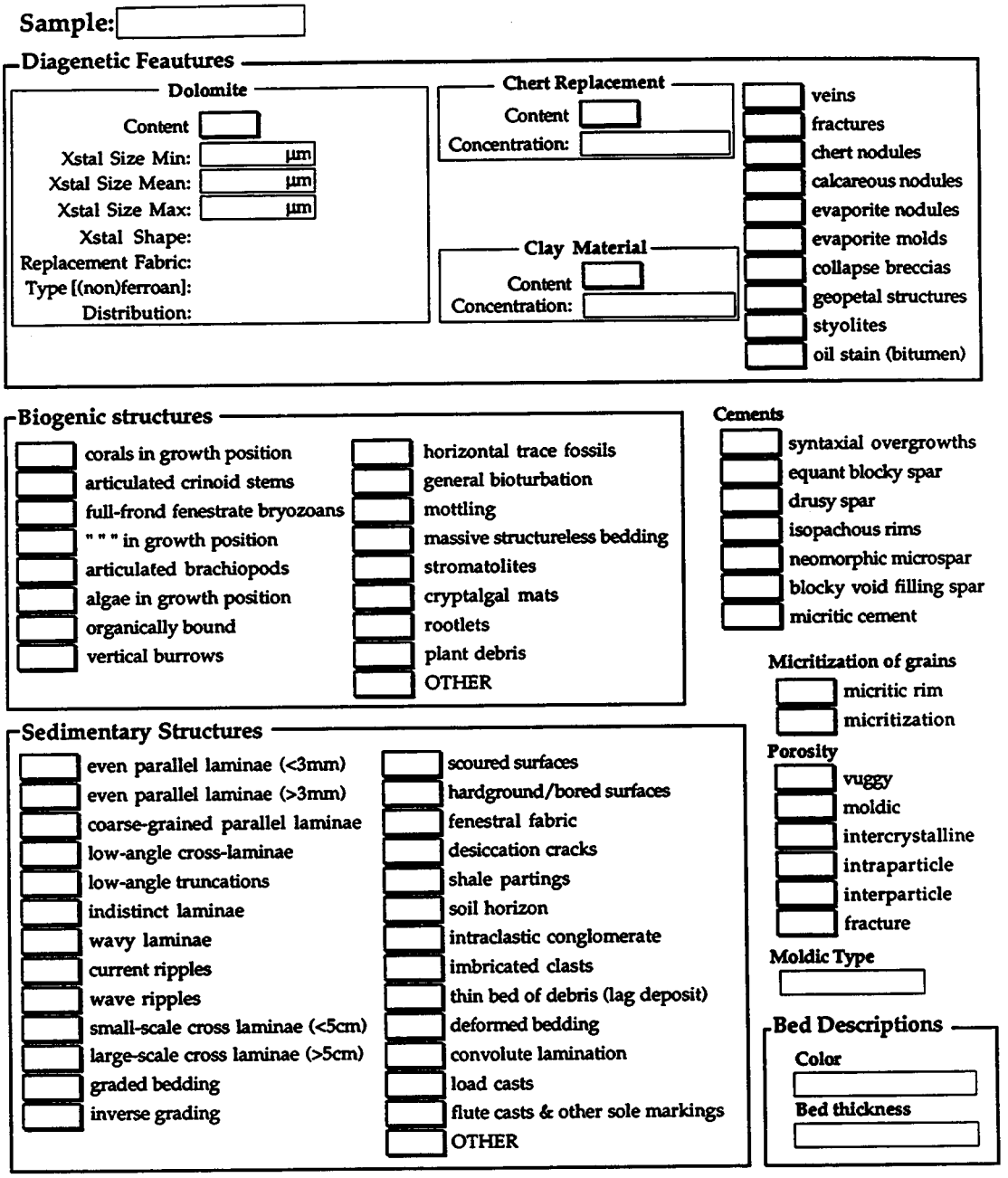

A C M R 0 - Abundant (>50%), Common (10-50%), Minor (1-10%), Rare (<1%), 0 (none), E (Exact number from point count)

Cyclicity as a Means of Correlation and Its Paleogeographic Significance

A north–south series of stratigraphic sections (Shublik Mountains, Fourth Range, and Plunge Creek) serves as a representative cross section across the south-dipping carbonate ramp upon which the Wahoo Limestone formed[1] (Figs. 2 and 3). The cyclic stratigraphy in each of these sections has been analyzed and used as a means of correlation between sections. Although individual cycles cannot always be correlated with certainty, bundles of cycles can be correlated with a higher degree of precision than is possible using biostratigraphy. The cycle correlations illustrate the lateral facies changes from shallower water paleoenvironments in the north and deeper water areas in the south. Overall, the upper Wahoo Limestone unit is regressive, transgressive, and then regressive with the

TABLE 2

Alternative Data Sheet

Sample: AK11M5.7
Researcher(s): Paul Gruzlovic
Rock Types: limestone
Carb Types: Packstone

SKELETAL GRAINS

C	Bryozoans		Coral (solitary)
C	Pelmatazoans		Coral (colonial)
M	Ostracods	M	Algae (undiff.)
	Brachiopods		Donezella
	Sponge Spicules		Asphaltina
M	Foraminifera		Bioclasts (undiff.)
M	Calcispheres	R	Fenestrate
	Gastropods		ramose
	Bivalves		OTHER
	Trilobites		

NON-SKELETAL GRAINS

	Ooid		Glauconite
	Superficial ooids	4	Pyrite
C	Peloids		Phosphate grains
	Intraclasts		Grapestone
	Oncolites		Hematite
5	Qtz sand or silt		Diagenetic quartz

MEAN GRAIN SIZE

☐ ☒ ☒ ☐ ☐
vf f m c vc

PRESERVATION OF GRAINS

Recrystalization of grains
○ none ◉ slightly ○ moderate ○ well

Grain Borings:
○ none ○ slightly ○ moderate ◉ well

Micritic Envelope Development:
partial complete
○ none ○ slightly ◉ moderate ○ well

Grain Roundness
○ well ○ moderate ◉ poorly

GRAIN SORTING
○ well ◉ moderate ○ poorly

DOLOMITE

Content: 25
Xstal Size Min: 10 µm
Xstal Size Mean: 0 µm
Xstal Size Max: 30 µm
Xstal Shape: subhedral-anhedral
Replacement Fabric: matrix

Date of Last Entry 5/3/90

CLAY MATERIAL
Content: C
Concentration: along styolites

CHERT REPLACEMENT
Content:
Concentration: grains

OIL STAIN
◉ high ○ moderate ○ low ○ none

SEDIMENTARY STRUCTURES

	Parallel laminae
	Small-scale X-laminae
	Wavy laminae
	Graded bedding
	Bioturbation
	Geopetal structures
	Stromatolite
	Fenestrae
	Birdseyes
	Breccia
	Evaporite repl. nods.
	articulated crinoid stems
	vertical burrows
	Scoured surfaces
	Imbricated clasts
	OTHER

CEMENTS

	Syntaxial overgrowths
	Equant blocky spar
	Drusy blocky spar
	Isopachous rims
	Neomorphic microspar
	Blocky spar cavity fills
	Micritic

POROSITY

	Vuggy
	Moldic
	Intercrystalline
	Intraparticle
	Interparticle
	Fracture

COMPACTION well

C	Sutured grains
	Broken rims or coats
	Strained grains
	Bent twins
C	Stylolites
wispy microstylolites	
	Fractures

Depositional Environment
lagoonal

Comments
rock type: highly dolomitic
photos: sutured and oil stained grains.

deepest-water facies situated approximately in the middle part of the unit. The smaller scale parasequences (shallowing-upward cycles) are super-imposed in these overall trends. Thus the differences are illustrated in the nature of shallowing-upward cycles that formed in shallow vs. deeper marine conditions.

Diagenetic Studies

Progress is being made at the University of Kansas in the studies of cement stratigraphy. Cathodoluminescence and other advanced techniques of analyzing variations in cementation histories have revealed several possible

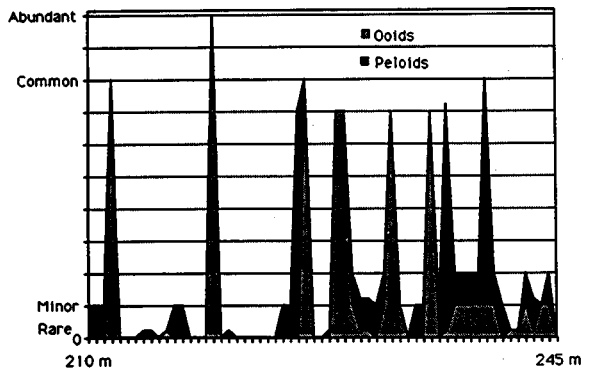

Fig. 1 Area graph generated using one of 4th Dimension's standard report forms illustrating variations in the content of ooids and peloids in the upper part of the Plunge Creek section. The cyclic variation indicates repeated migration of ooid shoals and peloidal lagoons resulting from relative sea-level fluctuations.

exposure surfaces. Limestones below the exposure surfaces are characterized by extensive early diagenetic non-ferroan calcite cements with numerous cathodoluminescent zones. In contrast, above the exposure surfaces, less abundant, early cements are uncommon and late diagenetic ferroan calcite cements generally have very dull luminescence.

Below the exposure surfaces, well-developed, early diagenetic cements apparently formed in the active freshwater phreatic diagenetic zone and preserved the loosely packed fabric between grains.[2] Thin (hairline thick), bright cathodoluminescent zones indicate that freshwater pore fluids contained manganese and other luminescent elements that were periodically precipitated under reducing conditions. Thicker dead or nonluminescent zones, alternating with the bright hairline zones, indicate that the majority of cementation occurred under oxidizing conditions. The paucity of early cements in grainstones above the exposure surfaces

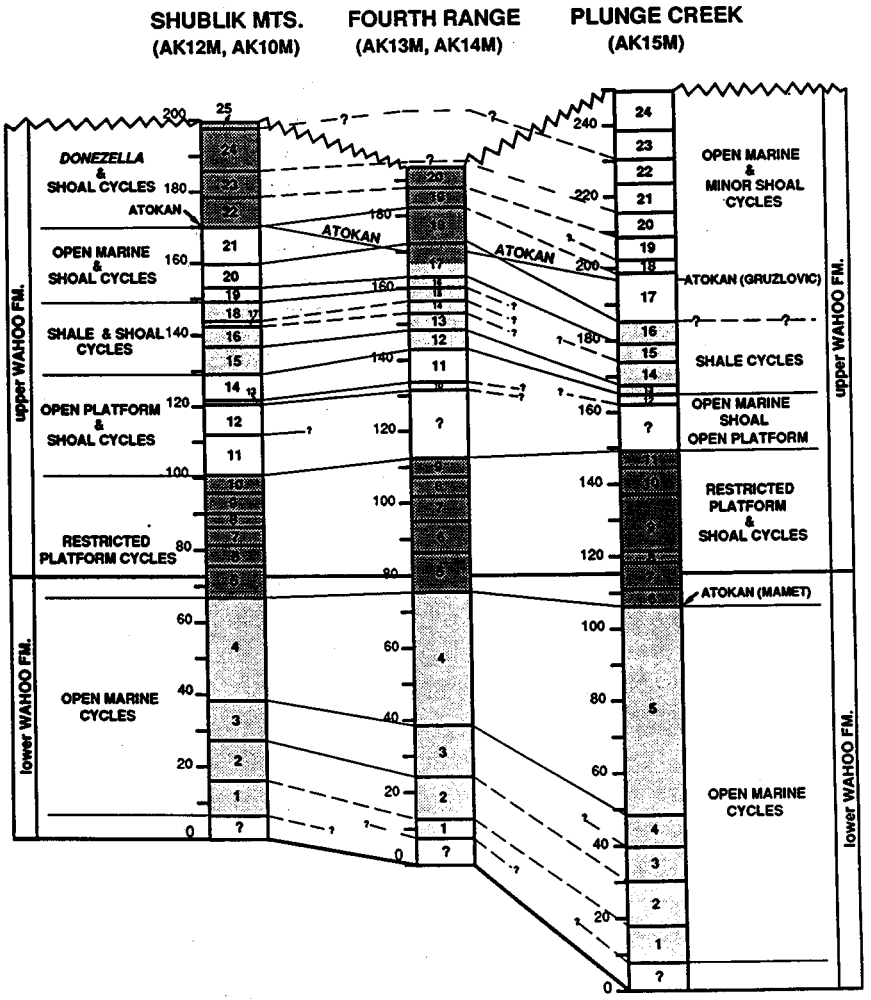

Fig. 2 Tentative correlation chart for lithographic cycles in the Wahoo Limestone illustrating how the cycles or bundles of cycles can be used as a means of detailed correlation.

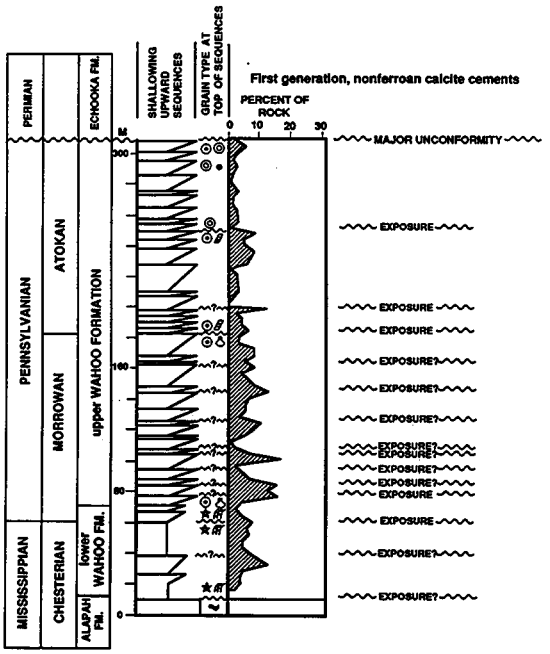

Fig. 3 Stratigraphic column showing the relationship of cyclic stratigraphy in the Wahoo Limestone to variations in cement stratigraphy and the position of suspected exposure surfaces.

indicates that such early freshwater diagenesis did not occur; this allowed these transgressive sediments to later become tightly compacted.[2]

Biostratigraphic Studies

The major accomplishments during the reporting period was setting up a lab at the University of Alaska at Fairbanks for processing conodont samples. Processing involves acid digestion of limestones to extract insoluble residues and heavy liquid separation of relatively dense conodonts from the other residues. Now that the lab has been organized, processing has begun on a backlog of samples collected during previous years. The first shipment of insoluble residues produced in the lab was sent for detailed analysis. A paper on conodont biostratigraphy of the Wahoo Limestone was presented at the annual Pander Society meeting (of conodont biostratigraphers).[3]

References

1. K. F. Watts, R. C. Carlson, P. Gruzlovic, T. A. Imm, and A. P. Krumhardt, Stratigraphic Framework and Depositional History of the Lisburne Group, Northeastern Alaska, *Geol. Assoc. Can., Programs Abstr.*, 15: A-138 (1990).
2. P. H. Heckel, Diagenetic Model for Carbonate Rocks in the Midcontinent Pennsylvanian Eustatic Cyclothems, *J. Sediment. Petrol.*, 53(3): 733-759 (1983).
3. A. P. Krumhardt and A. G. Harris, Conodont Biostratigraphy and Biofacies of the Wahoo Limestone (Carboniferous), Sadlerochit Mountains, Northeast Brooks Range, Alaska, *Geol. Soc. Am., Abstr. Programs*, 22(1): 12 (1990).

TORIS RESEARCH SUPPORT

Cooperative Agreement DE-FC22-83FE60149, Project BE2

National Institute for Petroleum and Energy Research Bartlesville, Okla.

Contract Date: Oct. 1, 1983
Anticipated Completion: Sept. 30, 1990
Funding for FY 1990: $210,000

Principal Investigator:
James F. Pautz

Project Manager:
Chandra M. Nautiyal
Bartlesville Project Office

Reporting Period: Jan. 1–Mar. 31, 1990

Objective

The objective of this project is to provide research support to the U.S. Department of Energy (DOE) Project Manager for the Tertiary Oil Recovery Information System (TORIS) in the areas of the enhanced oil recovery (EOR) project and reservoir database management, the EOR project and technology trend analysis, and oil production modeling.

Summary of Technical Progress

The trend in new EOR projects continues at a very slow rate. During the past 6 months, only five new EOR projects were identified, each with a different recovery process in three different states. The data on these five projects are shown in Table 1.

Transfer of information between computer systems and management systems is an important and challenging portion of data maintenance. One widely used data storage protocol that allows data exchange and transfer is the data interchange format (DIF) developed by Software Arts, Inc. This file standard is readable by dBase IV, RELIANCE, Lotus, and numerous other data management softwares. Unfortunately, the implementation of the DIF standard is not always consistently followed by all programs.

A variation of the implementation of DIF used by RELIANCE was identified and resolved in the NIPER data transfer program, LGRAF. The DIF format identifies the data type and then the value. For instance, the numeric value of 1 would be coded as 0,1. A slight variation of this was seen when a numeric value of 0 (zero) was transferred from RELIANCE. Instead of writing the number as 0,0, as

would be expected, RELIANCE did not write the zero value after the comma.

Normal DIF implementation	RELIANCE DIF Variation
0,0	0,

Other software capable of reading DIF provides a number after the comma and indicates an error when reading a RELIANCE-created DIF file that contains any zeroes.

TABLE 1

Summaries of the Status of Responses

Number	1	2	3	4	5
State	LA	WY	TX	TX	WY
Field name	Paradis	Wolf Draw	Sabine Tram	Stocum	Creek's Gap
Field code	539151	012313	623046	661557	171457
Operator	Texaco	Delcalta International Corp.	ARCO	Dallas Gas & Elect.	World Oil
Start date	1989	1989	1990	1990	11-90
Code	311	230	321	120	313
Process	CO_2 miscible	Polymer	Hydrocarbon	Steamflood	CO_2 cyclic
Area, acres			2010	65	
Reservoir formation	AB-1-sand 16	Upper Minnelusa "B"	Wilcox	Carrizo	Dakota
Production wells	2	4	7	70	1
Injection wells	3	1	1	13	1
Litho.	55	55	55	55	55
Depth, ft	9950	7260	11500	600	4910
Porosity, %	24.0		14.0	36	18
Permeability, mD	245	86	27.5	1200	300
Viscosity, cP		17.8	0.1	1200	1.0
Temperature, °F		145	271	72	150
Total prod. rate, bbl/d			550		
EOR rate, bbl/d			0		
Gravity, °API	38	21.5	49	19	38
Net pay, ft	10	18.6		30	60
Original pressure, psi		1636			
Current temperature, °F		223			
S_o,%				53	
S_w,%		21.7			
Pattern area, acres		40	320	5	
County			Newton	Anderson	Fremont
Remarks	Push–Pull				

THREE-PHASE RELATIVE PERMEABILITY

Cooperative Agreement DE-FC22-83FE60149, Project BE9

National Institute for Petroleum and Energy Research
Bartlesville, Okla.

Contract Date: Oct. 1, 1985
Anticipated Completion: Sept. 30, 1990
Funding for FY 1990: $305,000

Principal Investigators:
Matt Honarpour
Dan Maloney

Project Manager:
Edith Allison
Bartlesville Project Office

Reporting Period: Jan. 1–Mar. 31, 1990

Objectives

The objectives of this project are to improve the reliability of laboratory measurements of three-phase relative permeability for steady- and unsteady-state conditions in core samples and to investigate the influence of rock, fluid, and rock–fluid properties on two- and three-phase relative permeabilities.

Summary of Technical Progress

Sample Characterization

Pore and grain size distributions were determined for samples of the 2400-mD Bentheimer, 2000-mD Berea, and 700-mD Berea sandstones. Five hundred pores and 500 grains for each sample were measured by evaluating thin sections with the aid of a microscopic image analysis system. The grain and pore size distributions for each sample were found to be well approximated by lognormal distribution functions. Grain size distributions by number percent are shown in Fig. 1. Note that the y-axis is a log scale while the x-axis is a normal probability scale. The

Bentheimer sandstone had slightly larger grains than the two Berea samples, whereas the grain size distributions for the two Berea samples were almost identical. Pore size distributions are shown in Fig. 2.

Table 1 presents sizes corresponding to 84, 50, and 16 percentile values as well as σ results where

$$\ln \sigma = 0.5 \ln \left(\frac{d_{84}}{d_{16}} \right) \quad (1)$$

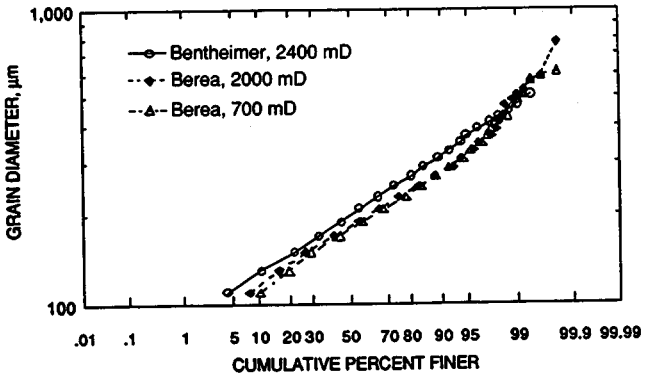

Fig. 1 Grain diameter distributions for Bentheimer and Berea sandstones.

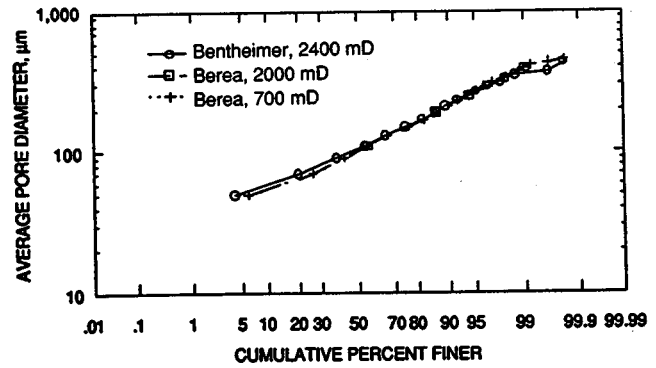

Fig. 2 Pore diameter distributions for Bentheimer and Berea sandstones.

As shown in the pore size data in Fig. 2 and Table 1, the pore size distributions for all three samples were very similar. Porosimetry tests are in progress to characterize the pore throat distributions for the three samples by mercury injection at pressures from 1 to 50,000 psia.

Centrifuge Capillary Pressure Experiments

Further centrifuge capillary pressure experiments were performed to compare the 2000-mD and 700-mD fired Berea sandstones. The samples were tested in heat-shrink Teflon tube sleeves to prevent radial fluid transfer during low centrifuge rotational speeds. Data for each sample were recorded at rotational speeds causing capillary pressures within the 0 to 6 psi range. Stabilization times of 24 h were allowed prior to recording data at each rotational speed during the first and second drainage and first imbibition cycles. A stabilization time of 1 h was allowed before recording data for the second imbibition and third drainage cycles. The 1-h stabilization time was selected as a means for evaluating the effect of equilibration time on capillary pressure results. The Hassler–Brunner approximation was used to calculate capillary pressures from the test data. Wettability results were calculated using the U.S. Bureau of Mines technique. Capillary pressure results are shown in Figs. 3 and 4.

As shown in Figs. 3 and 4, the 700-mD sample exhibited higher residual water and mineral oil saturations than the 2000-mD sample. The residual oil saturation for the 2000-mD rock was lower after the second and subsequent drainage cycles than that during the first drainage cycle. Data for the second and third drainage cycles for the 2000-mD Berea were almost identical, even though third drainage cycle data points were allowed only 1 h for stabilization. Drainage first and second cycle data for the 700-mD Berea were nearly identical, as were the data from both imbibition cycles. Wettability indices varied from 0.48 to 0.83 for both Berea sandstones from high and low capillary force tests. Results from tests with short stabilization times tended toward the lower wettability indices, erroneously implying lesser water-wet behavior.

Relative Permeability Measurements

A steady-state oil–water relative permeability experiment was performed on the 700-mD Berea sandstone using 1-cP

TABLE 1

Lognormal Distribution Function Characteristics for Bentheimer and Berea Sandstones

	Grain size, µm				Pore size, µm			
Permeability, mD	d_{84}	d_{50}	d_{16}	σ	d_{84}	d_{50}	d_{16}	σ
Bentheimer, 2400	290	203	140	1.439	181	105	66	1.656
Berea, 2000	253	184	130	1.395	180	105	60	1.732
Berea, 700	253	177	124	1.428	160	94	64	1.581

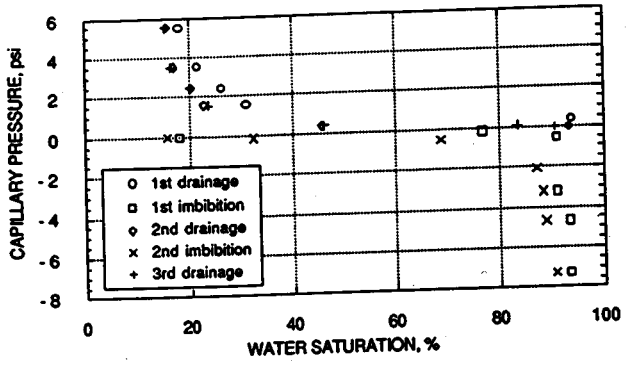

Fig. 3 Capillary pressure results for 2000-mD Berea.

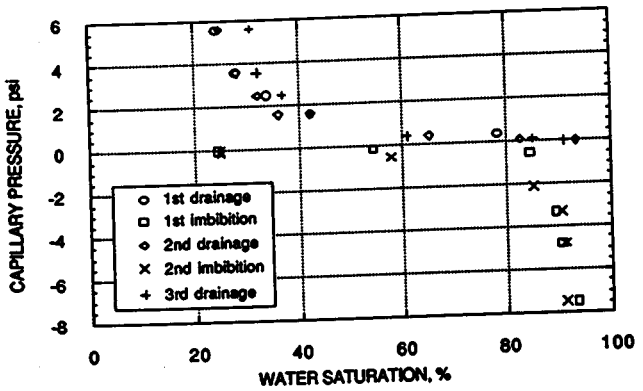

Fig. 4 Capillary pressure results for 700-mD Berea.

brine (1% by weight NaCl in water) and 1.4-cP oil tagged with 10% by weight iodododecane (X-ray tag). Four wire electrode resistivity and pH measurements were taken as the rock was initially flooded with brine at a pH of 7.3. The initial resistivity for the sample was 6.2 Ω-m, and the pH of the effluent from the rock was 11.33. The high pH of the effluent from the rock was the result of having fired the rock at 1000°C to stabilize clays. The high temperature is known to convert calcite and dolomite to CaO and MgO. After 2.3 pore volumes (PV) of brine were allowed to flow through the rock, the pH dropped to 11.2, and the resistivity increased to 6.8 Ω-m. The pH continued to drop to 10.4 after an additional 54 PV of brine was pumped, whereas the resistivity remained essentially constant. Mineral oil and brine permeabilities were measured for both drainage and imbibition cycles (decreasing and increasing wetting phase saturation). Four electrode resistivity measurements were recorded along with the permeability data. Saturations were determined using X-ray and microwave absorption techniques. For each steady-state saturation measurement, X-ray scans were taken for tube potential and current settings of 35 kV/10 mA and 45 kV/10 mA using a tungsten filament X-ray tube. The 35-kV tube potential was selected to be close to the "K" excitation potential of the iodine X-ray tag (33.2 kV) to give good contrast between the oil and brine. The emergent intensity of the X ray with the tube potential set at 45 kV was decreased by placing a lead filter in front of the beam as it emerged from the tube. The saturations calculated from the microwave data and 45-kV X-ray data were in excellent agreement. The 35-kV X-ray data were determined to be of little use for calculating fluid saturations. All subsequent X-ray scans on this rock will be performed with the tube potential set at 45 kV.

Figure 5 shows the permeability results, and Fig. 6 shows a plot used to calculate saturation exponents from the resistivity data. As shown by the two figures, saturation-dependent hysteresis is evident in both permeability and resistivity data. Additional drainage and imbibition cycles are in progress to investigate hysteresis effects.

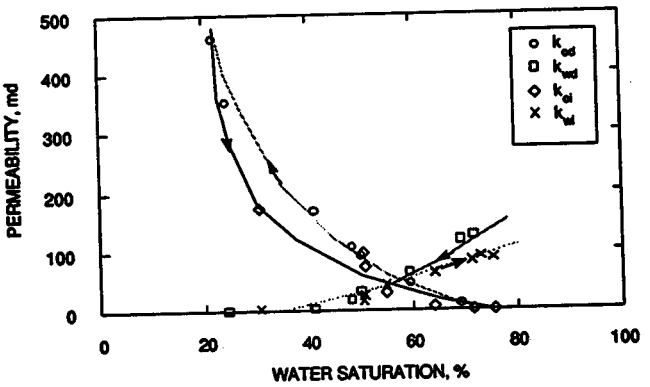

Fig. 5 Oil–water effective permeability tests results for 700-mD fired Berea.

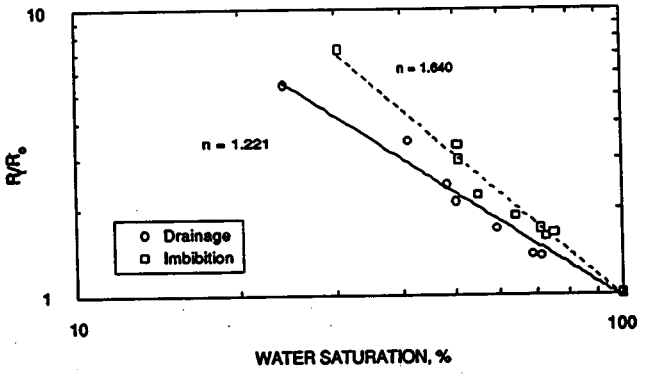

Fig. 6 Resistivity index vs. water saturation for 700-mD fired Berea measured during steady-state relative permeability tests.

RESERVOIR ASSESSMENT AND CHARACTERIZATION

Cooperative Agreement DE-FC22-83FE60149, Project BE1

National Institute for Petroleum and Energy Research
Bartlesville, Okla.

Contract Date: Oct. 1, 1985
Anticipated Completion: Sept. 30, 1990
Funding for FY 1990: $800,000

Principal Investigator:
Matt Honarpour

Project Manager:
Edith Allison
Bartlesville Project Office

Reporting Period: Jan. 1–Mar. 31, 1990

Objective

The objective of this project is to develop an improved methodology for effective characterization of barrier island reservoirs to predict oil saturations at interwell scales and flow patterns of injected and produced fluids.

Summary of Technical Progress

Progress was made in the following areas:

1. A second oil reservoir, Patrick Draw field, was selected for study because it meets requirements for further development of a generalized shoreline barrier model.

2. A method for improved reservoir evaluation for designing successful recovery projects was developed through systematic collection and integration of inexpensive, conventional production–injection data using the Hall plot method when knowledge of geological heterogeneities was available.

3. A method based on the difference between material balance and volumetric calculations of oil in place (OIP) was developed to identify heterogeneities in drainage areas of wells.

4. Comparisons of results of X-ray-diffraction (XRD) analyses conducted at the National Institute for Petroleum and Energy Research (NIPER) with those previously published indicate substantial similarities in mineralogy for upper Almond formation reservoir sandstones. Kaolinite and lesser amounts of illite are the dominant authigenic clays in upper Almond sandstones.

5. On the basis of dip-oriented, core-calibrated log correlations, the main producing sandstone units within the Almond formation at Patrick Draw field can be distinguished. In addition, producing sandstone UA-5 can be distinguished from the UA-6 sandstone, which is thin in the southern part of the field but is a good producer in the northern part of the field.

Selection of a Second Shoreline Barrier for Testing NIPER Reservoir Characterization Methodology

The process used to select the second reservoir for testing NIPER's reservoir characterization methodology was presented to the Bartlesville Project Office (BPO) Project Manager, and tentative approval for studying the Almond formation at Patrick Draw (Wyoming) field was obtained. At the United States Geological Survey (USGS) core-storage facility in Denver, Upper Cretaceous Almond formation cores from Patrick Draw field were examined. The objective of this examination was to evaluate the quality of 34 slabbed cores from wells primarily in the Arch Unit of Patrick Draw field for the development of a generalized shoreline barrier model and comparison with the Muddy formation at Bell Creek (Montana) field. It was concluded that the Arch Unit of Patrick Draw field represents a mesotidal setting, whereas Bell Creek field is a microtidal shoreline barrier. The internal architectures of barriers deposited in these tidal regimes differ in varying degrees in type of facies, vertical sequence of facies, and lateral continuity of productive sandstone.

Union Pacific Resources Co., the operator of Patrick Draw field, was visited to examine the quality of geological and engineering data for the development of a generalized shoreline barrier model. It was learned that adequate core analyses and production–injection data are available for both the Arch and Monel units. However, few well test data were collected in this field.

Patrick Draw field, located in the Greater Green River Basin in southwestern Wyoming, was selected for study as a second barrier island reservoir. Selection was based on the following considerations: (1) the Almond formation in Patrick Draw field meets depositional history requirements for study, (2) an abundance of information from previous studies and cores is available from the field, and (3) a cooperative response was received from Union Pacific Resources Co.

Studies of the Almond formation will provide data on component facies of a barrier–strand plain system and allow generalization of the model and methodology developed in Bell Creek. These improvements will extend capabilities to other reservoirs producing from barrier–strand plain deposits. A report[1] on the selection of the reservoir is being prepared.

Verbal agreement for releasing reservoir data from Patrick Draw field was given by Union Pacific Resources; however, no written agreement has been received. A representative of that company has indicated that transfer of information will probably occur in June 1990.

More log and completion information about Patrick Draw field was received which represents virtually all the

data that were available from the USGS. Compilation of all the collected data for a computer data file was continued.

A shoreline barrier literature database was initiated and is being continually updated. It now contains the collected references about the Almond formation, Patrick Draw field, petrography of barrier sediments, and formations and specific fields considered during the search for a second barrier reservoir to study.

Data from Patrick Draw field are being entered into a spreadsheet data file as they are collected. This organized, digitized form allows easy access to data for any purpose, including direct input of various parameters into computer mapping, log analysis, statistical analysis, graphics, and simulation programs. Direct transfer into a multipurpose geological database will be possible when the database becomes available.

The following parameters for 200 wells have been input into the spreadsheet data file:

1. Location (section, township, range, footage from section lines).
2. Elevation (ground level and Kelly bushing).
3. Core information (slabbed or full, interval cored, photographs available/on hand, percent core recovered, quality of core).
4. Total depth and tops of formations (Lance, Fox Hills, Lewis, Almond, and Erickson).
5. Logs run.
6. Well status (gas–oil producer, gas–water injector, shut-in, plugged and abandoned, temporarily abandoned, dry and abandoned, never drilled).
7. Initial production (perforated zones, perforation density).
8. Oil gravity.

Additional data on wells and engineering and production data will be added as they become available.

Production–Injection Analysis in the TIP Area, Bell Creek Field

Geological heterogeneities controlling fluid flow paths in the U.S. Department of Energy (DOE) Tertiary Incentive Project (TIP) area in Unit A of Bell Creek (Montana) field were identified and described with injection, production, pressure, pressure falloff, and pulse test data. Monthly injection rates and production data, over a period of 10 yr of line-drive waterflooding followed by 6 yr of 20-acre, five-spot, water and micellar–polymer injection, were analyzed with the Hall plot method.[2] Mathematical simulation results were integrated with information obtained from geological analysis and provided an improved interwell formation characterization. This integrative approach provided information about interwell reservoir properties, such as directional transmissivities, fluid-flow pattern, residual oil saturation, degree of continuity, presence of flow barriers, and permeability conduits.

In the TIP area, analysis of the injection data with the Hall method provided distinct directional formation transmissivity for the preflush, micellar, and polymer stages of injection. Analyses of pressure–pulse and falloff tests conducted before the application of the chemical flood provided a baseline for comparing directional flow characteristics. The influence of various geological heterogeneities, such as faults–permeability variations on fluid flow characteristics of the reservoir at various stages of line-drive waterflooding and chemical flooding, was identified. The results show good agreement with complementary information obtained from geological, petrophysical, and petrographical analyses. They also indicate that the effects of micellar and polymer adsorption/retention on fluid-flow characteristics of a reservoir can be quantified with the Hall plot method.

Long-term, predicted performances of chemical-injection wells based on short-term preflush performances (Region I) and long-term actual performances of chemical-injection wells (Region II) when postflush water injection was resumed were analyzed and are presented in Fig. 1. These performances were superimposed on long-term water-injection performances of all water-injection wells. The results showed that chemical-injection wells were initially similar in performance to water-injection wells. In fact, they exhibited better performance than most of the water-injection wells. The postflush performance of chemical-injection wells was similar to the performance of lower quality, diagenetically effected wells in the TIP area. The application of the micellar–polymer process reduced permeability contrast and magnitude of permeability by factors of 3 to 5. These performances were attributed to filtering/adsorption/retention of the injected polymer and reduction of permeability as a result of chemical injection.

It was also concluded that in the TIP area of Bell Creek field, faults behaved as sealing or semisealing barriers in the

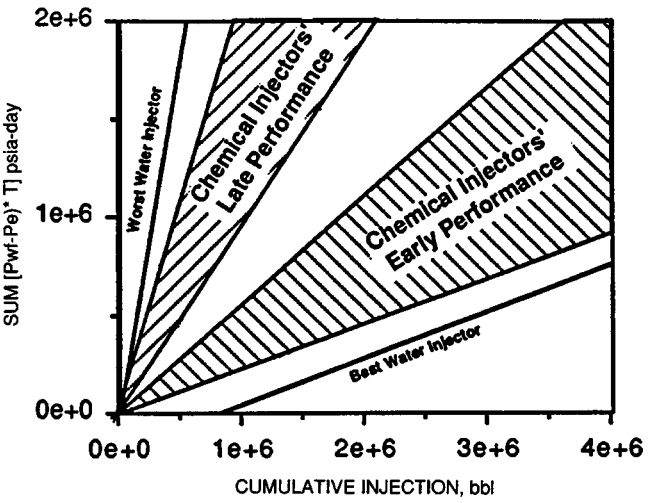

Fig. 1 Superposition of projected Hall plot chemical injection wells based on their early performance and their actual performance on Hall plot of water injection wells.

SW-NE direction and as a permeability conduit in the NW-SE direction. In addition, faults affected residual oil saturation distribution after line-drive waterflooding.

Application of Differential Oil in Place to Quantify the Effect of Geological Heterogeneities on Oil Production

A method was developed to calculate the differential oil in place (DOIP) of each well in a given reservoir. A well DOIP is defined by the equation: DOIP = volumetric oil in place (OIPV) at a given spacing minus material balance equation (MBE) OIP (OIPM). Equations for the OIPV and MBE analysis are given in Ref. 3. The DOIP is an indicator of the variation of individual well OIP, which could be the result of a variety of reasons. The OIPV can be considered a static evaluation based on petrophysical (core and log) data. OIPM, on the other hand, represents the effective or recoverable OIP of a well from production data, and, in this sense, the MBE computation is dynamic.

A highly positive DOIP will indicate more reserves than calculated by production data, and the drainage efficiency in the area is probably low. A highly negative DOIP will indicate that a well is draining more oil than is expected from the volumetrics.

Geologically, positive DOIP could be the result of a variety of reasons, such as high clay content, faults, or different types of flow barriers, whereas negative DOIP may imply production affected by highly permeable clean sands, fractures, etc. The essence of the proposed DOIP method is the use of MBE to compute OIP for an individual well and compare that with the OIPV (Ref. 4).

The computer MBE program developed earlier was used to analyze all available production data from wells in sections 22, 23, 26, 27, and 28. For the calculation of OIPV, available spontaneous potential, induction, sonic, density, and gamma-ray logs from the same 44 wells were interpreted to calculate porosity, clay content, pay thickness, and initial water resistivity and water saturation. These reservoir parameters, calculated at every foot interval, have been used to calculate the OIPV for 40-acre areas surrounding each well by the application of Simandoux's method. Where available, laboratory-measured porosity values, after compaction correction, have been used for cross-checking log-derived values. Results of volumetric OIP (OIPV), OIPM, and differential OIP (DOIP) are given in Table 1. Several potentially useful indexes also have been computed and are shown in the same table. They are relative differential OIP (RDOIP = DOIP/OIPV), ratio of OIPM to volumetric OIP (OIPM/OIPV), and effective well drainage area (area MBE). Effective drainage area is calculated by using the volumetric equation and the computed OIPM. Shown at the bottom of the table are the mean, standard deviation, mean – standard deviation, and mean + standard deviation of each related variable. The average OIPV is 798,000 stock tank barrels (STB) vs. 731,000 STB for OIPM. The average DOIP is 67,000 STB with a relative DOIP of 0.034, which indicates that each average well in the study area is draining slightly less than indicated by volumetric calculations. Note that the mean effective well drainage area is about 39 acres, which matches quite well with the expected 40-acre well spacing. This close agreement indicates that the five sections as a whole unit are draining nearly 40 acres for each well.

A plot of preliminary results of DOIP calculations for 44 wells in the study area is shown in Fig. 2. Areas with marked positive and negative DOIP anomalies are indicated. Two of the striking positive and negative anomalies are located along the depositional strike of the main sand body. The geological heterogeneities corresponding to the various anomalies are being studied. Preliminary analysis indicates that the pore drainage in section 22 is probably due to high clay content, whereas the large negative anomaly in sections 26 and 27 occurs in areas with very high permeabilities and relatively low clay content.

On the basis of current findings, the newly developed DOIP method can be used to (1) quantify the effect of geological heterogeneities on oil production; (2) characterize drainage efficiency of each well and its effective drainage area; (3) determine optimal well spacing in each section of a given reservoir; and (4) determine best injection and production well locations for waterflood, infill, and EOR programs. Two distinct advantages of this DOIP method are indicated as follows: (1) it requires only readily available production and basic petrophysical data; that is, the method is inexpensive and efficient; and (2) it can be applied at or before the end of primary production; that is, valuable reservoir information can be obtained early during the producing life of a reservoir and used prior to planning and implementation of waterflood, infill, and EOR programs.

Mineralogical Composition of the Almond Formation

Four upper Almond sandstone samples from Patrick Draw field were analyzed by XRD. The results (Table 2) have been compared with those of Keighin, Law, and Pollastro[5] who analyzed sandstone and shale samples from the upper portion of the Almond formation. The current samples (Table 2) tend to provide results similar to the shallow upper Almond samples (Table 3) in that quartz is the dominant mineral. Total average carbonate comprised 20% of the sandstone in the Keighin et al. study, whereas average carbonate was 39% in the four Patrick Draw samples. Feldspar, dominated by potassium-rich varieties, averaged 3.75 to 5%. Total clay content from shallow upper Almond samples in the Keighin et al. study averaged 18% and was dominated by kaolinite. The four Patrick Draw samples averaged only 3% total clay, but the samples were dominated by kaolinite.

A comparison of the two data sets (Tables 2 and 3) indicates that sandstones in Patrick Draw reservoir tend to

TABLE 1

Analysis of Differential Oil in Place in Bell Creek Field*

No.	Well name	OIPV, STB	OIP MBE, STB	DOIP, STB	RDOIP, frac	OIPM/OIPV, frac	Area MBE, acres
1	2201	824,014	791,593	32,421	0.0393	0.9607	38.43
2	2203	788,405	754,177	34,228	0.0434	0.9566	38.26
3	2205	822,901	753,675	69,226	0.0841	0.9159	36.64
4	2208	1,250,205	841,785	408,420	0.3267	0.6733	26.93
5	2209	1,157,382	1,012,221	145,161	0.0254	0.8746	34.98
6	2210	1,030,901	862,532	168,369	0.1633	0.8367	33.47
7	2211	1,243,829	734,009	509,820	0.4099	0.5901	23.60
8	2212	904,083	842,099	61,984	0.0686	0.9314	37.26
9	2213	1,121,054	546,942	574,112	0.5121	0.4879	19.52
10	2214	1,157,795	683,915	473,880	0.4093	0.5907	23.63
11	2216	1,009,824	1,134,693	–124,869	–0.1237	1.1237	44.95
12	2301	181,272	201,628	–20,356	–0.1123	1.1123	44.49
13	2303	810,311	682,370	1,227,941	0.1579	0.8421	33.68
14	2304	855,264	859,990	–4,726	–0.0055	1.0055	40.22
15	2305	939,229	886,498	52,731	0.0561	0.9439	37.75
16	2307	543,487	510,902	32,585	0.0600	0.9400	37.60
17	2310	440,239	565,837	–125,598	–0.2853	1.2853	51.41
18	2312	1,098,195	884,846	213,349	0.1943	0.8057	32.23
19	2314	997,236	705,679	291,557	0.2924	0.7076	28.31
20	2316	425,768	418,814	6,954	0.0163	0.9837	39.35
21	2601	425,407	327,334	98,073	0.2305	0.7695	30.78
22	2603	877,863	880,147	–2,284	–0.0026	1.0026	40.10
23	2604	1,122,719	1,534,428	–411,709	–0.3667	1.3667	54.67
24	2606	525,599	511,072	14,527	0.0276	0.9724	38.89
25	2607	588,598	622,952	–34,354	–0.0584	1.0584	42.33
26	2608	509,402	646,703	–137,301	–0.2695	1.2695	50.78
27	2609	394,353	489,481	–95,128	–0.2412	1.2412	49.65
28	2610	484,131	633,073	–148,942	–0.3076	1.3076	52.31
29	2612	1,017,402	1,017,526	–124	–0.0001	1.0001	40.00
30	2615	711,604	427,524	284,080	0.3992	0.6008	24.03
31	2616	406,153	532,093	–125,940	–0.3101	1.3101	52.40
32	2702	964,268	912,920	51,348	0.0533	0.9467	37.87
33	2703	1,033,282	642,351	390,931	0.3783	0.6217	24.87
34	2704	1,083,653	7,629,251	320,728	0.2960	0.7040	28.16
35	2705	1,982,850	722,506	260,344	0.2649	0.7351	29.40
36	2707	925,039	839,779	85,260	0.0922	0.9078	36.31
37	2709	637,893	1,112,908	–475,016	–0.7447	1.7447	69.79
38	2711	744,419	603.056	141,363	0.1899	0.8101	32.40
39	2712	900,765	839,090	61,674	0.0685	0.9315	37.26
40	2714	612,817	747,150	–134,333	–0.2192	1.2192	48.77
41	2715	623,456	1,139,464	–516,008	–0.8277	1.8277	73.11
42	2716	482,500	660,656	–178,156	–0.3692	1.3692	54.77
43	2808	703,903	423,390	280,513	0.3985	0.6015	24.06
44	2816	761,195	469,712	291,483	0.3829	0.6171	24.78
Mean		798,197	731,192	67,005	0.0340	0.9660	38.74
Standard deviation		265,172	242,522	234,321	0.2912	0.2912	11.65
Mean – standard deviation		533,025	488,670	–167,316	–0.2572	0.6748	26.99
Mean + standard deviation		1,063,369	973,714	301,326	0.3252	1.2572	50.29

*OIPV, volumetric oil in place; STB, stock tank barrels; OIP, oil in place; MBE, material balance equation; DOIP, differential oil in place; RDOIP, relative differential oil in place; OIPM, material balance equation oil in place.

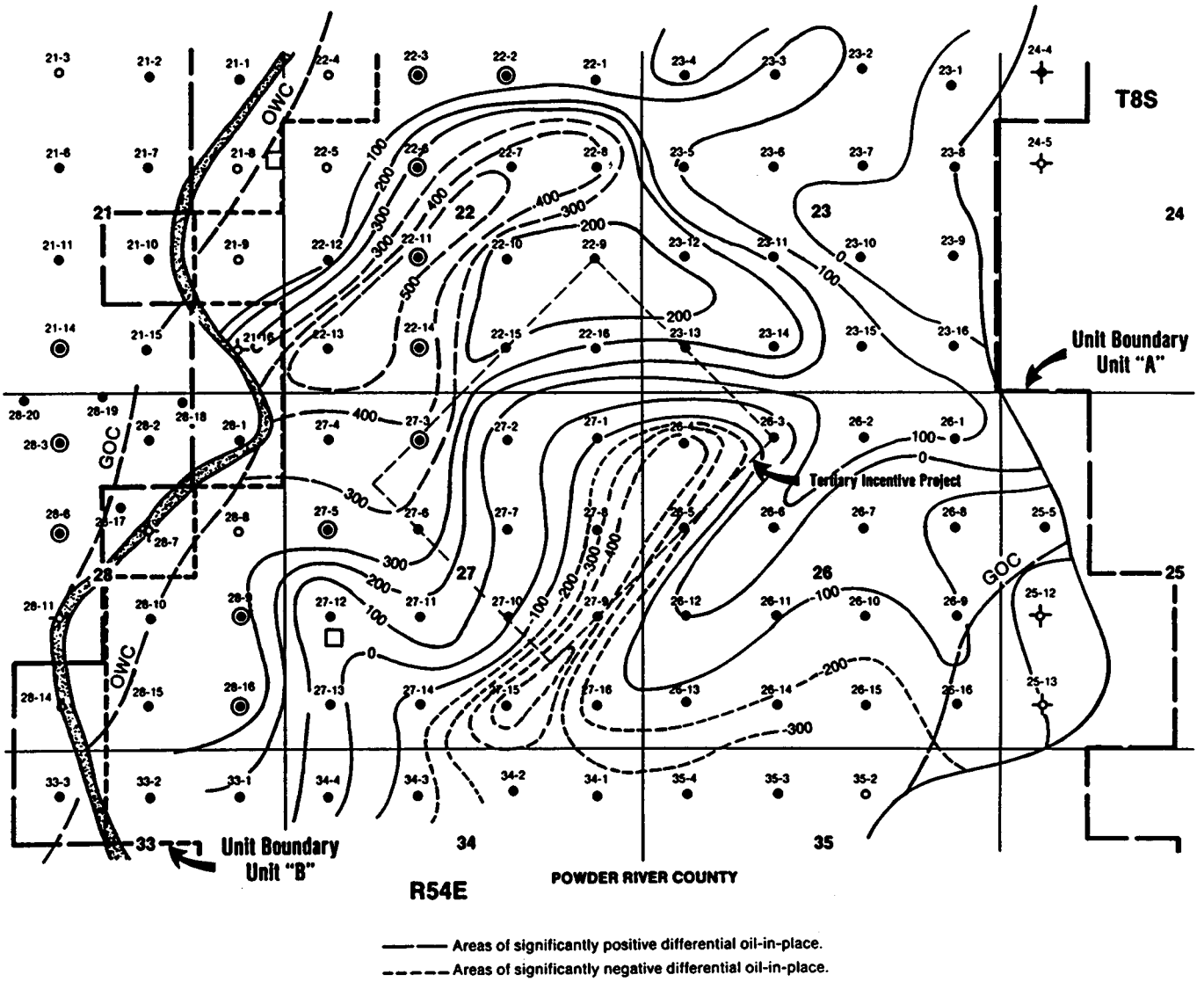

Fig. 2 Differential oil in place for the four sections surrounding the Tertiary Incentive Project area. Contours are in thousand of barrels oil difference between material balance equation and volumetric methods of oil-in-place calculation.

TABLE 2

Rock X-Ray-Diffraction Analysis (in weight percent) for Samples from Patrick Draw Upper Almond Formation Core Samples

Well	Depth, ft	Quartz	Plagioclase	K Feldspar	Calcite	Dolomite	Ferroan dolomite	Siderite	Pyrite	Kaolinite	Illite/mica	Illite/ smectite
7-18-1*	4945	61	4	4	3		21		3	3	1	tr
45-14-3†	4450	5		tr	93		tr			2	tr	tr
49-1-3‡	4515	69		2	1	10	15		1	1	1	tr
74-14-6§	4305	78	2	3	5	5	tr	2	1	2	2	tr

*Tightly-cemented, cross-laminated sandstone.
†Oyster rubble in silty, fine sandstone.
‡Faintly cross-laminated fine sandstone.
§Ripple-laminated sandstone and interbedded mudstone.

TABLE 3

Range and Mean of Rock X-Ray-Diffraction Analyses (in weight percent) of 46 Sandstone and 30 Shale Samples from the Upper Almond Formation*

	Shallow core samples†		Deep core samples‡	
	Sandstone	Shale	Sandstone	Shale
Quartz				
Range	25–81	22–52	38–91	22–43
Mean	57	37	67	33
Clay				
Range	13–25	44–67	3–26	47–72
Mean	18	51	8	59
Carbonates				
Range	0–55	0–19	0–42	0–31
Mean	20	10	12	5
Calcite	8	2	3	1
Dolomite	4	5	3	3
Ankerite	8	<1	6	<1
Siderite		<1	<1	1
Feldspar				
Range	0–15	2–5	0–12	1–6
Mean	5	3	3	3
Pyrite				
Mean		2		2

*From Ref. 5.
†Shallow core samples, 4,500–7,500 ft, 1,372–2,287 m.
‡Deep core samples, 9,600–13,700 ft, 2,928–4,178 m.

contain more carbonate minerals and less quartz than do upper Almond sandstones, which are buried to greater depths east of Patrick Draw. Quartz, however, is the dominant mineral [except in sample 45-14-3 (50 ft)], which is from an oyster rubble bed. K-feldspar is dominant over plagioclase, kaolinite is the dominant clay mineral, and illite as well as mixed-layer illite/smectite is present. Carbonates reported by Keighin et al.[5] included calcite, dolomite, ankerite, and siderite. They also noted that the amount of carbonate in the sandstone (most of which is authigenic in origin) varies greatly on the scale of a few inches. Excluding the sample from an oyster bed, calcite comprises less than 5 wt % in the four Patrick Draw samples indicated in Table 2; however, the combination of dolomite and ferroan dolomite comprised as much as 25% in one sample. Total carbonate content ranges from 12 to 93 wt % of the samples and is dominated by ferroan dolomite. The amount of dolomite from samples listed in Table 2 is much greater than that indicated by Keighin et al. The abundant ankerite reported in Table 3 is probably what is referred to as ferroan dolomite. There appears to be a complete solid solution series between ankerite, $Ca(Mg,Fe)(CO_3)$, and dolomite, $CaMg(CO_3)$, within Almond formation sandstones.

In a study of porosity occlusion in Upper Cretaceous sandstones from the Rocky Mountain Region (including the Almond formation), Jacka[6] noted that tops and bottoms of progradational barrier island sandstone bodies commonly exhibit greater concentrations of calcite cement than middle (foreshore beach and surfzone) intervals. Jacka concluded that calcite cement in the Upper Cretaceous barrier island sandstones of the Rocky Mountains is a function of the abundance of calcite nuclei upon which the calcite crystals can grow. Calcite nuclei may be provided by oyster fragments, disaggregated Inoceramus prisms, and planktonic and benthic foraminifera.

Petrographic analysis of Almond formation outcrop thin sections by Pryor[7] indicate a very similar mineralogical composition as compared with the XRD analyses by Keighin et al. Point count analysis by Pryor indicates an immature chert arenite composition for outcropping upper Almond sandstones.

Distribution of Geological and Petrophysical Properties in Patrick Draw Field

Investigation of the geological characteristics and the distribution of petrophysical properties of the barrier island sandstone deposit in Patrick Draw field was initiated by constructing a dip oriented stratigraphic section from log data in the north central part of the field. Lithological descriptions of cores performed by NIPER geologists are available from eight wells along this section to calibrate and correlate log signatures of the dominant geological features of the productive upper Almond sandstone formation. The main producing reservoir sandstone in this area is the UA-5 sandstone, interpreted to be a shoreline deposit. The sandstone deposit is composed of two sandstone bodies or "bars" separated from each other by a zone where the sandstone is absent. Below the UA-5 sandstone is a cyclic sequence of shales, sandstones, and coals that are distinguishable from combined studies of induction, gamma-ray, sonic, and density logs. The UA-6 sandstone, which is a sandstone unit from one of the cycles of sedimentation, is very thin or absent in this area but is a good producer from the northern part of Patrick Draw field.

The oyster-bearing shaley layer at the top of UA-5 sandstone, present along most parts of the section, is distinguishable by its characteristic high resistivity "kick" in the induction log. Abundant coal markers in the area, which normally separate different cycles of sedimentation, are distinguishable on logs by their sharp resistivity values on the induction logs and high transit time kicks on the sonic logs.

The UA-5 sandstone is well sorted and fine grained and has a uniform texture and composition and a minor degree of stratification. Calculations from density logs in well 107, section 11, indicate that the maximum porosity in UA-5 sandstone is around 19%, which is reduced to only 2% at the top of the sandstone as a result of dolomite

cementation. From studies reported by McCubbin and Brady,[8] the average permeability of the UA-5 sandstone ranges between 10.4 and 54.4 mD.

References

1. M. Szpakiewicz, R. Schatzinger, S. Jackson, B. Sharma, A. Cheng, and M. M. Honarpour, *Selection of a Second Barrier Island Reservoir System for Expanding the Shoreline Barrier Reservoir Model and Refining NIPER Reservoir Characterization Methodology,* DOE Report NIPER-472, 1990.
2. M. M. Honarpour and L. Tomutsa, *Injection–Production Monitoring—An Effective Method for Reservoir Characterization,* paper SPE/DOE 20262, presented at the SPE/DOE Seventh Symposium on Enhanced Oil Recovery, Tulsa, Okla., Apr. 22–25, 1990.
3. B. C. Craft and M. F. Hawkins, *Applied Petroleum Reservoir Engineering,* Prentice Hall, Inc., Englewood Cliffs, N.J., 1959.
4. National Institute for Petroleum and Energy Research, *Quarterly Technical Report for October 1–December 31, 1989,* DOE Report NIPER-463, Vol. II, February 1990.
5. C. W. Keighin, B. E. Law, and R. M. Pollastro, Petrology and Reservoir Characteristics of the Almond Formation, Greater Green River Basin, Wyoming, in *Petrogenesis and Petrophysics of Selected Sandstone Reservoirs of the Rocky Mountain Region,* E. B. Coalson et al. (Eds.), pp. 281-298, The Rocky Mountain Association of Geologists, 1989.
6. A. D. Jacka, Principles of Cementation and Porosity–Occlusion in Upper Cretaceous Sandstones, Rocky Mountain Region, *Wyo. Geol. Assoc., Guideb., 22nd Annu. Field Conf.,* pp. 265-285 (1970).
7. W. A. Pryor, Petrography of Mesaverde Sandstones in Wyoming, *Wyo. Geol. Assoc., Guideb., 16th Annu. Field Conf.,* pp. 34-46 (1961).
8. D. G. McCubbin and M. J. Brady, Depositional Environment of the Almond Reserves, Patrick Draw Field, Wyoming, *Mt. Geol.,* 6: 3-26 (1969).

MICROBIAL TECHNOLOGY

EFFECTS OF SELECTED THERMOPHILIC MICROORGANISMS ON CRUDE OILS AT ELEVATED TEMPERATURES AND PRESSURES

Contract No. DE-AC02-76CH00016

Brookhaven National Laboratory
Upton, Long Island, N.Y.

Contract Date: Mar. 1, 1989
Anticipated Completion: Sept. 30, 1990
Government Award: $155,000
(Current year)

Principal Investigators:
E. T. Premuzic
M. S. Lin

Project Manager:
Edith Allison
Bartlesville Project Office

Reporting Period: Jan. 1–Mar. 31, 1990

Objectives

The objective of this program is to determine the chemical and physical effects of thermophilic organisms on crude oils and cores at elevated temperatures and pressures. Ultimately, a database for use in technical and economic feasibility studies will be generated which will lead to field application.

Summary of Technical Progress

In the mass spectrometric analysis of mixtures containing organic compounds, such as crude oils, it is customary to use characteristic masses generated during fragmentation of organic molecules. For example, C_4H_9 (m/e 57) is used for alkanes and C_7H_7 (m/e 91) for substituted aromatics and others, all of which are characteristic molecular markers.[1] These diagnostic parameters were added to the systematic studies of oil–microbial interactions. For example, biotreatment of the teapot Naval Petroleum Reserve No. 3 (PR3) with Brookhaven National Laboratory (BNL) strain BNL-4-24 at 65°C under 2000 psi of nitrogen and 80 psi of carbon dioxide for 2 weeks yielded the following results: The single ion chromatogram monitored for mass 57 (Fig. 1) shows that the lighter alkanes (up to C16) are degraded over

that period of time, whereas those hydrocarbons which were larger than C16 and up to C30, based on peak comparison, were about 80% degraded. Similarly, Fig. 2 shows the effect of the biotreatment on alkylaranes (m/e 91), Fig. 3 on naphthalenes (m/e 169), and Fig. 4 on cyclic hydrocarbons, e.g., adamantane type (m/e 135). Considerable biodegradation of other cyclic saturated hydrocarbons, e.g., bicyclic sesquiterpanes (m/e 123), also occurs, as shown in Fig. 5. The ion-scan and other diagnostic parameters (such as sulfur monitoring) are being used in the development of a database that should ultimately determine trends and variations in the composition of crude oils caused by biotreatment by different strains of microorganisms under experimental conditions used.

As reported earlier,[2] during the biotreatment of crude oils, both acidification and emulsification occur as well as solubilization in the aqueous phase of some hydrocarbon components of the crudes. Such chemical changes can also influence the trace metal composition of crude oils. The metals are detected in the gas chromatogram selectively by their specific emission wavelength using a gas chromatograph (GC) with an atomic emission detector. Appropriate calibration allows the determination of metal species. For example, biotreatment of Wilmington (California) crude with BNL-4-22 resulted in a considerable reduction of the nickel porphyrin complex as shown in Fig. 6. In this analysis, the GC system was calibrated with

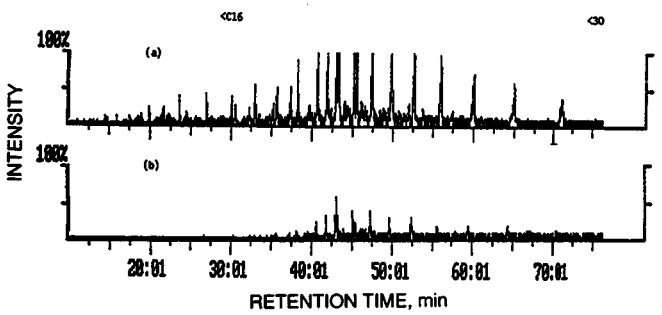

Fig. 1 Degradation of hydrocarbons before (a) and after (b) treatment; m/e 57 ion trace of PR3 crude treated with BNL-4-24.

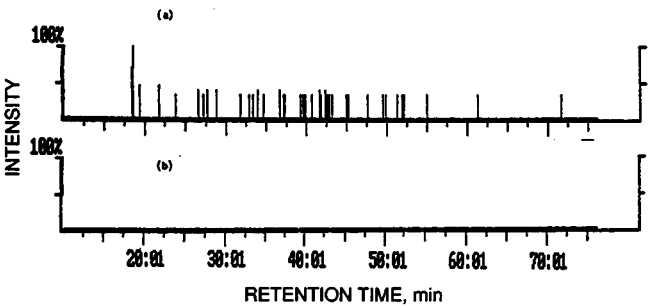

Fig. 2 Degradation of alkylarnes before (a) and after (b) treatment; m/e 91 ion trace of PR3 crude treated with BNL-4-24.

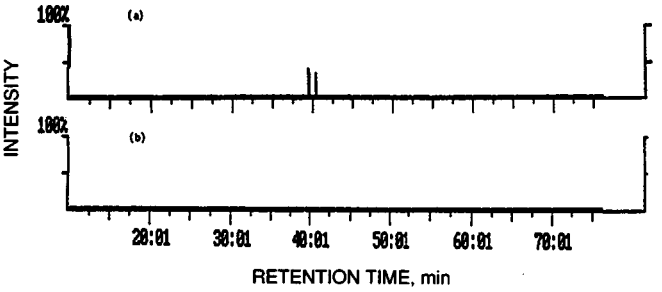

Fig. 3 Degradation of aromatic hydrocarbons before (a) and after (b) treatment; m/e 169 ion trace of PR3 crude treated with BNL-4-24.

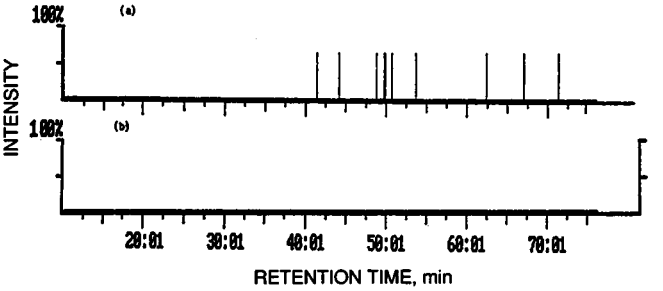

Fig. 4 Degradation of cyclic hydrocarbons before (a) and after (b) treatment; m/e 135 ion trace of PR3 crude treated with BNL-4-24.

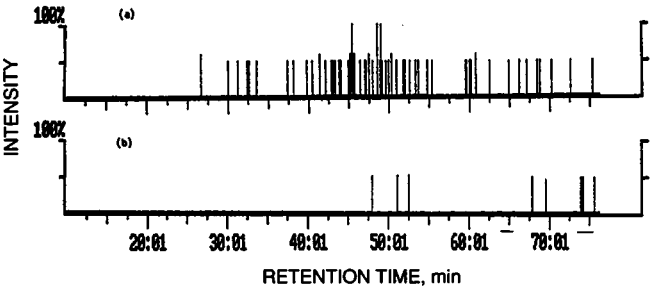

Fig. 5 Degradation of cyclic hydrocarbons before (a) and after (b) treatment; m/e 123 ion trace of PR3 crude treated with BNL-4-24.

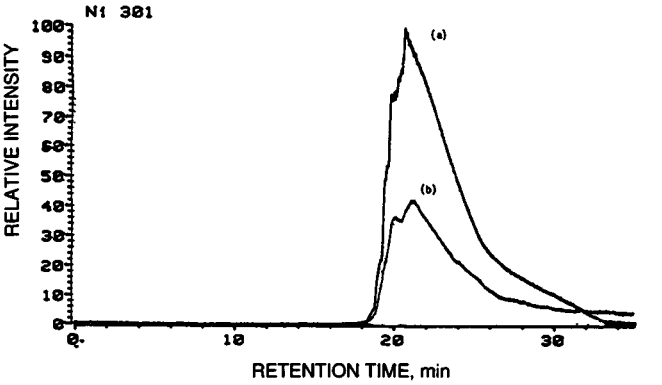

Fig. 6 Reduction of nickel porphyrin content in Wilmington (California) crude before (a) and after (b) treatment with BNL-4-22.

nickel octaethyl porphyrin eluting at 18.5 min and cobaltoactaethyl porphyrin eluting at 19.1 min. This is the first clear indication of removal of a trace metal from a crude oil by means of biotreatment under these experimental conditions.[3]

References

1. J. A. Williams, M. Bjorøy, D. L. Dolcater, and J. C. Winters, Biodegradation in South Texas Eocene Oils—Effects on Aromatics and Biomarkers, in *Advances in Organic Geochemistry, 1985*, Part I, Petroleum Geochemistry, D. Leythauser and J. Rullkötter (Eds.), pp. 451-461, Pergamon Journals, Ltd., U.K., 1986.
2. E. T. Premuzic and M. S. Lin, Interaction Between Thermophilic Microorganisms and Crude Oils—Recent Developments, in *Proceedings of the Bioprocessing of Fossil Fuels Workshop, Virginia, August 1989*, in press.
3. E. T. Premuzic and M. S. Lin, Patent pending, 1990.

ENHANCED OIL RECOVERY AND APPLIED GEOSCIENCE RESEARCH PROGRAM

Contract No. DE-AC07-76ID01570
Project 5AC3

Idaho National Engineering Laboratory
EG&G Idaho, Idaho Falls, Idaho

Contract Date: Oct. 1, 1988
Anticipated Completion: Sept. 30, 1995
Funding for FY 1990: $1,500,000

Principal Investigator:
C. P. Thomas

Project Managers:
I. Aoki
Idaho Operations Office

Edith Allison
Bartlesville Project Office

Reporting Period: Jan. 1–Mar. 31, 1990

Objectives

The objectives of this research program are to develop microbial enhanced oil recovery (MEOR) systems for application to reservoirs containing medium to heavy oils (12 to 20° API) and to evaluate reservoir wettability and its effects on oil recovery.

The MEOR research goals include:

1. Development of bacterial cultures that are effective for oil displacement under a broad range of reservoir conditions.
2. Improved understanding of the mechanisms by which microbial systems displace oil under reservoir conditions.
3. Determination of the feasibility of combining microbial systems with conventional enhanced oil recovery (EOR) processes, such as miscible and immiscible gas flooding, polymer and chemical flooding, and thermal methods.
4. Development of quantitative mathematical descriptions of microbial oil recovery mechanisms under reservoir conditions necessary for the development of reservoir simulation of MEOR processes.
5. Development of improved methods of characterization and simulation of heterogeneous reservoirs for design and application of EOR and MEOR processes.
6. Development of an MEOR field process design and implementation of an industry cost-shared field demonstration project.

The goals of the reservoir wettability project are to develop:

1. Better methods for assessment of reservoir core wettability.
2. More certainty in relating laboratory core analysis procedures to field conditions.
3. Better understanding of the effects of reservoir matrix properties and heterogeneity on wettability.
4. Improved ability to predict and influence EOR response through control of wettability in reservoirs.

Summary of Technical Progress

MEOR Research

The importance of microbial attachment at the oil–water interface as compared with the isolated metabolites to increase oil mobility via change in interfacial properties is currently being determined. Figure 1 shows evidence of the abilities of different microbes to adhere to the hydrocarbon phase of an oil–aqueous system. These experiments employ the Bacterial Adherence to Hydrocarbons (BATH) test to

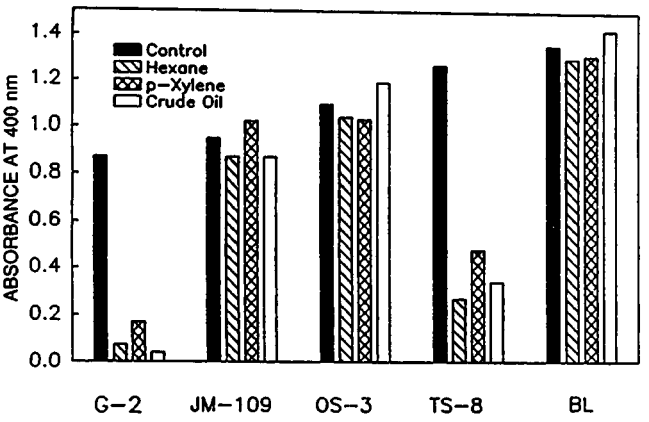

Fig. 1 Bacterial adherence to hydrocarbons.

ascertain the hydrophobicity of cell surfaces.[1] All the isolates demonstrate the ability to emulsify oil in aerobic shake flask tests except JM-109, which is added as a negative control. Although OS-3 shows no capacity for adherence to the hydrocarbon phase, other isolates (G-2, TS-8, and *Bacillus licheniformis*) demonstrate an ability to become attached to the hydrocarbon in the biphasic system. This suggests that different microbes interact with the hydrocarbons either directly via cell attachment or indirectly through surfactant production or by both mechanisms to cause emulsification.

Interfacial tension (IFT) measurements are conducted in a pendant drop apparatus with crude oil and solutions that contain: (1) a specific isolate plus the spent growth medium in which the culture grew (1:5 dilution), (2) the washed cells without the spent medium (1:5 dilution), or (3) the spent medium only without cells. Isolates OS-3, JM-109, TS-8, and G-2 along with the spent media associated with their growth show no evidence of altering IFT between the aqueous phase and the crude oil tested. In contrast, both *B. licheniformis* cells and the spent medium in which they grew show evidence of decreasing IFT between the aqueous phase and crude oil. Dilution was necessary to observe the dynamics of drop release in the apparatus. In all cases, these cultures are grown aerobically in trypticase soy broth (TSB) with no addition of oil. Although *B. licheniformis* clearly does not require the presence of oil to stimulate decreases in IFT, the other cultures may require the presence of oil to induce these properties.

A long-term assay for testing the ability of oil emulsifying cultures to modify crude oil has been initiated. With such an assay, separate isolates of mixed cultures can be tested for their ability to modify the surface characteristics of an oil-wet surface during extended incubations. Oil droplets are aseptically applied to a polystyrene petri dish lid. The lid is then inverted into a larger petri dish containing TSB medium that has been inoculated with isolate OR-1. OR-1 is an isolate that causes emulsification of oil in water and has been shown to attach to the hydrocarbon phase in the BATH test. Abiotic controls are set up in a similar fashion, and all plates are gently rotated at room temperature.

In dealing with inhibition of light chain hydrocarbon degradation, focus is on development of biocide-resistant bacterial strains with desirable characteristics for EOR. Current research is pursuing specific inhibition of light chain degradation; this will preserve and possibly improve the quality of crude oil in place. The organisms responsible for the degradation of light chains will be alleviated in a biocide flood, followed by a microbial flood containing biocide-resistant bacteria with desirable characteristics. Currently, strains of oil-degrading organisms and organisms that produce emulsifiers and/or surfactants are available. Organisms that have the ability to produce acids and/or gas as well as organisms capable of asphaltic degradation will be collected and isolated. This strategy will allow eradication of organisms in the reservoir and competition-free colonization of the desired microbes. Contingency biocides will be identified to control the injected strains.

Core aging studies have been initiated to determine the influence of oil in core residence time on residual oil recovery by waterflooding. The cores are waterflooded to a residual oil saturation condition and then placed in incubation for at least 1 week at 37°C. Preliminary results show no additional oil recovery from unfired Berea cores by waterflooding after the aging period. Additional experiments will be performed to evaluate longer periods of aging and to investigate the influence of salts, nutrients, etc., on the recovery of residual oil after incubation. These baseline studies will serve as controls for coreflood experiments involving microbial systems.

An experimental plan has been developed to investigate viscosity differences of various crude oils and their relationship to waterflood and microbial flood residual oil saturation. These corefloods are performed at the same temperature and brine concentration. IFT measurements are made for each system, and controls are run to determine if the nutrient alone produces additional oil recovery at waterflood residual oil saturation. Gas chromatography and elemental analysis are used to characterize and empirically compare premicrobial and postmicrobial flood oils.

This series of Berea coreflooding experiments using a *B. licheniformis* bacteria has been initiated to investigate the following parameters: (1) crude oil type, (2) crude oil viscosity, (3) aging and incubation time, (4) IFT, and (5) brine composition. Residual oil saturations resulting from waterflooding followed by microbial flooding as a function of these variables are compared. Six oils with API gravities ranging from 17.5 to 50.5° have been selected for use in these experiments. These experiments are to provide the basis for comparison of other microbial strains developed from the field samples and the effects of the amount of nutrient and other factors affecting microbial activity. Approximately one-half of the cores needed for this study have been prepared and waterflooded to residual oil, and several have been inoculated with the *B. licheniformis* bacteria.

Assembly of existing field and reservoir data has been initiated for reservoirs that are candidates for the focus of this MEOR research. Water analysis work to determine the characteristics of the produced brine and injection water for these fields has been completed. Viscosity measurements for the crude oil and produced brine from these fields have also been completed. Additional data will be assembled for these reservoirs to determine if they fit the criteria needed to be viable targets for MEOR application.

Evaluation of Reservoir Wettability and Its Effects on Oil Recovery

Investigation of the interactions between crude oil and mineral surfaces can be divided into two main groups:

(1) surface phenomena studies and (2) observations of flow behavior. In the surface phenomena studies, simple observations of adhesion or lack of adhesion when a drop of crude oil contacts a smooth solid surface covered with brine and more quantitative studies of the surface charge at crude oil–brine and solid–brine interfaces are being made. Several crude oils, under a wide variety of conditions of brine concentration, emulsion concentration and age, temperature, and oil composition, have been investigated.

A first step toward characterizing crude oils with respect to their effects on the state of reservoir wettability is to observe the three-phase contact between one solid phase and two fluids (crude oil and brine). Contact angle measurements are complicated by hysteresis and by potential alteration of the surface upon contact with crude oil components. A simple adhesion test has been developed to characterize crude oils on the basis of their surface interactions with smooth solids and varying brine composition. The standard initial mapping of the Schuricht Lease (Crook County, Wyo.) oil does not go to sufficiently high pH to determine the lowest ionic strength pH cutoff (Fig. 2).

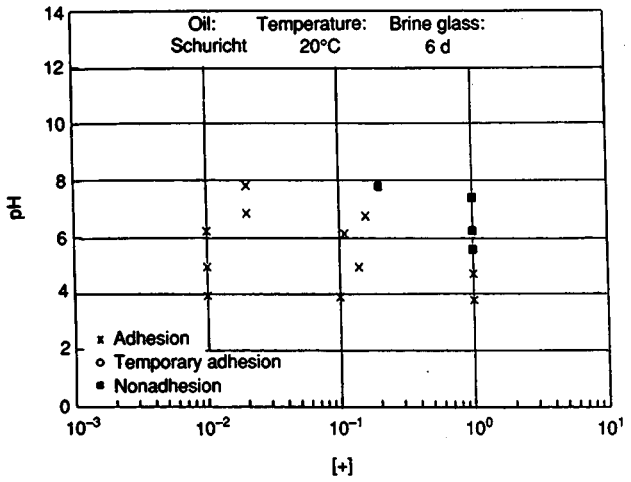

Fig. 2 Adhesion map for Schuricht lease crude.

Higher pH buffers are being tested, and this oil appears to have an unusual pH cutoff pattern: above pH 8 at 0.01*M* NaCl, dipping to pH 5 at 1.0*M* NaCl.

Emulsions of several crude oils have been tested to determine mobilities of emulsion droplets. All emulsions are prepared in pH 10 buffer; aliquots of the emulsion are added to the measurement solution immediately before observations. Some emulsions have limited stability, even at pH 10. The isoelectric points (IEP) are estimated from the plotted zeta potential data by measurement from graphs of pH value at which the line between the positive and negative zeta potentials closest to zero passes through zero. Reproducibility of the mobility measurements for a given emulsion batch for both the fresh emulsion and 2-week-old emulsion is very good (Fig. 3). For Moutray (West Texas),

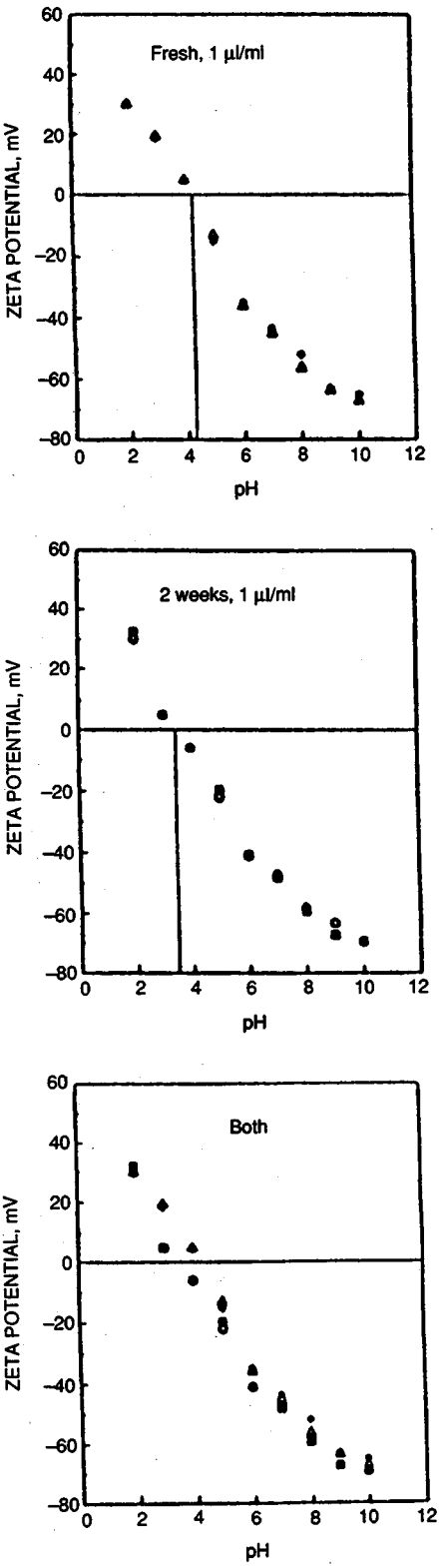

Fig. 3 Reproducibility of Zeta potential measurements for Moutray crude oil in 0.01*M* NaCl.

a difference in the IEP is found after 2 weeks of aging (from 4.3 to 3.5 pH units), although very limited change is found in either the positive or negative portions of the curves,

away from the IEP. For most of the oils studied, some aging was observed.

Reference

1. M. Rosenberg, *FEMS Symp.*, 9: 29-33 (1980).

MICROBIAL FIELD PILOT STUDY

Contract No. DE-FG22-89BC14246

University of Oklahoma
Norman, Okla.

Contract Date: Nov. 21, 1988
Anticipated Completion: May 15, 1991
Government Award: $202,272
(Current year)

Principal Investigators:
R. M. Knapp
M. J. McInerney
D. E. Menzie
J. L. Chisholm

Project Manager:
Edith Allison
Bartlesville Project Office

Reporting Period: Jan. 1–Mar. 31, 1990

Objective

The objective of this project is to perform a microbially enhanced oil recovery field pilot test in the Southeast Vassar Vertz Sand Unit (SEVVSU) in Payne County, Okla. Indigenous, anaerobic, nitrate-reducing bacteria will be stimulated to selectively plug flow paths that have been preferentially swept by a prior waterflood. This will force future floodwater to invade bypassed regions of the reservoir and increase sweep efficiency.

Summary of Technical Progress

Ecology of the Reservoir

Because the fluid composition of the reservoir brines can change the bacterial populations and their ability to metabolize certain carbon sources, frequent analysis of reservoir brines becomes necessary for the success of the microbial enhanced oil recovery (MEOR) process.

Brine samples were obtained from several wells in the field. The sample sites include wells 7-2, 1A-3, 1A-1, 1A-9, the makeup water source well, and the pump manifold. All samples were obtained with sterile techniques and were analyzed for bacterial numbers within 4 h. Samples were stored at 4°C until all the analyses had been completed. Chemical and bacteriological analyses were performed with methods previously described.[1]

The composition of the chemical species in brines did not vary significantly from those obtained previously (Table 1). The brines were highly saline with salinities ranging from 11.3 to 17.5%. The pHs of the brines were close to neutral, and moderate levels of alkalinity were detected. Although significant levels of nitrate and iron were detected in the brines, phosphate was present in only very low amounts.

Although high numbers of molasses–nitrate-using and anaerobic heterotrophic bacteria were detected in most of the brines, very few (or no) aerobic bacteria were detected in any of the brines (Table 2). Anaerobic molasses–nitrate-using bacteria were present in higher concentrations than anaerobic heterotrophic bacteria. Significant increases in the number of molasses–nitrate-using bacteria and anaerobic heterotrophic bacteria were detected in brines from the pumping manifold, well 7-2, and well 1A-3. Although the numbers of sulfate-reducing bacteria in most of the brines were low, significant levels were detected in brines from well 1A-3 and the pumping manifold. The presence of high numbers of bacteria in February 1990 brine samples indicates that microbial populations have recovered from the biocide treatment performed a few months earlier.

Studies show that the composition of the chemical species in the reservoir brines did not change significantly over a period of time. Results from bacteriological analysis indicate that brines from the SEVVSU do contain diverse populations of microorganisms whose growth and metabolism could be stimulated by the addition of nutrients.

Propagation of Nonmotile Cells

The mechanism of penetration of nonmotile *Escherichia coli* strain RP2912 was studied in 10-cm plastic cores saturated with motility growth medium. Duplicates of these cores were sacrificed at regular intervals and cut into 2-cm-long sections. Cell concentrations were determined for each of the sections. Motility growth medium (MGM) contained (per 100 mL) 0.45 g galactose, 0.5 g peptone, 0.5 g NaCl, 1.12 g K_2HPO_4, 0.48 g KH_2PO_4, 0.2 g $(NH_4)_2SO_4$, 0.025 g $MgSO_4$, 0.025 g methionine, and 0.00005 g $Fe_2(SO_4)_3$. The pH of MGM is 7.0. The conditions were identical to those used for the parental motile strain RP437.

As shown in Fig. 1, strain RP2912 took 60.5 h to move into the fifth section of the core. The penetration times of RP2912 and RP437 were comparable. The nonmotile strain moved and grew throughout the available pore volume. These do not support a model that assumes that

TABLE 1

Chemical Analysis of Brine Samples

Sample site	Date	Specific gravity	Total dry residue, mg/mL	Total suspended solids, mg/mL	Total hardness as $CaCO_3$	Calcium hardness as $CaCO_3$	NaCl salinity, mg/L	Total alkalinity, mg/L	Iron, mg/L	Phosphate, mg/L	Nitrate, mg/L	Nitrite, mg/L	pH
SW	4/87	1.075	129	3.88	36.8	25.0	116	38	10	<1	10	<0.02	
	6/87	1.080	134	4.20	20.4	13.5	123	34	10	<1	10	<0.02	7.0
	7/89	1.092	109	1.94	21.6	15.1	121	32	10	<1	10	<0.02	6.0
	2/90	1.072			21.6	17.2	113	36	10	1			
PM	6/89	1.115	111		25.2	17.2		82	10	<10	<5	<0.2	7.0
	7/89	1.112	110	1.78	24.6	18.1	164	86	10	1	5	<0.2	7.0–7.2
	2/90	1.081			23.6	17.4	158	72	10	1			
1A-1	4/89						160						
	6/89	1.046	113		26.2	17.9	156	162	30	<10	<5	<0.2	6.6–7.2
	7/89	1.090	111	2.7	26.2	18.2	168	176	10	1	5	<0.2	7.2–7.7
	2/90	1.093			26.2	19.6	165	144	5	1			
1A-7	4/87	1.106	197		61.6	41.8	182	382	160	<1	5	<0.2	
	6/87	1.110	194	5.95	31.9	22.1	196	42	30	<1	10	<0.2	6.9
	7/89	1.147	190	2.82	32.6	21.9	197	66	30	<0.1	10	<0.2	6.6–6.7
1A-9	4/89						161						
	6/89	1.050	114		27.0		166	144	20	<10	<5	<0.2	6.0
	7/89	1.092	112	2.41	26.8	18.1	164	144	20	1	10	<0.2	6.6–6.7
	2/90	1.091			26.8	19.8	166	108	20	1			
7-2	6/87	1.104	170		28.2	19.8	154	104	10	<1	5	<0.2	6.7
	4/89												
	6/89	1.132	113		26.6	16.5	159	112	30	<10	<5	<0.2	6.0
	7/89	1.111	112	2.91	25.2	21.9	15.1	110	30	1	5	<0.2	6.0–6.4
	2/90	1.087			25.6	18.2	17.5	28	80	1			
8-2	6/89	1.046			31.6	21.8			10	<10	<5	<0.2	6.0–7.0
8-3	4/89						186						
	6/89	1.127	188		30.4	21.6	186	60	20	<10	<5	<0.2	7.0
	7/89	1.122	184	1.9	30.4	22.7	185	30	30	1	5	<0.2	6.4–6.6

TABLE 2

Bacterial Numbers in Brine Samples

	Most probable number* (per mL)					
	Sulfate reducers		Molasses–nitrate users		Aerobic heterotrophs	Anaerobic heterotrophs
Sample location	7/89	2/90	7/89	2/90	2/90	2/90
Source well	110	<1	110	<1	0	0
Pump manifold	21	240	47	7490	2	1100
Well 7-2	46	46	110	1100	2	46
Well 8-3	15	NA	110	NA	NA	NA
Well 1A-3	NA	110	NA	462	2	462
Well 1A-1	24	<1	4	46	2	4
Well 1A-7	2	NA	21	NA	NA	NA
Well 1A-9	9	4	15	462	2	2

*Samples were incubated at 35°C for 45 d.

nonmotile bacteria grow through the core as a filament where the penetration time is dependent on the core length and the growth rate of the bacteria. A model that includes core length, bacterial growth rate, pore volume, and cell volume accurately predicted the penetration rate of nonmotile cells.

Coreflood Experiments

Coreflood experiments on four Berea cores were terminated in November 1989. Two cores remained shut-in in an incubator without additional nutrient treatments at reservoir temperature. One of the cores, Core 11, had been under this

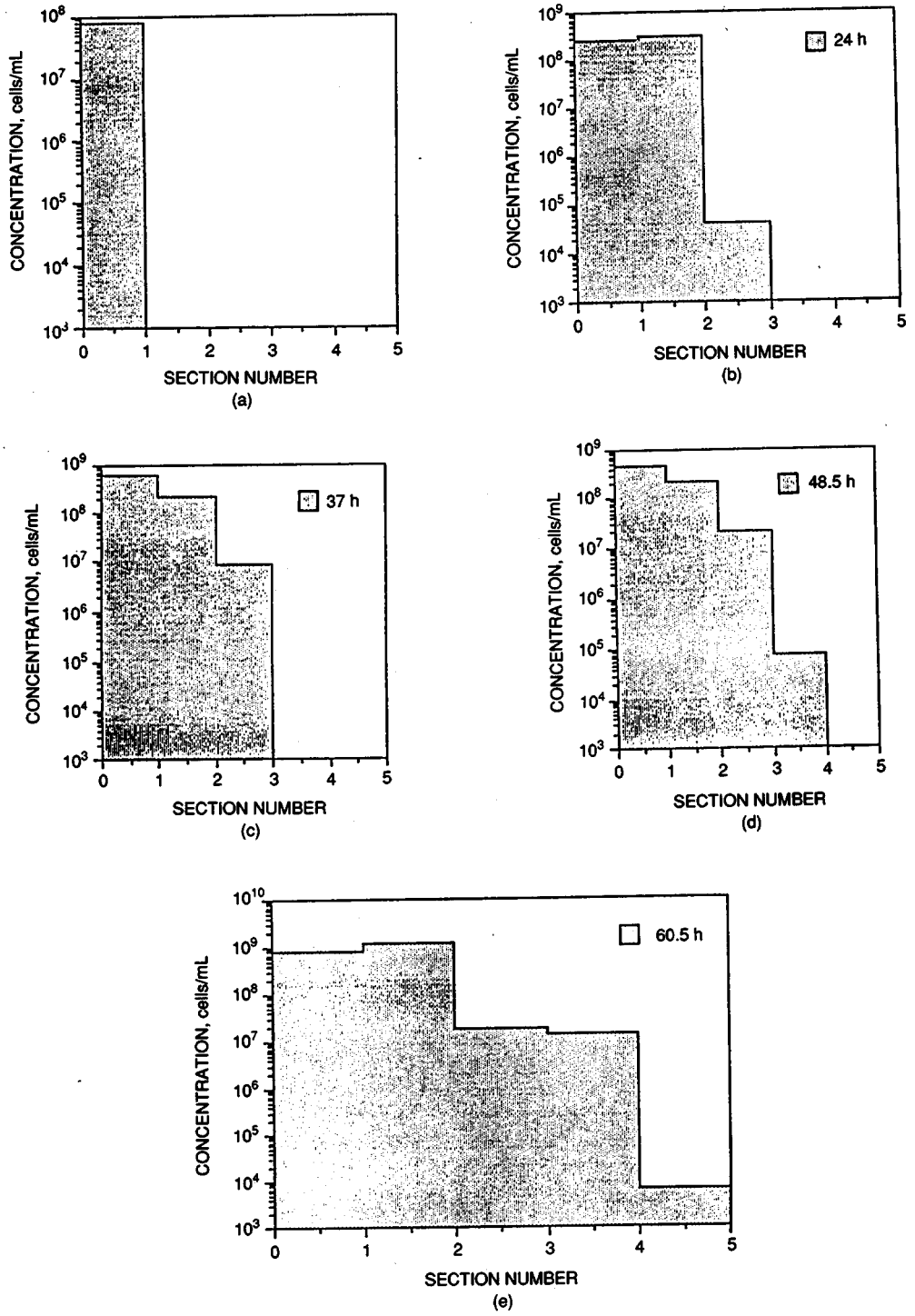

Fig. 1 Concentration vs. distance (section number) for nonmotile strain RP2912 at five time intervals. (a) 0 h, (b) 24 h, (c) 37 h, (d) 48.5 h, (e) 60.5 h.

extended incubation for 103 d and had a pore pressure of 12 psig. The pore pressure increase indicated that microbial activity had occurred in the core. Another nutrient treatment was tried to see what would happen.

Although this core had a poor response to MEOR during previous treatments, there was a substantial increase in oil recovery following extended incubation. The pressure of the core was slowly reduced to 2.8 psi, and 40 mL of nutrients was injected. A total of 3 mL of oil was recovered during this treatment. This was about 150% of the cumulative oil recovery from the eight treatments performed in fall of 1989. The brine permeability had increased slightly from

1.1 to 1.4 mD. A total of 26 mL of gas was recovered during this treatment.

Following this treatment, the core was allowed to incubate at 35°C while the pressure was monitored. When the pressure stopped increasing, another nutrient treatment followed. An additional 1 mL of oil was recovered during this additional treatment. The total oil recovery following these two treatments increased to 35% of S_{or}. The changes of recovery factor, permeability reduction factor (PRF), and cumulative gas production for treatments for Core 11 are shown in Fig. 2.

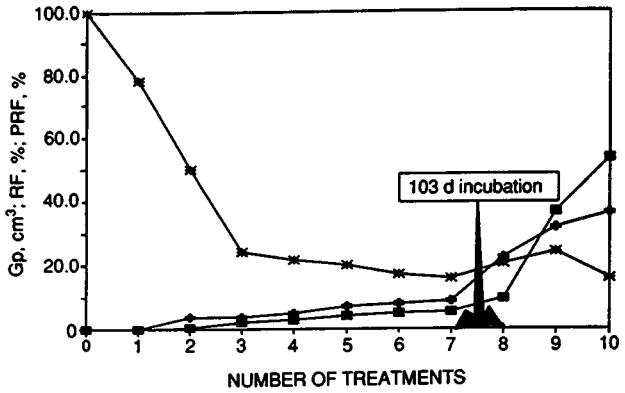

Fig. 2 Effect of nutrient treatments on the cumulative gas production (Gp) (-■-), recovery factor (RF) (-●-), and permeability reduction factor (PRF) (-✱-) in Core 11.

Microbial Modeling: Model Validation

A three-phase, seven-species, one-dimensional (1-D) model was developed to simulate the microbial process.[2] A 1-D version of the model was used to quantify biomass growth, product generation, and substrate consumption, and to predict permeability reduction in laboratory core experiments.

Experimental studies were conducted to investigate microbial mechanisms that recover oil remaining after waterflooding.[3] The injection, incubation, and continued nutrient-rich flood protocols used in the experiment on Core 6 were simulated using the model. A good match between experimental and simulation results was obtained for total gas production (Fig. 3).

The simulation indicated that after treatment ten the glucose consumption (carbon source for metabolism) reached its maximum level (Fig. 4) and that approximately 20% of the glucose remained unused in the effluent since the ammonium [nitrogen (N_2) source for bacterial growth] should have been totally consumed (Fig. 5). The model's chemical balance assumes that, for every glucose mol consumed, 1.2 mol of ammonium should be used for bacterial growth. Nitrate use predicted by the simulator was lower than that measured during the experiment. The reason may be that N_2 is considered the only product from nitrate

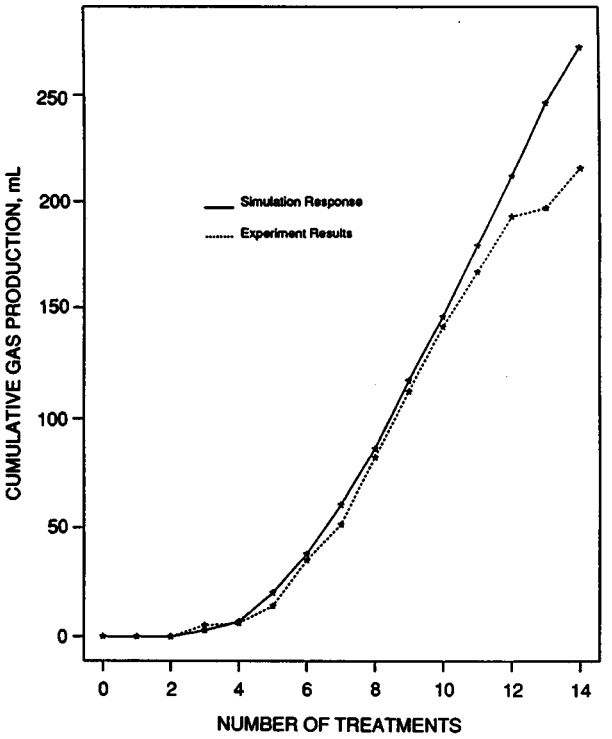

Fig. 3 Cumulative production of total gases (CO_2 and N_2) during MEOR process (Core 6).

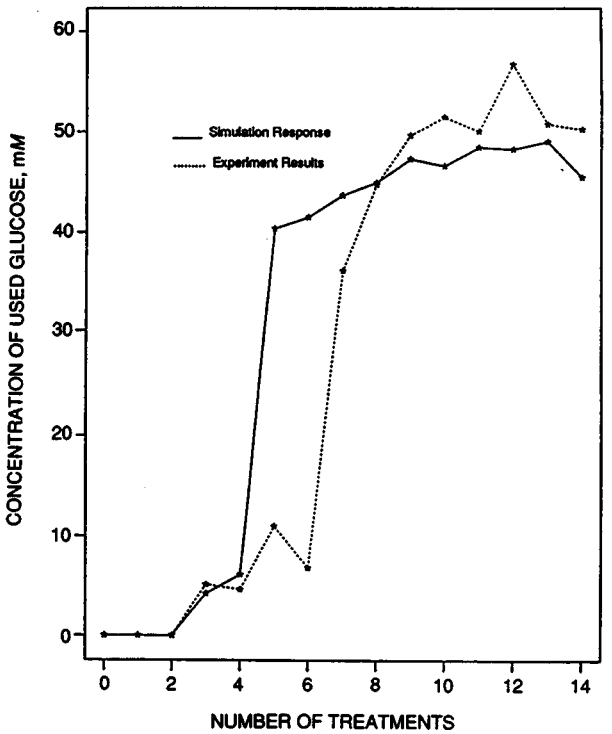

Fig. 4 Consumption of glucose during MEOR processes (Core 6).

in the model. If nitrate were being used to produce other products not monitored in the experiment or considered in the simulator, low nitrate use would be the expected simulation result.

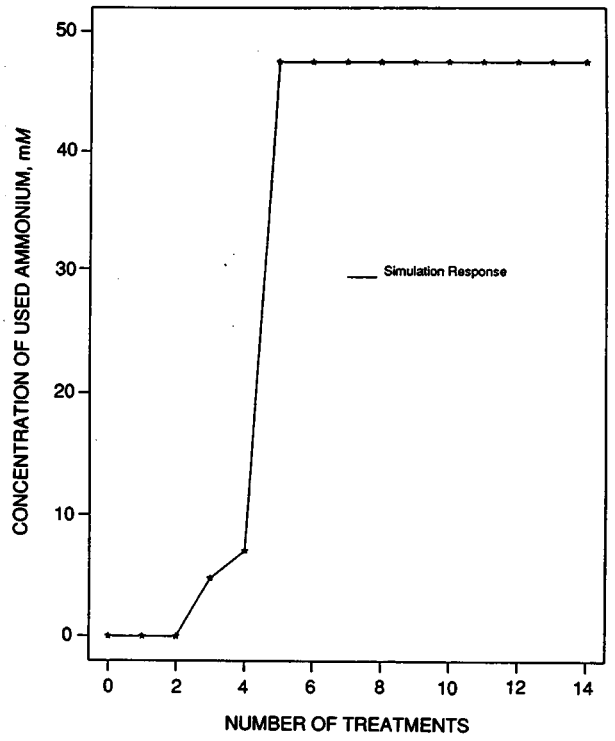

Fig. 5 Consumption of ammonium during MEOR processes (Core 6).

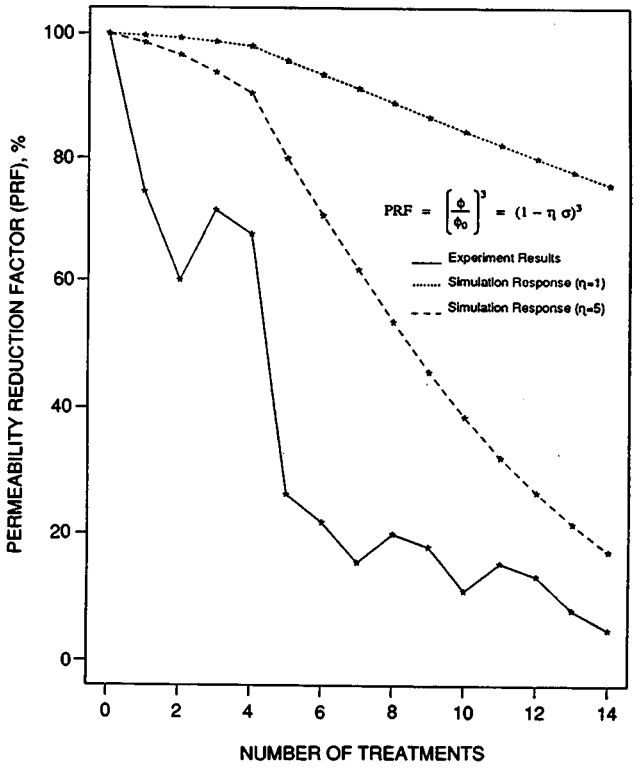

Fig. 6 Permeability reduction during MEOR processes (Core 6).

Since no significant growth and production occurred during the first four treatments, the observed experimental permeability reduction during this period may have been due to bacterial retention or facial plugging in the core. The ratio of the brine permeability after the ith treatment to the original brine permeability is defined as the PRF. After treatment four, in situ growth of bacteria and large production of biogenic gas resulted in a sharp reduction of permeability. However, simulation results have higher values of PRF than those of the experimental results (Fig. 6). There may be two reasons for this phenomenon. First, glucose consumption was underpredicted by the model. Second, bacterial plugging was considered the only factor reducing water permeability in the model. However, biogenic gas, either mobile or immobile, could also reduce the relative permeability to the flowing water phase.

The Southeast Vassar Vertz Sand Unit

During this quarter, new pressure gauges were installed on the 5-1, 5-2, 7-1, and 7-2 wells to be used in the field pilot study. More production and injection fluid samples were taken from various wells in the field for fluid analysis and microbial analyses. Some results of the analyses are reported in this report. Four turbine meters and totalizers were acquired for installation in the field.

At a meeting in Amarillo, Tex., on Feb. 27, 1990, with five Mesa Limited Partnership engineers, the following topics were discussed: planned treatment protocol, injection–production system design, status of oil produced from the pilot wells, nutrient injection system design and procedures, and separation of pilot-produced water from that normally used to inject in the field waterflood. Mesa Limited Partnership engineers expressed concern about the residual molasses content of pilot-produced water and suggested that the current injection lines could serve as production lines. Agreement was reached concerning the frequency of meetings. Mesa Limited Partnership engineers indicated support for the pilot and their willingness to expedite the field pilot.

The SEVVSU has been for sale by Mesa Limited Partnership since it was purchased from Tenneco Oil and Gas Company. During the first week of March, Mesa announced that Sullivan Oil Company, another working interest owner of the unit, has agreed to purchase Mesa's holdings. Sullivan and Mesa plan to close the sale late in April.

References

1. R. M. Knapp, M. J. McInerney, D. E. Menzie, and R. A. Raiders, *Microbial Field Pilot Study, Final Report,* U.S. DOE Report DOE/BC/14084-6, January 1989.
2. X. Zhang, *Mathematical Modeling of Microbially Enhanced Oil Recovery,* M.S. Thesis, University of Oklahoma, Norman Okla., 1990.
3. N. J. Sifanus, *Microbial Mechanisms for Enhanced Oil Recovery from High Salinity Core Environments,* M.S. Thesis, University of Oklahoma, Norman, Okla., 1990.

MICROBIAL ENHANCEMENT OF OIL PRODUCTION FROM CARBONATE RESERVOIRS

Contract No. AC22-90BC14202

University of Oklahoma
Norman, Okla.

Contract Date: Jan. 23, 1990
Anticipated Completion: Jan. 23, 1991
Government Award: $154,582

Principal Investigators:
Ralph S. Tanner
Roy M. Knapp
Michael J. McInerney
Emmanuel O. Udegbunam

Project Manager:
Edith Allison
Bartlesville Project Office

Reporting Period: Jan. 1–Mar. 31, 1990

Objectives

Work on this contract was initiated this quarter. Primary activities included changing the principal investigators on the contract, appointing research personnel, initiating the literature review of microbial enhanced oil recovery (MEOR) in carbonate reservoirs, and beginning investigation of microorganisms with potential utility in the coreflood and of mechanisms of oil displacement portions of the contract.

Summary of Technical Progress

Personnel

Notification of award of the contract was received during the last week of February 1990. The principal investigator on the contract was changed from Erle C. Donaldson to Ralph S. Tanner; Dr. Donaldson will leave the University of Oklahoma in June 1990. Dr. Emmanuel O. Udegbunam was appointed as a coinvestigator to help perform the tasks originally planned for Dr. Donaldson.

A graduate research assistant, an independent study undergraduate student, and a technician will be appointed to participate in coreflood and mechanisms of oil displacement experiments. Training of these individuals will be completed by May 31, 1990.

Review of MEOR in Carbonate Reservoirs

The review is under way. It is being approached from two directions: a microbiologically oriented review of MEOR in carbonate formations and a review of the geology and geochemistry of carbonate formations pertinent to MEOR. The initial work points to a paucity of actual MEOR data for carbonate reservoirs, which is expected given the state of the art. Geologically, carbonate reservoirs are more complex than sandstone formations. The initial review suggests that plugging of fractures in carbonate reservoirs may be an important factor in MEOR for these formations. This will be investigated in the laboratory segment of this work.

Carbonate Coreflood Experiments–Mechanisms of Oil Displacement by Microorganisms

Since microbial acid production may be an important phenomenon for MEOR in carbonate reservoirs, acid-producing halophilic microorganisms were isolated from sediments from the Great Salt Plains as a training exercise. Twenty-seven isolates were obtained. A preliminary analysis of 14 isolates is given in Table 1. In general, obligately halophilic, facultatively anaerobic gram-negative rods were recovered; these microorganisms could metabolize in an anaerobic core environment. The preliminary characterization also indicates that these microorganisms are representative of at least four previously undescribed genera.

TABLE 1

Preliminary Characterization of Acid-Producing, Halophilic Eubacteria with Potential Utility in Model Carbonate Core Studies*

Gram reaction	Cell morphology	Relation to oxygen	Catalase reaction	Relation to salt	Number of strains
–	Rod	Facultatively anaerobic	–	Obligately halophilic	5
–	Rod	Facultatively anaerobic	+	Obligately halophilic	3
–	Rod	Obligately aerobic	+	Obligately halophilic	2
–	Rod	Facultatively aerobic	–	Obligately halophilic	1
–	Rod	Facultatively anaerobic	–	Halotolerant	1
+	Rod	Facultatively anaerobic	–	Obligately halophilic	1
–	Coccus	Facultatively anaerobic	–	Obligately halophilic	1

*Strains were isolated from sediments obtained from the Great Salt Plains in media containing 15% NaCl.

Characterization of these and the other isolates is continuing.

Identification of an active, oil-producing carbonate reservoir for study of carbonate microbial ecology as a potential site for obtaining carbonate rock for the core studies is now in process.

DEVELOPMENT OF IMPROVED MICROBIAL FLOODING METHODS

Cooperative Agreement DE-FC22-83FE60149, Project BE3

National Institute for Petroleum and Energy Research
Bartlesville, Okla.

Contract Date: Oct. 1, 1983
Anticipated Completion: Sept. 30, 1990
Funding for FY 1990: $300,000

Principal Investigator:
Rebecca S. Bryant

Project Manager:
Edith Allison
Bartlesville Project Office

Reporting Period: Jan. 1–Mar. 31, 1990

Objective

The objective of this project is to develop an engineering methodology for designing and applying microbial methods to improve oil recovery.

Summary of Technical Progress

Prior work at the National Institute for Petroleum and Energy Research (NIPER) has identified the mechanisms of oil mobilization by certain microbial formulations. Mechanisms that have been shown to be important include wettability alteration, emulsification, solubilization, and alteration in interfacial forces. Recent experiments at NIPER have demonstrated that oil mobilization by microbial formulations is not merely the result of the effects of metabolic products from the in situ fermentation of nutrient. Further investigation of interfacial properties of microorganisms and localized transient concentrations of metabolic products at the oil–water interface is needed to further determine the mechanisms of oil mobilization. The relationships between transport of microbes, nutrients, metabolic products, and mobilized crude oil need to be clarified and interpreted with mathematical models for fluid flow in porous media. The effects of reservoir conditions, such as salinity, temperature, pH, and compositions of reservoir brine and rock, need to be studied to develop methods for designing microbial formulations that are optimal for recovering crude oil under specific reservoir conditions. The effects of injection strategies on oil recovery efficiency also need to be determined. The scope of work includes laboratory experiments to further define key mechanisms of oil mobilization, development of correlations and mathematical models to describe the physical phenomena that are important in microbial enhanced oil recovery (MEOR) methods, and development of a mathematical computer simulator to model and predict performance of microbial formulations in oil recovery laboratory tests.

Milestone 1, "Review Laboratory and Field Data and Design Plan for Development of Improved MEOR Simulator," was completed this quarter. Discussions of MEOR process mechanisms were conducted with senior reservoir engineers, and a plan for development of an improved laboratory MEOR simulator was designed. The major elements of the plan include: (1) numerical simulation work needed for microbial processes; (2) laboratory experiments and data that are necessary to verify the experimental model; and (3) identification of reservoir properties that affect MEOR processes in the field and how they relate to an MEOR reservoir simulator. While preparing this plan for the MEOR simulator, one of the more critical parameters required for the modeling appeared to be the effects of microbial formulations on relative permeability. Thus an apparatus for determining the relative permeability of microbial formulations was constructed. Preliminary runs with this apparatus have been conducted with mineral oil and Berea sandstone cores. Concurrent testing is also being done using the Amott and Bureau of Mines methods for determining the alteration of wettability by the same microbial formulation under the same conditions.

As part of the continuing experiments for milestone 2, "Finalize Determination of Effects of Microbial Formulations on Interfacial Properties," experiments were designed to visualize the interactions between a microbial formulation and crude oil in etched-glass micromodels. These experiments will focus on the effects of gas production and surfactant production by different microbial species and provide some indications of the effects of microbial products on crude oil trapped in a pore throat.

Work continued for milestone 3, "Define Importance of Process Variables in the Application of Microbial Methods." Flask experiments were conducted this quarter to obtain growth curve data for NIPER 1 and 6 in molasses. Table 1 and Figs. 1 and 2 show the results of these flask tests. Microbial counts were conducted with trypticase soy agar (TSA) and a selective medium for NIPER 1. The microbial counts of NIPER 1 with the selective media were

TABLE 1

Microbial Counts from Growth Curve Experiment*

F-1-A	F-1-AN	F-1-AB	F-1-ANB	F-2-A	F-2-AN	F-2-AB	F-2-ANB
3.70E+05	6.60E+04	1.70E+05	2.80E+04	4.68E+04	5.35E+04	1.08E+05	2.75E+04
6.85E+05	4.85E+04	3.50E+05	4.25E+04	4.25E+05	5.05E+04	1.39E+05	3.85E+04
6.35E+05	1.75E+05	2.70E+05	8.15E+04	1.00E+06	1.49E+05	1.38E+05	7.20E+04
3.45E+06	3.95E+06	2.15E+05	4.20E+05	5.30E+06	6.40E+06	3.60E+05	6.05E+04
7.65E+07	6.75E+07	1.04E+06	7.20E+05	6.25E+07	6.30E+07	3.60E+07	2.60E+07
7.15E+08	4.75E+08	2.80E+07	2.30E+08	2.90E+08	3.00E+08	1.17E+08	2.00E+07
1.20E+09	1.15E+09	7.75E+08	6.55E+08	5.10E+08	4.65E+08	5.00E+07	4.20E+07
5.15E+08	5.70E+08	3.45E+08	3.05E+08	5.15E+08	5.15E+08	5.65E+07	1.65E+08
1.20E+08	1.30E+08	8.75E+07	8.05E+07	3.35E+08	3.10E+08	1.65E+08	5.80E+07
8.50E+06	4.00E+06	1.00E+07	1.00E+06	3.35E+08	2.85E+08	8.50E+05	1.43E+07
1.60E+07	2.15E+07	1.00E+06	1.00E+05	3.65E+08	2.60E+08	1.35E+08	1.50E+08
6.40E+06	6.85E+06	4.10E+05	2.30E+05	1.20E+08	1.05E+08	2.80E+07	4.37E+07
1.10E+05	7.60E+05	4.25E+04	7.40E+04	2.40E+07	2.20E+07	1.86E+06	9.75E+06

*F-1-A, flask 1, nonsterile molasses, aerobic counts on TSA; F-1-AN, flask 1, nonsterile molasses, anaerobic counts on TSA; F-1-AB, flask 1, nonsterile molasses, aerobic counts on selective media; F-1-ANB, flask 1, nonsterile molasses, anaerobic counts on selective media; F-2-A, flask 2, sterile molasses, aerobic counts on TSA; F-2-AN, flask 2, sterile molasses, anaerobic counts on TSA; F-2-AB, flask 2, sterile molasses, aerobic counts on selective media; and F-2-ANB, flask 2, sterile molasses, anaerobic counts on selective media.

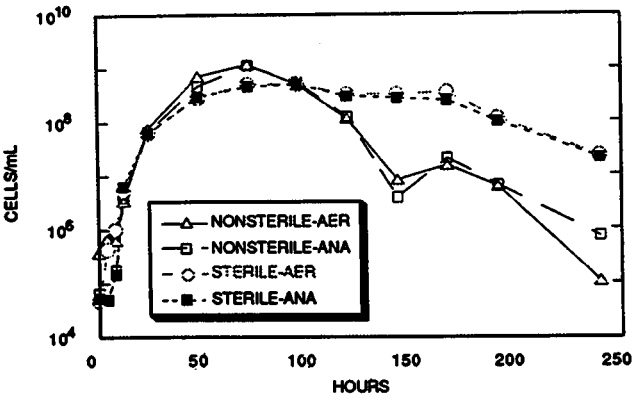

Fig. 1 NIPER 1 and 6 growth curves with the use of TSA for total bacterial counts.

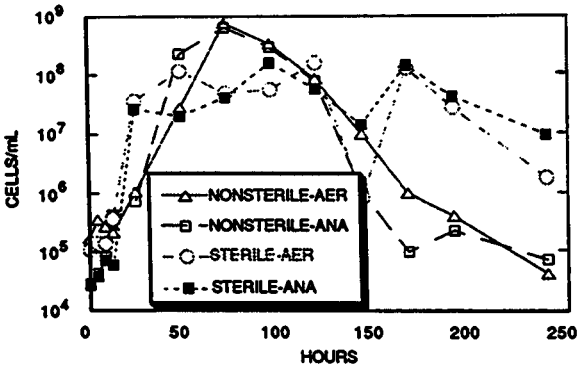

Fig. 2 NIPER 1 and 6 growth curves with the use of an antiticotic growth medium for NIPER 1 counts only.

comparable with the TSA; however, in both cases, the microorganisms remained at higher concentrations in the filter-sterilized molasses. This probably means that the indigenous microorganisms in the molasses may interfere with NIPER 1 and 6 growth after they have reached the stationary phase. This inhibition is likely the result of the higher alcohol production by indigenous microorganisms, which, after a growth period of over 120 h, builds up and begins to inhibit microbial growth. These effects are probably not observed during coreflood experiments, nor would they be expected in an oil field because the conditions of incubation are different. In a flask test, a buildup of products can occur, whereas in a flowing system, the products are continuously being swept away. Comparisons between molasses and other nutrients will be made to provide insight into nutrient effects on growth and metabolism of microbes. Carbonate rock from a reservoir in Ohio is being cut for microbial coreflooding experiments.

Work for milestone 6, "Complete Initial Work on Improved MEOR Simulator and Submit Status Report on Identified Improvements," progressed this quarter. A mathematical model has been developed to predict the propagation and distribution of microbes and nutrients in a one-dimensional core. Fluorescein tracer data from corefloods were used in the model to obtain a dispersion coefficient for nutrient. Microbial coreflooding data will now be incorporated into the model to predict the transport of microbes and nutrient when different injection strategies are used.

MICROBIAL-ENHANCED WATERFLOODING FIELD PROJECT

Cooperative Agreement DE-FC22-83FE60149, Project SGP13

National Institute for Petroleum and Energy Research
Bartlesville, Okla.

Contract Date: Oct. 1, 1983
Anticipated Completion: Sept. 30, 1990
Funding for FY 1990: $415,000

Principal Investigator:
Rebecca S. Bryant

Project Manager:
Edith Allison
Bartlesville Project Office

Reporting Period: Jan. 1–Mar. 31, 1990

Objectives

The objectives of this project are to determine the feasibility of improving oil recovery in an ongoing waterflood with microorganisms and to expand the initial pilot and determine the economics of microbial enhanced waterflooding. The scope of work for SGP13 includes continued monitoring of the Mink Unit Project and the injection of all injection wells on a particular pattern with microorganisms and nutrient for the waterflooding process. This portion of the project will be an expanded field pilot.

Summary of Technical Progress

A microbial-enhanced waterflood field project sponsored by the U.S. Department of Energy (DOE), Microbial Systems Corp. (MSC), and INJECTECH, Inc., and conducted in cooperation with the National Institute for Petroleum and Energy Research (NIPER) was initiated in October 1986. The field selected for the project is in the Mink Unit of Delaware-Childers field in Nowata County, Okla. This field pilot consisted of treating 4 of 21 injection wells on the Mink Unit. Weekly samples are continually analyzed for total dissolved solids (TDS), pH, surface and interfacial tensions, crude oil viscosity, microbial counts, molasses concentrations, oil production from the Mink Unit, water/oil ratios, injection pressures, and injection volumes.

The scope of work for FY90 includes continued monitoring of the Mink Unit Project through December 1989 and the injection of all injection wells on a particular pattern with microorganisms and nutrient for the waterflooding process. This portion of the project will be an expanded field pilot. In May 1988, Comdisco Resources, Inc., purchased property in Delaware-Childers oil field from B & N Oil Company. The Mink Unit leases were a part of this purchase. After much negotiation, an agreement was executed that compensated the project for relocating the planned expansion of the project from the selected Brown/Robertson/Johnson leases in the B & N property of Delaware-Childers field to an alternate site.

A site has been selected for the expanded microbial enhanced oil recovery (MEOR) project. The site is located in S8, T24N, R17E, of Rogers County. Figure 1 shows a map of the site. This site is part of Chelsea-Alluwe field in the Bartlesville formation. It was initially developed shortly after Delaware-Childers field. The site, owned by Phoenix Oil and Gas Ltd., is currently being waterflooded. This field is in a very isolated area, with virtually no other oil-producing leases nearby. Table 1 lists some of the reservoir properties. Although this field has much in common with the Mink Unit, there are some significant differences. The Phoenix field is not a freshwater flood; the water is recycled and injected and has an average TDS value of 3%. The permeability of the formation appears to be about 30 to 40 mD, which is less than that of the Mink Unit. Oil production information, reservoir core data, and data obtained from field sample analyses on the Phoenix site are being tabulated.

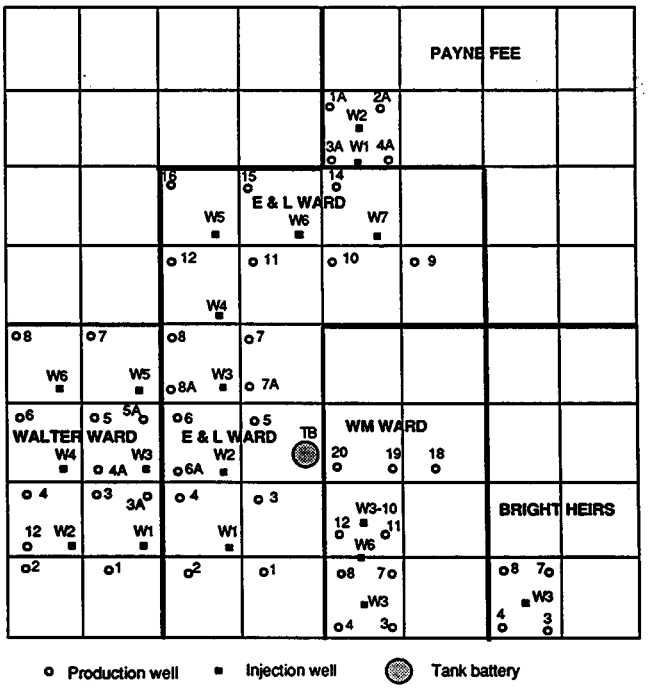

Fig. 1 Map of Phoenix field site.

All production wells from the five individual leases were tested for TDS and pH. These wells were tested to determine if any significant differences existed in the producing wells.

TABLE 1

Reservoir Properties for the Phoenix Field Test Site

Formation	Bartlesville Sandstone
Depth, ft	400
Number of injection wells	19
Number of production wells	40
Net pay thickness, ft	19 to 23
Well spacing, acres	2 to 5
Average formation temperature, °F	66
Average permeability, mD	16
Average porosity, %	20
Average water injection rate/well, bbl/d	111
Average oil production rate/well, bbl/d	1
Oil gravity, °API	34
Estimated average original S_o, %	65
Estimated average irreducible S_o, %	25

The data are presented in Table 2. The average results for the individual leases were: E & L Ward, pH of 7.72 ± 0.05, TDS of 2.97 ± 0.10; Walter Ward, pH of 7.80 ± 0.05, TDS of 3.02 ± 0.10; William Ward, pH of 7.15 ± 0.09, TDS of 2.94 ± 0.07; Payne Fee, pH of 7.85 ± 0.12, TDS of 2.65 ± 0.02; and Bright Heirs, pH of 7.95 ± 0.15, TDS of 2.47 ± 0.08. All wells averaged very close to 3% TDS and about a 7.8 pH with the exception of the William Ward lease, which averages a lower pH of 7.15.

Water samples were also used for baseline tracer analyses. Fluorescein will be injected as a tracer prior to microbial injection. The fluorescein will be analyzed with a spectrophotometric method, and it was important to determine if the produced water from the Phoenix site contained any trace minerals that might interfere with the analysis. By filtering the samples and adjusting them to a high pH, the analyses of fluorescein remained consistent. A filter from one of the injection wells was tested with fluorescein to ensure that no retention of fluorescein occurred during injection. It is anticipated that tracer will be injected soon.

An injection well on the Bright Heirs lease, W-3, was injected with microorganisms and molasses on Mar. 16, 1990. The well will remain shut in for 1 week; at which time it will be backflushed, and samples of the fluid will be analyzed for microorganisms. The wellhead pressure and volume will be recorded daily during the shut-in period. This single-well injection will provide pertinent information regarding the injectivity and survivability of the

TABLE 2

Total Dissolved Solids (TDS) and pH of Producing Wells in the Phoenix Field Site

Well	TDS, %	pH	Well	TDS, %	pH
E & L Ward			Walter Ward (continued)		
ELP-1	2.75	7.60	WAL P-5A	2.68	7.80
ELP-2	3.63	7.80	WAL P-6	3.13	7.55
ELP-3	2.65	8.00	WAL P-7	2.82	7.90
ELP-4	2.65	7.80	WAL P-8	3.00	7.75
ELP-5	2.67	7.95	WAL P-12	3.32	7.85
ELP-6	3.05	7.75	William Ward		
ELP-6A	2.98	7.80	WM P-3	2.62	6.80
ELP-7	3.10	7.70	WM P-4	3.07	6.95
ELP-7A	2.62	7.85	WM P-7	2.91	6.80
ELP-8	2.81	7.65	WM P-8	2.94	7.20
ELP-8A	2.74	7.75	WM P-11	2.83	7.00
ELP-9	2.69	6.95	WM P-12	3.20	7.60
ELP-10	3.02	7.80	WM P-18	2.68	7.40
ELP-11	3.12	7.60	WM P-19	3.01	7.30
ELP-12	2.83	7.80	WM P-20	3.24	7.30
ELP-14	3.66	7.70	Payne Fee		
ELP-15	3.16	7.60	PP-1A	2.65	8.00
ELP-16	3.00	7.85	PP-2A	2.61	7.50
Walter Ward			PP-3A	2.63	7.90
WAL P-1	3.75	7.80	PP-4A	2.70	8.00
WAL P-2	3.25	7.70	Bright Heirs		
WAL P-3	2.84	7.90	BH P-3		
WAL P-3A	2.76	7.90	BH P-4	2.55	7.80
WAL P-4	3.18	7.85	BH P-7		
WAL P-4A	2.49	8.10	BH P-8	2.38	8.10
WAL P-5	2.97	7.55			

microbial formulation. One significant finding with this single-well test is that the microorganisms and molasses were able to be injected from a centralized location at the injection plant. Microorganisms were inoculated into a 300-gal tank of molasses and incubated for 4 d. The molasses concentration in the tank before microbial inoculation was 3.75%, whereas that of the molasses at the time of injection at the wellhead was 1.8%, which indicates that the microorganisms had metabolized about half the nutrient during incubation. The complete results from the single-well test will not be available until April.

MICROBIAL ENHANCED OIL RECOVERY RESEARCH

Contract No. DE-FG07-89BC14445

University of Texas at Austin
Austin, Tex.

Contract Date: Sept. 1, 1989
Anticipated Completion: Aug. 31, 1991
Government Award: $80,650
(Current year)

Principal Investigators:
Mukul M. Sharma
George Georgiou

Project Manager:
Edith Allison
Bartlesville Project Office

Reporting Period: Jan. 1–Mar. 31, 1990

Objective

The objective of this project is to quantify and characterize microbial enhanced oil recovery (MEOR) processes through experimentation and computer simulation of bacterial metabolic processes, microbial transport through cores, and oil recovery processes resulting from the in situ production of biosurfactants. Computer simulation will be used to evaluate injection strategies and process optimization. The research will be conducted with *Bacillus licheniformis* JF-2.

Summary of Technical Progress

A mathematical model for MEOR processes was developed. The formulation of the model is discussed in detail in this report.

Mathematical Formulation of MEOR Process

The basic equations governing the transport of oil, water, bacteria, nutrient, and metabolites in MEOR processes are species mass conservation equations. In the formulation $(n_c - 1)$ component mass balance equations and one overall mass conservation equation–pressure equation are used. The constitutive relations, initial conditions, and boundary conditions must be specified to give full description of this initial boundary value problem. The components considered in the model are described in Table 1.

The process of growth and lysis of bacteria, generation of metabolites, consumption of nutrients, and transport of all the components through a permeable medium may be expressed in the form of a general mass balance equation on a unit bulk volume basis. For the problem to be more tractable, the following basic assumptions need to be made:

- Reservoir and fluids are incompressible. No gas component is considered.
- The reservoir is isothermal. Temperature changes resulting from chemical reactions are negligibly small.
- Pressure and volume changes resulting from chemical reactions are negligibly small.
- Ideal mixing holds (i.e., volume change of mixing is zero).
- Precipitation and dissolution, cation exchange, or redox reactions are not considered.
- Permeability or porosity does not change with flow of bacteria.
- Bacteria, nutrient, and metabolites are present in the aqueous phase only.
- Presence of only two phases (aqueous and oleic) is considered.
- Darcy's law applies (for non-Newtonian fluids, apparent viscosity of a phase is used).
- Dispersion follows Fick's law to multiphase flow in porous medium.

Material Conservation Equations

The differential form of material balance equations for isothermal, multicomponent, and multiphase transport of chemical–biochemical species in naturally occurring permeable media can be written as[1]

$$\frac{\partial W_k}{\partial t} = N_k + R_k \qquad (1)$$

where W_k, N_k, and R_k are the overall mass concentration, net flux, and source terms, respectively, of a component k. The porous medium has been assumed to be a homogeneous continuum with a fixed volume of domain in space.

TABLE 1

Index for Components, Coupled Components, Expressions for Dispersion Coefficients, and Specific Rate Constants for Different Components

Component (k)	Coupled component (k')	Name	Dispersion coefficient D_{kl}	Dispersion coefficient D'_{kl}	Rate constant R_{kl}	Rate constant R'_{kl}
1	*	Water	0.0	0.0	0.0	0.0
2	*	Oil	0.0	0.0	0.0	0.0
3	4	Nutrient	DF_{31}	0.0	0.0	$-[m + \mu/(Y_B)]$
4	3	Living bacteria	$(DB + DT + DF)_{41}$	$-DC_{41}$	$(\mu - k_d)$	0.0
6	4	Polymer	DF_{51}	0.0	0.0	$A_P{*}\mu + B_P$
6	4	Surfactant	DF_{61}	0.0	0.0	$A_S{*}\mu + B_S$
7	4	Inhibitor	DF_{71}	0.0	0.0	$A_I{*}\mu + B_I$
8	4	Spore	DF_{81}	0.0	0.0	0.0
9	4	Alcohol (cosurfactant)	DF_{91}	0.0	0.0	$A_{CS}{*}\mu + B_{CS}$
10	4	Acid	DF_{101}	0.0	0.0	$A_A{*}\mu + B_A$

The overall mass concentration (W_k) may be expressed as

$$W_k = \phi\left(1 - \sum_{k=1}^{n_c} \hat{C}_k\right)\sum_{l=1}^{n_p}(\rho_k C_{kl} S_l) + \phi\rho_k \hat{C}_k \quad (2)$$

where n_c = total number of components
n_p = total number of phases
(The change in pore volume caused by adsorption of components is accounted for by deduction of the cumulative volume of adsorption of all the components and expression of the phase concentration and saturation on the basis of fluid pore volume instead of on the basis of original pore volume.)
C_{kl} = volumetric concentration of component k in phase l
$\hat{C}_k$ = volumetric concentration of component k adsorbed on the rock surfaces based on original pore volume
ϕ = porosity of the medium
S_l = saturation of phase l
ρ_k = density of component k

The flux term (N_k) consists of convective and dispersive fluxes and may be expressed as

$$N_k = -\sum_{l=1}^{n_p}\{(u_l \rho_k C_{kl}) + \phi S_l [D_{kl} \cdot \nabla(\rho_k C_{kl}) + D'_{kl} \cdot \nabla(\rho_{k'} C_{k'1})]\} \quad (3)$$

where D_{kl} and D'_{kl} are hydrodynamic and coupled hydrodynamic dispersion coefficients, respectively. Subscript k' refers to the indices for the component with which component k is coupled. In MEOR processes there are diffusive fluxes in addition to the molecular diffusive flux. These are the result of bacteria that have a chemotactic diffusive flux driven by a nutrient concentration gradient (from a lower nutrient concentration toward a higher nutrient concentration) and a tumbling diffusive flux driven by bacteria concentration itself (from a higher concentration of bacteria toward a lower concentration of bacteria). These fluxes may be expressed mathematically for a permeable medium as

$$N_{Brownian} = -D_B \frac{\partial}{\partial x}(\phi S_w \rho_{bl} C_{bl})$$

$$N_{chemotactic} = D_C \frac{\partial}{\partial x}(\phi S_w \rho_n C_n)$$

where $D_C = (K_m/C_n)$ and K_m is the chemotatic coefficient[3]

$$N_{tumbling} = -D_T \frac{\partial}{\partial x}(\phi S_w r_{bl} C_{bl})$$

where subscript n = nutrient
subscript bl = bacteria
D_B = Brownian coefficient
D_C = chemotatic coefficient
D_T = tumbling diffusion coefficient

Chemotatic, tumbling, and Brownian diffusion coefficients may be 1000 times less than the value of the mechanical dispersion coefficient but may be important during static incubation and growth of bacteria inside the permeable medium. Here diffusion coefficients are already modified for permeable medium by dividing by medium tortuosity

($D = D^*/\tau$), where D^* refers to bulk diffusion coefficient in the absence of the permeable medium.

For this one-dimensional (1-D) model, hydrodynamic dispersion coefficients D_{kl} and D'_{kl} may be expressed in general as[1]

$$D_{kl} = (D_B + D_T) + a_{Ll} \frac{u_l}{\phi S_l}$$

or

$$D_{kl} = D_B + D_T + D_F$$

where $D_F = a_{Ll}\,(u_l / \phi S_l)$ and $D'_{kl} = D_C$

where a_{Ll} is the longitudinal dispersivity of the medium and D_F is the mechanical dispersion coefficient.

The source terms are a combination of all rate terms for a particular component (e.g., injection, production, growth, and death of bacteria component) and may be expressed as

$$R_k = \sum_{l=1}^{n_p} \phi S_l (R_{kl}\rho_k C_{kl} + R'_{kl}\rho_{k'} C_{k'l}) + \frac{Q_k \rho_k}{V_b} \quad (4)$$

where Q_k = rate of injection (sign is positive) or production (sign is negative)
V_b = bulk volume
R_{kl} = specific rate constant
R'_{kl} = coupled specific rate constant for component k in phase 1

First-order rate expressions have been used here for reaction rate terms. For example, in the case of nutrient, the coupled rate coefficient indicates that the rate of consumption is dependent upon the concentration of the live bacteria, and in the case of metabolites, the rate of generation depends on the concentration of bacteria (if nutrient is available).

For bacteria, the specific rate constant (R_{bl}), considering growth and death process, can be written as[2]

$$R_{bl} = \mu - K_d$$

where the specific growth rate (μ) can be approximated by the Contois model as

$$\mu = \frac{\mu_{max}}{[1 + B\,(C_{bl} / C_n)]}$$

where C_{bl} and C_n are concentrations of bacteria and nutrient, respectively; B is a parameter here.

This specific growth rate is further modified (μ_m) by introducing inhibition of growth by alcohols or acids, which becomes important toward the end of the growth process when the concentration of inhibitors becomes significant.

$$\mu_m = \mu \frac{k_i}{k_i + C_i}$$

where k_i is an experimentally determined constant and C_i is the concentration of inhibitor. The specific death constant value[2] for a particular species ($K_d = 0.01\ h^{-1}$ for most bacteria under limited nutrient condition may be considered as a constant) is included as a parameter.

The Leudeking–Piret equation[2] is used for modeling the generation of biosurfactant. In this model the kinetic rate constants for consumption of nutrient and generation of metabolites have been expressed in general as a linear relationship with respect to the specific growth rate of bacteria with a contribution from the bacterial population present. The specific rate constants may be a function of concentration of some other component or other variable that evolves from the coupled nature of this process. These terms for different components are shown in Table 1.

In the case of limiting nutrient, the specific rate constant can be written as

$$R_n = A_n \mu + B_n$$

In popular terminology

$$A_n = Y_B^{-1}$$

$$B_n = m$$

where Y_B is yield and m is maintenance coefficient of bacteria. For metabolites, A_k and B_k are the yield (generation or consumption) parameters of a component with respect to growth and maintenance of bacterial population, respectively.

Now, if values are substituted for W_k, N_k, and R_k in Eq. 1

$$\frac{\partial}{\partial t}\left[\phi\left(1 - \sum_{k=1}^{n_c} \hat{C}_k\right)\sum_{l=1}^{n_p}(\rho_k C_{kl} S_l) + \phi\rho_k \hat{C}_k\right]$$

$$= -\sum_{l=1}^{n_p} \frac{\partial}{\partial x}(u_l \rho_k C_{kl})$$

$$+ \sum_{l=1}^{n_p} \frac{\partial}{\partial x}\left[D_{kl}\phi S_l \frac{\partial}{\partial x}(\rho_k C_{kl})\right]$$

$$+ \sum_{l=1}^{n_p} \frac{\partial}{\partial x}\left[D'_{kl}\phi S_l \frac{\partial}{\partial x}(\rho_{k'} C_{k'l})\right]$$

$$+ \sum_{l=1}^{n_p} \phi S_l (R_{kl}\rho_k C_{kl} + R'_{kl}\rho_{k'} C_{k'l}) + \frac{Q_k \rho_k}{V_b} \quad (5)$$

If ρ_k is assumed to be constant and accumulation, flux, and source terms are divided by ρ_k, the accumulation term can be written as

$$W_k = \phi\left(1 - \sum_{k=1}^{n_c} \hat{C}_k\right)\sum_{l=1}^{n_p}(C_{kl}S_l) + \phi\hat{C}_k$$

or

$$W_k = \phi\left(1 - \sum_{k=1}^{n_c} \hat{C}_k\right)C_k + \phi\hat{C}_k$$

or

$$W_k = \phi\tilde{C}_k$$

where

$$C_k = \sum_{l=1}^{n_p}(C_{kl}S_l)$$

and

$$\tilde{C}_k = \left(1 - \sum_{k=1}^{n_c} \hat{C}_k\right)C_k + \hat{C}_k$$

The flux term becomes

$$N_k = -\sum_{l=1}^{n_p}\left\{(u_l C_{kl}) + \phi S_l \times\left[D_{kl}\frac{\partial}{\partial x}(C_{kl}) + D'_{kl}\frac{\rho_{k'}}{\rho_k}\frac{\partial}{\partial x}(C_{k'l})\right]\right\}$$

The source term becomes

$$R_k = \sum_{l=1}^{n_p}\phi S_l\left(R_{kl}C_{kl} + R'_{kl}\frac{\rho_{k'}}{\rho_k}C_{k'l}\right) + \frac{Q_k}{V_b}$$

So the material balance equation (Eq. 5) can be written as

$$\frac{\partial}{\partial t}(\phi\tilde{C}_k) = -\sum_{l=1}^{n_p}\left\{(u_l C_{kl}) + \phi S_l \times\left[D_{kl}\frac{\partial}{\partial x}(C_{kl}) + D'_{kl}\frac{\rho_{k'}}{\rho_k}\frac{\partial}{\partial x}(C_{k'l})\right]\right\} + \sum_{l=1}^{n_p}\phi S_l\left(R_{kl}C_{kl} + R'_{kl}\frac{\rho_{k'}}{\rho_k}C_{k'l}\right) + \frac{Q_k}{V_b} \quad (6)$$

Pressure Equation/Overall Component Balance Equation

The continuity equation describing the conservation of total mass can be obtained by summing the species conservation equation over all components.[1,4]

$$\frac{\partial}{\partial x}\sum_{l=1}^{n_p} u_l = \sum_{l=1}^{n_p}\phi S_l\left[\sum_{k=1}^{n_c}\left(R_{kl}C_{kl} + R'_{kl}\frac{\rho_{k'}}{\rho_k}C_{k'l}\right)\right] + \sum_{k=1}^{n_c}\frac{Q_k}{V_b}$$

Darcy's law for multiphase flow is written in vector notations as

$$\vec{u}_l = -\vec{\vec{k}}\cdot\lambda_{rl}(\vec{\nabla}P_l - \gamma_l\vec{\nabla}D) \quad (7)$$

If the continuity equation and Darcy's law are combined

$$-\frac{\partial}{\partial x}\sum_{l=1}^{n_p}\vec{\vec{k}}\cdot\lambda_{rl}\frac{\partial}{\partial x}(P_l - \gamma_l D) = \sum_{l=1}^{n_p}\phi S_l\left[\sum_{k=1}^{n_c}\left(R_{kl}C_{kl} + R'_{kl}\frac{\rho_{k'}}{\rho_k}C_{k'l}\right)\right] + \sum_{k=1}^{n_c}\frac{Q_k}{V_b} \quad (8)$$

From the capillary pressure relation

$$P_{cll'} = P_l - P_{l'} \quad (\text{for } l \neq l') \quad (9)$$

If l' is considered to be aqueous phase (1)

$$P_l = P_l + P_{cll'} \quad (10)$$

If the capillary pressure relation and Eq. 10 are combined

$$-\frac{\partial}{\partial x}\left[k\lambda_{rT}\frac{\partial}{\partial x}(P1)\right]=-\sum_{l=1}^{n_p}\frac{\partial}{\partial x}k\lambda_{rl}\gamma_l\frac{\partial}{\partial x}(D)$$
$$+\sum_{l=2}^{n_p}\frac{\partial}{\partial x}\left[k\lambda_{rl}\frac{\partial}{\partial x}(P_{cl1})\right]$$
$$+\sum_{l=1}^{n_p}\phi S_l\sum_{k=1}^{n_c}\left(R_{kl}C_{kl}+R'_{kl}\frac{\rho_{k'}}{\rho_k}C_{k'l}\right)$$
$$+\sum_{k=1}^{n_c}\frac{Q_k}{V_b} \qquad (11)$$

where total relative mobility (λ_{rT}) is expressed as

$$\lambda_{rT}=\sum_{l=1}^{n_p}\lambda_{rl} \qquad (12)$$

If gravity is neglected

$$-\frac{\partial}{\partial x}\left[k\lambda_{rT}\frac{\partial}{\partial x}(P1)\right]$$
$$=\sum_{l=2}^{n_p}\frac{\partial}{\partial x}\left[k\lambda_{rl}\frac{\partial}{\partial x}(P_{cl1})\right]+\sum_{k=1}^{n_c}\frac{Q_k}{V_b}+\sum_{l=1}^{n_p}\phi S_l$$
$$\times\sum_{k=1}^{n_c}\left(R_{kl}C_{kl}+R'_{kl}\frac{\rho_{k'}}{\rho_k}C_{k'l}\right) \qquad (13)$$

Constitutive and Auxiliary Relations

The constitutive and auxiliary relations (initial and boundary conditions) for isothermal, multicomponent, and multiphase flow have been described by Lake[1] and adapted for micellar polymer flooding by Gupta.[4] For the sake of completeness, those relations have been briefly outlined. The enclosed quantity by the side of the subheading shows the number of independent relations.

Saturation constraint (1)

$$\sum_{l=1}^{n_p}S_l=1$$

Phase concentration constraint (n_p)

$$\sum_{k=1}^{n_c}C_{kl}=1$$

Total concentration constraint (n_c)

$$C_k=\sum_{l=1}^{n_p}S_lC_{kl}$$

Adsorption isotherm (n_c)

$$\hat{C}_k=\hat{C}_k(C_{kl})$$

Phase equilibrium relations [$n_c(n_p-1)$]

$$k_{rl}=k_{rl}(\vec{S})$$

Capillary pressure relations (n_p-1)

$$P_{cl1}=P_l-P1$$

Phase densities (equation of state) (n_p)

$$r_l=r_l(C_{kl})$$

Phase viscosities (n_p)

$$\mu_l=\mu_l(C_{kl})$$

Relative permeabilities (n_p)

$$k_{rl}=k_{rl}(s)$$

When the number of independent relations are combined, there is a total of $n_p(n_c+5)+n_c$ relations. With the addition of (n_c-1) species conservation equations and one pressure equation, there are a total of $n_p(n_c+5)+2n_c$ equations. The total number of dependent variables also has been shown to be $(n_c+5)+2n_c$.

List of dependent variables

Variable	Number
C_k	n_c
C_k	n_c
C_{kl}	$n_c \cdot n_p$
S_l	n_p
k_{rl}	n_p
μ_l	n_p
g_l	n_p
P_l	n_p
Total	$n_p(5+n_c)+2n_c$

The preceding set of equations therefore completely describes multicomponent, two-phase, 1-D flow in the MEOR process.

Initial and Boundary Conditions

A general description of the initial and boundary conditions for flow under equilibrium and nonequilibrium conditions is presented by Lake et al.[5] The special cases of those conditions applicable for isothermal incompressible flow are described here.[4]

Initial Conditions

Specification of initial values for $(n_c - 1)$ overall component concentrations for species conservation equations and an aqueous phase pressure value for the pressure equation are necessary.

$$C_k = C_{k0}$$

$$P1 = P1_0$$

Boundary Conditions

The boundary conditions for no-flow, inflow, and outflow boundaries are treated in the following manner:

No flow condition: The normal component of the flux across impermeable boundaries is zero.

$$\vec{n} \cdot \vec{N}_{kl} = 0$$

It is equivalent to

$$\vec{n} \cdot \vec{u}_l = 0$$

$$\vec{n} \cdot \vec{D}_{kl} \cdot \vec{C}_{kl} = 0$$

For the 1-D flow,

$$\frac{\partial}{\partial x}(u_l) = 0$$

$$\frac{\partial}{\partial x} C_{kl} = 0$$

This no-flow boundary condition is not needed in this model but has been mentioned here for the sake of completeness.

Inflow condition: For inflow across a permeable boundary, the normal component of the flux needs to be specified as a function of time.

$$\vec{n} \cdot \vec{N}_{kl} = \alpha(t)$$

This condition can be specified by specifying $(n_c - 1)$ overall component concentrations and the total injection rate or a phase pressure of the injected fluid.

Outflow condition: For outflow across a permeable boundary, the continuity of flux across the boundary needs to be maintained.

$$(\vec{n} \cdot \vec{N}_{kl})_- = (\vec{n} \cdot \vec{N}_{kl})_+$$

where (–) indicates the upstream side (reservoir) and (+) indicates the downstream side (well) of the outflow boundary. If dispersion is neglected on the downstream side, the preceding equation becomes

$$n \cdot \{(u_l \rho_k C_{kl}) + \phi S_l [D_{kl} \cdot \nabla (\rho_k C_{kl}) + D'_{kl} \cdot \nabla (\rho_{k'} C_{k'1})]\}_-$$

$$= n \cdot (u_l \rho_k C_{kl})_+$$

This leads to

$$n \cdot (D_{kl} \cdot \nabla C_{kl})_- = 0$$

$$n \cdot (D'_{k'1} \cdot \nabla C_{k'1})_- = 0$$

In case of 1-D flow, this becomes

$$\frac{\partial}{\partial x}(C_{kl}) = 0$$

$$\frac{\partial}{\partial x}(C_{k'1}) = 0$$

From constitutive relationships, this provides $(n_c - n_p)$ relations.

It is further assumed that capillary pressure at the downstream end is zero.

$$0 = P_l - P_{l'} \quad (\text{for } l \neq l')$$

This relation provides another $(n_p - 1)$ relation, and in combinations with the preceding equations, gives $(n_c - 1)$ relations.

It is further necessary to specify a phase pressure or the total flow rate at the outflow boundary to obtain total n_c relations.

In the case of incompressible flow, the total flow rate at the inflow boundary should be equal to that at the outflow boundary, so at least one end of the system must be pressure constraint.

Physical Property Modeling

Modeling of physicochemical properties and phase behavior is a very important aspect of a compositional simulator. The approach taken here is very much similar to that taken in UTCHEM with respect to some properties.

Interfacial Tension

The interfacial tension between oleic and aqueous phases, for surfactant concentration above a critical value, is expressed as

$$s = s_{max} - \frac{s_{max} - s_{min}}{C_{smax} - C_{sc}} C_s$$

The parameters s_{min}, C_{smax}, and C_{sc} are to be determined from experiments.

Capillary Desaturation

The residual phase saturations under high capillary number flow condition[6] are calculated as

$$S_{rl} = S_{rlw}\, T_{l1} [\log (N_{cl}) + T_{l2}] \quad (\text{for } l = 1,2)$$

where, for 1-D flow,

$$N_{cl} = \frac{k\,(\partial P/\partial x)}{s_{ll'}}$$

The parameters T_{l1} and T_{l2} are to be determined from experimental capillary desaturation curves. These have been measured for Berea sandstone.

Relative Permeabilities

The relative permeability model, for different phases, used in the simulator[6] is

$$k_{rl} = k^{o}_{rl} S^{e_l}_{nl}$$

where

$$S_{nl} = \frac{S_l - S_{rl}}{1 - \sum_{l'=1}^{2} S_{rl'}} \quad (\text{for } l = 1,2)$$

The end-point relative permeability k^{o}_{rl} and the curvature parameter e_l are expressed as a function of residual saturations.

For $l \neq l'$

$$k^{o}_{rl} = k^{o}_{rlw} + \frac{S_{rl'w} - S_{rl'}}{S_{rl'w} - S_{rl'c}} k^{o}_{rlc} - k^{o}_{rlw}$$

$$e_l = e_{lw} + \frac{S_{rl'w} - S_{rl'}}{S_{rl'w} - S_{rl'c}} e_{lc} - e_{lw}$$

The subscript w indicates parameters measured under low capillary number condition, and similarly subscript c indicates a high capillary number condition.

Capillary Pressure

The capillary pressure is modeled as a function of porosity, permeability, interfacial tension, and saturation.[6]

For $l \neq l'$

$$P_{cll'} = C_{pc} \left(\frac{\phi}{k}\right)^{1/2} \frac{\sigma_{ll'}}{\sigma_{wo}} (1 - S_{nl})^{n_{pc}}$$

where

$$S_{nl} = \frac{S_l - S_{rl}}{1 - \sum_{l'=1}^{2} S_{rl'}}$$

where C_{pc} and n_{pc} are capillary pressure parameter and capillary pressure exponent, respectively. The values for those parameters are determined by curve fitting a plot of water–oil capillary pressure vs. normalized water saturation and are available for Berea sandstone. The subscript l indicates wetting phase and l' indicates nonwetting phase. In this case, $l = 1$ and $l' = 2$. $\sigma_{ll'}$ and σ_{wo} are interfacial tension between phases l and l' and water and oil, respectively.

Adsorption of Biosurfactant and Biopolymer

The adsorption of biosurfactant and biopolymer is modeled with a Langmuir type of isotherm and assumed to be reversible and independent of salinity and pH of the aqueous phase.

$$\hat{C}_k = \frac{aC_{kl}}{1 + bC_{kl}}$$

The empirical parameters a and b are to be determined experimentally.

Adsorption of Microorganisms

The flowing concentration of bacteria may be modeled as a function of total concentration as

$$C_f = 0 \quad (\text{for } C_T < C^*)$$

or

$$C_f = C_T - C^* \quad (\text{for } C_T > C^*)$$

$$\hat{C}_k = C_T - C_f = C^*$$

where C^*, C_f, $\hat{C}_k$, and C_T are critical, flowing, adsorbed, and total (adsorbed and flowing) concentrations of bacteria, respectively.

Alternatively, the process may be modeled as

$$C_{fD} = \frac{a\, C_{TD}}{(1 + b\, C_{TD})}$$

where $C_{fD} = C_f / C_T$ and $C_{TD} = (C_T - C^*)/C_T$

So

$$C_f = C_{fD} \, {}^*C_T$$

$$\hat{C}_k = C_T - C_f$$

where C_{fD} and C_{TD} are dimensionless flowing and effective total concentrations of bacteria, respectively. The parameters a and b are to be determined experimentally.

Phase Viscosities

The aqueous phase viscosity will be a function of the biopolymer concentration (C_{pol}) and may be represented as

$$\mu_l = \mu_w + m\, C_{pol}$$

The parameter m must be determined experimentally.

The oleic phase is assumed to consist of oil component only, so the viscosity remains the same as that of oil.

Phase Densities

Phase densities are expressed as (ρ_k may be a function of pressure, temperature, and composition, but in this model it is assumed to be a constant)

$$\rho_l = \sum_{k=1}^{n_c} \rho_k C_{kl}$$

where ρ_k and C_{kl} are density of component k and concentration of component k in phase l, respectively.

Phase Behavior

Previous researchers have reported the formation of an emulsion in the presence of a biosurfactant. More work needs to be done in the area of phase behavior for MEOR applications.

A simple approach has been taken by assuming that the oleic phase consists of only the oil component and that the bacteria, nutrient, and produced metabolites remain in the aqueous phase. This is a good realistic assumption.

The phase saturation may be expressed as

$$S_o = C_o$$

$$S_w = 1 - S_o$$

The phase concentration of aqueous-phase components may be expressed as

$$C_{kw} = \frac{C_k}{S_w}$$

Nomenclature

C_{bl}	Concentration of bacteria in aqueous phase
$\hat{C}_k$	Concentration of component k adsorbed on the stationary phase
$\tilde{C}_k$	Overall concentration of component k adsorbed on the stationary phase
C_k	Concentration of component k (volume of component/volume of liquid phase)
C_{kl}	Concentration of component k in phase l
C_n	Concentration of nutrient in aqueous phase
D'_{kl}	Coupled dispersion coefficient for component k in phase l
D_{kl}	Dispersion coefficient for component k in phase l
e_l	Relative permeability exponent for phase l
e_{lc}	Relative permeability exponent for phase l at high capillary number
e_{lw}	Relative permeability exponent for phase l at low capillary number
k	Absolute permeability in the flow direction
K_d	Specific death rate constant
k_{rl}	Relative permeability of phase l
k^o_{rl}	End-point relative permeability of phase l
k^o_{rlc}	End-point relative permeability of phase l at high capillary number
k^o_{rlw}	End-point relative permeability of phase l at low capillary number
n_c	Number of components
N_{cl}	Capillary number of phase l
N_k	Net flux of component k [mass/(area · time)]
N_{kl}	Net flux of component k in phase l
n_p	Number of phases
Pl	Pressure in aqueous phase
$P_{cll'}$	Capillary pressure between phase l and l′
P_l	Pressure in phase l
Q_k	Rate of injection (+ve sign) or production (–ve sign) of component k
r_l	Density of phase l
R_{bl}	Specific rate constant for bacteria
R'_{kl}	Coupled specific rate constant for component k in phase l
R_k	Rate of injection, production, generation, or consumption (mass/time) of component k
R_{kl}	Specific rate constant for component k in phase l
S_l	Saturation of phase l
S_{rl}	Residual saturation of phase l
t	Time

T_l	Transmissibility of phase l
T_t	Total transmissibility
u_l	Darcy velocity (flux) of phase l
V_b	Bulk volume
W_k	Overall mass concentration (mass/bulk volume)

Subscript

k	Index for a component
l	Index for a phase
	1 Water
	2 Oil
max	Maximum
min	Minimum

Superscript

n	Old time level
n+1	New time level

Greek Symbols

ϕ	Porosity of porous medium
μ	Specific growth rate of the bacteria
μ_{max}	Maximum specific growth rate of the bacteria
μ_m	Modified specific growth rate
ρ_k	Density of component k
μ_l	Viscosity of phase l
λ_{rl}	Relative mobility of phase l
λ_{rT}	Total relative mobility
∇	Difference operator
$s_{ll'}$	Interfacial tension between phase 1 and l′

References

1. L. W. Lake, *Enhanced Oil Recovery,* Prentice Hall, Englewood Cliffs, New Jersey, 1989.
2. J. E. Bailey and D. F. Ollis, *Biochemical Engineering Fundamentals,* 2nd edition, McGraw Hill, 1986.
3. M. Y. Corapcioglu and A. Haridas, Microbial Transport in Soils and Groundwater: A Numerical Model, *Adv. Water Resour.,* 8: 188-200 (December 1985).
4. A. Datta Gupta, *Three-Dimensional Simulation of Chemical Flooding,* M.S. thesis, Department of Petroleum Engineering, University of Texas, Austin, Tex., May 1985.
5. L. W. Lake, G. A. Pope, G. F. Carey, and K. Sepehrnoori, Isothermal, Multiphase, Multicomponent Fluid Flow in Permeable Medium, *In Situ,* 8(1): 1-40 (1984).
6. D. Bhuyan, *Development of an Alkaline–Surfactant–Polymer Copositional Reservoir Simulator,* Ph.D. dissertation, Department of Petroleum Engineering, University of Texas, Austin, Tex., December 1989.

Appendix

The overall mass conservation equation may be obtained by adding the component mass conservation equations over all the components.

$$\sum_{k=1}^{n_c} \frac{\partial}{\partial t} W_k = -\sum_{k=1}^{n_c} \nabla \cdot N_k + \sum_{k=1}^{n_c} R_k$$

$$= -\nabla \cdot \sum_{k=1}^{n_c} N_k + \sum_{k=1}^{n_c} R_k$$

The accumulation term

$$\sum_{k=1}^{n_c} \frac{\partial}{\partial t} W_k = \frac{\partial}{\partial t}\left[\phi\left(1-\sum_{k=1}^{n_c}\hat{C}_k\right)\sum_{k=1}^{n_c} C_k + \phi \sum_{k=1}^{n_c}\hat{C}_k\right]$$

but

$$\sum_{k=1}^{n_c} C_k = 1$$

So

$$\sum_{k=1}^{n_c} \frac{\partial}{\partial t} W_k = \phi \frac{\partial}{\partial t}\left(1-\sum_{k=1}^{n_c}\hat{C}_k + \sum_{k=1}^{n_c}\hat{C}_k\right)$$

$$= 0$$

The total flux term

$$\sum_{k=1}^{n_c} N_k = \sum_{l=1}^{n_p}\left\{\left(u_l \sum_{k=1}^{n_c} C_{kl}\right)\right.$$

$$\left. - \phi S_l \sum_{k=1}^{n_c}\left[D_{kl}\frac{\partial}{\partial x}(C_{kl}) + D'_{kl}\frac{\rho_{k'}}{\rho_k}\frac{\partial}{\partial x}(C_{k'l})\right]\right\}$$

but

$$\sum_{k=1}^{n_c} C_{kl} = 1$$

and total dispersive flux is zero, thus

$$\sum_{k=1}^{n_c} N_k = \sum_{l=1}^{n_p} (u_l)$$

The source terms become

$$\sum_{k=1}^{n_c} R_k = \sum_{l=1}^{n_p} \phi S_l \sum_{k=1}^{n_c} \left(R_{kl} C_{kl} + R'_{kl} \frac{\rho_{k'}}{\rho_k} C_{k'l} \right) + \sum_{k=1}^{n_c} \frac{Q_k}{V_b}$$

Now, if overall terms for accumulation, flux, and source terms are substituted in overall main conservation equation

$$\frac{\partial}{\partial x} \sum_{l=1}^{n_p} u_l = \sum_{l=1}^{n_p} \phi S_l \left[\sum_{k=1}^{n_c} \left(R_{kl} C_{kl} + R'_{kl} \frac{\rho_{k'}}{\rho_k} C_{k'l} \right) \right] + \sum_{k=1}^{n_c} \frac{Q_k}{V_b}$$

ENVIRONMENTAL TECHNOLOGY

TECHNICAL ANALYSIS FOR UNDERGROUND INJECTION CONTROL

Cooperative Agreement DE-FC22-83FE60149, Project SGP23

National Institute for Petroleum and Energy Research
Bartlesville, Okla.

Contract Date: Oct. 1, 1989
Anticipated Completion: Sept. 30, 1990
Funding for FY 1990: $74,500

Principal Investigator:
Michael P. Madden

Project Manager:
Alex Crawley
Bartlesville Project Office

Reporting Period: Jan. 1–Mar. 31, 1990

Objective

The objective of this project is to provide technical assistance to the U.S. Department of Energy (DOE) on matters related to underground injection control (UIC) or other environmental topics related to oil and gas production.

Summary of Technical Progress

At the request of the DOE Technical Project Officer, two documents were reviewed, "EPA Statement of Groundwater Principles" and "State/Federal Relationships Options Paper," prepared by the Environmental Protection Agency (EPA) Groundwater Task Force. The review was submitted as NIPER Report SGP23-9. A portion of the introduction of the report is given below verbatim.

The paper prepared by the EPA Groundwater Task Force is very broad. Their statement could be interpreted, by a congressional committee or others, as implying that nothing has been done or is being done to protect groundwater. Such an interpretation would be false because there are tough laws in effect at the present time. This statement may give the EPA the ammunition they need to virtually shut down the petroleum industry by overregulating brine disposal, integrity testing of onshore producing and injection wells, protection of recharge zones, etc. Severe restrictions would impact not only oil producers, but also the Nation's petroleum reserves.

☆U.S. GOVERNMENT PRINTING OFFICE:1990 -561 -029/20063